Universität Rostock Traditio et Innovatio

ONLINE MONITORING SYSTEM USING REACTOR AND MASS SPECTROMETRY

Thesis

To

The acquisition of the academic degree

Doctor of Engineering (Dr. Eng)

Faculty of Computer Science and Electrical Engineering

University of Rostock

Rostock, 2017

Submitted by:
M.Sc Vinh Quang Do
From Vietnam
Born on 16.10.1984 in Can Tho

Advisors:
PD. Dr.-Ing. habil. Heidi Fleischer
Prof. Dr.-Ing. habil. Kerstin Thurow

urn:nbn:de:gbv:28-diss2018-0044-1

Reviewers:

1. Reviewer:

   Prof. Dr. -Ing. habil. Kerstin Thurow

   Institute of Automation, University of Rostock, Germany

2. Reviewer:

   PD. Dr. -Ing. habil. Heidi Fleischer,

   Institute of Automation, University of Rostock, Germany

3. Reviewer:

   Prof. Robin A. Felder, Ph.D.

   Department of Pathology, University of Virginia School of Medicine, USA

Date of Submission: 5th , September, 2017

Date of Defense: 5th , March, 2018

ABSTRACT

An online reaction monitoring system can offer fast data acquisition at different reaction stages of every time-point in a reaction process. This facilitates the study of reaction mechanism and reaction kinetics through the monitoring of reactants, products and transient species. And at a higher level, reaction conditions can be influenced automatically based on feedback data so that reaction parameters such as reaction rate, product quality or product quantity can be optimized. For constructing an online reaction monitoring system with basic operations, different tasks in different areas of engineering are involved such as: (chemical engineering) determining purposes of the system construction and its main functions, system configuration as well as component devices; (mechanical and control engineering) suitable arrangement, housing and control of individual devices if necessary; (computer engineering) combination of discrete functioning of component devices into an automation process for performing meaningful actions; and creation of the Graphical User Interface (GUI) for ease and convenience in control to operators. A mobile reaction system coupling to an ESI-TOF-MS for online analysis purpose has been implemented in our lab. The system implements the flow injection (FI) idea that solution from the micro reactor outflow is injected into a carrier stream which is coupled to an analyzer. The system is computer-based controlled with its all actions to be automated through the GUI. In this work, a modification and extension of an existing online reaction monitoring system are aimed at so that the system performance as well as its utilities can be improved. Different tasks have been performed to accomplish the goal.

1) Addition of the dilution module so that the problem associated with sample overloading can be avoided.

2) Integration of the micro reactor system to the ICP-MS for metal detection.

3) Modification of the monitoring method (or sampling method) for saving time and materials.

4) Modification of the heating module for tempering a reaction.

5) Correction for the errors of peak missing and double-sized peaks in sampling of the existing system. This helps bring the standard deviation in sampling replication down to less than 10%.

6) Modification of the existing control software for accommodating new functions and modules.

7) Communication with the analyzer's control software for a convenience in operation and data extraction.

ACKNOWLEDGEMENTS

In order to be at this phase of my Ph.D. program, I have received a lot of support from my supervisors, my family, and my friends.

Firstly, I would like to express my sincere thanks to Frau Prof. Kerstin Thurow for giving me a chance to follow this Ph.D. program which I had never dreamed of even after my bachelor graduation. Her instructions are valuable for me during the years. I would like to send my deepest gratefulness to my supervisor Frau PD. Dr. Heidi Fleischer who has accompanied me during the last duration. She not only guided me with her care, patience and enthusiasm but also encouraged me a lot during this long and challenging period. I would like to thank also other members in Celisca for their kind supports, especially Dr. Thomas Roddelkopf, Herr Lars Woinar, Herr Heiko Engelhardt, Dr. Steffen Junginger, Frau Grit Koch, Frau Sybille Horn.

Secondly, I am extremely grateful to my family who always love me and stay by my side no matter where I am and what I do. I would like to thank my friends, especially Ankit, Ali, Kim Chi, Minh Thu, Trang Thuy, Ha Giang, Xuan Hong, Phuong Linh, Xuan Can and Van Muot, for their kind helps and encouragement and for the pleasure time we had.

Finally, I would like to thank the Vietnam Ministry of Education and Training for the Project 911 Scholarship for the financial support of my study. This gives me a chance to study in Germany where people love to work and willing to share their knowledge. Time when I have been here is a meaningful experience and unforgettable memory in my life.

Thank you again and wish you all the best.

CONTENTS

LIST OF FIGURES

LIST OF TABLES

CHAPTER 1 INTRODUCTION

A chemical reactor is a device properly designed for reactions to occur under controlled conditions toward specified products [1]. It can be roughly categorized into batch reactors and flow reactors although there are other types of reactor available such as semi-batch reactors, continuous stirred tank reactors, organelles, cells, and tissues. In batch reaction such as a reaction in a flask and a beaker, the concentration of species evolves with time or concentration is a function of time. Meanwhile, for a flow reaction at its steady state, the concentration at each specific location is unchanged with time but evolves with spatial location along the reactor. In other words, concentration in flow reactor is a function of position [2]. The residence time in flow reaction is defined as the time for which the solution resides in the flow reactor. It can be considered equivalent to a certain elapsed time for a reaction in batch reactor. For setting different residence time in flow reaction, either the reactor volume or stream flow rate can be varied. Batch reaction is widely used in fine chemicals and drugs. Meanwhile, flow reaction is more dominated in mass manufacture such as petrochemical and commodity chemical industry [3].

Micro reactor is a branch of flow reactor which has been investigated since the mid-1990 as a tool for chemical research by academic researchers. Today, this technology is not limited to the field of chemistry but is used in biotechnology, pharmaceutical industry and medicine, life science, clinical and environmental diagnostics [4].

Advantages and disadvantages: An advantage of micro reactors is rapid mixing that occurs due to short diffusion distances and therefore side reactions that occur due to poor mixing can be suppressed [4][5]. Efficient mass transfer that increases reaction selectivity[1] [6] and efficient heat transfer that enables higher temperatures and pressures applied to slow reactions as well as safer operations with exothermic reactions are further advantages [7]. Micro reactors can be modulus since different functioning blocks can be connected together such as mixing modules, reaction modules, and heating modules. Therefore, a micro reactor system can be easily scaled up by numbering up channels and is flexible enough to respond to changes in the market or supply chain [8]. In addition, process conditions in micro reactors can be well controlled such as flow pattern, efficient mixing, uniform or gradient temperature distribution [9][10]. Indeed, those factors of small size, robustness, controllability, and scalability of micro reactors make it beneficial for implementing chemistry-related automation system in lab scale. One drawback of micro reactors is not being tolerant to particulates whose size exceeds 10% of the smallest dimension of the system channel [8].

Some applications relating to micro reactors include:

- High-throughput screening: isomerization of allylic alcohols, gas/liquid asymmetric hydrogenation [11].
- High purity chemical products such as photo cyclization, photocycloaddition, photo isomerization reactions [12].

[1] The selectivity may be defined as the conversion of the reactant to the desired product divided by the overall conversion of the reactant. It may also be stated as the rate of conversion of the feed to the desired product divided by the overall conversion rate of the feed.
http://www.eptq.com/qandaquestion.aspx?q=c37ac6f6-3748-4704-8dcf-dfed451ee54e

- Highly exothermic reactions: Nitration of toluene using concentrated nitric acid as the nitrating agent with a packed bed micro reactor [13], reaction of methyl chloroformate with amines to form methyl caramates [14].
- Reaction at elevated temperature: Newman-Kuart rearrangement involving O-(2-nitrophenyl)-N,N-dimethylthiocarbamate at 170^{o}C with CYTOS system [14], hydrogen production at >700^{o}C [15].
- Fuel cell construction: hydrogen production from ceramic micro reactor [15].
- Emulsification and microencapsulation [16].
- Precision particle manufacture: calcium carbonate precipitation and silver particle synthesis [17].
- Portable chemical analysis: Lab on chip or total analysis system [18].

Motivations: Combination of micro reactors and analytical devices for online monitoring of chemical processes even widens the application of this field in industry and research. This combination exploits the advantages of micro reactors and the advantages of analytical devices for fast and reliable data acquisition. Therefore, with an online reaction monitoring system, the qualitative, quantitative and structural information of analytes can be derived [19]. Therefore, reaction mechanism and reaction kinetics can be studied conveniently through the monitoring of reactants, products and transient species. And at a higher level, reaction conditions can be influenced automatically based on feedback data so that reaction parameters such as reaction rate, product quality or product quantity can be optimized [20]. This technology of automated optimization of reactions, catalysts, and solvents exploits the revolutionary algorithm or self-optimization (i.e. the Nelder-Mead simplex algorithm NMSIM or the stable noisy optimization by branch and fit SNOBFIT algorithm), design of experiments (DoE) and kinetic parameters [21].

For monitoring a chemical reaction, there are 3 techniques namely *online*, *inline* and *offline*. For the first two techniques, samples are not required to be transferred remotely; the process can be measured at real-time and the transient intermediates in millisecond range can be detected [22]. In the inline technique, all the flow is continuously analyzed or the probe is inserted into the reactor, whereas representative aliquots are periodically analyzed or the reactor is hyphenated to an instrument in the online technique [23][24]. In the offline technique, the time the process properties are obtained is normally longer than the time the process properties are changed. Therefore, this method is often impossible to detect short-lived intermediate. *In situ* or *inline* monitoring techniques has advantages for not introducing sampling delays and less disturbing the reaction process. Meanwhile, in online methods more realistic reaction conditions such as heating, cooling, inert or reactive gas atmosphere and mixing are easily realized [24].

Online reaction monitoring can be realized by the integration of physical sensors or spectroscopic methods. Via installation of physical sensors, the reaction temperature can be monitored by thermometer, bimetal, thermistor, thermal-couple; and reaction flow rate can be measured with micro pressure sensors, micro flow anemometers, optical fiber cantilevers. In spectroscopic methods fluorescence spectroscopy, ultraviolet-visible spectroscopy (UV/VIS), infrared spectroscopy (IR), Raman spectroscopy, X-Ray spectroscopy (XRF) and nuclear magnetic resonance spectroscopy (NMR) are common techniques of

employment by measuring electromagnetic signals. Mass spectrometry is used via the detection of the mass to charge ratio (m/z) of a chemical element or compound.

Practically, all control systems implemented today are based on computer control [25]. Since the pioneering period (≈ 1955), computer-based control has advanced rapidly through the direct-digital-control, minicomputer, microcomputer, general use of digital control and distributed control, and recently Internet of Things (IoT). Parallel to the advancement of computer technology is the increasing of the mean time between failure (MTBF) and the steady decreasing in price of the computer unit. These factors contribute to the popularity of computer controlled systems nowadays.

As the author's understanding, the idea of control is to mainly deal with how a device or system behaves when a change in setpoint or a disturbance occurs. This relates to the problems of Trajectory tracking or Servo problem and regulatory problem respectively. Meanwhile, automation is normally to integrate some or many component devices (which are already well controlled) to automate a desired operation/process so that human labor can be released. The two concepts are interrelated and both are included in a computer control system.

In the lab, a computer-based automation system has been built order to realize the benefits as well as to investigate the analytical capability of the combination. The aim of this project is to construct a mobile online reaction system (ORMS) coupled to a spectrometric method for online monitoring chemical reaction in a micro reactor. The system can facilitate users with different tools and utilities necessary for the analytical work. The system should be automated so that users can conveniently manipulate the process as well as the resulting data. An initial setup of the system with the control software (ORMS software) was available that it can perform basic functions of sampling and injection. In this work, a modification and extension of the existing system are aimed at in order to improve the system performance as well as to elaborate the system functioning. This includes:

1) Addition of the dilution module so that the problem associated with sample overloading can be avoided.

2) Integration of the micro reactor system to the ICP-MS for metal detection.

3) Modification of the monitoring method for save of time and materials.

4) Modification of the heating module for tempering a reaction.

5) Correction for the errors of peak missing and double-sized peaks in sampling of the existing system. This helps bring the standard deviation in sampling replication down to less than 10%.

6) Modification of the existing control software for an accommodation of new functions and modules.

7) Communication with analyzer's control software for a convenience in operation and data extraction.

Text arrangement: The first chapter briefly introduces micro reactors and reaction monitoring techniques. An overview of the project's aims and tasks are also included. The second chapter gives the state of art of different technologies applied for online reaction monitoring in micro reactors or micro fluidic devices.

Chapter 3 introduces the system in the laboratory as well as the objectives of the work in more details. Chapter 4 verifies the performance of the system components. Chapter 5 introduces different sampling methods and the proposed *fast sampling method* for time and materials saving. Chapter 6 presents the heating module with different heating configurations and the automatic heating algorithm. Chapter 7 discusses the integration of the dilution module with different dilution configurations and the algorithm for automatic dilution. Chapter 8 presents the system in coupling to the ICP-MS with two proposed configurations. Testing of the dilution module in coupling with the ICP-MS system is also shown in this chapter. Chapter 9 focuses on the GUI modification of the control software (ORMS software) and the communication to the analyzer's control software using the Graphical User Interface (GUI) automation techniques. Chapter 10 is the summary, conclusion and future work. Finally, chapter 11 summarizes all chemicals and parameter settings for the analytical device that are used for testing and experiments.

CHAPTER 2 THE STATE OF ART

In this chapter, operation principles and some applications of popular spectroscopic methods are reviewed briefly such as fluorescence spectroscopy, ultraviolet-visible spectroscopy (UV/VIS), infrared spectroscopy (IR), Raman spectroscopy, nuclear magnetic resonance spectroscopy (NMR) and mass spectrometry. In particular, the integration of those methods to micro reactors for online reaction monitoring purposes will be considered. A short introduction to micro reactors is presented first.

2.1 *Micro Reactors*

Micro reactors are considered as devices containing typically a micro channel with lateral dimensions of <1mm in which a continuous flow reaction can take place [26]. There are different types of micro reactor depending on reaction types such as: micro reactors for liquid phase process; micro reactor for gas-liquid process; and micro reactor for gas phase reaction. Regardless of their specialized usage, a micro reactor is often a planar surface with ducts or channels machined into. Sometimes, the reaction volume can be in a T-mixer or a capillary. Some types of micro reactor are shown in Figure 2-1. For a liquid-based micro reactor, the typical cross sectional dimensions of the channels used are normally in a range of 10–500 μm [27].

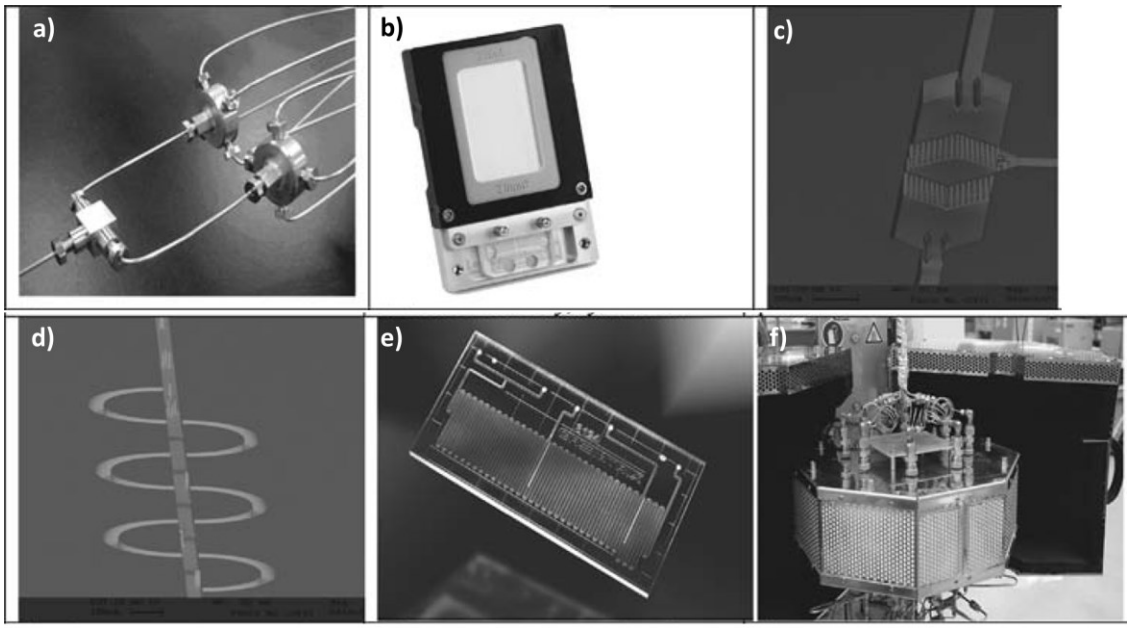

Figure 2-1: Various types of micro reactor and other micro fluidic components [26]: a) branch capillary micro reactors using couplers, b) glass micro reactor integrated within chip-to-word coupling interface, c) silicon micro reactor with integrated frit to hold catalytic particles, d) silicon micro reactor with integrated high aspect-ratio posts and flow disruption features, e) glass micro reactor chip for catalyst reactions, f) commercial multi-micro reactor based system

Materials and fabrication techniques: Micro reactors can be fabricated from different materials such as metal (stainless steel, copper), silicon, glass (FOTURAN), fused silica and quartz, thermal plastic (polymethylmethacrylate-PMMA, polycarbonate-PC and Topas®-COC), thermoset polymers (SU8,

Kapton), elastomers (polydimethylsiloxane-PDMS), thermoplastic elastomers, fluorinated homopolymers (polytetrafluoroethylene-PTFE), fluorinated copolymers (perfluoroalkoxy-PFA, Teflon AF, fluorinated ethylene propylene-FEP), ceramic, polytheretherketone-PEEK etc. There are many considerations on materials for fabrication of micro reactors, for example, thermal tolerance to processing conditions, temporal stability of surface energy, surface chemistry, the chemical inert, thermal and electrical properties, compatibility with reagents/analytes and solvents used, light transparency, compatibility with fabrication protocol used and compatibility with the analyzing techniques [26][28]. Different techniques have also been adapted or developed for processing micro reactors such as laser ablation, wet chemical etching, abrasive micromachining, deep reactive ion etching, molding, embossing, casting and milling.

Manufacturers: The field of micro flow reactor is now growing bigger that there are more and more companies get involved in this market. They offer (1) complete products or integrated systems in which different operations (pumping and metering of reagents, mixing, temperature control, chemical or thermal quench, pressure control, product collection) are integrated into a compact unit as well as (2) separate components (component-based system) for more flexibility of the system [3]. Some of the known manufacturers are mentioned below with some of their typical products about micro reactor system:

Ehrfeld Mikrotechnik (Germany): The company offers a variety of products and modules for flow chemistry from laboratory scale (Modular MikroReaction System – MMRS) with a yield of 0.05 - 10 L/h to production scale (Miprowa®) with a yield of 40 – 10,000 L/h [29]. Most of the modules offered are made from metal (stainless steel, hastelloy). Reactors are varied from micro reactors to mini-structured reactors. A reaction system is normally a combination of separate modules. A process automation system for MMRS named LabManager® is also offered by the company.

Chemtrix (Netherland): The manufacturer also offers products used for laboratories (Labtrix® with glass micro reactor, Protrix® with ceramic (SiC) reactor) and for ton scale production (Plantrix® with ceramic (SiC) reactor). Labtrix® S1 with dedicated control software enables the automatic data logging, sample collection and control [30]. In addition, 3D printed flow reactors, glass reactor modules (Gramflow®, Kiloflow®) can be found in the company's product list.

Uniqsis (UK): This company offers small scale applications with three lines of flow reaction models called FlowLab, FlowLab Plus and FlowSyn. Each module as well as material options can be selected for specific use. This manufacturer and other like manufacturers such as Syrris, ThaLesNano, Accendo Corporation are more focused on small scale and integrated systems which are more suitable for application analysts than for engineers. They can be operated manually via a built-in keypad or automatically via a control software. These systems are built in order to facilitate for the self-analysis or being integrated to an external analyzer.

Other manufactures for micro reaction systems can be referred to are: Cetoni, Amar equipment, Little Things Factory (LTF), Corning, Sigma-Aldrich, HiTec Zang, Institute for microtechnich Mainz, Mikroglas, Synthesechemie Dr. Penth, Micronit.

Table 2-1: Some commercial micro reactor systems available on the market

Manufacturers	Products	Properties and applications
Ehrfeld Mikrotechnik	Modular MicroReaction System (MMRS)	Different modules can be combined easily and quickly. Can be used for research and development, and for small-quantity production such as mixing/emulsification/dispersion/particle precipitation; homogeneous/heterogeneous synthesis; photochemistry.
	ART® plate reactors	Milli-structured plate reactors with excellent heat transfer; quick and easy scale-up. Suitable for research & development or production application. Application in multi-purpose plants for flexible product change-over.
	Miprowa®	Highly efficient reactors and heat exchangers. Fast upscaling from miniature to production level. Suitable for laboratory scale, pilot plant or production application.
Chemtrix	Labtrix® S1	'Plug and play' continuous flow reaction system. Dedicated software which provides automatic data logging, sample collection, and control. Suitable for assessment of process feasibility; exploration of novel reaction conditions; process parameter optimization and process validation.
	Plantrix®	Ceramic continuous flow reactors which are suitable for chemically challenging reactions such as fast, highly exothermic reactions; reactions with aggressive media; reactions employing unstable intermediates and hazardous reactions not accessible under batch conditions.
	3D printed flow reactor	Flexible tool for high pressure and high temperature flow chemistry applications. Suited for process development and kg production. High temperature applications (-100 to 300°C) High pressure applications (<100 bars). Customized 3D printing of reactors is possible.
Uniqisis	FlowLab Plus™	A modular flow chemistry system with some features: Dedicated control software. Remote Wi-Fi or LAN operation. -40 to +300 °C temperature range options. Versatile dual channel high pressure flow reactor system. Compatible with standard Uniqsis reactors.
	FlowSyn series	A series that include various products with keys features: FlowSyn: for single reactions. FlowSyn Maxi: For scale up and high throughput processes. FlowSyn Multi-X: Multi-experiment package for reaction sequences. FlowSyn Auto-LF: For automated combinatorial experiments. FlowSyn Polar Bear™: Advanced cooling for flow chemistry. FlowSyn Cold: For low and multi-zone temperature experiments.

2.2 *Reaction Monitoring Technologies*

Knowing what is happening in real-time of a reaction process offers a lot of benefits. In R&D phase, reactions can be designed and controlled in an optimal way such as to increase product yields, improve product purity, reduce side reactions and therefore by-products, reduce production costs and risks from unexpected processes. In manufacturing phase, online monitoring helps operators know the progressing of the process and have an early intervention before something unexpected may occur. In scientific research, the abundance real-time data allows researchers to determine kinetics, mechanisms of reactions that can be exploited for online reaction optimization or for synthesizing new compounds. There are different techniques can be used for online reaction monitoring including spectroscopic techniques such as infrared (IR), Raman, ultraviolet-visible (UV-vis) and nuclear magnetic resonance (NMR) spectroscopies) as well as other methods such as calorimetry, mass spectrometry, electrochemistry, chromatography, and chemical analysis [24]. For spectroscopic methods such as IR and UV-vis, the absorbance spectrum is what can be used to identify functional groups or chemical bonding of compounds which are useful for identification of species and study of reaction mechanisms. In addition, by using standard calibration solutions, concentrations of educts or products as a function of time can be derived and employed to determine reaction kinetics. For NMR, the absorption spectrum of radiowaves by nuclei (of some combined atoms in molecule) in a magnetic field are useful for studying the shape, structure of molecules and their concentrations, chemical equilibria, reaction kinetics, motion of molecules, and intermolecular interactions [31]. For mass spectrometry, mass spectrum (*m/z*) and their relative abundance can be used to determine structures and elemental compositions of molecules and to calculate their concentrations (using standard calibration samples).

2.2.1 Background

A light can be considered as a wave, which is represented by its frequency *(v)*, wavelength *(λ)* and amplitude, or as a stream of particle (*photon*) with *energy* of each photon represented as

$$E = h * v = \frac{h * c}{\lambda} \tag{2-1}$$

h: *Planck's constant*, 6.626×10^{-34} J.s
c: velocity constant of light in vacuum, 2.997×10^{8} m/s

The *radiation power P* (*energy per second per unit area*) or *intensity I* (*power per solid angle*) of a light beam is related to the square amplitude of that light beam.

There is an interaction between *electromagnetic radiation* (light) with *matter*; this interaction is also the study subject of *spectroscopy* [31]. Under the relevant interaction with radiation, matter (in this case includes atoms, ions, molecules) which is always in constant motion, changes their energy in form of changing in motion and in electron energy level. In order words, they are in *transition state*. It is important to note that the *transition state* in molecules and in atoms or monoatomic ions are different as compared in Table 2-2. For molecules, there are *vibrational transitions, rotational transitions, electronic transitions*, etc. in which the transitional energy is *vibration* < *rotation* < *electronic*. However, for atoms

or monoatomic ions, they do not have either *vibrational* or *rotational transitions* but *electronic transitions*. Even the electronic transition state of molecules and of atoms are somehow different.

Table 2-2: Transition state in molecules and in atoms

Transition State	Molecule	Atom
Vibration	X	-
Rotation	X	-
Electronic	X	X
	Outer (valence) electrons promote from ground state molecular orbitals to higher energy molecular orbitals (i.e. bonding π-> antibonding π *). (Molecular orbitals are formed by the combination of electrons from atoms).	Outer (valence) electrons promote from ground state orbitals to higher energy orbitals (i.e. 2p -> 2s).

Due to different transitional states existing in molecules, an *absorption*/*emission* of energy involves a combination of changes in rotational, vibrational and/or electronic energy. In other words, a molecule can absorb/emit various wavelength depending on the state it will be excited to or released from. This explains for the broad absorption/emission band in molecules and narrow band in atoms. A demonstration is shown in Figure 2-2 which shows an emission spectrum of a flame that includes polyatomic species and atomic elements.

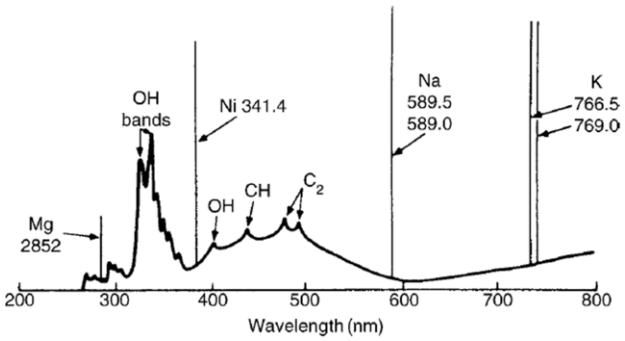

Figure 2-2: Emission spectrum of a flame. The broad background emission bands from polyatomic species such as OH and CH are seen. Superimposed on the broad background emission are the very narrow atomic emission lines from the elements Mg, Ni, Na, and K [31]

A transition in energy state of matter can take place only when the *absorption energy*/*emission energy* exactly equals the energy difference between the initial (E_0) and the final (E_1) state.

$$\Delta E = E_1 - E_0 = \frac{h * c}{\lambda} \tag{2-2}$$

Absorption Laws

Matter can only absorb light of certain *frequencies* (*wavelengths*) as related to its *photon energy* defined in equation (2-1). In addition, *intensity* at a particular frequency that can be absorbed/emitted (of the matter) is also unique. Frequencies of maximum absorption result in absorption peaks (or maxima) in the

absorption band. It is important to note that, the *intensity* of a light beam (which is closely related to the average energy transport) is independent of its frequency, but the *energy* of *photons* depends on its frequency. In order words, if two beams of light have the same intensity but different frequencies, the one with higher frequency produces fewer photons than the other. The absorption law relates the intensity of incoming light (I_0) and of outgoing light (I_1) as it passes through a sample.

$$A = \log(\frac{I_0}{I_1}) \tag{2-3}$$

With A the absorbance of the sample

The Beer–Lambert–Bouguer Law further describes the relationship between the absorptivity and concentration of absorbing species if the path length and wavelength of the radiation beam are kept unchanged:

$$\frac{I_0}{I_1} = e^{-abc} \tag{2-4}$$

a: absorptivity, (ε: molar absorptivity, L/mol*cm)
b: path length of the sample, cm
c: concentration of absorbing species, mol/L

2.2.2 Reaction Monitoring with Fluorescent Spectroscopy

2.2.2.1 Overview of Fluorescence Spectroscopy

Fluorescence of molecule is their emission of light when they absorb *visible* or *ultraviolet radiation* in the range of 180 nm – 800 nm. Molecules via the absorption of radiation are transitioned from the ground state to a vibrational excited electronic state. The emission of photons when molecules return to the ground state is instantaneous after 1-20 ns of the excitation. Due to the non-radiation loss of vibrational energy, the emitted photons have lower energy (longer wavelengths) than the excited photons. Fluorescence can occur in gas, liquid or solid chemical compounds and a molecule with fluorescence capability is called a *fluorophore* [32].

Relationship Between Fluorescence Intensity and Concentration

Fluorescence intensity (F) can be defined as:

$$F = (I_0 - I_1)\phi \tag{2-5}$$

I_0 and I_1 are the intensity of the incoming light and outgoing light respectively
$\phi = \frac{No.of\ quanta\ emitted}{No.of\ quanta\ absorbed}$, is the quantum efficiency

From the Beer's law, substitute for I_1 into equation (2-5):

$$F = I_0(1 - e^{-abc})\phi \tag{2-6}$$

The fluorescence intensity depends on the analyte concentration, quantum efficiency, intensity of the exciting radiation and the absorptivity of the analyte.

When abc is sufficiently small, (2-6) becomes $F = I_0 abc\phi$. The fluorescence intensity is linear to the analyte concentration, from 10^{-9} – 10^{-4} M.

The shape of the emission (fluorescence) spectrum and wavelength of the fluorescence maximum (peak) do not depend on the excitation wavelength. It means that for any wavelength that the compound can absorb, the same fluorescence spectrum is obtained. But the fluorescence intensity depends on the excitation wavelength and its intensity [31]. Therefore, it is the best to select an excitation wavelength that provides good intense fluorescence but also avoids decomposing the compound.

Information from the wavelength, intensity of the obtained fluorescent can be used, for instance, to determine the detection limit of an optical system, to investigate the mixing quality of a micro mixer, to study kinetic parameters of a reaction. Fluorometry is applied in the analysis of clinical and environmental samples, pharmaceuticals, and natural products. There are fluorescence methods for steroids, lipids, proteins, amino acids, enzymes, drugs, inorganic electrolytes, chlorophylls, natural and synthetic pigments, vitamins, and many other types of analytes [31]. Fluorescent is also applied in most microtiter plate and continuous flow biochemical assays that are based on fluorescent labels [33].

Some advantages of using fluorescence: high sensitivity due to a zero background signal (the receiving path is normally orthogonal to the emitting path); high specificity because not all molecules fluoresce and two wavelengths (excitement and emission) are used; and large linear dynamic range (6-7 order of magnitude) [31].

However, the fluorescent spectrum is subjected to interference possibly from other fluorescent compounds, other emission or scattering processes; the reversal of fluorescent or self-quenching at high concentration; photochemical decomposition or photochemical reaction due to intense light sources. In addition, changes in pH, temperature, and viscosity may cause changes in fluorescence intensity [31]. In addition, the fluorescent spectroscopy is material-specific and in most cases requires an addition of reporter molecules, which might sometimes cause extra time for labeling reaction and multiple derivatization products [34].

2.2.2.2 Integration Schemes and Applications

Integration schemes: Fluorescent measurement is a widely used method in chemical analysis for its characteristics of extremely high sensitivity with a limit of detection (LOD) in some cases in the range of parts per billion (10^{-15} - 10^{-4} mole/lit), which is 10 to 1,000 times better than that of absorption spectroscopy [35]. In addition, a large range of linear relationship between analyte concentration and fluorescent intensity is another advantage being exploited for in most applications. Moreover, fluorescent emission lifetime and excitation spectrum are also useful information for the analytical purpose [36].

A common setup for fluorescent detection in micro reactor includes basically a source of radiation (laser, LEDs, lamps), transmission fibers, fluorescent substances, and a fluorometer. Emitted light is in a range of wavelength in visible region with different intensity and is detected by the fluorometer. Some integration schemes for micro reactor to fluorescent spectroscopy can be seen as in the following.

In a trivial arrangement as in Figure 2-3 [37], an exciting source is coupled to an inverted microscope. Fluorescence is filtered before reaching to the CCD camera while the reflected light from the exciting

source is blocked. This detection scheme, however, used large size optical elements so that other integration schemes have been proposed to miniaturize the system and to improve the detection limit. Optical fibers, waveguides, and micro lenses have been integrated into chips. The use of planar waveguides, in addition, can enable multipoint detection by beam splitting.

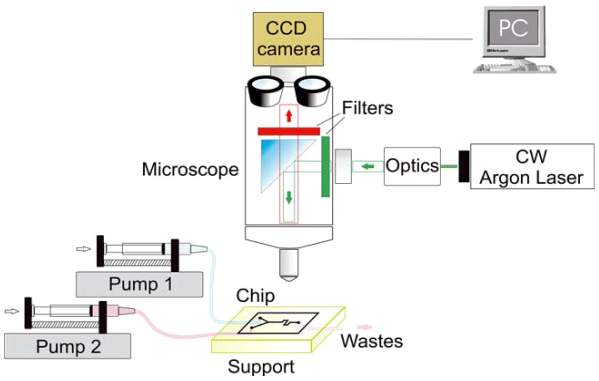

Figure 2-3: Integration scheme using an inverted microscope [37]

In Figure 2-4, a simple integration of an on-chip optical fiber was performed by SYLWESTER ET AL. [38]. To increase the intensity of the excitation light, a chip with a V-groove engraved on was used for positioning the optical fiber, whose tip contacts with fluid in the micro channel. The second fiber which was perpendicular to the first fiber collected the emitted fluorescence to the spectrofluorimeter. ROULET ET AL. created a chip with micro lenses on both of its sides so that excitation beam could be focused on the micro channel and emitted fluorescence could be focused on the detection device, which is placed nearby (Figure 2-5) [39]. MOGENSEN ET AL. fabricated a chip with planar waveguides of SU8 material and fiber-to-waveguide couplers that ensured self-alignment between the optics and the fluidics (Figure 2-6) [40]. The system is applied to characterizing coupling loss, sensitivity and limit of detection for measurements of the dye bromothymol blue.

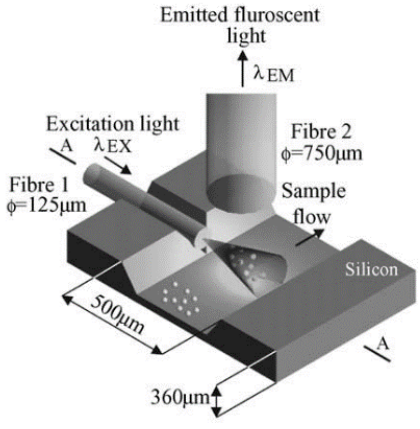

Figure 2-4: Schematic view of spectrofluorimetric microdetector [38]

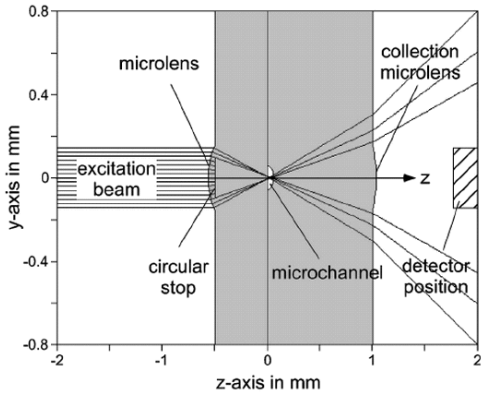

Figure 2-5: Microlens ewide (focal length 550 μm) [39]

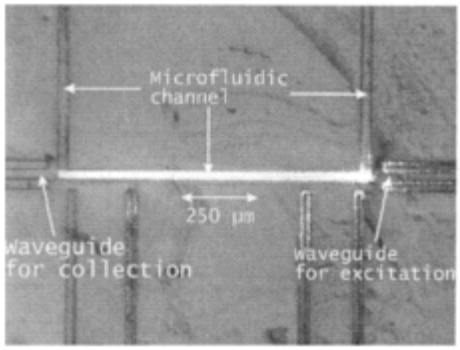

Figure 2-6: Light coupled along a microfluidic channel segment [40]

Applications: The application of fluorescence is often based on the following forms: (a) Some analytes are themselves fluorescent so that they can be detected directly. Cy5™ (Amersham Life Science Ltd.) solution was used to test the detection limit of micro lenses-integrated-on chip and the result found to be 20 nM [39]. HOFFMANN ET AL. employed Rhodamine B to investigate mixing quality and specific contact area between species in the T-shaped micromixers [41]. Not all chemicals are fluorescent, however, they can be detected indirectly. (b) A reaction of two nonfluorescent compounds can produce a fluorescent compound. ISMAGILOV ET AL. used Fluo-3 (pentaammonium salt), which is essentially a nonfluorescent compound, to combine with calcium ion of $CaCl_2$ to form a strongly fluorescent complex [42]. This combination was applied to examine the transverse broadening of two chemical solutions in laminar flow in micro channels. KERBY ET AL. used alkaline phosphatase (AP) enzyme as an immobilized substrate for dephosphorylation of 6,8-difluoro-4-methylumbelliferyl to fluorescent 6,8-difluoro-4-methylum-belliferone [43]. The reaction was applied for measuring kinetic properties of AP. (c) Nonfluorescent compounds bind with fluorescent dyes to form fluorescent products. LU used a derivatized 4-fulfonic calix [6] arene binding with UO_2^{2+} to detect uranium (VI) with the limit of detection of 4.4 μM for UO_2^{2+} [44]. Moreover, effects of chemical environment to fluorescence of a substance were also exploited. HOFFMANN ET AL. took advantage of the dependence of fluorescent intensity on *pH* [41]. Disodium

fluorescein, which is active above $pH = 4$ and excited by Arion-laser at wavelength 488 nm, was applied for monitoring product concentration of the neutralization reaction between NaOH and HCl so that mixing and reaction along the micro channel could be studied.

2.2.3 Reaction Monitoring with UV-VIS Spectroscopy

2.2.3.1 Overview of UV-VIS Spectroscopy

Ultraviolet and visible light are light at wavelength ranging from 200 nm – 400 nm and 400 nm – 800 nm respectively. The UV-VIS absorption spectroscopy is an analytical technique based on the absorption capability of chemical species with electromagnetic radiation in the UV-VIS range. Via the absorption, an electron will be excited from an occupied molecular orbital to an unoccupied (or singularity occupied) molecular orbital [45]. *Chromophores* is a term used to indicate molecular groups that can absorb UV-VIS light. There are multiple *vibrational* and *rotational energy levels* in each electronic energy level which constitutes to the broadband of the UV-VIS absorption. In more details, if there are initially a million molecules mostly in the ground state, they may be in various vibrational states after excitation [31].

In order to analyze a sample, each wavelength in the UV/VIS spectrum is sequentially directed to the sample for absorption measurement. The wavelength of absorption peaks and their intensity are most interested in identifying species and their concentration in the sample. And the fundamental relationship between the absorptivity and concentration of an analyte is described by the Beer's law, which is represented in the previous section of this chapter.

Bonding electrons are excited as a result of light absorption. Therefore, the bonding types in molecules can be correlated to the wavelengths of the absorption peaks. In order words, functional groups in a molecule can be identified via molecular absorption spectroscopy [35]. In addition to qualitative analysis, UV-VIS absorption spectroscopy can be employed to evaluate dissolution of active pharmaceutical ingredients from formulations, compounds stability, reaction kinetics, equilibria, metal or ligand binding and quantitative analysis [45]. It can be found in research, clinical analysis, industrial analysis, environmental analysis, and many other applications. Some typical applications of UV absorption spectroscopy include the determination of the concentration of phenol, nonionic surfactants, sulfate, sulfide, phosphates, fluoride, nitrate, a variety of metal ions, and other chemicals in drinking water in environmental testing; natural products, such as steroids or chlorophyll; dyestuff materials; and vitamins, proteins, DNA, and enzymes in biochemistry [31]. LOD in UV-VIS depends on the molar absorptivity of the analyte being measured and can be in micro molar range [45]. A limitation for using UV/VIS is its spectrum does not contain as much information as that of the IR and Raman spectroscopy [46]. In addition, the linear working range for spectrophotometry, one to two orders of magnitude, is smaller than that of fluorescence [31].

2.2.3.2 Integration Schemes and Applications

Integration schemes: The integration of UV/VIS spectroscopy to micro reactors has been done in different schemes. LU ET AL. aligned a microscope above the micro channel to create an optical cell for detection of colchicine and four alkaloids [47]. However, this arrangement often faces with difficult and complex optical alignment process. FERSTL ET AL. used flow-through cells that connected externally to the output of a micro reactor for studying toluene nitration [46]. BARZIN ET AL. also monitored *pH* in a micro mixer indirectly by using a Z-shaped micro-flow-through cell as shown in Figure 2-7 [48]. YUE ET AL. employed a cross-type flow-through cell for online process analysis of gold nanoparticle synthesis in segmented flow [49]. The use of flow-through cells for online analysis helps reduce time for analysis compared to the offline analysis method. It also simplifies the fabrication process for micro reactors compared to the in-situ integration method that it will be considered in the next paragraphs. These advantages make it commercially available. As a general concern in spectroscopic techniques, materials for micro reactor chips are considered an important factor not only in detection limits but also in aspects of auto fluorescence, price, and ease of fabrication. Improvement in optical condition is also important. These concerns can be achieved by using improved optics or integrating waveguides on chips for a better light transmission. PARK ET AL. fabricated an Integrated MicroAmmonia Analysis System (IMAAS) as shown in Figure 2-8 [50]. The system included a micro reactor and two in-plane optical fibers acting as a source and a detector for ammonia analysis of reaction rate and reaction concentration at different temperatures. The micro detection cell with SiO_2 windows of 2 μm thickness lied between the optical source and detector. The alignment of optical fibers was precise by using new techniques in micro channel guiding for optical fiber (silicon deep RIE process based on Berthelot reaction). PETERSEN ET AL. integrated waveguides and a 750 μm detection cell in a microfluidic device to evaluate the absorbance sensitivity by measuring the absorbance at 254 nm of caffeine, paracetamol, ketoprofen and ascorbic acid [51]. PRABHAKAR ET AL. fabricated a microchip incorporated with U-bend waveguides along with micro channels for evanescent field absorption [52]. This integration increased length of detection cell and reduced the problem of light scattering. The limit of detection for methylene blue was found to be 10 μM. An Automatic Continuous Online Monitoring of Polymerization Reactions (ACOMP) system is available in the commercial market. The system employs different detectors in series (static light scattering, UV-Vis spectroscopy, differential refractometry, viscometer) to monitor polymerization reactions by withdrawing a steady stream of product from the reactor and diluting it [53]. The system is highly automated that it is controlled by the LABVIEW software interface.

Applications: Applications of UV/VIS spectroscopy in reaction monitoring are usually through measuring solution concentration of a reaction evolution. LU ET AL. monitored pinacol formation in a photochemical reaction of benzophenone in isopropanol [54]. Two detection schemes were presented: (1) coupling with a separate chip for detection, and (2) integrating reaction and detection functions on the chip. UV absorption of the reaction mixture was measured at different flow rates and compared with the measurement of standard solution to determine the conversion. The result is in agreement with the analysis using high performance liquid chromatography (HPLC). FERSTL ET AL. compared the analysis precision of three spectroscopic methods: Raman, near infrared and visible spectroscopy by monitoring

the toluene nitration reaction with pure nitric acid, which showed the highest precision of Raman spectroscopy [46]. In the second experiment of toluene nitration reaction using mixed acids, equivalent precision was obtained for three methods. WAGNER ET AL. reported an application of in situ UV/VIS spectroscopy for online monitoring and kinetic measurements of gold and silver nanoparticles production by monitoring reduction of metal salt solutions with borohydride [55]. EDEL ET AL. used UV-VIS spectrometer to study CdS nanoparticles synthesis via its absorption spectrum [56].

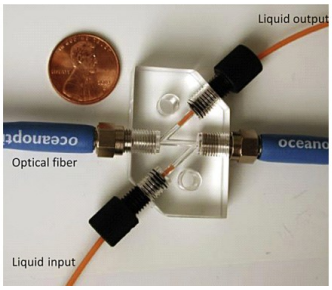

Figure 2-7: Z-shaped micro-flow thorough cell with 50 µl inner volume [49]

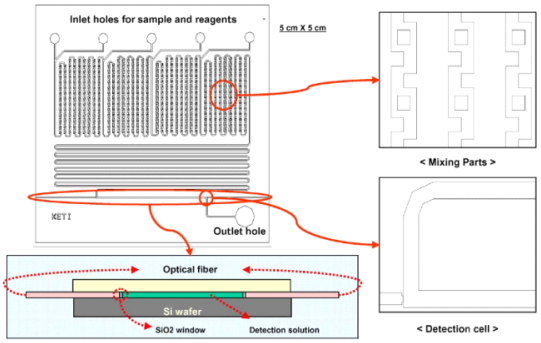

Figure 2-8: Schematic top view of the IMAAS [50]

2.2.4 Reaction Monitoring with Infrared Spectroscopy

2.2.4.1 Overview of IR Spectroscopy

Infrared spectroscopy is an analytical technique employing the infrared spectrum for identification and quantitative measurement of a myriad of molecular species. The infrared spectrum is further divided into three sub-regions: near-IR (0.75-2.5 µm), mid-IR (2.5-20 µm), and far-IR (20-200 µm) in which mid-infrared spectroscopy (MIR) is the most widely used technique. The working principle of this technique is based on molecular absorption that results in vibration of their chemical bond: stretching and bending (with IR excitation wavelength from 1 – 100 µm) and rotation (with IR excitation wavelength from >100 µm) [57]. And, the vibrational frequency of a chemical bond is intrinsic to the chemical bond of interest [58]. In order for a molecule to absorb IR radiation, (1) the molecule must have covalence bonds; (2) the natural vibrational frequency of the molecule must be equal to the incident radiation frequency; (3) the radiation energy must equal the energy difference between the vibrational states involved; (4) the dipole

moment of the molecule must be changed by the vibration; (5) The amount of radiation absorbed is proportional to the square of the rate of change of the dipole during the vibration; (6) The energy difference between the vibrational energy levels is modified by coupling to rotational energy levels and coupling between vibrations [31].

The frequency of stretching vibration of two atoms in a molecule can be estimated as in (2-7), with f measures the strength of the chemical bond of two atoms. f and μ are constant for a given set of atoms and chemical bonds. Therefore, the radiation absorbed by the system has the same frequency and is constant for a given set of atoms and chemical bonds [31].

$$\bar{v} = \frac{1}{2\pi c}\sqrt{\frac{f}{\mu}} \tag{2-7}$$

$\bar{v}$: the wavenumber of the absorption maximum (cm^{-1})
c: the speed of light (cm/s)
f: force constant of the bond (dyn/cm)
μ: the reduced mass (g)

$$\mu = \frac{M_A M_B}{M_A + M_B}$$

M_A, M_B: mass of atom A, B respectively in molecular AB

In MIR, absorption, reflectance, and emission could be measured and the spectrum is often divided into regions: a) Group frequency region is often useful for initial guess about the presence of organic functional groups; b) “Fingerprint” region is often helpful for compound identification by matching with spectrums of known pure compounds [35]. The detection limit can be at micro mole [59][60].

Infrared spectroscopy is sensitive to chemical composition and molecule architecture. Infrared spectrum carries high information content; has large a range of application from small soluble proteins to large membrane proteins, high time resolution (down to 1 μs), short measuring time, low amount of sample required (typically 10-100 μg) and relatively low costs of the instruments [57]. Although there is a strong mid-IR absorption of many solvents (particularly water) that limits the quality of analyte solution [61], this technique is one of the most important analytical techniques to scientists today [57]. No solvent is transparent to the entire mid-IR region so that the analyst must choose a solvent that is transparent to the region of interest.

IR spectroscopy can be applied to identify organic molecules, inorganic molecules and investigate dynamic processes (i.e. chemical reactions, phase transitions, sedimentations) [62]. In the field of polymer, IR spectroscopy can be used to identify the composition of polymers, monitor polymerization processes, characterize polymer structure, examine polymer surfaces and investigate polymer degradation processes. It is also applied to biological system for study of lipids, proteins, peptides, bio membranes, nucleic acids, animal tissues, diseased tissues, microbial cells, plants and clinical samples; to pharmaceutical applications such as evaluation of raw materials used in production, the active ingredients and the excipient; to food science such as the study of fats, oils, milk, wine and other alcoholic beverages, or quantitative measurement of water, proteins, fats and carbohydrates; to agriculture such as qualitative

and quantitative study major constituents of grains (water, protein, oil, fiber, minerals and carbohydrates); to pulp/paper industries, paint industry, and environmental applications such as measurement of trace gases, atmospheric compositions, investigation of solid pollutants [63].

2.2.4.2 Integration Schemes and Applications

Integration schemes: For integration of micro reactors to IR detection devices, a straightforward scheme is to place the micro reactor in the sample compartment of the IR spectrometer. Pumps placed outside to supply solutions and IR light passing through the reactor from the bench is recorded for the transmission spectrum [64]. KEOSCHKERJAN ET AL. arranged the FTIR spectrometer as a unit in the modular micro reaction system to monitor the chemical process of diethyl-urea dissolved in dichloroethane as in Figure 2-9 [65]. The micro channels were deposited with gold so that MIR and NIR reflection spectroscopy could be performed.

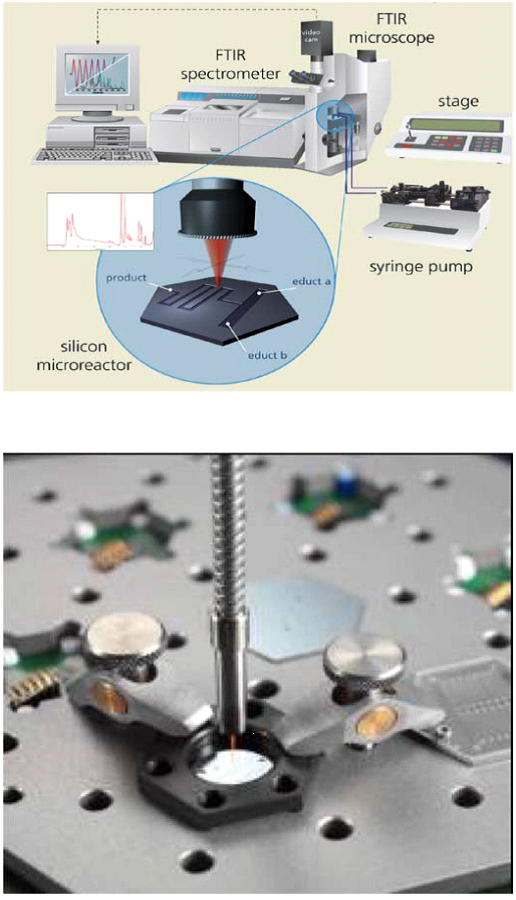

Figure 2-9: Schematic of the IR-measurement set-up: (top) measurement in the MIR-range using a high-resolution FTIR-microscope; and (bottom) measurements in the NIR-range using a NIR-fibre optic probe [65]

PRIM ET AL. connected a microfluidic system to a flow-through cell with IR-transparent windows made of CaF_2 for online monitoring the conformation of protein under the *pH* variation [66]. The use of flow-through cell releases the difficulty in fabricating micro reactors with materials, which are transparent at

the IR wavelength. HINSMANN ET AL. used a Time-Resolved Fourier Transform Infrared Spectroscopy (TR-FTIR) device to measure the spectrum of reactants before and during the reaction in a flow-through cell at the stopped-flow mode [67]. The reaction of acetic acid and NaOH, formaldehyde and sodium bisulfite, and methyl monochloracetate and NaOH were performed as a demonstration.

ATR FTIR spectroscopy method is capable of decreasing the problem of strong absorbance solvents to MIR spectrum [61]. CARTER ET AL. used a ATR flow cell which was directly connected to the FT-IR device in one end and indirectly connected to the output of the reaction coil at the other end via the quenching and cleaning up column (Figure 2-10) [68]. The system performed online monitoring of reagent/analyte consumption, product formation and short-lived intermediates such as fluorination reaction; oxazole formation from isocyanide and acid chloride; or hydrogenation of BDA-derivative 11.

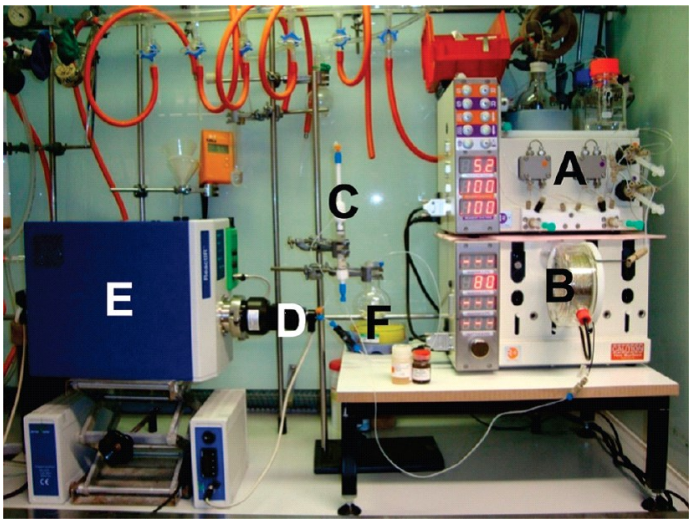

Figure 2-10: Exemplary setup for monitoring the product formation within a continuous flow processing using the Vapourtec R2+/R4 flow chemistry system. a) R2+double pump unit, b) R4 unit with CFC reactor connected, c) Omnifit column filled with polymer supported scavenger, d) MT IR flow cell, e) ReactIR 45m, f) flask containing product solution [68]

Applications: GREENER ET AL. integrated a micro reactor to an ATR FTIR device such that solution inside the micro reactor contacts directly to the surface of the ATR crystal [69]. The integration was verified by detecting PNIPAm and PEG polymer at a concentration down to 5 and 10 µmole respectively. Further experiments were also performed to monitor the concentration of PNIPAm and PEG mixture by varying the mixture ratio and to verify that the effect of flow rates on the absorbance was unchanged.

FLOYD ET AL. presented an integrated micro chemical system with micro mixing, reaction channel, IR detection region, and temperature control to monitor and study the kinetics of liquid phase reactions [64]. The mixing was evaluated by an acid-base reaction. The rate constants were calculated via monitoring the alkaline hydrolysis of methyl formate. KEYBL ET AL. used a ATR-FTIR device in a micro reactor system to determine homogeneous catalyst kinetic parameters of high-pressure gas-liquid continuous flow [70]. A reaction kinetic determination of rhodium catalyst in the hydroformylation reaction was performed as a demonstration of the system usage.

Other applications of IR spectroscopy for reaction monitoring can be mentioned such as HERZIG-MARX ET AL. monitored the kinetics of ethyl acetate hydrolysis over a range of HCl concentration and the amidization of surface-tethered amine groups [61]. BRODMANN ET AL. used a micro scale ReactIR flow cell that attached to the micro reactor as an inline analytical tool for monitoring the Grignard formation [71]. RUEPING ET AL. also used an inline ReactIR flow cell to monitor the asymmetric organo catalytic hydrogenation of benzoxazines, quinolines, quinoxalines and 3H-indoles for its capability of fast and convenient optimization of the reaction parameters [72].

2.2.5 Reaction Monitoring with Raman Spectroscopy

2.2.5.1 Overview of Raman Spectroscopy

Raman spectroscopy is an analytical technique based on the inelastic collision of molecules from monochromatic light. The result of this inelastic collision is a shift in wavelength of the scattered light to lower energy (Stoke Raman scattering) and to higher energy (anti-Stock Raman scattering). The excitation source is normally in the UV/VIS or near-IR region. The Raman spectrum can be treated as the finger print of a compound, similar to other vibrational techniques such as IR absorption, vibrational resonant sum frequency generation, or high resolution electron energy loss spectroscopy [73]. Raman spectroscopy utilizes scattered light to gain knowledge about molecular vibrations which can provide information regarding the structure, symmetry, electronic environment and bonding of the molecule, thus permits the quantitative and qualitative analysis of the individual compounds [74]. There are two major technologies for collecting the Raman spectra, Dispersive Raman spectroscopy and Fourier transform Raman spectroscopy, and other different advanced Raman techniques include: surface-enhanced Raman spectroscopy (SERS), confocal Raman microscopy, coherent anti-Stokes Raman scattering (CARS), resonance Raman spectroscopy (RRS), tip-enhanced Raman spectroscopy (TERS), Raman sensing. Those techniques help improve the limit of detection (up to 10^{-18} mol/l [73]), efficiency, cost and size of the instrument.

Some applications of this technology can be seen in forensic science such as analysis of fibers, explosives, drugs, paints, inorganic, lipsticks; in biology such as analysis of hemoglobin-oxygen saturation in living tissue, structural information about the change in proteins, water and lipids of muscle food, analysis of toxic agents, drugs, diseases, cell death and differentiation; in diagnostics such as examination and characterization of the outermost layer of human skin, endoscopic imaging and quantization of biochemical constituents, analysis of blood, human epidermal keratinocytes; in material science such as structural characterization and investigation of semiconductor properties, measurement of stress, crystal lattice disorder, phase-separation of supersaturated solid solutions and homogeneity of materials, online monitoring of NO_2^-/NO_3^- in waste water; in pharmaceuticals such as characterization of drug formulations, elucidation of kinetic processes in drug delivery; in nanotechnology such as probing and characterization of nanomaterials like nanosensor, nanotube and nanowire [75]. Raman spectroscopy has been found coupled with many hyphenated analytical techniques like HPLC, micro chromatography,

scanning tunneling microscopy atomic force microscopy, etc. and given a possibility for useful analysis at trace level studies.

Raman spectroscopy offers a number of advantages over other spectroscopic techniques for chemical analysis and has been used effectively for process analysis monitoring in recent years [76]. Organic species without UV/VIS chromophores can be analyzed by Raman spectroscopy. Unlike IR method, Raman spectroscopy is almost unabsorbed by water, therefore, it is suited for analyzing aqueous based reaction media [77]. The technique can achieve multi-component detection in a solution as each component would exhibit its own fingerprint bands in the acquired Raman spectrum. Therefore, it is possible to achieve simultaneous monitoring of multiple analyte components in a microfluidic channel [78]. The technique is also independent of the excitation wavelength and conveniently works with glass and quart cell. Weak scattering signal that may make it overwhelmed by a strong spectral background and fluorescence interference from analyte or solution matrices are two major disadvantages of this method [78] [79]. However, using longer wavelength sources in the near-IR region can help suppress unwanted fluorescence background signal [80]. In relative to UV/VIS methods, the sensitivity of Raman spectroscopy is poor and hence either high concentrations, long data acquisition times or the use of specialist Raman techniques such as surface or resonance enhancement techniques are required [77].

2.2.5.2 Integration Schemes and Applications

Integration schemes: Raman spectroscopy instruments have been integrated to micro reactors in different schemes for qualitative and quantitative analysis. URAKAWA ET AL. placed the Raman probe directly in front of the micro reactor (Figure 2-11) to monitor phase behavior and reaction performance of heterogeneous catalytic reaction, cyclohexene hydrogenation in dense carbon dioxide [81]. FERSTL ET AL. monitored a toluene nitration process via a small flow-through Raman cell [46]. FLETCHER ET AL. used a Raman microscope spectrometer for monitoring the synthesis of ethyl acetate from ethanol and acetic acid [77] are examples of straightforward integration schemes with conventional instrumentations.

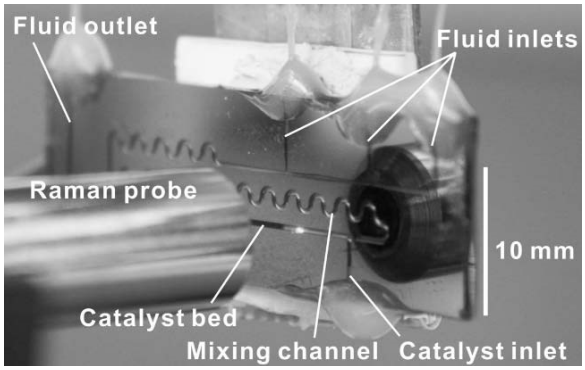

Figure 2-11: Photograph of on-chip Raman analysis [81]

ASHOK ET AL. created a Raman spectroscopic detection scheme called Waveguide Confined Raman Spectroscopy (WCRS) by embedding fibers on the PDMS chip for exciting and collecting Raman spectra

(Figure 2-12) [78]. The limit of detection for this scheme is 80 mM for urea detection. The reaction of acetic anhydride and ethanol was monitored to demonstrate the system capability to study the reaction dynamics. The portability of this scheme makes it possible to be integrated with different Raman spectroscopy techniques such as SERS or resonance Raman spectroscopy.

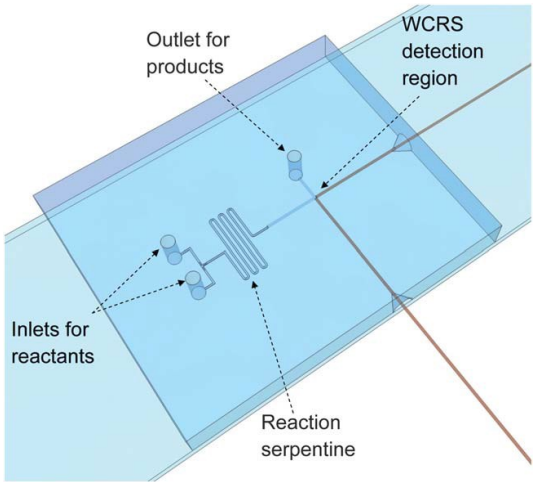

Figure 2-12: Schematic of a micro reactor integrated with waveguide confined Raman spectroscopy [78]

Applications: Microfluidic Raman spectroscopy (MRS) has been used for a variety of chemical and biological applications ranging from basic analyte detection to reaction monitoring in a micro reactor [78]. KIM ET AL. used the surface-enhanced Raman scattering to detect Turnip yellow mosaic virus (TYMV) in Chinese cabbage plants [82]. FLETCHER ET AL. used an inverted Raman microscopic spectrometer to profile the micro channel network, to describe spacious image for the mixing of ethanol and acetic acid, and to monitor the concentration of reagents and product of this catalytic reaction [77]. WILSON ET AL. demonstrated the improvement in detection limit of both surface-enhanced Raman scattering (SERS) and surface-enhanced resonance Raman scattering (SERRS) techniques [83]. The system is applied in R6G detection (with detection limit at 50 fM) and identification of scytonemin (with a limit of detection at 10 pM). LISZKA ET AL. designed a microfluidic chip coupled with a confocal Raman imaging spectrometer. This specific-designed system is tested by imaging biological cells, that were transported by flow into the microfluidic chip [84].

2.2.6 Reaction Monitoring with NMR Spectroscopy

2.2.6.1 Overview of NMR Spectroscopy

NMR spectroscopy is an analytical technique based on measuring the interaction between an oscillating radio frequency (RF) radiation and a collection of nuclei (with magnetic dipoles), which are immersed in a strong external magnetic field [85]. It is one of the most powerful techniques available for studying the structure of molecules [86]. This method is applicable for both qualitative and quantitative analyses, particularly of organic compounds [87]. The fundamental to NMR is the ***Larmor equation***, which can be derived as follows.

Let E be the energy of a nucleus at a certain nuclear energy level in a magnetic field B_0

$$E = -m\left(\frac{\mu}{I}\frac{h}{2\pi}\right)B_0 = -m(\gamma\frac{h}{2\pi})B_0 \tag{2-8}$$

With m is the *magnetic quantum number*; μ is the *nuclear magnetic spin*; B_0 is the *applied magnetic field*; I is the *spin angular momentum*; γ is the *magnetogyric ratio*; and h is *Plank's constant*.

The energy required for transition between two quantum levels of a nucleus should be equal to the energy absorbed by the nucleus from the RF radiation, $\Delta E=hv$.

For the case of *1H* nucleus ($I=1/2$), this equality is expressed as:

$$\Delta E = hv = -\left(+\frac{1}{2}\left(\frac{\mu}{I}\frac{h}{2\pi}\right)B_0\right) - \left(-\frac{1}{2}\left(\frac{\mu}{I}\frac{h}{2\pi}\right)B_0\right)$$

$$\Delta E = hv = \left(\frac{\mu}{I}\frac{h}{2\pi}\right)B_0 = \left(\gamma\frac{h}{2\pi}\right)B_0$$

Therefore, the frequency v (in *Hz*) that can be absorbed from a transition of ΔE is:

$$v = \gamma\frac{1}{2\pi}B_0$$

Or

$$\omega = 2\pi v = \gamma B_0 \tag{2-9}$$

With ω is the frequency in (*rad/s*)

This (2-9) is the *Larmor equation*. For a given nucleus there is a direct relationship between the frequency v of RF radiation absorbed by that nucleus and the applied magnetic field B_0 [31]. The equation can be utilized in the way that B_0 is kept constant and the frequency of RF can be varied to measure the absorption. Or vice versa, the RF is kept constant and varies B_0.

However, the continuous wave (CW) or field sweep NMR (that varies either the frequency of RF radiation or magnetic field B_0) often requires much time and gives limited resolution that all modern NMR spectrometers are Fourier Transform instruments (FT-NMR) [31].

In FT-NMR, the strong magnetic field (B_0) helps align the random-oriented nuclei which results in a net magnetic moment (M) from the sample. This magnetization behaves as a magnet so that it rotates when there applies a current to a surrounding coil. The RF pulse (on the order of 10 μs and a few second interval between pulses) is applied at the right angle to B_0. This generates the second magnetic field B_1 perpendicular to B_0 and causes this magnetization moment misaligned from B_0. When the RF is discontinued, M begins rotating at an angle to B_0. This induces a current at radio frequencies on the detector coil placed around the sample. The larger the magnetic field B_0, the stronger the signal can be generated [88]. The energy involved in RF radiation is too small to vibrate, rotate, or electronically excite molecules as UV/VIS or IR radiation. However, it is great enough to affect the nuclear spin of atoms in molecules [31].

Some applications of NMR include: to study chemical equilibria, reaction kinetics, the motion of molecules, and intermolecular interactions. NMR instruments and experimental methods allow the determination of the 3D structure of proteins (as large as 900,000 Da) as well as studying solids such as polymers, 13C, 19F, 31P, 29Si, and other nuclei. NMR imaging techniques or magnetic resonance imaging (MRI) are wildly used in noninvasive diagnosis of cancer and other medical problems. NMR instruments coupled to liquid chromatographs and mass spectrometers for separation and characterization of unknowns are commercially available [31].

As other discussed techniques, NMR is a noninvasive method that it does not destroy samples. In addition, it is flexible that can be used to investigate various chemical and biological processes [89]. However, this technique can only be used to measure nuclei with magnetic moments. In addition, it may be less sensitivity than other spectroscopic methods, that it requires higher sample amount for analysis [88]. With modern instruments, the detection and identification of *ppm* concentrations of substances can be achieved and detection limits are approaching *ng* levels [31]. However, in real world, due to the purity problems, the practical lower limit for most structural elucidation by NMR is to be close to 500 ng. The high magnetic field working environment has potential to impact on human health and on electronics or computer controlled devices. In addition, its motion sensitivity may lead to signal distortions [88].

NMR has been hyphenated with LC, MS or HPLC to form different techniques such as LC-MS-NMR, LC-NMR that can increase sensitivity or the capability of solving structural problems of mixtures of unknown compounds. Other chromatographic techniques coupled online to NMR include size-exclusion chromatography (SEC)-NMR, solid-phase extraction (SPE)-NMR, capillary electrophoresis (CE)-NMR, and capillary-based HPLC (capLC)-NMR [86].

2.2.6.2 Integration Schemes and Applications

Integration schemes: For integration of the micro reactor to the NMR instrument, the direct scheme is to fit the micro reactor into a conventional NMR flow probe. TAKAHASHI ET AL. fabricated a MIcro Channeled Cell for Synthesis monitoring (MICCS) for real-time monitoring of the Wittig reaction and Grignard reaction [90]. The MICCS was placed into a 5 mm NMR sample tube as in Figure 2-13. By similar integration, NAKAKOSHI ET AL. was able to detect unstable intermediates in the radical addition reaction of oxime ether 1 mediated by triethylborane (Et(3)B) [91]. SANS ET AL. developed a self-optimizing synthetic organic reactor system based on LABVIEW control [92]. A coil reactor was connected to a flow-cell which was based on a 5 mm NMR tube. The system was tested by monitor, kinetic study and structural characterization of the imine (N-bezylidenbenzylamine) formation. Furthermore, by using NMR instrument as a sensor for feedback data, the author demonstrated the possibilities of reaction self-optimization with the catalytic synthesis of an imine using aniline as the catalyst. The low sensitivity of NMR especially when sample volume is reduced has motivated researchers to look for better solutions.

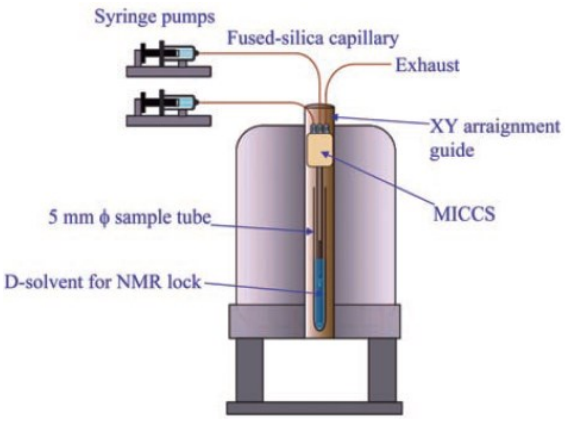

Figure 2-13: Schematic diagram of MICCS-NMR [90]

There are many solutions that have been implemented such as higher magnetic field strengths, cryogenic probes, and hyperpolarization techniques and micro coil probes [93]. Micro coil is the more concerned method to reduce sample volume and to increase the measurement sensitivity. The findings are that the smaller the diameter of the detector coil is, the more efficient the solenoid measures the NMR signal [94]. The integration could be simply to wrap a solenoid RF micro coil around an NMR flow cell which is connected to a micro reactor output [95]; or a micro solenoid wound around a capillary [96]; or to fabricate a planar on-chip micro coil [97] in which the micro channel passes through a wire bonded micro coil as in Figure 2-14 or the design of microstriplines that intrinsically improves sensitivity to solenoid and planar coils [98]; or the use of micro slot probes that show its capability to obtain NMR spectra of sample quantity in 100 pmol range [99]. The limitation for a fixed fluidic infrastructure to accommodate the sample of those integrations has led to the development of the contactless microfluidic chip. In this configuration, the planar micro coils are inductively coupled to the NMR probe assembly [100]. A wider and deeper look on this integration can be found in the report of Fratila and Velders [93].

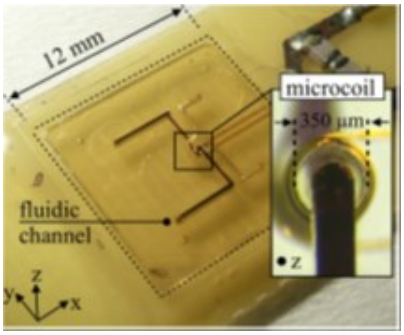

Figure 2-14: The NMR microchip with a fluidic channel passing through a wire bonded micro coil [97]

Applications: The integration of NMR to micro reactor can be used for different applications such as to monitor a chemical reaction, identification of intermediate and product, to study reaction conditions and kinetics. TAKAHASHI ET AL. with the MICCS as mentioned above performed real-time monitoring of the Wittig reaction and Grignard reaction [90]. The system is also useful for qualitative detection for microchip-based synthesis. KAKUTA ET AL. integrated a micro mixer and a micro coil NMR probe to

study the conformation of Ubiquitin in interaction with methanol solutions under low *pH* [95]. The change of Ubiquitin from native state to A-state was observed for evaluation of Ubiquitin transition kinetics. Reactions in timescale of *seconds* can be measured. CIOBANU ET AL. used a continuous-flow NMR spectroscopy with multiple micro receiver coil detection to demonstrate the possibility of NMR to study chemical kinetics of small amount of materials and reaction time (a few seconds). The reaction kinetics of D-xylose and borate reaction was investigated [101]. The three coils wrapped around the capillary at different positions after the mixer helped decrease the detection volume down to 31 nL and consequently the sample volume required. WENSINK ET AL. demonstrated the design, fabrication, and testing of a micro reactor chip with an integrated micro coil for NMR measurement [102]. The system was applied to monitor the reaction kinetics of benzaldehyde and aniline to form imine. He found that the kinetics of this reaction in the microchip was two times faster than that took place in the conventional NMR probe due to better mixing condition. GOMEZ ET AL. implemented a microliter-microwave reactor (flow cell < 2μL) hyphenated with a custom-made nanoliter NMR spectrometry (6 nL detection volume microfluidic with an integrated planar radio frequency transceiver micro coils). An online monitoring of the Diels-Alder cycloaddition of 2,5-dimethylfuran and dimelthylacetylene dicarboxylate was performed to demonstrate the capability of this microwave-NMR concept in rapid optimization of reaction conditions [103]. BART ET AL. presented a microfluidic high-resolution NMR flow probe based on a stripline detector chip for monitoring reaction kinetics at full NMR resolution [98]. An online monitoring of reactant and product of the toluene diisocyanate and pure ethanol was performed. Reaction time range of 30 min could be studied (depending on the flow rate). The system was further applied for real-time monitoring the acetylation of benzyl alcohol with acetyl chloride in the presence of N,N-diisopropylethylamine (DIPEA) and study of the human cerebrospinal fluid (CSF).

2.2.7 Reaction Monitoring with Mass Spectrometry

2.2.7.1 Overview of Mass Spectrometry

Mass spectrometry (MS) is an analytical technique for creating gas phase ions of molecules or atoms in a sample, followed by separating the ions according to their mass-to-charge ratio, m/z, and measuring the abundance of the created ions. It is one of the most powerful modern physical-chemical methods for identifying compounds, and for studying their structure and reactivity [104]; and is currently one of the most rapidly advancing fields of instrumental analysis [31]. MS offers advantages over conventional spectroscopic assays because it enables structural determination of reactants while preserving temporal resolution [31]. Due to its detection capability of short-lived reaction intermediates or labile metabolites, this tool is used for study of chemical reactions, chemical kinetics and biochemical dynamics [105] [33]. MS offers diverse information ranging from the structure of complex organic and biomolecules to quantitative determination at ppb concentrations of elements and molecules in samples. This is one of the cornerstone techniques used to elucidate the structure of biomolecules, especially high molecular weight proteins up to >10,000,000 Da [106]. MS is also widely applied for real-time monitoring of chemical/biochemical reactions for its ability of fast response, high sensitivity and multiple-components measurement [107].

There are some major steps in the MS technique: ionization of the sample; separation of ions based on their mass-to-charge ratio; and detection of the ions.

Ionization techniques as its name are responsible for converting analyte elements into molecular ions or atomic ions. There are techniques for molecular (usually applied for organic analyte) and atomic (usually applied for inorganic analyte) ionization. Some of the ionization techniques are listed in Table 2-3.

Table 2-3: Ionization techniques for molecules and atoms

Ionization Techniques	Principle	Category
Fast Atom Bombardment	A beam of fast moving neutral inert gas atoms is used to ionize large molecules.	Molecular ionization
Electron Ionization (EI)	Use an electron beam to bombard the sample to create molecular ions.	Molecular ionization
Chemical Ionization (CI)	Assisted reagent gas is ionized by an electron beam initially. This ionized gas then collides with analytes for ionization.	Molecular ionization
Electrospray ionization (ESI)	Sample flows through a metallic capillary, which is subjected to a strong electric field, and becomes dispersed into fine spray of electrically charged. Drying gas helps evaporate the solvent so that analyte ions can be desorbed from the droplets.	Molecular ionization
Atmospheric Pressure Chemical Ionization (APCI)	Sample is nebulized into fine droplets without an applied potential at the spray tip. The fine droplets are evaporated by heated sheath gas (heated from ceramic tubes). Corona discharge of electrons from a sharp-high voltage-metal needle ionizes air first (N_2^+, O_2^+, H_2O^+, NO^+), then reagent (solvent) and finally sample molecules (like the CI process).	Molecular ionization
Laser Desorption and Matrix-Assisted Laser Desorption Ionization (MALDI)	Dried sample is radiated by intense pulses of laser. The matrix absorbs most of the energy from the radiation and is heated rapidly. This causes the desolvation and ionization of analytes.	Molecular ionization
Glow Discharge Sources (GD) and Spark Sources	High potential imposing across the electrodes helps ionize the argon gas and create a plasma. Electrons and argon ions accelerated in high electric field sputter off atoms from the cathode material, which is the sample (analyte). The sample atoms collide with electrons or excited argon in the plasma to form ions; The method is more suitable for solid samples.	Atomic ionization
Inductively Coupled Plasma (ICP)	Radio Frequency (RF – 27 MHz or 40 MHz) in a load coil surrounding at end part of the quartz torch forms an intense electromagnetic field. This field helps cascade the creation and sustain of electrons, argon ions and finally the plasma (after the argon gas is sparked by high-voltage). A sample solution is introduced to the nebulizer, then to the plasma where the sample aerosols are dried, vaporized, atomized and ionized.	Atomic ionization

Mass analyzer is the heart of the system and is responsible for separating different ions according to their mass-to-charge ratio (*m/z*). A list of different mass analyzer techniques is represented in Table 2-4.

Table 2-4: Different mass analyzer techniques

Technique	Principle	Type
Magnetic and Electric Sector	An ion with electric charge (z) and velocity (v) of the ion moving through a magnetic field will be imposed an attractive force in proportion to the applied field (B) which curves the ion's route. Changing B allows ions of different m/z values passing through a fixed radius flight tube. Electric Sector that separates ions according to their kinetic energy acts as an energy filter; only ions with a very narrow kinetic energy distribution can pass through.	One ion is scanned at a time
Quadrupole	Separate ions in a time-variation electric field (the quadrupole field). The field is created by applying a constant DC voltage to a set of 4 metal rods and an oscillating radio frequency (RF) voltage as AC voltage. Ion separation can be achieved by varying the potentials of the DC and RF fields (keeping their ratio constant) and keep the oscillation frequency of the RF field constant.	One ion is scanned at a time
Time of Flight	Ion pulses are extracted at frequencies of 5 – 20 kHz and accelerated in voltages up to 30kV in a drift tube of 1 – 2m. If all ions have the same kinetic energy and the same charge, the ion separation is based on their mass. Lighter ions will reach to the detector sooner than heavier ions.	Simultaneous transmission of all ions
MS-MS or Tandem MS	Two or more stages of MS are connected which then combines with a process so that mass of interested ions can be changed.	Simultaneous transmission of all ions
Quadrupole Ion Trap (QIT)	Ions can be formed and confined in a trap by an electric field and/or magnetic field. Extraction of ions from the trap is enabled by changing the amplitude of the field.	Simultaneous transmission of all ions
Fourier Transform Ion-Cyclotron Resonance (FTICR)	Each m/z moves in a circular orbit at a specific cyclotron frequency in the presence of a high magnetic field. The RF pulse (a few milliseconds) containing a range of frequency is selected to excite the desired m/z range. The excitation causes the ions to move in larger circular orbits at unchanged frequencies. When the RF pulse is off, image currents are induced in the receiver plates as all ions exit. The application of Fourier transform mathematically converts output current containing all frequencies and magnitude information from all presenting ions into a mass spectrum.	Simultaneous transmission of all ions

And for detection of ions, there are the techniques of electron multiplier (EM), Faraday cup or array detectors.

Applications and properties:

MS has a wide range of applications and can be found from clinical chemists, pharmaceutical chemists to nuclear science because of its sensitivity and selectivity. The applications are as diverse as determination of molecular weight, molecular structure, reaction kinetics, dating of minerals, fossils and artifacts, fundamental studies of ion–molecule reactions, and quantitative analysis of elements and compounds at

sub-ppb concentrations, analysis of inorganic and organic solids, liquids and gases, study of subcellular structures [31]. MS is a key technique in the expanding field of proteomics. It is the choice for many environmental, industrial, clinical, and forensic analyses [104].

The MS techniques offer high sensitivity and the detection limit can reach nanomolar [108]. It is more suitable for short timescale measuring than other spectrometric techniques such as UV/VIS, IR, NMR that reactions in less than 1s can be screened [109]. MS can simultaneously detect multiple analytes. Due to its ability to induce chemical transformations, MS is a unique technique that can obtain information about the intrinsic properties of isolated ions and molecules, solvates, clusters, non-covalent complexes [104]. In addition, by combining with different ionization techniques, the number of analytes that can be potentially detected increases. Although MS is a destructive technique, it does not consume much samples. However, MS technique, especially in elemental analysis, requires hyphenating with other separation techniques (i.e. GC, LC, IC, CE) to be useful for structural analysis [110]. Another drawback of the technique is its requirement for sample preparation such as different columns and optimization of ionization conditions, which is less demanding in other nondestructive spectroscopic methods (i.e. NMR) [108].

2.2.7.2 Integration Schemes and Applications

Combinations of various types of micro reactors and mass spectrometers have been successfully realized. OOSTERBROEK ET AL. performed two simple designs, namely a monolithical interface and a modular approach, for direct coupling to an MS with electrospray ionization (ESI-MS) [111]. The connection was applied to study the reaction kinetics of β-cyclodextrine and adamantine. SANTOS ET AL. directly coupled a micro reactor to an ESI quadrupol time-of-flight MS (ESI-QTOF-MS) to study the Ziegler-Natta polymerization of ethane with a homogeneous catalyst [Cp_2ZrCl_2]/MAO (methyl aluminoxane) [112]. In this configuration, a commercially available PEEK Mixing Tee that acts as a micro reactor was connected to another micro mixer for reaction quenching purpose before coupled to the analyzer as shown in Figure 2-15. MARTHA ET AL. combined a coil reactor with atmospheric pressure chemical ionization MS (APCI-MS) for the demonstration of the system capability to simultaneously determine product formation, substrate conversion and catalyst identification [113]. This system implements the flow injection analysis (FIA) concept that sample is periodically injected into the solvent carrier stream. BROWNE ET AL. coupled a miniature MS to the Uniqsis FlowSyn flow chemistry system, that used the FIA concept, for online reaction monitoring [23] (Figure 2-16). This commercial flow system, that was expanded with the diluting function, was used to study the generation of benzyne and its subsequent reaction with furan. Micro reactor with FIA concept is also applied to ICP-MS to trace metals in drinking water samples as demonstrated by HSU ET AL. [114]. The micro reactor is coated with an immobilized reagent for separating trivalent [Cr(III)] and hexavalent [Cr(VI)] chromium species in aqueous samples. More about the integration between micro reactor to equipment for elemental analysis will be discussed in CHAPTER 8.

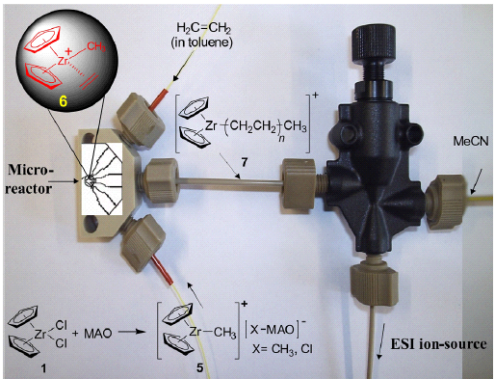

Figure 2-15: Micro reactor coupled online to ESI source with the reaction quenched at the second micromixer [112]

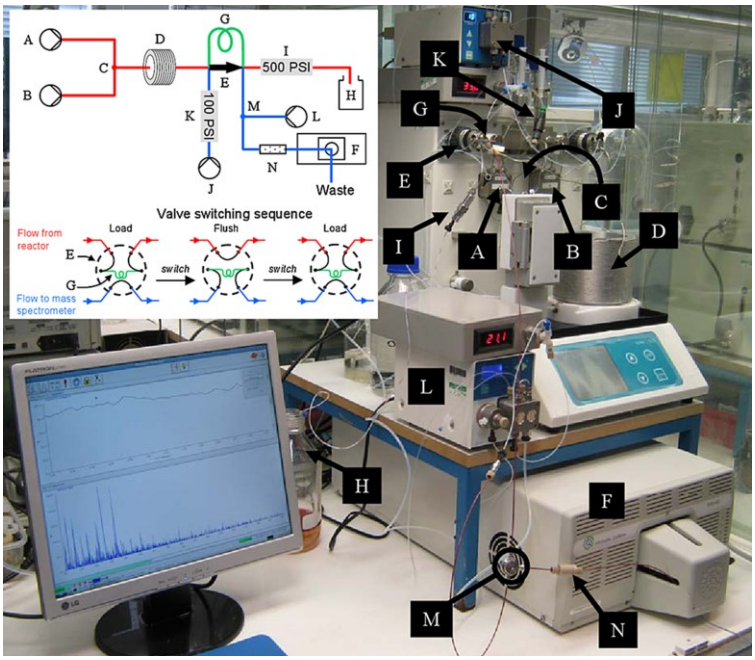

Figure 2-16: Microsaic 3500 MiD miniature mass spectrometer coupled to a Uniqsis FlowSyn flow chemistry system[23]

BRIVIO ET AL. connected an on-chip microfluidic device to a matrix-assisted laser desorption ionization TOF-MS (MALDI-TOF-MS) for real-time monitoring of different organic syntheses and biochemical reactions [115]. CLARKE ET AL. coupled a capillary-based reactor to an ESI Fourier transform ion cyclotron resonance MS (FTICR-MS) to obtain the kinetic parameters for the hydrolysis of p-nitro phenyl acetate by enzyme chymotrypsin [116]. The first nanomixer was used for mixing the two educts; the second nanomixer was used for quenching the reaction (Figure 2-17). BARNES ET AL. implemented an ESI ion trap TOF-MS to study the oxidative degradation of quercetin in an aqueous solution at pH 5.9 and 7.4 [105]. The influence of heat as well as the mechanism and pathway of oxidative degradation of quercetin was investigated. The reaction time in the range of 2 – 21 minutes could be adjusted by varying flow rate of the syringe pump, the diameter of the outer tube and position of the inner tube. DANIEL ET

AL. reported a development of a new Internet-based software system (LeyLab) that can be used for monitoring and controlling chemical reactions from anywhere in the world via the Internet [117]. The software was tested by connecting a reaction system with an online MS and later an inline IR detector for monitoring and self-optimizing (via feedback data from the detector) 1) the conversion of 3-Cyanopyridine over MnO_2 to its amide 2) Appel reaction, respectively.

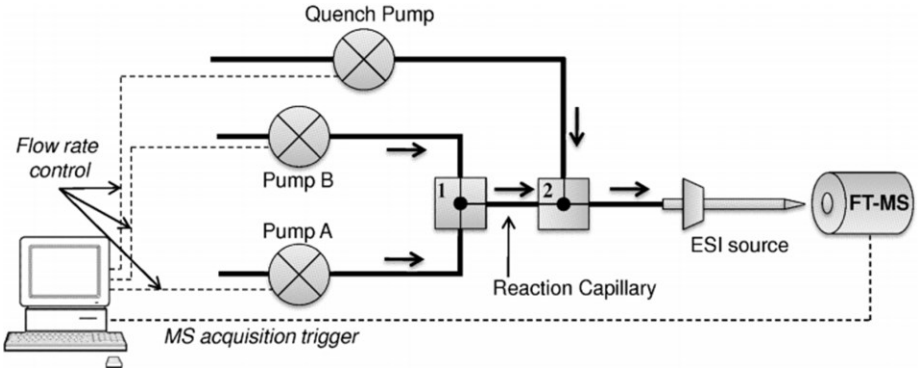

Figure 2-17: Schematic diagram of the online quench-flow micro reactor used for time-resolved ESI-FTICR MS experiments [116]

There are many applications for the combination between micro reactor and MS in chemical and biological reactions. ARAKAWA ET AL. reported the application of ES-MS to observe the photo substitution reactions of metal complexes of bidentate in acetonitrile [118]. Intermediates and products with lifetimes of minutes can be investigated by exciting the quart cell; and short-lived intermediates in the range of milliseconds can be detected by irradiation at the spray tip. SILVA ET AL. employed the ESI-MS/MS to investigate the Sandmeyer reaction online [109]. The short-lived intermediates and products are reported to be identified and characterized. His team also carried out the investigation of the Ziegler-Natta polymerization of ethane with a homogeneous catalyst and the Brookhart polymerization of ethane and 1-butene with homogeneous catalyst diimine using the ESI-MS. The solution was then diluted with acetonitrile online via another micro reactor before being fed to the ESI-MS for direct detection and characterization of transient species. BRIVIO ET AL. monolithically and later modularly integrated a reaction chip to a nanoflow ESI-TOF-MS [28]. The modular integration scheme was used to investigate the metal-ligand interactions of Zn-porphyrin with N-containing ligands in acetonitrile and the encapsulation of small organic molecules into β-cyclodextrin. BOER ET AL. showed the integration of an HPLC to a reaction system for detecting enzyme inhibitor in complex samples [33]. The HPLC was used to separate each component in the samples and the coil was where reactions took place. In his later work, two reaction coils were replaced by a two-stage microchip for bioactivity screening of complex mixtures [119]. The amount of samples was reduced and a more flexibility in using materials, dimensions and design for the microchip was enabled. WANG ET AL. coupled a microfluidic, which was used for metal extraction purpose, to an ElectroThermal Vaporization (ETV) - ICP MS [120]. Trace Cu, Zn, Cd, Hg, Pb and Bi in $HepG_2$ cell, Jurkat T cells and human serum was quantitative determined with the limit of detection found to be in the range of 6.6 – 89.3 pg/mL.

2.3 *Summary for Different Spectroscopic Methods*

From the survey, it can be seen that the combination of micro reactor and analytical devices is popular to academic research and industrial sectors with a variety of integrations and applications. Some reactor systems are manually operated [111] [112] via buttons on component devices; some systems with their components can be controlled individually through an in-house software [116] but not the software for the whole system; and some systems are automated with the control software commonly written in LABVIEW [53][121]. Feedback control is implemented in some systems as well with the control algorithm usually done in MATLAB [121][122][123][124]. A review for this innovation of using feedback can be seen in [125]. A chemical reaction is further monitored, controlled and autonomously self-optimized reaction parameters via the Internet [117]. A summary of the presented methods is shown in Table 2-5.

Different spectroscopic methods employ electromagnetic spectrum at different ranges of wavelength to interact with matter (molecules, atoms). The matter via energy absorption enters the excited state such as electronic transition, vibration, rotation in which information about the matter can be obtained, for example functional groups, unsaturated bonds presented in molecules (UV/VIS/IR/Raman/Fluorescence method), or number and type of protons and carbon atoms, position of the nuclei in the molecule relative to each other (NMR method). This information is useful in identification and quantitation of matter and finds many applications in reality. Except for the fluorescence spectroscopy with very high sensitivity (ultratrace/subtrace level of detection limit), other methods of this family fall into the micromolar range (trace level) of detection limit, which is less sensitive than that of the MS method.

For every technique, there are some benefits as well as some drawbacks which make them suitable or not suitable for certain applications. Spectroscopies are fast that they can be used as real-time feedback techniques to access the steady state of a continuous flow reactor. Fluorescent spectroscopy is very sensitive but restricts itself in applications containing fluorescence species. UV/VIS spectroscopy does not contain as much information as that of the IR and Raman spectroscopy [50] and is replaced by NMR and IR for organic compound identification [31]. IR spectroscopy is strongly absorbed by aqueous solvents, complex in spectra, and difficult to calibrate for multi-component systems [21]. NMR spectroscopy can provide more structural information but easier to analyze than IR. However, NMR systems (i.e. miniaturized low-field bench-top NMR spectrometers) normally have less sensitivity than other methods otherwise the price is very high for high magnetic field strength instruments. Although MS method is a destructive method, the amount of sample consumption is not considerable (with input flow rate normally smaller than 1 mL/min). In addition, the MS technique offers higher sensitivity and lower detection limit than other spectroscopic methods (except Fluorescence) and is versatile that analytes are not limited to a specific category such as fluorescence species or chromophore species. By coupling a micro reactor system to different types of MS, organic (molecular form) or inorganic (atomic form) analytes can be detected. Moreover, they are fast, capable of multiple analyte detection and suitable for short timescale measuring so that they could be used to investigate transient species which are often not suitable for UV/VIS, IR, or NMR spectroscopy [109]. Furthermore, a flow-through cell, which is

commonly employed for convenient integration of micro reactors to spectroscopic methods, is not required when integrating with MS. This reduces the additional reaction volume to the system. Finally, the technique is currently one of the most advancing fields of instrumental analysis that provides qualitative and quantitative information (i.e. masses of molecules and atoms in samples as well as molecular structures of organic and inorganic compounds) that it is interesting to investigate their power.

There have been a number of integration of micro reactors with MS of different types as well as their applications. Some of the integrated systems operate manually, semi-automated or automated with feedback control for autonomously self-optimized. There are different configurations in which the system can simply send the reagent directly from the micro reactor to the MS or use the FIA concept for sending pulses of sample. Different modules such as heating, quenching and diluting for the solution are also concerned through the design. One of the typical characteristics of a continuous flow system is the variation of the reagent flow rate due to different settings of the resident time. This flow rate variation usually causes difficulty to achieve a dilution module with stability and high dilution ratio. A Mass Rate Attenuator (MRA) or Active Splitter can be used for the dilution purpose. However, the device is often operated manually and is not seriously concerned about the variation of the input flow rate. Therefore, it is necessary to have a dilution module which can dilute at high ratios and automatically change its settings to adapt to the input condition. In addition, micro reactors which are widely integrated with molecular mass spectrometric techniques find little application in the field of atomic spectrometry in general or ICP-MS in specific. In the found literature, when being coupled to ICP-MS, the micro reactor was only functioned as a separation element (as a column to separate analytes) but not as its main purpose of a compartment in which chemical reaction can take place. Therefore, an attempt to connect the micro reactor system to the ICP-MS to detect metal contamination from the ORMS system to the sample would be interesting. The dilution module can also be included for testing its functionality by using ICP-MS. These are the two main tasks as well as the main contribution of this work.

Table 2-5: A summary for different spectroscopic techniques

	Fluorescence	**UV/VIS**	**IR**	**Raman**	**NMR**	**MS**
Absorption Wavelength	180 – 800 nM [31]	180 – 800 nM [31]	0.75 – 200 μM [31]	200 – 1064 nM [126][127]	0.5 – 10 m [31]	-
Emission wavelength	>180 – 800 nM	-	-	-	-	-
Detection limit	10^{-15} - 10^{-4} mole/lit [36]	micromolar range [45]	micromolar range [69]	micromolar range [128]	micromolar range [31]	nanomolar range [108]
Operation principle	Shared electrons in molecular orbitals absorb photons, promote to vibrationally excited electronic state, then emit photons at longer	Shared electrons in molecular orbitals absorb photons and promote to electronic excitation states.	Covalent bond of molecules absorbs IR photons which causes excitation of molecules to vibrational transition state (stretching and bending of	Inelastic collision of molecules from monochromatic light that results in a shift in wavelength of the scattered light to lower energy (Stoke Raman	Interaction between an oscillating radio frequency (RF) radiation and a collection of nuclei (with magnetic dipoles), which are immersed in a	Creating gas phase ions from the molecules or atoms in a sample; followed by separating the ions according to their mass-to-charge ratio, *m/z*; finally

	wavelengths.		chemical bonds) or rotational transition state.	scattering) and to higher energy (anti-Stock Raman scattering).	strong external magnetic field.	measuring the abundance of the formed ions.
Applications	Determination of unsaturated compounds, particularly aromatics [31]. Determination of the detection limit of an optical system. Investigation of the mixing quality of a micro mixer [129]. Study of kinetic parameters of a reaction.	Identification of functional groups (e.g., -(C=C)n-, -C=O, -C≡N) [31] and structure of molecules containing unsaturated bonds [31]. Detection of inorganic compounds (e.g., transitional metal complex). Quantitative determination of unsaturated compounds [31].	Identification of organic molecules (via identifying functional groups), inorganic molecules and investigation of dynamic processes (i.e. chemical reactions, phase transitions, sedimentations) [71]. Quantitative analysis of organic compound (at % concentration level).	Fingerprint information for organic and inorganic compounds. Quantitative and qualitative analysis of the individual compounds [74].	Qualitative and quantitative analyses, particularly of organic compounds [87]. Study of chemical equilibria, reaction kinetics, motion of molecules, and intermolecular interactions [31].	Determination of molecular weight and elemental composition. Characterization of structures of complex bio-organic molecules. Analysis of polymers and proteomics. Quantitative determination of organic components of solid, liquid or gas sample or elements at ppt concentrations [31].
Advantages	High sensitivity, high specificity [130]. Large linear dynamic range [31].	Fast and easy analysis capability.	Infrared spectrum carries high information content. High time resolution (down to 1 μs), short measuring time, low amount of sample required (typically 10-100 μg). Relatively low costs of equipment [57].	Organic species without UV/VIS chromophores can be analyzed by Raman spectroscopy [77]. Suitable for analyzing aqueous based reaction media [27]. Multi-component detection in a solution [78].	Probably the most powerful tool for determining molecular structures of many organic and inorganic compounds [131]. Can be used for investigating various chemical and biological processes [132].	High sensitivity and low detection limit [108]. Suitable for short timescale measuring [109]. Simultaneous detection of multiple analyte. Obtaining information about the intrinsic properties of isolated ions and molecules [104].
Disadvantages	Require fluorescence species [31]. Subject to interference from quenching effects or from spectral overlap from other compounds [31].	Spectrum does not contain as much information as that of the IR and Raman spectroscopy [46]. Replaced by NMR and IR for organic compound identification [31].	Strong mid-IR absorption of many solvents (particularly water) [61].	Weak scattering signal that may make it be overwhelmed by a strong spectral background. Fluorescence interference from analytes or solution matrices [78] [79].	Applicable to nuclei with magnetic moments. Insensitivity in comparison to other spectroscopic methods, which requires a higher sample amount for an analysis [88].	Destructive analysis technique. Requirement of hyphenating with other separation for structural analysis [110]. More effort requirement in sample preparation [108].

CHAPTER 3 SYSTEM OVERVIEW

3.1 *System Concept*

In chemical engineering, monitoring chemical reactions as well as qualitative and quantitative determination of reactants and resulting products are generally performed by online analysis systems [19]. As described in the previous chapter, an online monitoring system of chemical reaction in micro reactor has many advantages in reaction efficiency and fast data acquisition. In order to realize such benefits as well as to investigate the analytical capability of such a system, a mobile reaction system coupled to an analyzer has been planned in the laboratory. Some features and functionalities are required for the system:

- A chemical reaction can be performed and monitored at real-time.
- The system is effectively and simply coupled to a high sensitive analyzer.
- The system operation is automatic through a control software.
- The system can perform various functionalities:
    - Taking sample at different reaction stages
    - Enabling multiple sampling at every reaction stage
    - A sampling method for saving waiting time and materials between different reaction stages
    - A heating module for tempering chemical/reagent/analytical solution in micro reactor
    - A dilution module that allows users to set different dilution ratios
    - A quenching module to extinguish the reacting process
    - The control software can communicate and perform some basic functions to the analyzer's control software for convenience in data acquisition and data analysis
- Micro reactors of different sizes and types can be easily plugged in for various possible measuring time, in which good mixing has to be guaranteed.
- The system can be coupled to different types of analyzers so that molecules and atoms (or organic and inorganic components) can be measured.
- The system has a good robustness and repeatability.

In order to realize the system, two important decisions are (1) to decide an analyzer from different possibilities and (2) to determine an integration scheme for sending analyte to the analyzer. From the literature review in CHAPTER 2, it can be seen that there are various integration schemes of micro reactors to spectroscopic/spectrometric techniques. Such developments are benefits for followers that they have massive sources of reference. Advantages and disadvantages of every spectroscopic/spectrometric technique as well as of every integration scheme are also discovered. Therefore, a constructing for an online monitoring system can select a monitoring technique and an integration scheme that best fit their specifications. They can either follow an existing integration scheme or develop their own scheme based on the reference resources.

1) For the existing system, the MS technique (ESI-MS and ICP-MS) are selected for coupling to the micro reactor system instead of the spectroscopic techniques. The detailed comparison is given in section 2.3 and in Table 2-5. A summary is listed as the following:

- The MS technique offers higher sensitivity and lower detection limit than other spectroscopic methods (except Fluorescence) and the analytes are not limited to specific categories such as fluorescence species or chromophore species.
- By coupling the micro reactor system to different types of MS, organic (molecular form) or inorganic (atomic form) analytes can be detected.
- They are fast, multiple analyte detection and suitable for short timescale measuring.
- In addition, a flow-through cell, which is commonly employed for a convenient integration of micro reactors to spectroscopic methods, is not required when integrating to the MS. This reduces additional reaction volume to the system.

2) For a stable operation of the MS and therefore of the signal, the MS flow must be stable and below a threshold (commonly 1 mL/min). A direct connection of the micro reactor system to the MS is not suitable because the micro reactor flow rate varies according to the residence time (or reaction stage) and normally is greater than 1 mL/min. Therefore, the flow injection analysis concept (FIA) or (SIA – sequential injection analysis) is selected. The idea is to inject a liquid sample into a moving, non-segmented uninterrupted carrier stream of a suitable liquid [133]. The technique supports automated sampling which is helpful for the consistency of data; lowers impurities and improves accuracy over manual sampling [134]. It also offers many advantages such as high sampling rate, high throughput, low cost, low reagent consumption, and ease of design. It was proved to minimize clogging from salt deposition onto the sampler and skimmer cones of the interface to the MS and help reduce material consumption and fast contamination to the MS [135] because the MS almost contacts with a suitable solvent only. Therefore, the technique is extensively used in pharmaceutical chemistry, clinical chemistry, environmental monitoring, and forensic analysis.

3.2 *Initial State of the System*

The system in the laboratory is basically a computer controlled system. Components used in the system offer their functions that are well-controlled (via their manufacturers) for the automatic control purpose. The control software (called ORMS software) coded in C++ language helps corporate those components so that a variety of system's functionalities could be achieved. In general, the ORMS software calls and combines functions from the components for bigger automation tasks. There is no implementation of truly closed loop control in the software except setting for an input so that the corresponding component adjusts itself to reach the setpoint. Data communication in the system is realized via RS232 interfaces and from RS232 hubs to a computer by USB interface. The MassHunter Workstation Software from Agilent Technologies is responsible for data acquisition and analysis from the mass spectrometer.

Initially, the system was set up by experts in our lab. It was later developed by students and DI Fröhlich in her Ph.D. work [136]. The system is shown in Figure 3-1. As mentioned, the system implemented the

FIA concept that solution from the micro reactor outflow can be sampled and injected into a carrier stream. The carrier stream, which is manipulated by a mass flow controller, sends the sample to the analyzer. The system with its control software (ORMS software) can operate some basic measuring tasks such as to set flow rate for the carrier solvent stream, for educt pumps, to switch the multiport valve as well as the communication with the analyzer's control software using the API functions from Microsoft Windows.

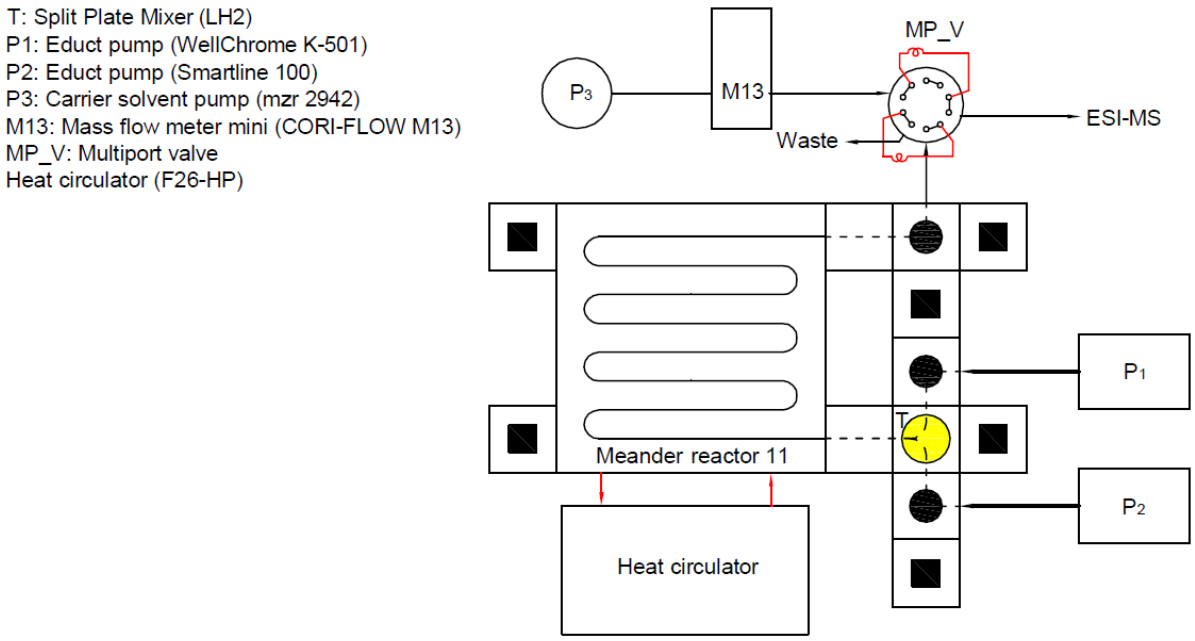

Figure 3-1: Initial configuration of the Online reaction monitoring system: (T) mixer, (P_1) educt pump, (P_2) educt pump, (P_3) carrier solvent pump, (M13) mass flow controller, (MP_V) multiport valve

However, for better performance and for an elaboration of functioning, the system needs to be improved:

- There is a problem of operation missing due to the loss of command from the control software such as missing command of taking a sample that results in peak missing. The problem is identified to be caused by the simultaneous reading and writing to the same object.
- The heating module is integrated but the heating rate is very slow (≈ 1°C/min).
- The idea of exploiting the elapsed time in the occurred reaction stage to save waiting time and materials is great but the algorithm is not efficient.
- The requirement of a dilution module that can function stably under different flow rates of the micro reactor and possible to dilute at high ratios.
- Integration to the ICP-MS to enable elemental analysis of the system.
- An expansion of the control software interface to accommodate new functions of the system.
- There are different utilities such as AutoIt, UIPath, Automa, Selenium, AutoHotKey, etc. that can be used for GUI automation instead of using API functions of Windows.

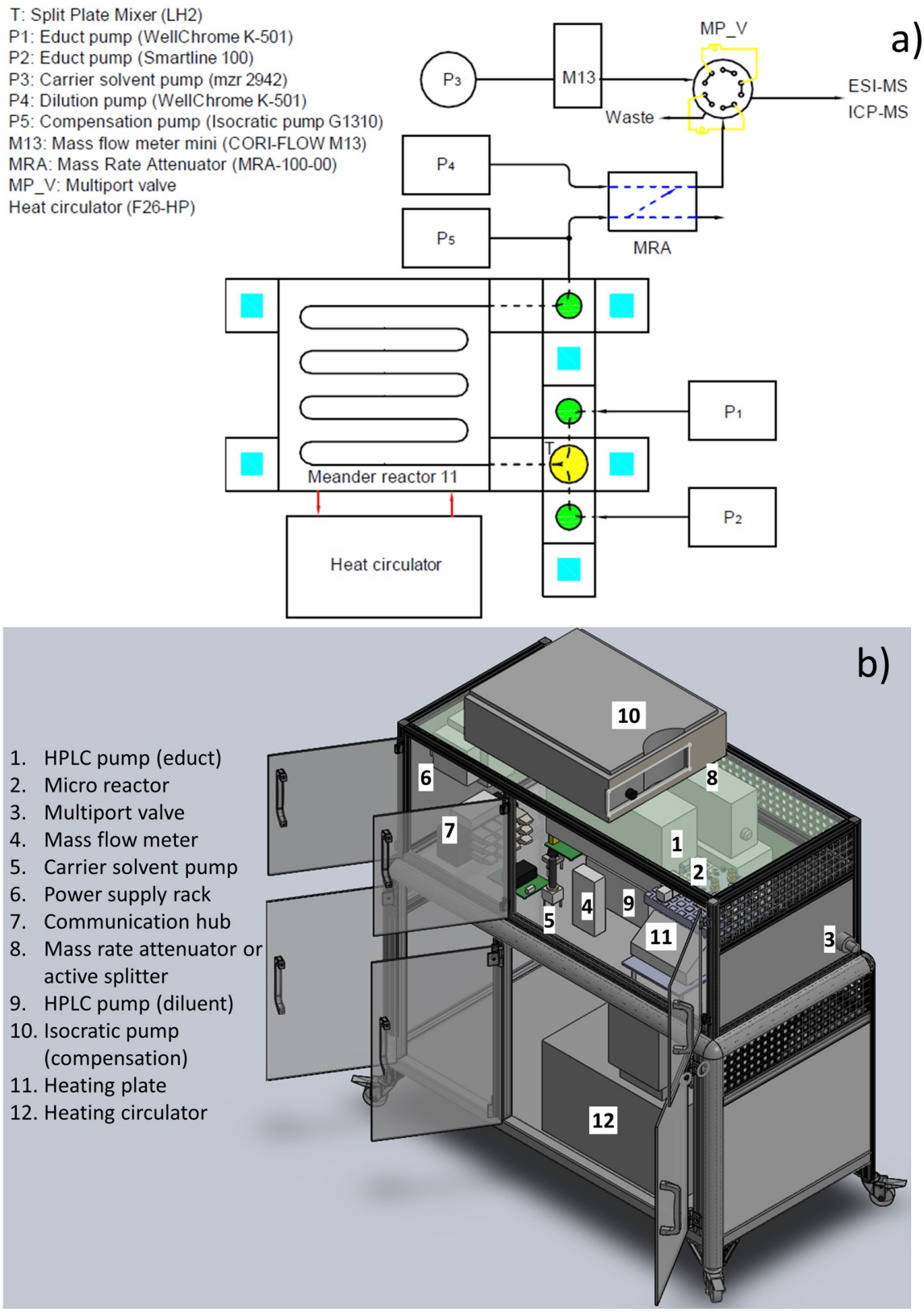

Figure 3-2: Current configuration of the Online reaction monitoring system: a) schematic diagram, b) 3D model

3.3 *Current State of the System*

The current configuration of the system is shown in Figure 3-2. The system includes the following main components: Two educt pumps HPLC WellChrom K-501 and Smartline 100 (Knauer, Berlin, Germany) are used for transferring reactants/educts to an 11.2 mL meander reactor (Ehrfeld Mikrotechnik BTS, Wendelsheim, Germany). Solution temperature in this micro reactor can be controlled by a F26-HP refrigerated/heating circulator (Julabo, Seelbach, Germany) and an additional heating/chilling plate (Cole-Parmer, Kehl/Rhein, Germany). After leaving the micro reactor the solution is diluted by the dilution module (Mass rate attenuator (Rheodyne, L.P., Rohnert Park, CA, USA)) before entering a multiport valve assembled with a two-position micro electric valve actuator (Valco Instruments Co. Inc, Schenkon, Switzerland). This valve is used for sample injection. The sample is then transferred to the analytical device (TOF-MS G1969A, Agilent Technologies, Waldbronn, Germany) by the Micro annular gear pump mzr-2942 (HNP Mikrosystem GmbH, Schwerin, Germany). The flow rate of this pump is controlled by the mass flow meter mini CORI-FLOW™ model M13 (Bronkhorst Mättig, Kamen, Germany). Later, the micro reactor system is connected to the Agilent 7700x ICP-MS (Agilent Technologies, Waldbronn, Germany). The system specification is shown in Table 3-1.

Table 3-1: System specifications

Micro reactor volume (mL)	11.2
Maximum flow rate of each educt pump (mL/min)	7
Allowable range of reaction stage (min)	0.8 – 56
Solvent carrier flow rate (mL/min)	<1
Dilution ratio	10 – 100,000
Temperature range (^{o}C)	-20: +180
Heating solvent	Thermal H10, Julabo

When the sample reaches the MS, the signal appears as a peak as in Figure 3-3. The concentration of a particular reagent can then be derived by specifying its *m/z* for extracting the chromatogram and relating its peak height or the area under the peak profile (peak area) to a standard calibration curve.

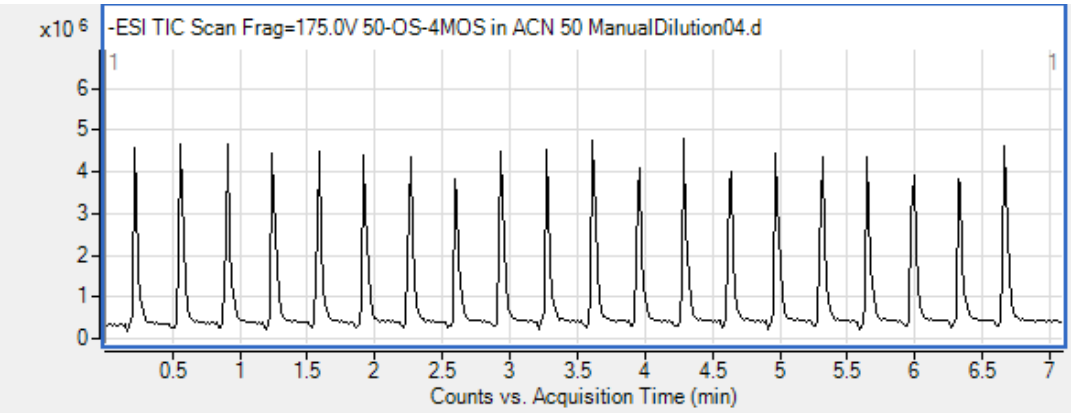

Figure 3-3: Each sample transferred to the MS is recognized as a peak

3.4 *Main Functions*

The system can be operated in *manual operating mode* and in *automatic operating mode*. In *manual operating mode*, users can set flow rates for the educt pumps, take samples by switching the multiport valve, set temperature for the heating component, and set flow rate and split factor directly for the dilution module. In *automatic operating mode*, there are the *slow sampling method* (SSM) and *fast sampling method* (FSM) that enables multiple reaction stages to be specified (in time ascending order), for example, reaction stages of a reaction at 1 min, 2 min, 3 min. The *reaction stage* in this case reflects a certain state of a reaction and is defined as the *residence time*, which is the duration of traveling of a solution from the input to the output of the micro reactor (Figure 3-4). This residence time (or reaction stage) should be distinguished to the *reaction time,* which is considered in this work as elapsed time of a reaction since reactants are mixed. Details about this two sampling methods will be discussed in CHAPTER 5.

In general, the two methods can execute all reaction stages sequentially in one run. Flow rates for the pumps are calculated and samples are taken automatically based on those reaction stages. In the *slow sampling method*, for every reaction stage, completely new reactant solutions are used or a reaction starts from time zero for every new stage. Meanwhile, the idea in the *fast sampling method* is to exploit the reaction time that has elapsed in previous reaction stages to begin a new stage. Therefore, intuitively, the *fast sampling method* has advantages over the *slow sampling method* in time and material consumption.

A heating module is integrated with the control software so that the solution temperature can be conditioned. Two operation modes of the heating module are available. *Preheating mode* uses the internal heating mode of the circulator for manipulating the heating reagent to the setpoint. Meanwhile, the *automatic heating mode* uses the external heating mode of the circulator, which is interconnected with the *automatic operation mode* of the system, to heat up a solution in micro reactor to the setpoint. In this mode, a reaction stage can begin only when the solution temperature is close enough to the setpoint. The topic is presented in CHAPTER 6.

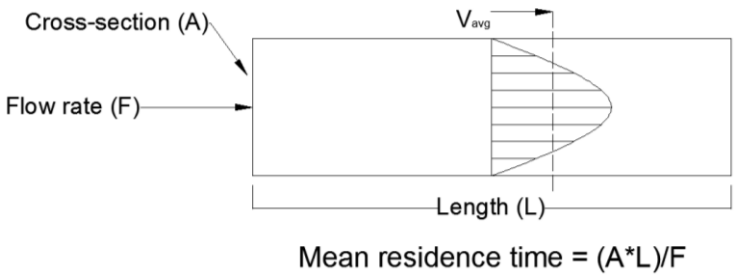

Figure 3-4: Velocity profile of a fully developed laminar pipe flow and formula of mean residence time

A dilution module using the low flow compensation approach is employed for diluting reaction solution to different dilution ratios (up to 100,000) in different conditions of the micro reactor flow rate. This module can operate in *manual* and *automatic diluting mode*. In *manual diluting mode*, each component of

the module can be controlled manually. Also, a dilution ratio can be specified, then, settings for each component will be done automatically but not taking consideration of the micro reactor flow rate. In *automatic diluting mode*, the flow rate in micro reactor for every reaction stage is considered in calculating parameters of the dilution module. In order words, setting for the dilution module is performed for every reaction stage. This mode is active only when the system is in the *automatic operating mode*. This module is discussed in CHAPTER 7.

In addition to integrating with ESI-MS for molecular analysis, the micro reactor system has been integrated with ICP-MS for elemental analysis via one of the two concepts. The first concept includes a direct coupling of the micro reactor to ICP-MS without the use of the auto sampler (ALS). The second concept integrates an ALS that increases the flexibility in sample handling. This second concept also enables the standard start-up of ICP-MS with warm up, calibration and tuning. Finally, the dilution module is included and tested with the ICP-MS system. Details of this implementation are treated in CHAPTER 8.

Finally, for automation purposes, the ORMS control software not only controls the hardware devices (pumps, multiport valve etc.) but also be enabled to control the analyzer's control software. The MassHunter Workstation Software LC/MS Data Acquisition Version B.04.00 for the ESI-TOF-MS (Agilent Technologies, Waldbronn, Germany) and the MassHunter 4.2 Workstation software for ICP-MS Top version C.01.02 (Agilent Technologies, Waldbronn, Germany) are automated so that some sequences of operation in these softwares can be performed via the ORMS software. The approach called GUI automation is applied to fulfill the task. A library from the AutoIt scripting language has been applied for this task instead of using functions from Windows API. This topic is discussed in CHAPTER 9.

3.5 *Objective and Contributions of the Thesis*

The objective of this thesis is to improve the system performance according to the requirements specified in Section 3.1. The system can facilitate users with online monitoring of a chemical reaction and with different tools and utilities necessary for the analytical work. In more details, after sample preparation finishes, users only have to specify different parameters for the experiment. The system will do its tasks automatically. Data acquisition and extraction can be performed directly from the control software. In order to achieve the goals, different tasks have been done:

- Implementation of a dilution module to enable the system to work with highly concentrated reagent without sample overloading problem.
- Integration of the system to an ICP-MS for elemental measurement.
- Insertion of the dilution module in testing with the ICP-MS in which the sample concentration can be quantified conveniently using spectrum mode of the acquisition method.
- Modification of the *fast sampling method* to make it more efficient in reducing waiting time and materials in a series of reaction stages.
- Modification of the heating module for temperature conditioning of a reaction.

- Correction for the problem of peak missing due to simultaneous object accessing from two threads.
- Verification of performance of the system components to make sure they work correctly.
- Modification of the Graphical User Interface (GUI) of the ORMS control software due to system expansion. The modified GUI has different tabs in which similar control functions are grouped into a tab.
- The ORMS software can communicate with the operational and analytical software of the MS for convenience in data acquisition and extraction.

Throughout the thesis, there are always replications for every measurement. The values of average, standard deviation (STD), coefficient of variation (or STD in %) of the measurements are often included in the result table to show mean values as well as distribution of the measurements. Formulas for calculating are listed below:

- Mean value: $\bar{m} = \frac{m_1+m_2 \ldots +m_n}{n}$, m_i: i^{th} measured values, n: number of measurement
- Standard deviation: $\delta = \sqrt{\frac{\sum_{i=1}^{n}(m_i-\bar{m})^2}{(n-1)}}$
- Coefficient of variation: $CV = \frac{\delta}{\bar{m}} * 100$

CHAPTER 4 SYSTEM VERIFICATION

In order to evaluate the system performance, it is necessary to verify the performance of main components in the system. In other words, a system can work well when its components are well-functioned. The system setup for the testing is in Figure 4-1. The chapter begins by validating the educt pumps, carrier solvent pump, and the multiport valve. The chapter ends by estimating reaction stages that can be performed by the system, and by estimating the time gap between two consecutive samplings so that peak overlapping does not occur.

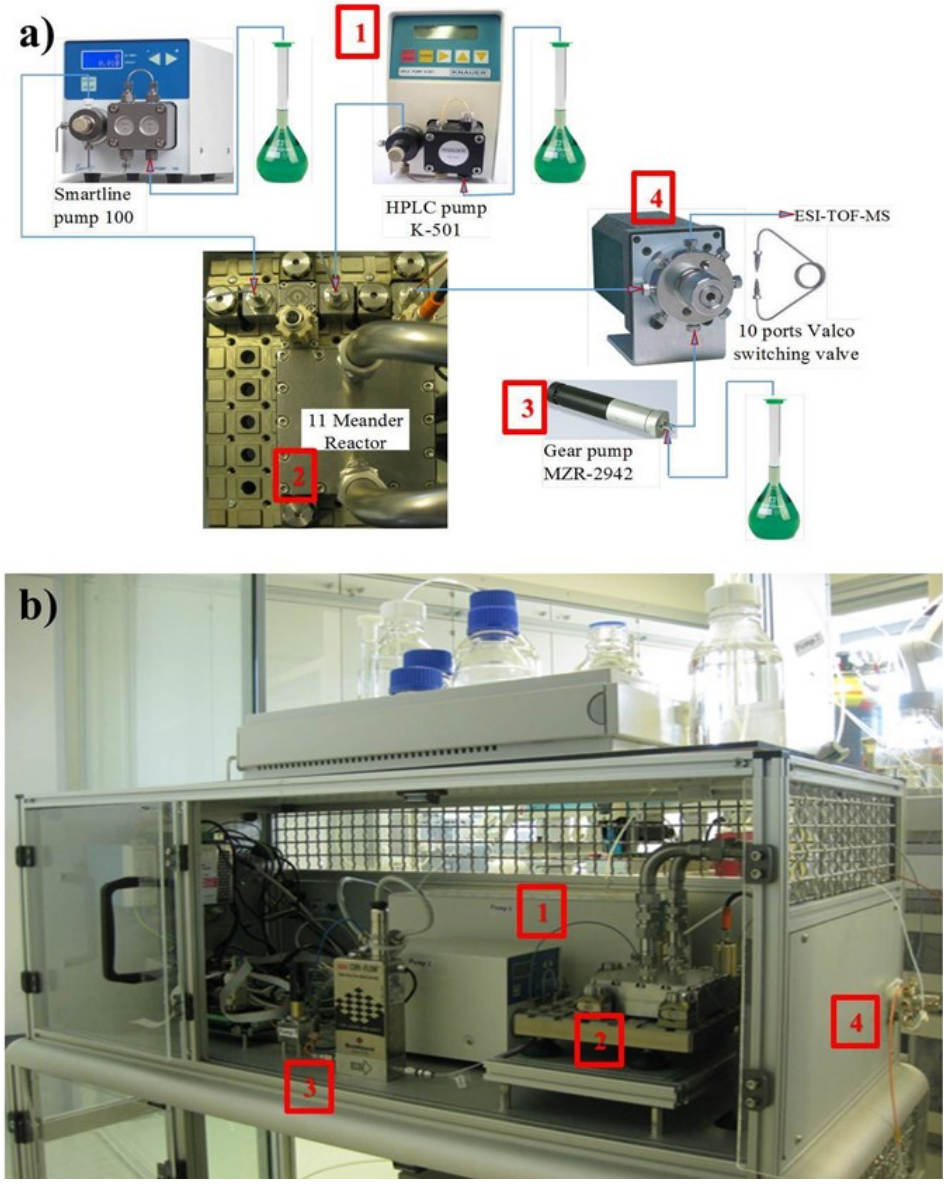

Figure 4-1: Configuration scheme of the measurement structure: 1) pump module, 2) micro reactor, 3) carrier solvent module, 4) multiport valve

4.1 *Verification of Pump Operation*

The two HPLC pumps were tested for their performance. Figure 4-2 shows the response of two HPLC pumps (P_1 and P_2) to different flow rate setpoints. The output from micro reactor is connected to the mass flow meter for measuring the flow rate of two pumps. The FlowDDE and FlowPlot software (Bronkhorst Mättig, Kamen, Germany), that manipulate the mass flow controller (Coriflow M13), were applied for indicating the flow as in the figure. The flow rate of each pump was varied from 0.01 mL/min to 2 mL/min. It can be seen that at a high flow rate ($F \geq 0.5$ mL/min), the pump responses instantly to the command and in less than 5s the flow rate reaches the setpoints without overshooting. At lower flow rates, the pump is slower in reaching the setpoint (≈ 10s) and the flow is also more oscillating due to slow movement of the two pistons. This pulsating behavior of the pumps is reduced after the micro reactor and the sample loop, which act as a capacitor. At higher flow rate ($F \geq 0.5$ mL/min), the pulse is more condensed so that the oscillation seems disappeared.

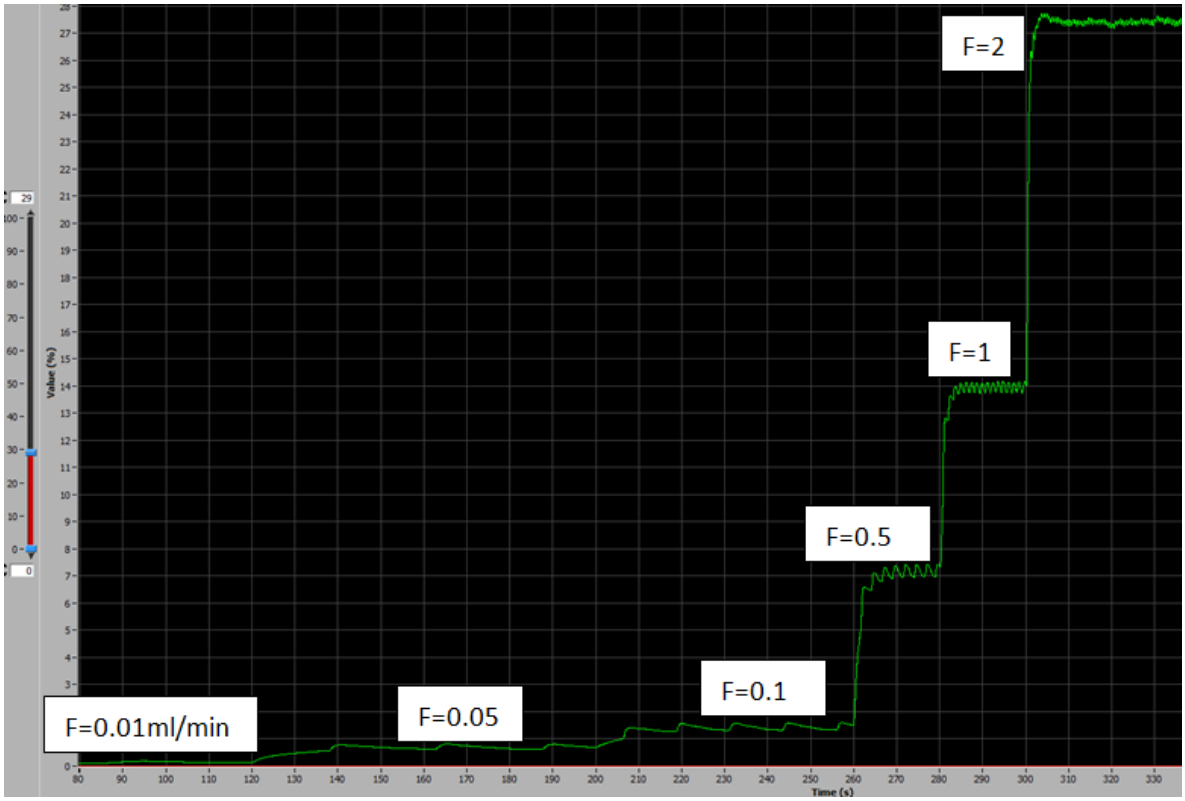

Figure 4-2: Response of Knauer pumps to different flow rate settings

Liquid was also collected in order to determine the actually deliveried volume (V). In this test, flow rates of both pumps were varied from 0.1 mL/min to 7 mL/min. Operating duration of the pumps was calculated so that the total volume corresponding to every tested flow rate is 11.2 mL. The experiment ran three times. Measurement results are shown in Table 4-1.

Table 4-1: Determination of pump's accuracy in transferring liquid

Flow rate P_1,P_2 (mL/min)	0.1	0.5	1	2	3	5	7
Pressure (0.1 Mpa)	1	2	4	7	11	20	32
Tap Water Density (mg/mL) at 21°C	998.02						
Expected Weight (g)	**11.18**	**11.18**	**11.18**	**11.18**	**11.18**	**11.18**	**11.18**
Mean Weight (g)	**11.42**	**11.56**	**11.54**	**11.47**	**11.43**	**11.24**	**11.00**
STD (in g)	0.10	0.00	0.00	0.01	0.02	0.02	0.11
STD in % or Coefficient of Variation (%)	0.9	0.0	0.0	0.1	0.2	0.2	1.0

The result demonstrates a good performance of the pump in supplying accurate volume at different working range (from 0.1 mL/min to 7 mL/min). In most cases, the pump gives more flow than the specified value. This is a good compromise for the additional volume from capillaries, mixer or connectors. In addition, the deviations from the 3 replications are very small (< 1.5%) that shows a very good precision of the pumps.

Remarks: The most easily damaged parts of these pumps are the two check valves. The next parts are the piston seals and O-rings. Therefore, when the pump does not give sufficient flow, it is recommended to examine the check valve first and run the pump again before making replacement one of those parts.

4.2 *Verification of the Carrier Solvent Pump*

A stable carrier flow to the MS is very important in giving a reliable measurement. The solvent carrier flow has been tuned and verified for its operation [137]. The pump works fine afterward. As in Figure 4-3, the pump can reach to a new flow rate in less than 20s. Its response to a disturbance (when the multiport valve switches that it blocks the flow instantly) is good that the flow quickly returns to its stability in less than 4s. Some remarks for this pump: The pump is under PID control by the mass flow meter (Coriflow M13). An aggressive setting for the controller (K_p large, T_i small; i.e. K_p*=15.27,* T_i*=0.01*), therefore, results in short transient response time but large overshoot and oscillation of the actuator. With this settings, the pump can work well under the high pressure of the ESI-MS but in atmospheric pressure and low flow rate, the pump does not perform well. Therefore, it is better to tune the pump with K_p smaller and T_i larger (i.e. K_p*=12.27,* T_i*=0.03*). The transient response time is longer; however, the pump flow rate is more stable under various working pressure and disturbance from the switching of the multiport valve as can be seen in the figure.

In addition, the MS is very sensitive that any debris, dirt in the solvent or from the gear pump will cause the signal up-hill. In this case, flushing the pump with MeOH can solve the problem. Moreover, a blockage of the micro filter behind the MS connector with the ORMS system increases the pressure of the stream that makes the pump run at higher speed. This often results in an unstable flow rate of the pump and sometimes puts the pump controller board into error mode (LED turns red). As a practical experience, at 0.6 ml/min, if the pump speed is more than 4,300 revolutions/min the micro filter should be renewed.

Normal speed of mzr 2942 pump when connecting to the ESI-MS in the lab is around 2,200 revolutions/min when a new micro filter is used. Finally, the ORMS software only uses a function to send the desired flow rate value to the Coriflow controller. Therefore, tuning the *PID* value to adjust the flow response has to be performed directly in the FlowDDE and FlowPlot software.

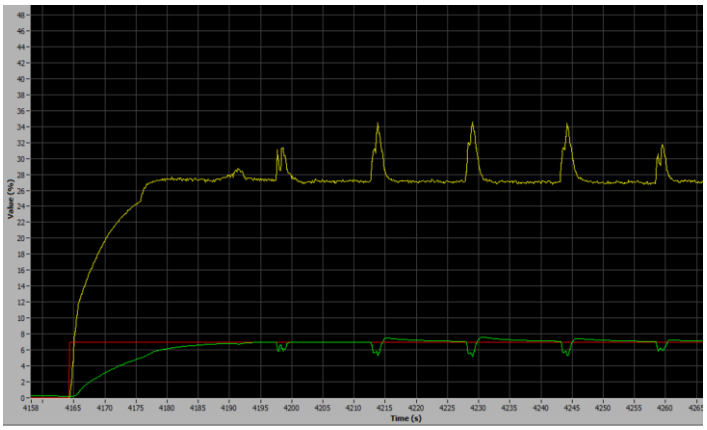

Figure 4-3: Response of the mzr 2942 to a step input and to sampling: yellow line is the input power; red line is the setpoint; green line is the measured flow rate

4.3 *Testing the Switching Valve*

When the multiport valve switches, it disturbs the carrier flow temporarily. It may cause the flow become unstable and send an erroneous amount of sample to the MS. This can make high STD for the sampling replication. Therefore, a test was performed to know the effect of this component onto the system (or to the current setting for the carrier solvent flow so that modification of the PID parameters for this has to be made if necessary). Tests for the switching valve was carried out using 4-Methyloctanoic acid (4-MOS) as an internal standard in acetonitrile (40%)/ultrapure water (60%) (ACN/H_2O) solvent. The system was configured as in Figure 4-1 for this test. The measurement was repeated two times with 50 samplings for each run. The result shows that the STD values are in the range of 6-7%. This result shows a normal operation of the multiport valve and its insignificant effect on the measurement. Details of system settings are shown in Table 4-2.

Table 4-2: Testing results for the switching valve

Solution	4-MOS in ACN/H_2O	
Micro reactor flow rate (mL/min)	2	
Carrier solvent flow rate (mL/min)	0.4	
Peak replicate	50	
Sampling duration (s)	0.2	
Sampling interval (s)	25	
	Run 1	**Run 2**
Average (Abr. Unit)	1,324,599	1,340,779
STD	87,252	81,824
STD in %	**6.6**	**6.1**

4.4 *Estimation of the Possible Residence Time*

The residence time of a solution in the micro reactor is calculated followed:

$$T_{res} = \frac{V}{F}$$

With T_{res}: mean residence time (s)
V: micro reactor volume (mL)
F: flow rate of solution in micro reactor (mL/min)

Intuitively, a certain reactor volume can accommodate a solution with any flow rate or with any residence time. However, for a chemical reaction, two reagents must be guaranteed to be well-mixed at the micro reactor input instead of relying on the dispersion effect. Therefore, flow rate of the reagents must be high enough for good mixing at the mixer. This limits the minimum input flow rate. The system uses the Micromixer (Ehrfeld LH2) which has recommended flow rate of greater than 0.2 mL/min for good mixing. Therefore,

$$T_{res\_max} = \frac{11.2}{0.2} = 56\ min$$

In addition, the two pumps (WellChrom HPLC-Pump K-501 and Smartline Pump 100) have each maximum flow rate for safe operation of the system: 7 mL/min (max: 10 mL/min). This limits the maximum input flow rate to 14 mL/min.

$$T_{res\_min} = \frac{11.2}{7 * 2} = 0.8\ min$$

Therefore, a **suitable working range of flow rate** for the system is from 0.2 mL/min to 14 mL/min (two pumps). Consequently, a **suitable range of residence time (or reaction stages)** of the current system is from 0.8 min to 56 min.

4.5 *Time Resolution of the System*

The time resolution of the system determines how close the two samplings can be taken without overlapping to each other. Therefore, a good approximation of this parameter will enable time and material saving without losing analytical information. For the *slow sampling method*, time resolution limits the minimum *sampling interval* which is a time interval between two adjacent sampling in one reaction stage. And for the *fast sampling method* that will be presented in chapter 5, the time resolution determines the maximum number of stages between the first and the last stage in every run.

The system measures the sample as peaks. A peak width depends on the *sampling duration, flow rate of carrier solvent to the analyzer*, *solution concentration* and *solution composition*. Theoretically, the switching time of the micro electric valve actuator (Valco Instruments Co. Inc) from position A to position B or vice versa is 140ms = 0.14s, total delay time: 2ms, sampling duration: 0 - 60s. Thus, a sampling cycle takes minimum <300ms or 0.3s. Therefore, time between two adjacent samplings cannot be smaller than 0.3s.

An experiment with 80 µL/L Octanoic acid (OS) and 40 µL/L 4-Methyl Octanoic acid with different sampling intervals and different carrier solvent flow rates was performed in order to estimate the time resolution of the system. The experiment settings are tabulated in Section 11.2 (*Experiment 1*). The results are represented in Table 4-3.

Table 4-3: Effect of sampling interval on the peak area with different flow rate of carrier solvent

Flow rate (P_3-mL/min)			**Sampling Interval (s)**					
			7	*10*	*15*	*20*	*30*	*40*
0.4	**Average peak area (Abr. Unit)**	**OS**		12,320,748	17,867,092	20,234,200	18,404,470	24,861,466
0.6			5,138,024	8,344,905	9,485,880	8,848,170	9,629,238	8,980,851
0.4		**4-MOS**		18,938,242	23,784,822	25,768,129	24,722,108	28,373,156
0.6			9,339,217	12,341,667	13,582,125	13,642,310	14,083,772	14,185,010

As shown in the table, the carrier solvent flow rate impacts on the peak area by diluting sample and changing ionization efficiency of the analyzer. In addition, a higher flow rate decreases the residence time of the sample in the nebulizer so that lesser ions can get into the MS. As a result, an increase in the carrier solvent flow rate from 0.4 mL/min to 0.6 mL/min causes a decrease in peak areas by roughly half in this case. In addition, if the sampling interval gets smaller than a certain threshold, overlapping occurs which results in a reduction in the peak area. In the case of OS with carrier solvent flow rate 0.4 mL/min, there is a big difference in the peak area between sampling interval 15s (17,867,092) and 10s (12,320,748). This indicates the happening of peak overlapping. It can be concluded from the table that, with peak areas around 20 million (arbitrary unit), sampling interval 15s would be sufficient; and with peak area around 14 million, sampling interval 10s would be sufficient. In practice, it is better to first estimate the sampling interval and run for one time in order to determine the final value of the sampling interval for the afterward runs. Figure 4-4 is shown to additionally visualize the situation of peak overlapping occurred in this experiment. As can be seen, the base line is lifted up and the peaks get smaller.

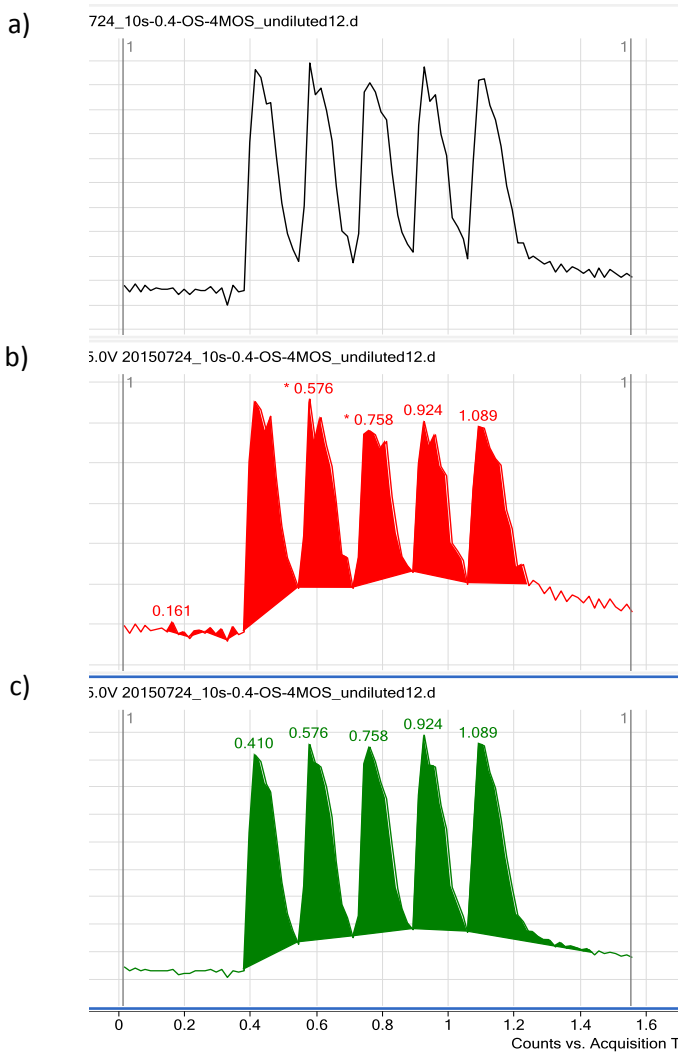

Figure 4-4: Peak overlapping caused by dense sampling which rises the base line and reduces peak areas. a) Total ion current (TIC) chromatogram, b) Extracted ion chromatogram (EIC) for OS, c) EIC signal for 4-MOS

CHAPTER 5 MODIFICATION OF THE FAST SAMPLING METHOD

An important aspect after system construction is to optimize the system operation so that equivalent analytical results can be achieved with less time and material consumption. This factor contributes to the economics of the system. In the current system, for monitoring a series of reaction stages sequentially in one run (multiple reaction stages), there are two methods namely *slow sampling method* (SSM) and *fast sampling method* (FSM). In SSM completely new reactant solutions are used for every reaction stage and the reaction time starts from zero for every new stage. Meanwhile, the idea in FSM is to exploit the reaction time that has elapsed in previous reaction stages to begin a new stage [19]. The chapter begins by discussing the existing algorithm of the SSM, FSM and their limitations. The two improved approaches are presented next. And, the chapter continues by comparing those sampling approaches in the aspect of time and material consumption and closes by monitoring a chemical reaction using the SSM and FSM.

5.1 *Existing Algorithm of the Slow Sampling and Fast Sampling Method*

In the *automatic operation mode*, there are the SSM and FSM in which flow rates for the educt pumps are calculated and samples are automatically taken based on the reactor volume and reaction stages. In the SSM, for every reaction stage, flow rate (F_i) is set based on the whole reactor volume (V) and the current reaction stage (T_i) following the relation $F_i = V/T_i$. The reaction time starts from zero (Figure 5-1a) for every reaction stage. Meanwhile, the FSM exploits the reaction time that has elapsed in previous reaction stages to begin a new stage [19]. In other words, the reaction time of a new reaction stage (except for the first stage) does not start from zero (Figure 5-1b). Flow rate (F_i) for every two reaction stages (starting from stage 2) is set equal the smaller flow rate (or flow rate of the later reaction stage with larger time), so that total time to perform two reaction stages equals the time of the later stage only or $\Delta T_{2n}+\Delta T_{2n+1}=T_{2n+1}$. In general, the result of this method is a time reduction of all even stages.

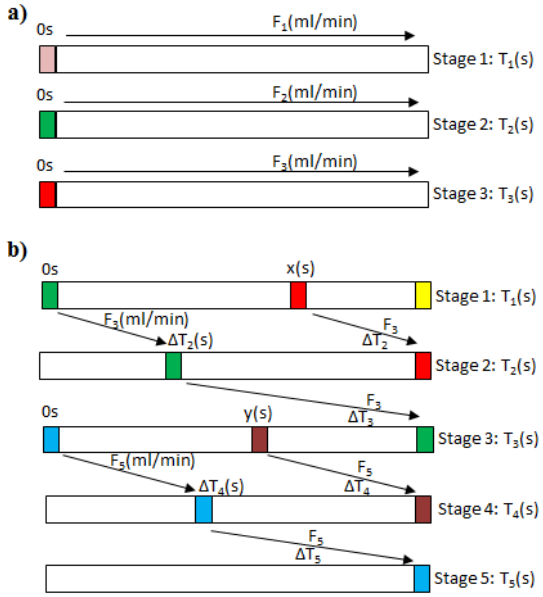

Figure 5-1: Principle of sampling methods: a) *slow sampling method,* b) the old *fast sampling method*

However, the algorithm is quite complicated. Also, the formula for calculating the *waiting time for sampling* (or *additional reaction time* (ΔT)) of a new stage has two cases for odd and even reaction stages with the even stage depending on the afterward stage, which may not always be available. Therefore, a new algorithm to overcome the mentioned limitations as well as to further reduce time and material consumption would be necessary. Two approaches for fast sampling have been proposed and implemented. Here, the *additional (reaction) time* (ΔT_i) is defined as the waiting time from stage *i-1* to stage *i* for sampling.

5.2 *Approach 1*

5.2.1 A Simple Case with 3 Nodes

Consider a reaction volume to have channel-type with an equal cross area so that the flow condition is identical over the reactor. A simple case of the modified algorithm for the purpose of understanding is sketched as in Figure 5-2. The idea is to divide the reactor volume (V) into 2 equal parts by 3 nodes (starting from node 0). After the first reaction stage completes, for every reaction stage afterward, the timing starts from the middle of the reactor (node 1). At this point, the current reaction stage has elapsed for a certain amount of time. For example, when the first reaction stage set at 60s has reached, at the middle of the reactor, the reaction has elapsed 30s. Therefore, to reach the second reaction stage of 120s, the reaction solution needs to move from the middle point to the sampling point in just 90s more. In other words, an amount of 30s is saved for the second reaction stage. It is similar for the third stage that has to wait 150s more instead of 240s because the reaction has been started for 90s at the middle point. In general, the additional time ΔT_i to stage i is: $\Delta T_i = T_i - \Delta T_{i-1}$ (with $i>1$), which is also the saving time to stage $i+1$ (Table 5-1). Similarly, by starting a new reaction stage in the middle of the reaction volume, the required materials for every following stage are also reduced by 50%.

Table 5-1: Step by step derivation of the fast algorithm with 3 nodes.

Node 0	Node 1	Node 2
0	$\Delta T_1 = \frac{T_1}{2}$	T_1
0	$\Delta T_2 = T_2 - \Delta T_1$	T_2
0	$\Delta T_3 = T_3 - \Delta T_2$	T_3
…	…	…
0	$\Delta T_i = T_i - \Delta T_{i-1}$	T_i
…	…	…
0	$\Delta T_n = T_n - \Delta T_{n-1}$	T_n

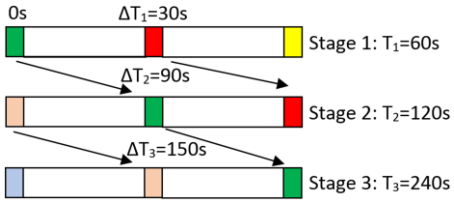

Figure 5-2: Principle of the FSM approach 1with 3 nodes

Derivation of Total Working Time and Total Reaction Material

Total working time (***δT***) is the time to finish all reaction stages in each run. As specified in Table 5-1 this is a series problem that sequentially sums all ΔT_i $(i>1)$ and T_1. Detailed steps for deriving the general equation for this simple case is presented below with $\boldsymbol{\delta T_i}$ the total working time until reaction stage *i*:

$$\delta T_1 = T_1$$

$$\delta T_2 = \Delta T_2 + \delta T_1 = T_2 - \frac{T_1}{2} + T_1 = T_2 + \frac{T_1}{2}$$

$$\delta T_3 = \Delta T_3 + \delta T_2 = T_3 - \Delta T_2 + \Delta T_2 + \delta T_1 = T_3 + T_1$$

…

$$\delta T_i = \Delta T_i + \delta T_{i-1} = T_i - \Delta T_{i-1} + \Delta T_{i-1} + \delta T_{i-2}$$

…

$$\delta T_n = \Delta T_n + \delta T_{n-1} = T_n - \Delta T_{n-1} + \Delta T_{n-1} + \delta T_{n-2}$$

It can be noticed that the total working time until stage *n* equals the current reaction stage (*n*) plus the total working time until stage *n-2*. Therefore, the total working time in this case can be formulated as:

$$\delta T_{fast} = T_1 + \Delta T_2 + \cdots + \Delta T_n = \sum_{i=0}^{floor(\frac{n-1}{2})} T_{n-2*i} + \frac{mod\left(\frac{n-1}{2}\right)}{2} * T_1 \quad (5\text{-}1)$$

With *n* is the number of stage; $floor(\frac{n-1}{2})$ is the largest integer not greater than $\frac{n-1}{2}$ and $mod\left(\frac{n-1}{2}\right)$ is the Modulo operation that finds the remainder of $\frac{n-1}{2}$.

Similar to the total working time, the total reaction material (δV) is the material amount required to complete all reaction stages of each run. Both two values might be important to analysts for the sample amount they need to prepare and time when they could check for results and start another experiment.

It can be noticed that except for the first stage that requires a full reaction volume, the remaining reaction stages require only half of the reaction volume. Therefore,

$$\delta V_{fast} = V_1 + \frac{V_2}{2} + \cdots + \frac{V_n}{2} = \frac{V}{2} + n * \frac{V}{2} = (1+n)\frac{V}{2} \quad (5\text{-}2)$$

As a continuation of the example mentioned above, for 3 reaction stages 60s, 120s, 240s, if the SSM is applied $\delta T_{slow} = 60 + 120 + 240 = 420s$ and $\delta V_{slow} = 11.2 + 11.2 + 11.2 = 33.6\, mL$.

Meanwhile, $\delta T_{fast} = 60 + 90 + 150 = 300s$ and $\delta V_{fast} = 11.2 + \frac{11.2}{2} + \frac{11.2}{2} = 22.4\, mL$.

5.2.2 Extension of the Fast Sampling Method to M+1 Nodes

The philosophy of reducing the waiting time and reaction solution can be extended by further dividing the reactor volume into 3, 4 … or to any *M* equal parts by *M+1* nodes. For reaction stage *n* (T_n, $n>1$), its starting time will be counted starting from the elapsed reaction time at node *M-1* of stage *n-1* ($X_{n-1,M-1}$).

Therefore, additional time to reach reaction stage n is $\Delta T_n = T_n - X_{n-1,M-1}$ (with $n>1$). Similarly, required materials are also reduced to one volume portion (V/M). In that case, the flow rate for both educt pumps will be changed according to this volume portion (V/M) and the additional time (ΔT_n). Step by step derivation of the algorithm is shown in Table 5-2.

From node *M-1* of stage *i-1*, the additional time required to reach stage i is ΔT_i (in bold). This additional time is also the elapsed reaction time of the reaction solution at node *1* (X_{i1}) of stage i. The reaction time of solution at node *2* (X_{i2}) of this stage *(i)* now equals the reaction time at node *1* ($X_{i-1,1}$ of stage *i-1*) plus this additional time ΔT_i. It is similar for every node afterward of the stage that it has to add this additional time to reach the next node. The total working time and total reaction material for this general case are formulated and shown in equations (5-3) and (5-4), where M denotes the number of parts equally divided from the reactor. The algorithm is illustrated in Figure 5-3 with $M=3$.

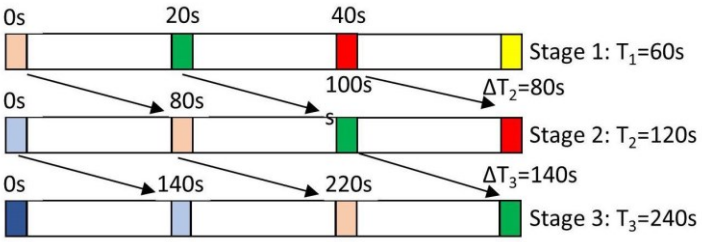

Figure 5-3: Extension of the FSM approach 1

Table 5-2: Step by step derivation of the fast algorithm with *M+1* nodes

Node 0	Node 1	Node 2	…	Node M-1	Node M
Unit: Time					
0	$\mathbf{\Delta T_1}=X_{11}=T_1/M$	$X_{12}=2T_1/M$	…	$X_{1,M-1}=(M-1)*T_1/M$	T_1
0	$\mathbf{\Delta T_2}=X_{21}=T_2-X_{1,M-1}$	$X_{22}=X_{11}+\mathbf{\Delta T_2}$	…	$X_{2,M-1}=X_{1,M-2}+\mathbf{\Delta T_2}$	T_2
0	$\mathbf{\Delta T_3}=X_{31}=T_3-X_{2,M-1}$	$X_{32}=X_{21}+\mathbf{\Delta T_3}$	…	$X_{3,M-1}=X_{2,M-2}+\mathbf{\Delta T_3}$	T_3
…	…	…	…	…	…
0	$\mathbf{\Delta T_i}=X_{i1}=T_i-X_{i-1,M-1}$	$X_{i2}=X_{i-1,1}+\mathbf{\Delta T_i}$	…	$X_{i,M-1}=X_{i-1,M-2}+\mathbf{\Delta T_i}$	T_i
…	…	…	…	…	…
0	$\mathbf{\Delta T_n}=X_{n1}=T_n-X_{n-1,M-1}$	$X_{n2}=X_{n-1,1}+\mathbf{\Delta T_n}$	…	$X_{n,M-1}=X_{n-1,M-2}+\mathbf{\Delta T_n}$	T_n

$$\delta T_{fast} = T_1 + \Delta T_2 + \cdots + \Delta T_n = \sum^{floor(\frac{n-1}{M})} T_{n-M*i} + \frac{mod\left(\frac{n-1}{M}\right)}{M} * T_1 \tag{5-3}$$

$$\delta V_{fast} = V_1 + \frac{V_2}{M} + \cdots + \frac{V_n}{M} = \frac{(M-1)V}{M} + n * \frac{V}{M} = (M-1+n) * \frac{V}{M} \tag{5-4}$$

In the SSM, the total working time and material requirement (in case the sampling replication is 1) are:

$$\delta T_{slow} = T_1 + T_2 + \cdots + T_n = \sum^{n} T_i \tag{5-5}$$

$$\delta V_{slow} = V_1 + V_2 + \cdots + V_n = n * V \tag{5-6}$$

Therefore, percentage of time and material saving of the FSM over the SSM can be represented respectively:

$$\delta T(\%) = \left(\frac{\delta T_{slow} - \delta T_{fast}}{\delta T_{slow}}\right) * 100 = \left(1 - \frac{\delta T_{fast}}{\delta T_{slow}}\right) * 100 \tag{5-7}$$

$$V(\%) = \left(1 - \frac{\delta V_{fast}}{\delta V_{slow}}\right) * 100 \tag{5-8}$$

5.3 *Approach 2*

This approach is the extension of the original idea in [136] that is presented in Section 5.1. In this extension, after the first reaction stage finishes, the flow rate of all remaining stages is set equal to that of the last reaction stage. Therefore, the total working time and reaction volume are always equal to the summation of the first and the last stage. The additional waiting time for sampling (ΔT_i) for other stages is calculated and taken in between the first and the final stage.

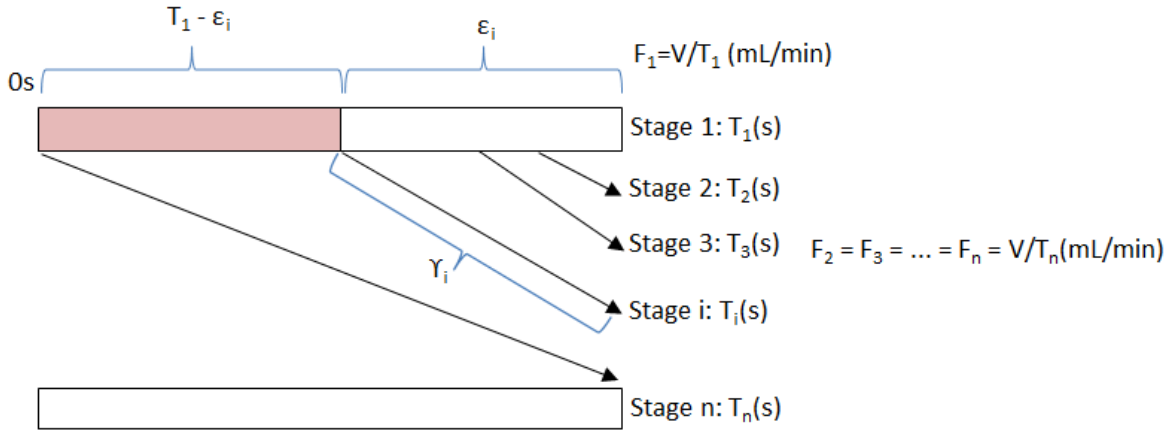

Figure 5-4: Principle of the second approach

5.3.1 *Derivation of the Additional Reaction Time from Reaction Stage i-1 to Reaction Stage i*

For realization the concept in the control software, an algorithm must be derived. The idea is to find the additional time (ΔT_i) to reaction stages T_2, T_3, ..., T_n so that the software knows when to take sampling for each reaction stage.

Call γ_i the additional time from reaction stage *1* (after stage *1* completed) to the i^{th} reaction stage.

$Q_1=V/T_1$, flow rate at reaction stage *1*

$Q_n = V/T_n$, flow rate of the last reaction stage (also equal to flow rate of other remaining reaction stages)

We have two balance conditions (refer to Figure 5-4):

+ Volume portion (V_1) filled at flow rate Q_1 for time (T_1- ε_i) + Volume portion (V_i) filled at flow rate Q_n for time γ_i = reactor volume (V).

+ Reaction time with flow rate Q_1 (T_1–ε_i) + additional time at flow rate Q_n to stage i^{th} (γ_i) = reaction stage i (T_i)

This can be expressed mathematically:

$$\begin{cases} (T_1 - \varepsilon_i)Q_1 + \gamma_i * Q_n = V \\ T_1 - \varepsilon_i + \gamma_i = T_i \end{cases} \quad (5\text{-}9)$$

$$\begin{cases} (T_1 - \varepsilon_i)\dfrac{V}{T_1} + \gamma_i * \dfrac{V}{T_n} = V & (1) \\ T_1 - T_i + \gamma_i = \varepsilon_i & (2) \end{cases}$$

Substitute ε_i from *(2)* into *(1)*:

$$(T_1 - T_1 - \gamma_i + T_i)\frac{1}{T_1} + \frac{\gamma_i}{T_n} = 1$$

with some reduction we have:

$$\boldsymbol{\gamma_i = \frac{T_n(T_i - T_1)}{T_n - T_1}} \quad (5\text{-}10)$$

Call ΔT_i the additional time from stage *i-1* to stage *i (*starting from stage *2*)

$$\Delta T_i = \gamma_i - \gamma_{i-1}$$

Therefore,

$$\boldsymbol{\Delta T_i = \frac{T_n(T_i - T_1)}{T_n - T_1} - \frac{T_n(T_{i-1} - T_1)}{T_n - T_1}}$$

$$\boldsymbol{\Delta T_i = \frac{T_n(T_i - T_{i-1})}{T_n - T_1}} \quad (5\text{-}11)$$

5.3.2 Calculation of the Total Working Time and Total Material Consumption

Similar to the first approach, total working time and total material consumption are calculated to estimate the required time and material for every run and also to evaluate the efficiency of the algorithm in comparison to other approaches.

Total working time:

$$\delta T_{fast} = T_1 + T_n$$

Total material consumption:

$$\delta V_{fast} = V_1 + V_n$$

5.4 *Testing and Results*

5.4.1 Quantification of Reduction Capability of the Algorithm

An experiment has been performed to quantify the actual reduction capability in time and materials of FSM over SSM. Six reaction stages 1, 2, 4, 7, 11, 16 min were sequentially executed in each run. SSM was repeated 3 times; FSM approach 1 was repeated 9 times (3 runs for each *M=2, M=4, M=6*) and approach 2 was repeated 3 times. Average amount of material (water) consumption and time consumption for each sampling method were measured and shown in Table 5-3 as in row "Measured". Those theoretical values were also calculated from equation (5-3), (5-4), (5-5) and (5-6) and shown in row "Estimated" in the same table in order to compare to the actual measured values. Note, in theoretical calculation, the additional volumes apart from the reactor such as capillaries, mixer, etc. were accounted for that made the reaction volume larger (11.2 mL + 0.98 mL (additional volume from capillaries, mixer, etc.) = 12.18 mL). The table also includes the percentage of reduction of FSM over SSM approach that was calculated for both theoretical values and practical values, and for both time and material consumption.

Table 5-3: Measurement of time and material consumption with slow and fast sampling method

Sampling method		**SSM**		**Existing FSM**	**FSM – Approach 1**			**FSM – Approach 2**
Number of Node - 1		-		-	M = 2	M = 4	M = 6	-
Reaction stage (min)		1, 2, 4, 7, 11, 16						
Peak per reaction stage		1	4	1	1	1	1	1
Total time consumption (min)	Estimated	41	47	32	25.50	18.25	16.83	17
	Measured	41.35	47.44	-	25.58	18.32	16.91	17.13
Reduction percentage over SSM (%)	Estimated	-	-	22.0	37.8	55.5	59.0	58.2
	Measured	-	-	-	38.1	55.7	59.1	58.6
Total educt consumption (mL)	Estimated	73.07	98	48.72	42.63	27.40	22.33	24.36
	Measured	78.33	104.20		45.17	28.50	23.33	25.33
Reduction percentage over SSM (%)	Estimated	-	-	33.3	41.7	62.5	69.4	66.7
	Measured	-	-	-	42.3	63.6	70.2	67.7

It can be seen that the estimated time and material consumption are approximate to those measured values for both sampling methods. This proves an agreement between theoretical calculation and actual performance. The physical measurement again shows an advantage in time and material of the FSM over the SSM (with one sampling per reaction stage). This can be seen by the smaller amount of time and

material consumption or the higher percent of reduction of the FSM than the SSM such as 38.1% (*M=2*), 55.7% (*M=4*) and 59.1% (*M=6*) in time with the first approach and 58.6 % with the second approach; and 42.3% (*M=2*), 63.6% (*M=4*) and 70.2% (*M=6*) in volume with the first approach and 67.7% with the second approach. However, if the SSM has more sampling repetitions per reaction stage, the average time (or volume)/peak will be reduced significantly. This is proved when 4 samples/reaction stage requires 47.43 minutes (104.2 mL) or in average, one sample requires less than 12 minutes (26 mL). This value is smaller than 18.32 minutes (27.40 mL) of the case with *M=4* in the first approach.

Between the two fast sampling approaches, the second approach requires time and materials in this case less than that of the first approach with *M = 2, 4* and similar to *M = 6*. The reduction will further increase when there are more reaction stages because to total time and material consumption do not change for the second approach. In addition, approach 2 offers a simpler algorithm, therefore, it is simpler in implementation to the software. The total working time and volume are calculated easily by adding the first and last stage. Finally, flow rate (except reaction stage 1) does not change for every reaction stage as in approach 1. This helps reduce possible disturbance and increase the reliability of the measurement.

By comparing to the existing (old) FSM, the two new FSM are more efficient with the measuring time and material less than 50%. Therefore, the two new FSM was further implemented to monitor a real chemical reaction.

5.4.2 Implementation with Acetylation Reaction

The sampling methods have been implemented in the control software and tested through the acetylation of N-DL-tryptophan (*NDL*, *MW=204.2*) using acetic acid anhydride (*AAA*) to form N-Acetyltryptophan (*NAT, MW=246.26*) with the internal standard N-Formyl-DL-tryptophan (*NFT, MW=232.24*).

5.4.2.1 First Approach of FSM vs. SSM

The acetylation reaction was measured at reaction stages 1.5 – 3 – 4.5 min using the FSM (*M=2, 4, 6*) and SSM. Detailed settings for this test can be referred to in the table of *Experiment 2* in Section 11.2. The result is represented in Figure 5-5 and Table 5-4. Sampling peaks of the reaction product (NAT) are shown in plot (a), (b) and (c) for the FSM (with *M = 2, 4, 6* respectively) and in (d) for the SSM. The table shows the average, STD and STD in % of peak areas of educt, internal standard, and product measured by those sampling methods.

In (a), (b) and (c), the density of peaks increases as *M* increases, which means more time-saving. Those waiting time are visually smaller than those of the SSM in (d). This result is in agreement with the demonstration in Table 5-4 of the previous section.

Table 5-4 provides a more detailed summary of 3 runs of each sampling method. The average peak areas reflect the common sense of a reaction that there is an increase of product formation, a decrease of reactant or educt, and a stability of internal standard when the reaction time increases. This can also be seen in Figure 5-5 by noticing on the peak height and peak width. However, there are higher standard

deviations at some measurements especially in the FSM at higher *M* and higher flow rate, for example, 23.5%, 18.0% at reaction stage of 1.5 minutes with *M=4* and *M=6* respectively. This can be caused by a significant change in flow dynamics when a sudden change from high flow rate to lower flow rate occurs. The table also indicates an acceptable similarity in peak areas among different values of *M* of the FSM and also between the SSM and FSM in their measurement. This proves the equivalent of two sampling methods. This result is relevant to the expectation that the measurement should depend on the reaction time, or sampling duration but not on the sampling method.

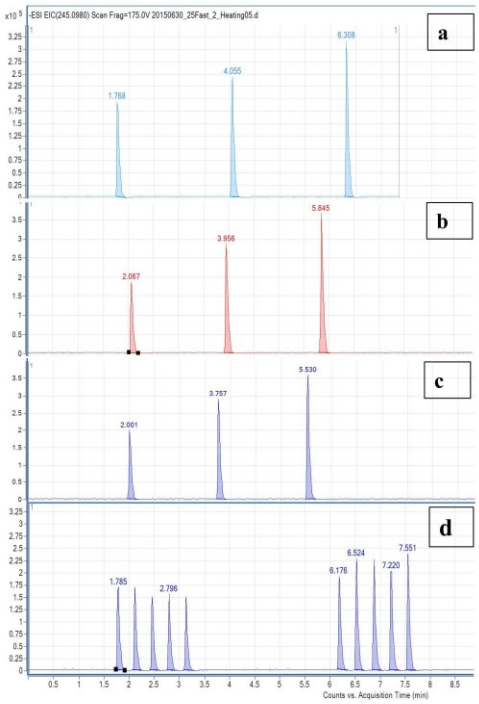

Figure 5-5: Measurement signals for the *slow* and modified *fast sampling method* approach 1 with reaction stages at 1.5, 3, 4.5 minutes: a) FSM (*M=2*) with product signal, b) FSM (*M=4*) with product signal, c) FSM (*M=6*) with product signal, d) SSM with product signal

Remarks: In theory, it is possible to number *M* up to any value, however, signal peaks from the sampling may overlap. This M_{max} depends on the time difference between two adjacent reaction stages and the peak width. It should be selected so that $\Delta T_i >$ peak width. For example, stage *i* is 60s; stage *i+1* is 70s and peak width is 21s. If $M_{max} \geq 6$, $\Delta T_i \leq 20$s, which means that peak overlapping occurs because ΔT_i (20s) < peak width (21s). Also, the flow rate may get too low for the pumps to operate accurately when *M* is high.

The accuracy of the algorithm depends on the accuracy of the pumps as well as the external physical effects to the flow. If a quick blocking of the flow due to sampling or a sudden change in flow rate does not cause a considerable change in the flow dynamics, reaction time from node to node can be added algebraically as shown in Table 5-2. In addition, due to including different flow rates in one reaction stage, the reaction time of solution at every position in the micro reactor is not so stable as in the SSM but drifts continuously. Therefore, the method is not suitable for multiple sampling. However, it is more suitable for fast data acquisition of a reaction or when there is a limitation in time and material amount.

Table 5-4: Summary for the acetylation reaction using the SSM and FSM approach 1

Slow method	Educts (N-DL)			Internal Standard (NFT)			Product (NAT)		
Reaction stage	**1.5 min**	**3 min**	**4.5 min**	**1.5 min**	**3 min**	**4.5 min**	**1.5 min**	**3 min**	**4.5 min**
Average (Abr. Unit)	1,273,243	1,326,340	1,224,797	1,030,422	1,096,525	1,092,907	532,276	652,629	944,128
STD (Abr. Unit)	189,896	41,519	18,831	122,203	28,321	19,501	32,438	45,965	21,556
STD (%)	14.9	3.1	1.5	11.8	2.6	1.8	6.1	7.0	2.3
Fast method									
M=2									
Average (Abr. Unit)	1,404,264	1,248,841	1,207,518	1,127,043	1,052,131	1,037,548	650,912	821,058	998,965
STD (Abr. Unit)	34,159	31,421	27,353	31,692	30,534	36,632	19,336	30,258	17,340
STD (%)	2.4	2.5	2.3	2.8	2.9	3.5	3.0	3.7	1.7
M=4									
Average (Abr. Unit)	1,210,125	1,201,483	1,138,898	1,064,294	1,093,723	1,054,787	846,057	999,938	1,166,445
STD (Abr. Unit)	62,586	76,100	25,643	12,038	56,185	23,512	198,558	99,923	81,241
STD (%)	5.2	6.3	2.3	1.1	5.1	2.2	23.5	10	7.0
M=6									
Average (Abr. Unit)	1,219,733	1,172,089	1,108,064	1,060,928	1,063,522	1,074,421	835,783	1,007,770	1,219,847
STD (Abr. Unit)	60,536	18,074	28,400	8,516	13,637	6,235	150,783	110,536	71,322
STD (%)	5.0	1.5	2.6	0.8	1.3	0.6	18.0	11.0	5.9

5.4.2.2 Second Approach of FSM vs. SSM

The acetylation reaction was measured at 10 reaction stages (1 – 2 – 3 – 4 – 5 – 6 – 7 – 8 – 9 – 10 min) using the FSM approach 2 and the SSM. Detailed settings for this test can be referred to in the table of *Experiment 3* in Section 11.2. The result is represented in Figure 5-6, Figure 5-7 and Table 5-5. Measurement with the FSM and its plots are shown in Figure 5-6 and Table 5-5 for the educt, internal standard and product respectively. And the table shows the average, STD and STD in % of peak areas of the educt, internal standard, and product of 3 runs with SSM and 5 runs with FSM.

The result is logical with an increase of the product, decrease of the educt and quite stable of the internal standard in both SSM and FSM. Figure 5-7 also compares the SSM and FSM visually. Both methods show good agreement with the other. This agreement is reflected in the table as the average peak area of every reaction stage of both methods are approximately similar. However, closely look at the STD in the table for the SSM, there is an abnormal issue that makes their STD high up to 32%. The first peak in each sampling series is smaller than the rest due to a sudden drop of the baseline after the first sampling (Figure 5-8a). The situation occurs with the current system when using acetic acid as a solvent. It does not happen when using MeOH, ACN, or ACN/H_2O as solvents (Figure 5-8b) or when the HPLC system is

used for sampling solution with acetic acid solvent (Figure 5-8c). So far, we have no explanation for this issue.

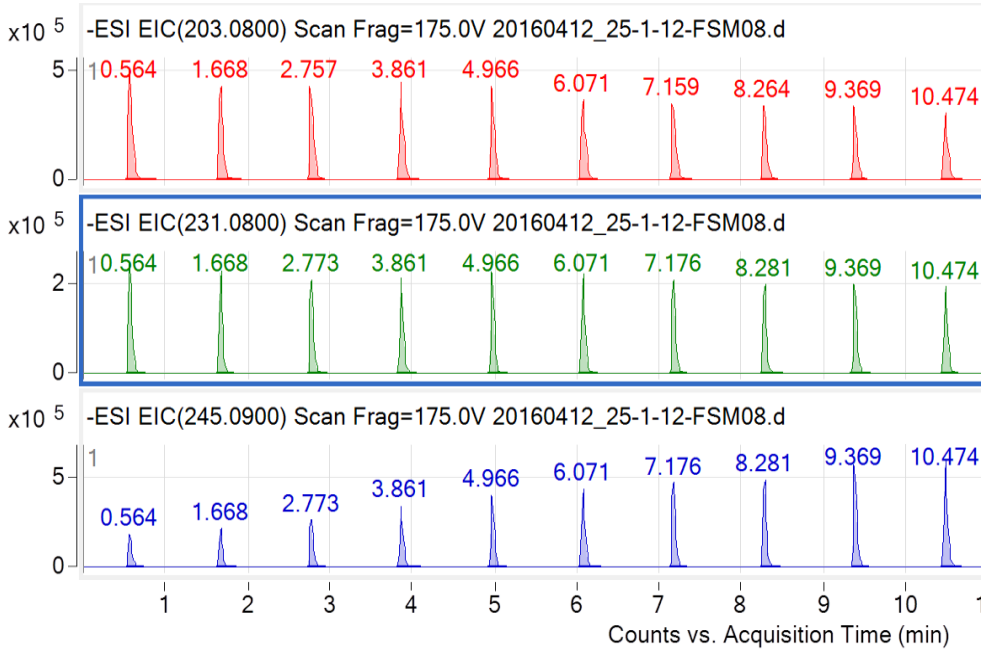

Figure 5-6: Measurement signals of educt, internal standard and product with the FSM approach 2: red curve is signal of the educt; green curve is signal of the internal standard; blue curve is signal of the product

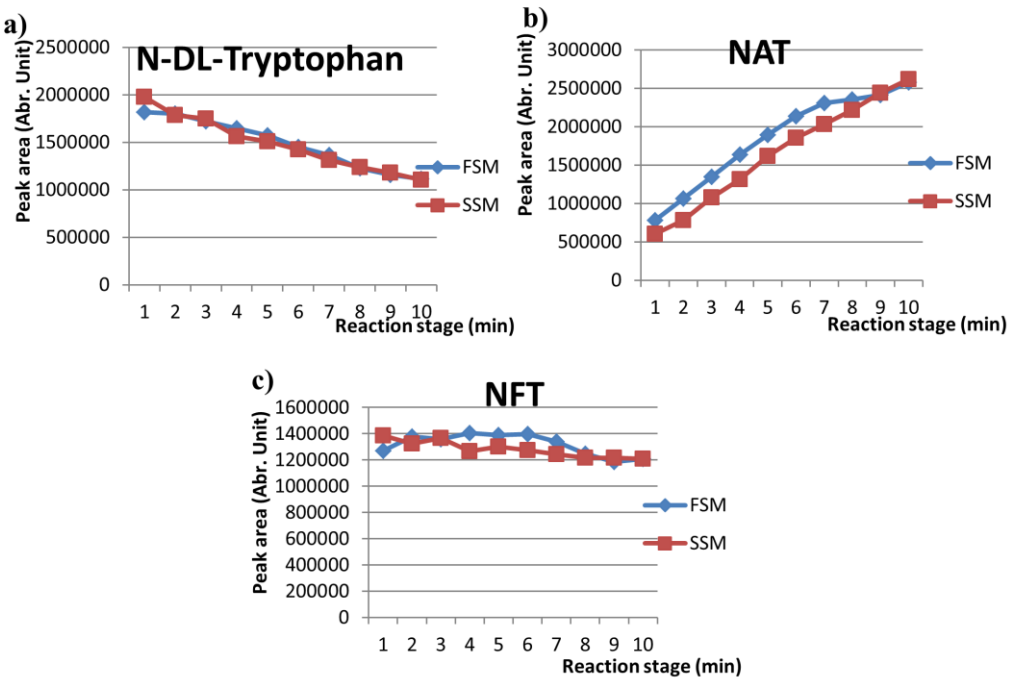

Figure 5-7: Plots of educt (a), internal standard (b) and product (c) with the FSM approach 2 vs. SSM

Table 5-5: Summary for the acetylation reaction using the SSM and FSM approach 2

	FSM			SSM			FSM			SSM			FSM			SSM		
	N-DL-Tryptophan						NFT						NAT					
Stage (min)	Average	STD	STD in %	Average	STD	STD in %	Average	STD	STD in %	Average	STD	STD in %	Average	STD	STD in %	Average	STD	STD in %
1	1,816,997	65,245	3.6	1,981,060	217,129	11.0	1,269,361	75,239	5.9	1,387,976	202,986	14.6	777,607	25,127	3.2	603,800	56,112	9.3
2	1,803,280	86,938	4.8	1,784,482	266,526	15.0	1,377,832	100,153	7.3	1,323,534	272,473	20.6	1,061,485	64,678	6.1	779,690	84,190	10.8
3	1,724,704	62,646	3.6	1,750,527	308,238	17.6	1,357,502	82,668	6.1	1,365,372	352,098	25.8	1,344,938	89,221	6.6	1,077,592	190,408	17.7
4	1,648,366	58,095	3.5	1,563,922	218,733	14.0	1,406,139	116,668	8.3	1,268,450	263,580	20.8	1,634,494	152,210	9.3	1,311,669	178,659	13.6
5	1,576,215	85,890	5.5	1,510,427	255,210	16.9	1,388,178	116,684	8.4	1,301,476	315,564	24.3	1,893,852	157,195	8.3	1,619,244	236,376	14.6
6	1,454,011	19,959	1.4	1,424,123	262,378	18.4	1,396,323	26,425	1.0	1,273,852	328,114	25.8	2,137,071	44,155	2.1	1,851,415	274,292	14.8
7	1,366,333	52,197	3.8	1,312,932	252,309	19.2	1,338,072	72,889	5.5	1,244,141	341,715	27.5	2,309,483	108,045	4.7	2,032,306	329,751	16.2
8	1,228,540	56,142	4.6	1,237,094	269,785	21.8	1,246,551	63,277	5.1	1,215,054	390,032	32.1	2,356,421	108,260	4.6	2,215,963	464,874	21.0
9	1,161,037	55,994	4.8	1,178,138	209,978	17.8	1,184,948	103,374	8.7	1,216,209	324,086	26.7	2,411,995	191,519	7.9	2,440,708	397,847	16.3
10	1,116,191	18,406	1.7	1,106,721	210,030	19.0	1,210,559	67,494	5.6	1,207,132	346,931	28.7	2,578,639	128,860	5.0	2,619,771	470,836	18.0

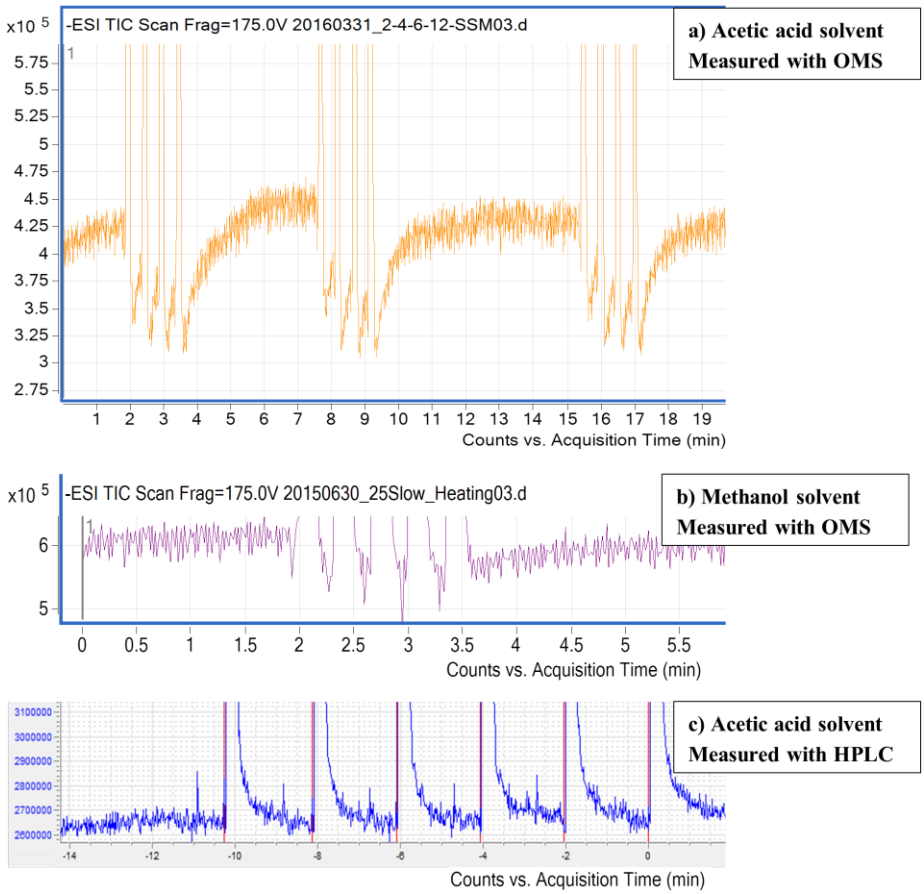

Figure 5-8: a) first smaller peak with acetic acid solvent measured by the ORMS, b) peaks are normal with methanol solvent, c) peaks are normal with acetic acid solvent measured by an HPLC system

5.5 *Summary*

Two sampling approaches for fast sampling are presented for saving time and material consumption of a reaction series. Both of them fulfill this purpose. The first approach is more complicated than the second approach in the algorithm. In addition, the first approach includes different reaction flow rates for every reaction stage which may cause the measurement unreliable. Therefore, the second approach is more preferred for implementation in the control software.

In general, the SSM with multiple sampling capabilities is more economical in measurements that require sampling repetitions. Meanwhile, the FSM is more suitable for fast data acquisition of a reaction or when there is a limitation in time and material amount.

CHAPTER 6 INTEGRATION OF THE HEATING MODULE

6.1 *Overview*

Temperature has significant effects on many physical, chemical and biological processes. It impacts on the reaction rate through the number of high energy molecules as well as their collision probability. An increase in temperature causes molecules to move faster, therefore, improves the mixing efficiency of reagents. An accurate control of temperature is therefore very important in managing reaction rate and improving product purity. In smaller scale applications, temperature is further used to modulate electrophoretic mobility for detection of low-concentrated species in small volume or to drive particles in microfluidic devices [138]. Some applications of temperature in biology include keeping cells alive by maintaining constant temperature [139]; controlling temperature cycling for Polymerase Chain Reactions [140]; or to drive droplets in droplet-based microfluidic applications in which the droplets are considered as discrete biological reactors [141].

Heat can be transferred by conduction, convection or radiation process [142]. Conduction takes place when heat is transferred through a stationary medium; convection mode is when heat is transferred between a moving fluid and a surface. And radiation occurs when heat is transferred in form of electromagnetic waves. The control of temperature profile in micro reactors includes *homogeneous temperature regulation*, which attempts to create a homogeneous heat on a controlled surface, and *temperature gradient* (or *linear temperature profile*), which creates a temperature gradient over the controlled surface. Different techniques have been implemented to achieve the heating/cooling purpose. They are listed in the below table:

Table 6-1: Different heating methods

Heating Methods			
External Heating	**Integrated Heating**		**Electromagnetic Radiation**
	Joule Heating	**Chemical reaction**	
Preheated liquid, Peltier elements	Electric current passes through the conductor	Endothermic and exothermic processes	Microwaves, laser

External heating includes the use of preheated liquids [143] or commercial components [144] as the external heating sources. Liquids are heated and circulated through a micro reactor for heat exchange or a micro reactor is in contact with Peltier elements or a heating/cooling plate. The integrated heating method exploits the heat diffusion from the integrated heating sources such as Joule heating [145] and chemical reaction [146]. The Joule heating method employs heating resistors embedded in a micro reactor system and the chemical reaction heating uses energy consumed/generated by an endothermic/exothermic process for heat exchange with the solution in the microfluidic channels. In these techniques, heat transferred is dominated by convection and conduction. Finally, the non-contact delivery energy approach uses electromagnetic radiation such as microwaves [147] and laser [148] for the heating purpose. These techniques employed the heat radiation process.

6.2 *Derivation of Parameters for the PID Controller*

The heating method applied in our system is the external heating method that uses preheated oil circulating around the micro reactor for heat exchange (Figure 6-1). The Julabo heating device, with 2000W heating capacity and *PID* control, has two operating modes: the internal control mode uses a sensor located in the circulator bath as a feedback signal to control temperature of the heating solvent; and the external control mode uses signal from the PT100 located at the micro reactor output to control temperature of the reagent/analytical solution.

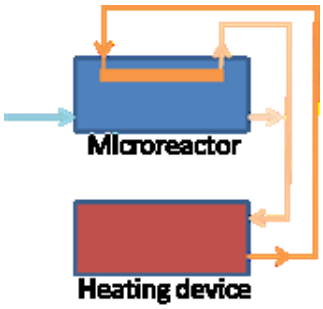

Figure 6-1: External heating configuration

Both the internal and external heating modes are able to bring a reagent solution to a desired temperature. However, the external mode was selected as a main heating mode due to its capability to quickly and precisely bring the solution's temperature to steady state. The possibly big gap in temperature between the heating solvent and the setpoint allows compensating for heat requirement from the metallic reactor block and heat loss as well as boosting the thermal transmission between materials. However, this mode may also cause high-temperature overshoot to the reagent solution. Meanwhile, the internal mode, which is safer but slower, can be used for preheating the reactor.

For the Julabo F26-HP in the laboratory, the *PID* controller works well with the internal control mode as the heating solvent reaches the setpoint fast with no overshoot. However, in the external control mode, the system is sluggish that it takes >10 mins to heat up 10^{o}C for a solution in micro reactor. Therefore, Ziegler-Nichols tuning method is applied to this closed-loop system. The procedure is presented [149]:

- Remove the integral and derivative action, in this case, by setting the *integral time constant* to its maximum value *(T_n)* and the *derivative time constant* to its minimum value *(T_v)*.
- *Proportional gain (K_c)* will be tuned so that the response will oscillate constantly as shown in Figure 6-2.
- Determine the *ultimate proportional gain* (K_u) and *ultimate period of oscillation (P_u)*.
- Determine parameters for the *PID* controller based on Table 6-2. If a *P* controller is used, only K_c is derived following the second row of the table. If a *PI* controller is preferred, K_c and T_n can be derived following the third row of the table. And the last row is for deriving parameters of the *PID* controller.

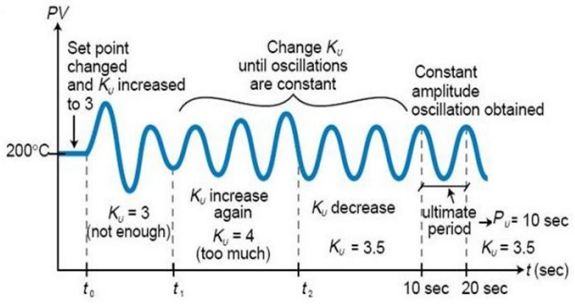

Figure 6-2: System tuned using the Ziegler-Nichols method [81]

Table 6-2: Closed-loop calculation of K_p, T_n and T_v

	K_c	T_n	T_v
P	$K_u/2$		
PI	$K_u/2.2$	$P_u/1.2$	
PID	$K_u/1.7$	$P_u/2$	$P_u/8$

This procedure is then applied to the Julabo circulator. There is a slight difference in the notation of *PID* parameters used in the Julabo circulator and those commonly used. In this case:

- $X_p=100/K_c$: *Proportional band* (X_p)= inversion of the *proportional gain* (K_c) times *100.*

The parameter set in the device for an oscillatory response is $X_p=0.1;\ T_n=5000;\ T_v=0$. The system response is shown in Figure 6-3. From the response, the *ultimate proportional band* (X_p) and *ultimate period of oscillation* (P_u) is found ($X_u=100/K_u=0.1$ *or* $K_u=1000$ and $P_u=60$). In this case, the *period of oscillation* is determined by looking at the power signal (green line) but not the reagent solution temperature because it is not as clear as the power signal. It can be seen that the power oscillation is not constant but damping. However, it is selected because that is the minimum proportional band that the system can reach. After that, implementing Table 6-2 gives the sets of parameters for the controller.

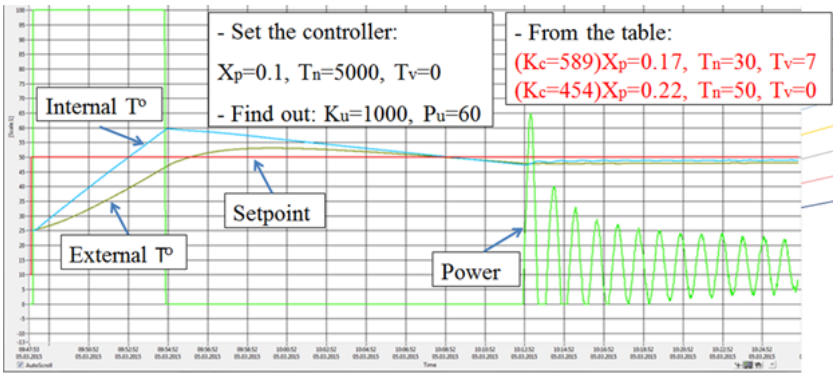

Figure 6-3: Oscillatory response of the system for derivation of PID parameters

The found sets of *PID* parameters (X_p=*0.17,* T_n=*30,* T_v=*7*) and *PI* parameters (X_p=*0.22,* T_n=*50,* T_v=*0*) were applied to the Julabo circulator. Large overshoot was observed with those values. Therefore, a fine tuning is necessary. Due to its simplicity and popular usage in industrial control, the *PI* scheme was selected for fine tuning. The *proportional gain* (K_c) was reduced (or increase the *proportional band* X_p) and the *integral time constant* (T_n) was increased. The chosen set of parameters was X_p=*0.4-0.6,* T_n=*100-150,* T_v=*0*. System temperature response with some sets of *PID* parameters is shown in Figure 6-4.

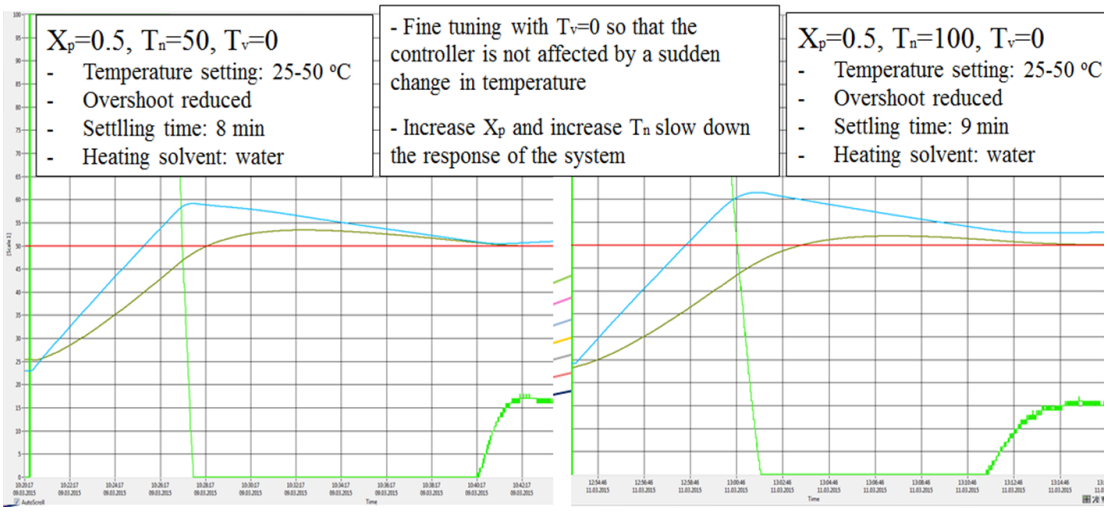

Figure 6-4: System response to different sets of PID parameters

As can be seen, the heating solvent temperature (blue curve) is higher than of the reagent solution (olive green curve) to compensate for heat loss and heat requirement by the reactor. Temperature of reagent solution reaches the setpoint (red curve) with low overshoot. The steady state is maintained with no oscillation of the input power (green curve).

6.3 *A Simplified Modeling of the Heating Problem*

The heat transfer problem is simplified as the model shown in Figure 6-1. Due to a huge mass difference between the reactor metal block (2,200g) and the analytical (reagent) solution (V=*11.2mL* ≈ *11.2g*), it is assumed that the outflow solution can reach to the temperature setpoint only when the reactor block has reached to that temperature. Therefore, the problem is simplified to heating a solvent that circulates around a metal block.

The heating solvent is powered by the heating coil, which can supply maximum 2000W power. The *PID* controller manipulates the heating power. Temperature of the heating solvent (T_{hs}) is a function of time that depends on the heating time (t) and heating power $u(t)$ as in equation (6-1). Temperature of the heating solvent can also be derived directly from the data obtained from the temperature response of this heating solvent.

$$T_{hs}(t) = \int_0^t 0.2 * u(t)dt \tag{6-1}$$

With *0.2: actual heating rate of the heating solvent (oil) when heating power is 100% ($^oC/s$)*
u(t): heating power (%)

Energy required by the reactor block to increase its temperature by 1 degree (Q_R).

Properties of the micro reactor:
Material: Stainless steel 316
*Specific heat: 0.5 kJ/(kg*K)*
Density: 7.99 g/cm^3
Thermal conductivity k_w: 16.2 W/(m.K)
Mass: 2200g

$$Q_R = m * C * \Delta T = 2.2 * 0.5 * 1 = 1.1\ kJ = 1100\ J$$

The heating solvent gives energy and the metal block receives energy. Heat transfer rate is calculated as:

$$Q_T = U * A * \Delta T$$

U: Total heat transfer coefficient - W/(m^{2o}C)
A: contact area of the fluid and the metal surface – m^2
ΔT: temperature difference between them - ^oC

The heat transfer rate in this situation is dominated by the convection (from heating fluid to the reactor) and conduction process (heat conduction in the reactor). Total heat transfer coefficient *U* in this case:

$$\frac{1}{U} = \frac{1}{h_h} + \frac{L_w}{k_w} = \frac{1}{170} + \frac{0.01}{16.2}$$

$$U = 154\ \frac{W}{m^2\ ^oC}$$

h_h: convection heat transfer coefficient from Oil to stainless steel: 60-1800 W/m^{2}K: select 170
L_w: thickness of the micro reactor metal block: 10 mm=0.01m
k_w: Thermal conductivity - 16.2 W/(m.K)

Contact area $A = n * a * b = 2 * 0.1 * 0.1 = 0.02\ m^2$ (*a, b* are the length and width of the reactor; *n* is the two reactor surfaces that contact with the heating fluid.

Therefore, the heat transfer rate (Q_T) between the heating solvent and the reactor when $\Delta T = 1\ ^oC$ can be estimated

*154*0.02*1= 3.08 J/s.*

Total energy transfered from the heating solvent to the reactor (Q) over time

$$Q = \int_0^t 3.08 * \Delta T(t)dt$$

With *ΔT(t)* is the temperature difference between the heating solvent (T_{hs}) and the reactor (T_r):

$$\Delta T(t) = T_{hs}(t) - T_r(t) = T_{hs}(t) - \frac{Q(t)}{1100}$$

Substitute for the above equation, we have

$$Q = \int_0^t 3.08 * (T_{hs} - \frac{Q}{1100})dt$$

This can be solved in the discrete time domain

$$Q_k = \sum_{k=0}^{t} 3.08(T_{hs,k} - \frac{Q_{k-1}}{1100}) \quad (6\text{-}2)$$

The model has been implemented to simulate the temperature response of the analytical solution according to the heating solvent input (Figure 6-5). The upper figure is the real measurement data from the circulator with the red curve is temperature of heating solvent (input) and the blue curve is temperature of reagent solution (output). By estimating input data as a polynomial using Excel or Matlab, temperature of the reagent can be estimated according to equation (6-2) as shown in the lower part.

A further idea for this model is to integrate the *PID* controller for feedback control. The controller will manipulate the heating power which influences the heating solvent and, as a consequence, the reagent solution. Temperature of the reagent solution is compared with the set temperature for the error (difference). This error is fed to the controller for modifying the heating power.

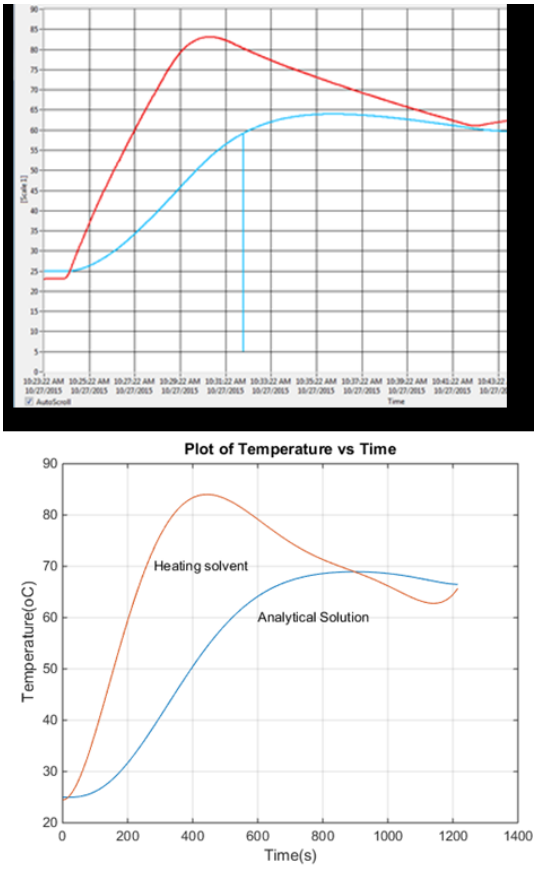

Figure 6-5: Temperature response of the real system (upper) and temperature response from model simulation (lower)

6.4 *Selection of Suitable Heating Schemes*

The new *PID* parameters for the external control mode help the solution reach the setpoint faster. However, the heating rate is still small and a further improvement is required. Therefore, different heating configurations were attempted for possible improvements and the results are summarized in Table 6-3. For homogeneous testing condition, oil (Thermal H10, Julabo, Seelbach, Germany) is used as the heating solvent. The flow rate of solution (water) in micro reactor is fixed at 4 mL/min. The temperature test range is selected between 20^{o}C to 55^{o}C.

The first configuration (*a*) uses only the Julabo with its original configuration in which the heating stream is circulated around the Julabo and heat exchanger of the micro reactor (Figure 6-6a). This configuration gives a heating rate about 4.29^{o}C/min. When there is insulation of tubes and the reactor (*b*) for reducing heat loss, the heating rate is slightly improved to 4.37^{o}C/min (Figure 6-6b). An addition of 3x25W resistors (*c*) indirectly on the micro reactor via an aluminum plate under its base further improves the heating rate to 4.7^{o}C/min (Figure 6-6b). A simple removal of the curvature connectors in the tubing system (*d*) helps increase the heating rate remarkably because flow rate through the heat exchanger is enhanced (Figure 6-6c). The heating rate in this case is at 4.85^{o}C/min. However, changing to soft tubes (instead of metal tubes) with similar length (*e*) decreases the heating rate to 4.37^{o}C/min due to its high specific heat capacity that absorbs heat from the flow. In configuration (*f*), the whole micro reactor block including its base is placed on a heating plate (EKT Hei-Con, 800W, Germany) (Figure 6-6d). The heating plate with high power capacity is responsible for initial heating of the micro reactor. It is turned on for 3.5 minutes to supply initial aid for heating. Heat is transferred from the heat source through the base plate, the aluminum plate and finally to the reactor. In combination with the Julabo, it is expected to increase the heating rate significantly, however, the heating rate is only at 5.38^{o}C/min. The inefficient heat transfer between the base plate surface, which is not flat but has grooves, and the aluminum plate, and between the aluminum plate and the micro reactor is one of the reasons. In addition, the *PID* controller of the Julabo reduces its power when the heating rate is fast enough in order to avoid overshooting in temperature response. Moreover, the cooling rate of the system is decreased because this heating plate does not have a cooling function and heat is stored in the base plate of the micro reactor. The EKT is replaced by the NeoLab heating plate (400W, NeoLab) for its capability of communication to computers (*g*). Temperature setpoint for the heating plate is the same as for the Julabo. In this case, the heating rate is at 5^{o}C/min but experienced the slow cooling as reasoned above. An integration of another heating/cooling plate (Cole-Parmer, 50W) (*h, k*) slightly improves both the heating rate (5^{o}C/min) and cooling rate (1.03^{o}C/min). This configuration is observed later to help stabilize the temperature reading of external sensor from flow rate fluctuation in micro reactor better than in the case of the standalone Julabo. The reason is that both the upper and lower surfaces of the micro reactor are heated so that a homogeneous temperature condition over the whole micro reactor is achieved.

The last three concepts use the heating circulator from another manufacturer (Huber, Offenburg, Germany) (*l, m, n*). The Huber MiniStat 125 with 1,000W heating capacity and only internal control mode has the worst performance of all the configurations (1.79^{o}C/min in heating). The more advanced

device, Huber Tango, with 1.5kW (at 230V) and 3kW (at 400V – not tested) performs superior to the Julabo in cooling (2.6°C/min) but worse in heating (4.37°C/min). Further reducing the transmission hoses from 2m to 0.5m helps slightly increase its performance (heating: 4.67°C/min; cooling: 2.9°C/min).

In all tested configurations, the application of the Huber thermostat offers the optimal performance in heating and cooling. The technology applied with this method does not heat/cool the complete heating solvent as with the Julabo F26-HP, instead, the solvent with low self-heating capacity is heated/cooled inline. However, this Huber device has a large size, which makes it not really suitable for the current construction. Therefore, configuration (h) is chosen for further integrated into the control software and tested with chemical reactions.

Table 6-3: Different configurations for heating/cooling

Schemes	Notes	Temperature range (°C)	Time (min)	Heating rate (°C/min)	Cooling rate (°C/min)	Controllable by software
Julabo (a)		30	7	**4.29**		**Yes**
Julabo+Insulation (b)		35	8	**4.37**	35/37=**0.946**	**Yes**
Julabo+Power resistor+Insulation (c)	Resistors: 3x25W=75W	33	7	**4.7**		**Yes**
Julabo+Removal of lower curve tubes (d)		34	7	**4.85**	35.3/39=**0.93**	**Yes**
Julabo+Soft tubes (e)		35	8	**4.37**		**Yes**
Julabo+Heating plate (EKT Hei-Con) (f)	800W Heating plate setpoint: 150°C Turn ON in 3.5 minutes	35	6.5	**5.38**	35/40=**0.875**	Heating plate: **No**
Julabo+Heating plate (NeoLab) (g)	400W Heating plate setpoint = 55°C	35	7	**5**		**Yes**
Julabo+Cole-Parmer Heating/Chilling Plate (h)	50W Heating plate setpoint = 55°C	35	7	**5**	36/35=**1.03**	**Yes**
Julabo up to micro reactor level+Cole-Parmer (k)	50W Heating plate setpoint: 55°C	35	7.5	**4.67**		**Yes**
Huber MiniStat 125 (l)		25	14	**1.79**		**No**
Huber Tango (m)	2x2m hoses	35	8	**4.37**	34/13=**2.615**	**Yes**
Huber Tango (n)	2x0.5m hoses	35	7.5	**4.67**	35/12 =**2.9**	**Yes**

6.5 *Integration into the Control Software*

For automatic operation, the heating module has been integrated to the ORMS control software. The GUI is shown in Figure 6-7. It contains 3 buttons for temperature settings; turn on and turn off the heating devices (Julabo circulator and Cole Parmer heating/cooling plate). Additionally, the current status of the heating module is indicated such as internal temperature, external temperature, status (ON/OFF/ERROR).

The module has two modes of operation, manual and automatic heating mode. In manual heating mode, pressing the preheat button, the internal heating mode is used. The main purpose of this button is to condition temperature for the metal block while the operator is busy with sample preparation tasks. The internal control mode is chosen for safety reason. When the reagent solution is in standstill, its temperature changes slowly. Therefore, temperature at the external sensor changes slowly too. If the external mode was selected, the controller had to increase power to the heating solvent to accelerate the heating process. This would cause a large difference in temperature between the reagent and heating solvent, which is not desired.

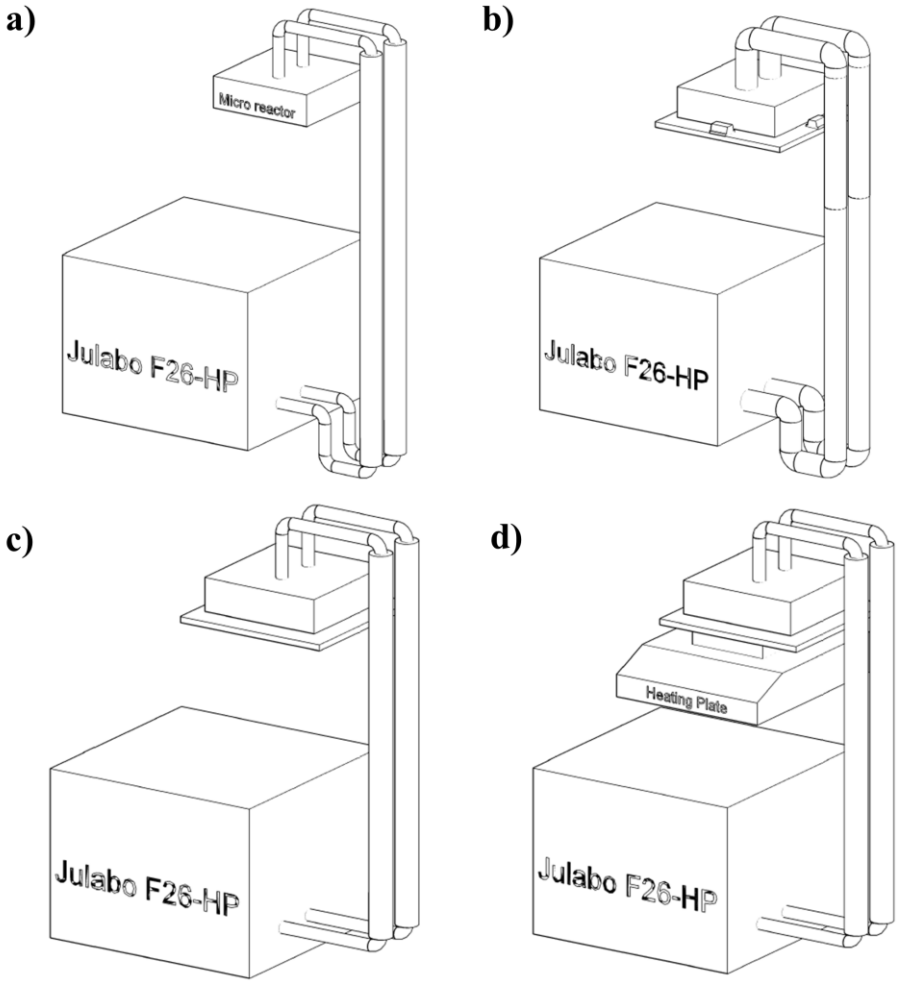

Figure 6-6: Different Heating configurations: a) initial configuration of Julabo circulator and micro reactor, b) insulation was installed on the piping system and micro reactor; later, 3 resistors was applied indirectly to the micro reactor, c) curvature connectors was removed from the piping system, d) a heating/chilling plate was installed for additional heating/cooling

The heating module changes to automatic heating mode after the temperature is set and the *automatic operation mode* is triggered. Figure 6-8 shows the algorithm for both heating and cooling when the automatic operation mode is selected. In general, the controller is switched to the external heating mode and the educt pumps P_1, P_2 are set to a certain flow rate to wait for temperature of the reagent solution

close to the setpoint (to save materials). The reaction series is triggered when the reagent's temperature is within ±2°C around the setpoint.

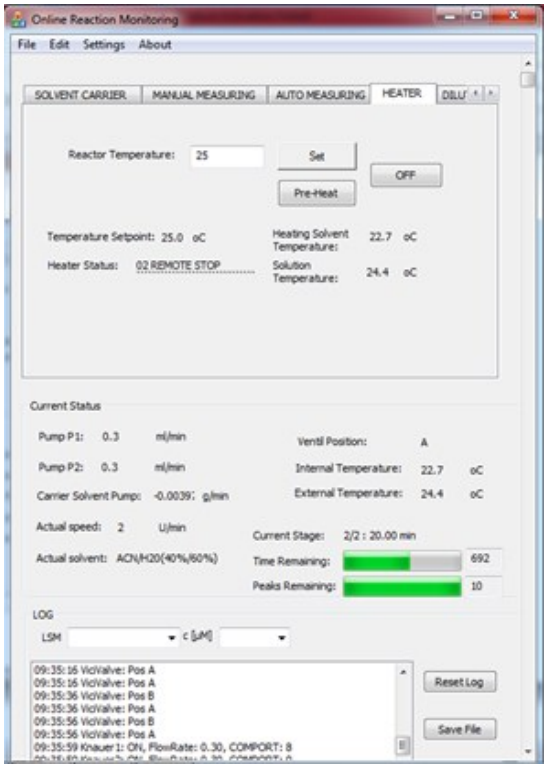

Figure 6-7: GUI of the heating module

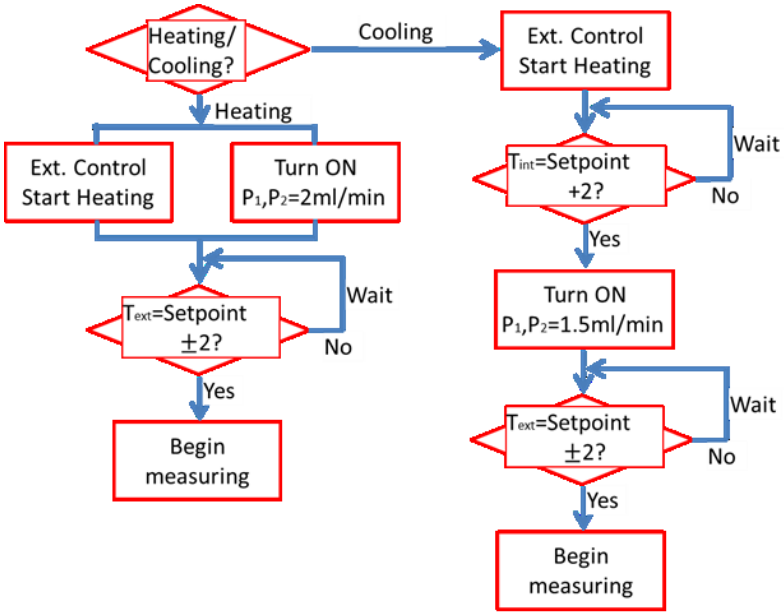

Figure 6-8: Algorithm for Heating/Cooling in automatic measuring mode

6.6 *Testing and Results*

Again the acetylation of N-DL-tryptophan (*MW=204.2*) using acetic acid anhydride (AAA) to form N-Acetyl tryptophan (NAT, *MW=246.26*) with the internal standard N-Formyl-DL-tryptophan (NFT, *MW=232.24*) was performed. Materials and equipment settings are presented in *Experiment 4* in Section 11.2. The reaction was measured at 1.5 – 3 – 4.5 min at 25°C and 55°C using the FSM approach 1 and SSM. The results are plotted in Figure 6-9.

The effects of different reaction temperatures and reaction time on chemical reactions are shown in Figure 6-9. The stability of the internal standard (NFT) with time and temperature is confirmed (plot a). All measured signals (peak areas) are equivalent to each other (with 2.8% deviation). The signal intensity of educt (N-DL-Tryptophan) decreases by increasing reaction time from 1.5 min – 3 min – 4.5 min. There is a significant difference in educts consumption between 25°C and 55°C as shown in plot (b). At lower temperature, fewer educts are consumed (or more educts remains) which results in higher peak areas than at 55°C. The opposite trend is observed for the product N-Acetyl tryptophan (NAT) as in plot (c). The signals are growing with increasing reaction time and temperature.

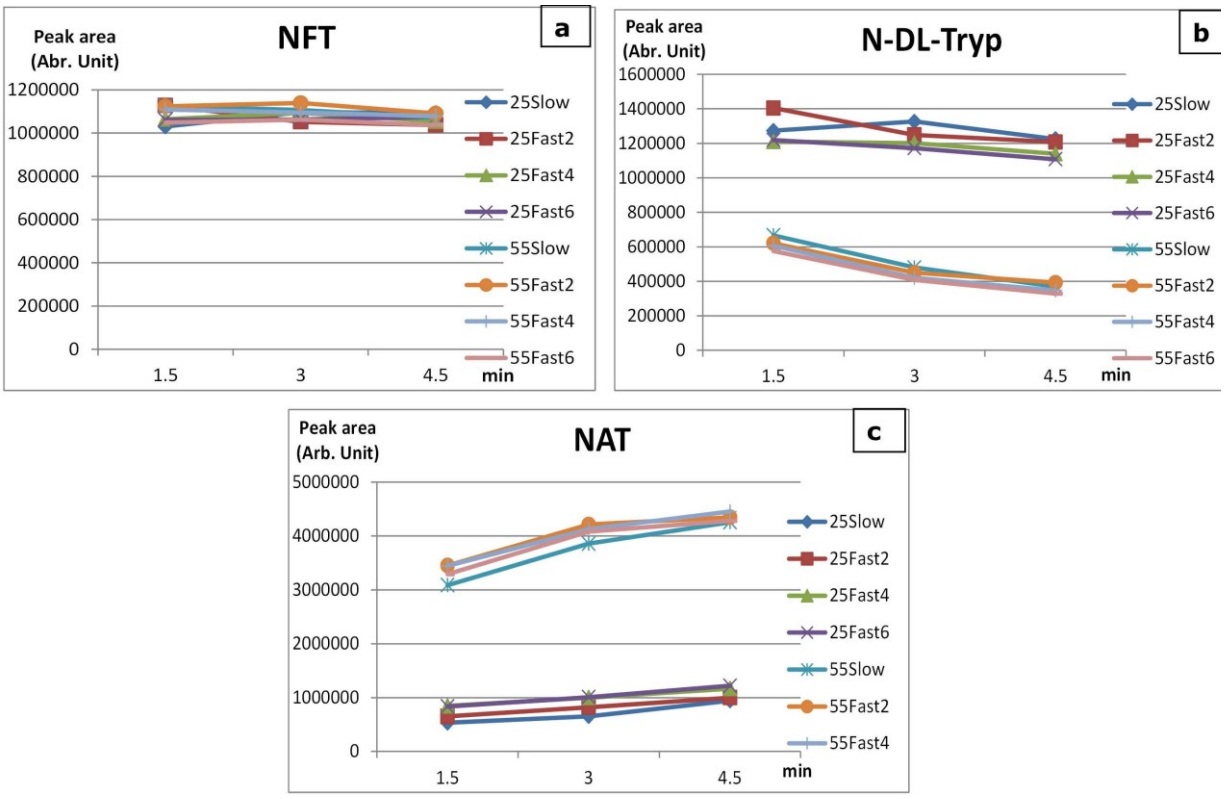

Figure 6-9Measurement results of acetylation reaction according to reaction time (1.5, 3 and 4.5 min) and temperature (25°C and 55°C) using *SSM* and *FSM* (M=2, 4, 6): a) internal standard, b) educts, c) product

These plots also compare the system performance between the SSM and the FSM approach 1. In the FSM, measurements with *M=2* give similar results to those measured with *M=4* and *M=6* with standard deviations at 25^{o}C in the range of 1.41% – 11.53% and 1.64% – 7.57% at 55^{o}C. Those results of FSM are similar to results measured by the SSM with standard deviation in the range of 1.77%-18.40% and 1.77%-6.70% at 25^{o}C and 55^{o}C respectively. The relevance of both methods is indicated in the plots via groups of lines that represent effects of time and temperature on a reaction.

6.7 *Summary*

Although different heating configurations have been attempted, the heating performance remains unsatisfied. It takes a long time to increase solution temperature in the micro reactor (7, 8 minutes for $\Delta T=35^{o}C$). Some of the possible reasons are:

- Heat required by a large quantity of the heating solvent (4.5L).
- Heat required by the micro reactor block (2,200g)
- Small inlet/outlet size of the micro reactor, which reduces flow through the heat exchanger for an efficient heat exchange.

However, the module is able to condition temperature of reagent in the micro reactor to a setpoint. Both heating modes (internal/external) have been exploited to compromise between the heating speed and safety. Finally, a chemical reaction was performed to demonstrate the influence of temperature on reaction kinetics.

CHAPTER 7 DILUTION MODULE

7.1 *Overview*

Sample overloading due to the high molar concentration of reaction mixtures is a further important issue in online monitoring of chemical reaction. The problem causes an excitation of the detector operation range associated with a detector overload and a shorter detector lifetime. This also may result in the contamination of the mass spectrometer and in distorted mass spectra [150][151].

For solving this problem, there are two major approaches: modification of the ionization techniques and dilution of the analytical solution. The introduction of ionization techniques such as low temperature plasma (LTP), extracted electrospray ionization (EESI), and direct analysis in real-time (DART) shows their capability to analyze chemical reactions at molar concentrations [107]. However, a more flexible approach is to dilute the analytical solution, which comprises the precise metering of two or several solutions, followed by mixing [152]. The dilution can be based on the ratio of input flows such as dilution by variation of the flow rate [153], frequency [154], time [152], or based on the ratio of volume [155]. For high dilutions up to 100, 200, 500, 1,000, in addition to serial dilution, another dilution method is to use an Active Splitter or Mass Rate Attenuator (MRA), which can reach a dilution ratio up to 100,000. Some of the dilution works are presented.

CLINTON ET AL. used a microporous membrane interface to achieve high dilution ratios ($\frac{\text{initial volume}}{\text{final volume}}$) [156]. A donor solvent containing the sample was pumped to waste through the groove on one side of the membrane interface. Acceptor solvent was pumped through the other side of the membrane in the opposite direction into an atmospheric pressure chemical ionization-quadrupole mass spectrometer (APCI-MS). A dilution ratio of approx. five orders magnitude was achieved for the Michael addition reaction of phenylethylamine (PEA) and acrylonitrile in ethanol. However, the analytical response was influenced to changes in pressure and flow rate of the donor and acceptor solvents. DELL'ORCO ET AL. reported the application of HPLC pumps and a flow splitter to dilute the concentration of the reaction mixtures by approximately 3,000 times [150]. The delay time in this configuration was 4-6 minutes for the sample introduction to the mass spectrometer. However, this is not a true “dead” time since the reaction was quenched by the diluting agent. The important reaction intermediates and reaction kinetic time scale were identified although quantitation of these species was still problematic. Using also HPLC pump and splitter coupled with an atmospheric pressure chemical ionization mass spectrometry (FIA/APCI-MS), ZHU ET AL. has reported to have quantitative real-time monitoring of a model reaction performed at 1.63M level, a concentration often required by process control [107]. The incorporation and step by step testing of an automatic internal sample injector, a post injection splitter, an ion-transport capillary and an optional FIA solvent modifier were performed. And, the corresponding consequence was the increment of the upper-limit of solution concentrations that were still in the linear dynamic range of the spectrometer. It can also be observed in this work (from Figure 7-1) that for different concentrations and flow rates of the analytical solution, the linear dynamic range of the mass spectrometer is not the same. For example, with undiluted solution and flow rate of 1 mL/min, the upper-limit of linearity for

peak area of the extracted ion profiles (XIPs) is larger than 2.0e+7 (curve A); with 1:10 splitting ratio, the corresponding value is less than 5.0e+6 (curve B); and with 1:100 splitting ratio, this value is around 2.5e+6 (curve C).

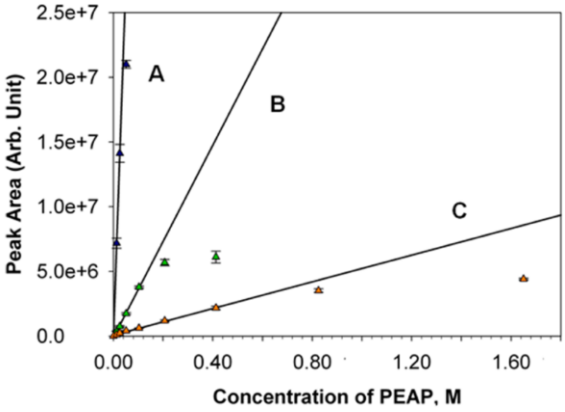

Figure 7-1: Linear dynamic range for splitting ratio [107]

7.2 *Selection of Dilution Scheme for Integration to the System*

For our system, different dilution concepts have been proposed and tested [157].

(1) Post-Sampling Dilution: In this configuration, flow from a dilution pump is added to the carrier solvent flow (from pump P_3) right after the multiport valve via a T-mixer (Figure 7-2a). Due to the possible smaller pressure of pump P_3, a check valve is added before the multiport valve to avoid back pressure. Dilution ratio is adjusted via flow rate variation of dilution pump only (additive mixing) or of both dilution pump and carrier solvent pump (relative mixing) to have a constant total flow rate to the mass spectrometer. The concept is simple because only one pump is required additionally for dilution. Different testing shows that the additive mixing configuration could work well at lower flow rate of pump P_3. However, the configuration is only suitable for low dilution ratio due to limitation of flow rate to the analyzer and of pump accuracy. In addition, there is high potential of long tail of detected peaks because the mixing occurs behind the switching valve.

(2) Volumetric dilution: This dilution concept uses the principle of volumetric ratio. There are two loops with optional ratio, one for the sample and another for the solvent, that can be coupled for mixing (Figure 7-2b). For higher dilution ratio, serial dilution is applied in which the initial diluted solution is mixed further by keeping the sample loop but flushing the solvent loop with new solvent. The dilution performance for this configuration is good with linear dilution capability. However, there are many factors effects on the dilution process such as solvent filling time, switching time, mixing time, mixing speed which contribute to the complication of this concept for integration to the main system. In addition, the dilution may require many steps to achieve a required concentration, which makes it a slow dilution process. Moreover, the diluted sample of every step flows into the mass spectrometer in which there may have peaks at very high concentration.

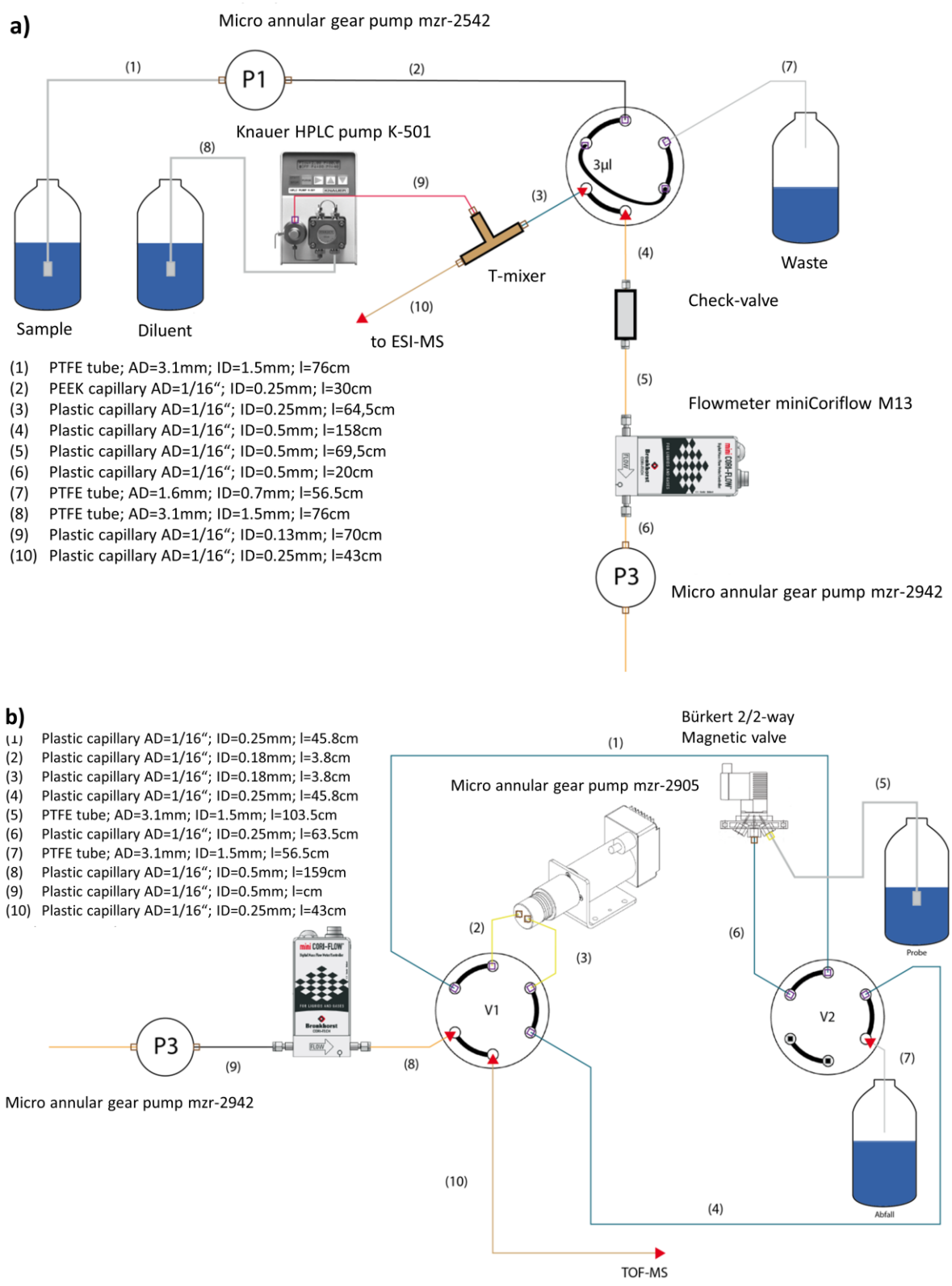

Figure 7-2: a) Post-sampling dilution, b) Volumetric dilution [157]

(3) Active splitting dilution: This dilution scheme is based on a commercial active splitter or mass rate attenuator (MRA). This configuration is selected for integration to the main system for its good performance in dilution due to the main device is a commercial product and is specialized for dilution, and the integration is not too complicated.

7.3 *Related Results in the Literature*

The application of MRA for dilution is not new. CAI ET AL. reported the use of MRA in replace for the passive splitting device in coupling an MS to preparative HPLC in a purification system [151]. They showed the benefit in system plumbing, volume reduction of the collected fraction and its evaporating time to reclaim the purified products. Similar applications of MRA in purification of combinatorial libraries, drug metabolites or characterizable impurities can be found in the work of TORIBIO AND LEISTER [158][159]. BRISTOW ET AL. coupled the MRA in their online monitoring system for continuous flow chemical synthesis for sampling and transferring the analyte to the make-up flow (dilution flow) [160]. This flow is then directly sent to a portable, small footprint MS. The system was applied to monitor one of the stages of an industrial chemical process, the Hoffman degradation reaction. JEURISSEN ET AL. also employed the MRA after the HPLC column for diluting extracts (inhibitors of human cytochrome P450 1A2) in an online HPLC detection system [161]. However, in those applications, the main usage of the MRA is to decrease the solution concentration down to a suitable working range of the mass spectrometer. In other words, there is no focus on the accuracy of the dilution by comparing different dilution ratios or comparing with manual dilution. In addition, due to the restricted information from the manufacturer, the MRA is mostly operated manually by setting the keypad for a desired split factor. Therefore, an automated dilution module which is able to automatically select its parameters based on a desired dilution value is necessary.

7.4 *Integration of the Active Splitting Dilution to the Main System*

Figure 7-3 shows a diagram of the system with the dilution module. Solution stream from the micro reactor (called *HPLC flow* according to the device manual or *micro reactor flow* as in this work) enters the MRA where a portion of it is transferred to the second flow (as in Figure 7-4). This second flow (*MS flow* or *dilution flow* or *make-up flow*) is supplied by another HPLC pump (called *dilution pump* – P_4). The remaining of the micro reactor flows to waste, meanwhile, the dilution flow with sample goes to the switching valve where it is sampled and sent to the analyzer by the carrier solvent stream of pump P_3. It should be noticed that, by using the MRA, the original micro reactor flow is not used after the MRA but the diluted flow. It means that flow to the micro reactor will always be diluted before it reaches the MS.

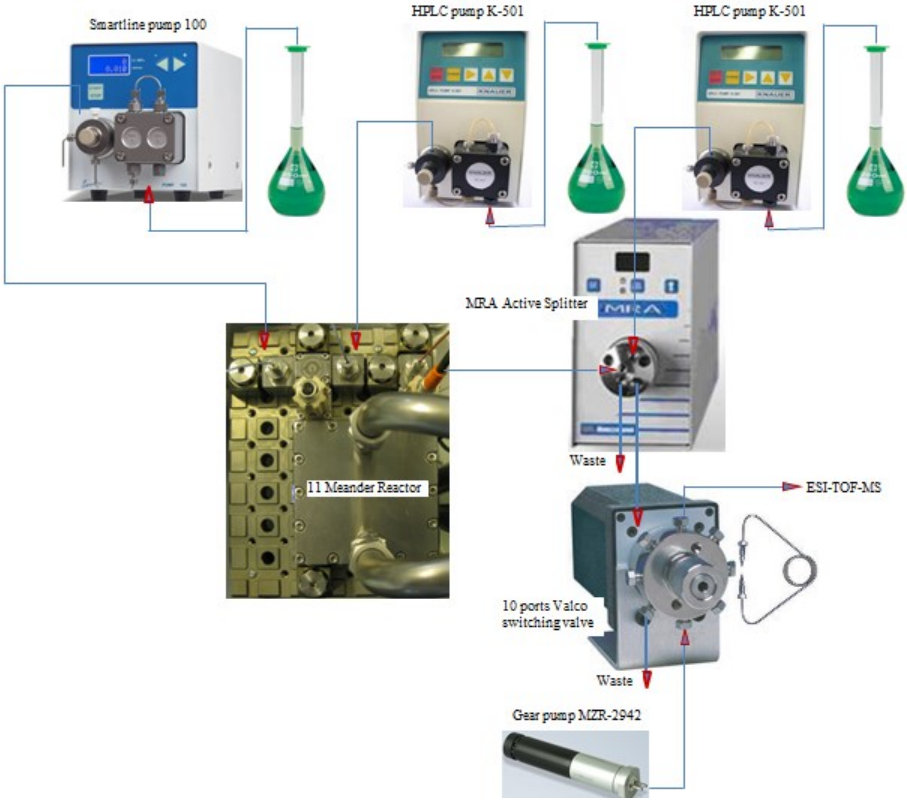

Figure 7-3: Diagram of the system integrating with the active splitter or mass rate attenuator (MRA)

In the active splitter, the amount of sample from the micro reactor flow transferred to the dilution flow is determined by the **split factor** (SF) programmed on it as shown in Table 7-1. There are 59 *split factors* in which each of them decides the transfer frequency (0.2 Hz–2 Hz) as well as the aliquot volume (22 nL, 100 nL, 300 nL). It is important in this case to understand the **split ratio** in the table. *Split ratio* is the ratio of flow being transferred (or split) relative to the micro reactor flow. For example, if a *split ratio* is 100:1 and micro reactor flow rate is 100 mL/min, then the split flow rate is 1 mL/min. Therefore, in the table, from left to right, by increasing the *split ratio*, less sample is transferred to the dilution flow; and from top to bottom, the *split ratio* is unchanged but more sample is transferred to the dilution flow because the nominal micro reactor flow rate increases and the split factor changes.

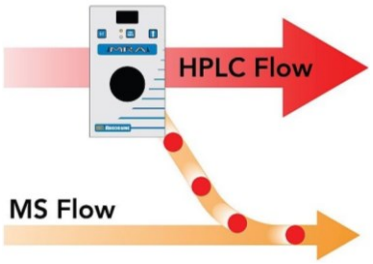

Figure 7-4: Working principle of the active splitter

There are two main parameters that could be manipulated in order to achieve a desired **dilution ratio or dilution factor** ($\frac{\text{initial volume}}{\text{final volume}}$), namely *split factor* and the dilution flow rate. The first determines the sample volume and the latter determines the diluent volume.

Table 7-1: Table for selection of split factor depending on flow rate of the micro reactor and the split ratio

Micro reactor flow rate (mL/min)	Split Ratio						
	100:1	**500:1**	**1000:1**	**4000:1**	**10000:1**	**20000:1**	**100000:1**
1	1	4	12				
2	2	5	13	22			
4	3	6	14	23	34		
6		7	15	24	35	45	
8		8	16	25	36	46	
10		9	17	26	37	47	
15		10	18	27	38	48	
20		11	19	28	39	49	
30			20	29	40	50	55
40			21	30	41	51	56
60				31	42	52	57
80				32	43	53	58
100				33	44	54	59

7.5 *A Problem with Variation of Micro Reactor Flow Rate*

A typical feature of our system is that the micro reactor outflow varies according to different reaction stages. Therefore, the input to the MRA is variable too. For a stable dilution ratio, however, the split flow should be stable to different input flow conditions.

In theory, sample amount in an MRA (V_f) that can be transferred depends on the sample flow rate (Q_s *in mL/min*) and half of switching cycle (*1/2f*):

$$V_f = \frac{Q_s}{60} * \frac{1}{2 * f}$$

For example, with $Q_s = 0.2$ mL/min, $f = 2.222$

$$V_f = 0.75\ \mu L/cycle = 750\ nL/cycle$$

This V_f is greater than the largest aliquot volume (300 nL) of the MRA. In other words, even with a very low flow rate of the micro reactor (0.2 mL/min) and the highest switching frequency of the MRA (2.2 Hz) all aliquot volumes should be fully filled.

However, initial testing showed a strong dependency of the signal amount (peak area) of the diluted solution on the micro reactor flow rate as shown in Figure 7-5. The plot was obtained by varying only the micro reactor flow rate from 0.2 mL/min to 6 mL/min. At micro reactor flow rate from 0.2 mL/min to 3 mL/min, the concentration of diluted octanoic acid varies roughly from 200,000 to 4,000,000. The

dilution is quite stable at a flow rate higher than 3 mL/min. This influence of flow rate variation to the MRA is unexpected and impacts the dilution results. Therefore, different approaches have been attempted to circumvent the issue.

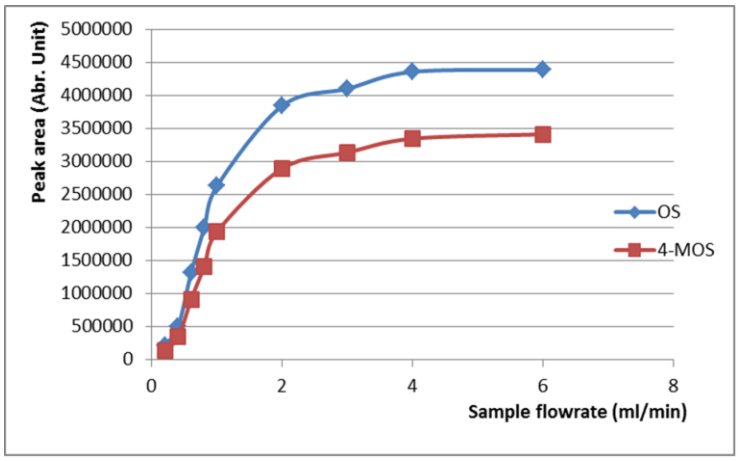

Figure 7-5: Dependency of a diluted solution on the flow rate of micro reactor. In this experiment, the split factor (3) and dilution flow rate (1 mL/min) are fixed. Only the micro reactor flow rate (or sample flow rate) is varied. Solution: Octanoic acid (OS) and 4-Methyl octanoic acid (4-MOS) in Methanol

7.6 *Back-Pressure Approach*

The assumption is that, at a very low flow rate, the micro reactor pressure is not high enough to fill in the aliquot. Therefore, this concept attempts to increase the pressure in front of the aliquot on the rotor seal by using a back-pressure regulator (Figure 7-6).

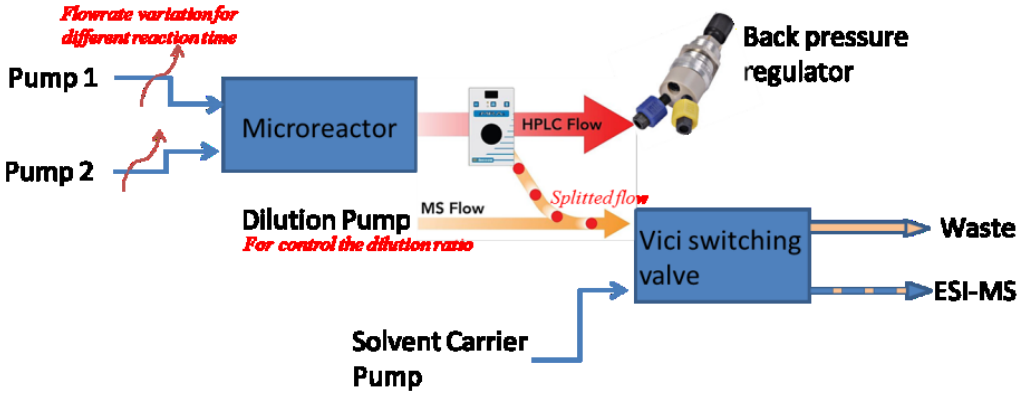

Figure 7-6: Back-pressure regulation concept

Testing with this concept was performed at 5 bars of educt pumps using 4-methyloctanoic acid as internal standards. The results are plotted in Figure 7-7. The dilution still strongly depends on the micro reactor flow rate as it is varied from 0.5 mL/min up to 6 mL/min. At higher flow rate, the diluted solution has

higher concentration (peak area) than the one at lower flow rate. Therefore, this concept does not solve the current issue.

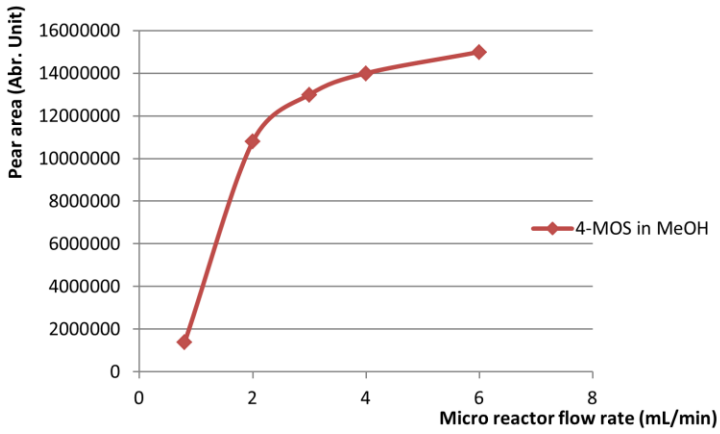

Figure 7-7: Dilution with a back-pressure regulator. Measuring with pressure in micro reactor 5 bars, Split factor (SF)=3 and different flow rate of the micro reactor

Another idea is to estimate the dependency curve by a formula as in Figure 7-8. This formula is applied to calculate the compensation factor corresponding to every micro reactor flow rate. After that, this compensation factor is multiplied by the nominal dilution flow rate to get the actual dilution ratio (assumed that the relation between the dilution ratio and dilution flow rate is linear). This approach can reduce the dependence on flow rate variation of the micro reactor. However, the practical approach is not recommended because the derived function depends on each split factor as well as on the chemicals used. In other words, for different split factors or different reagents, the estimated curve could be different.

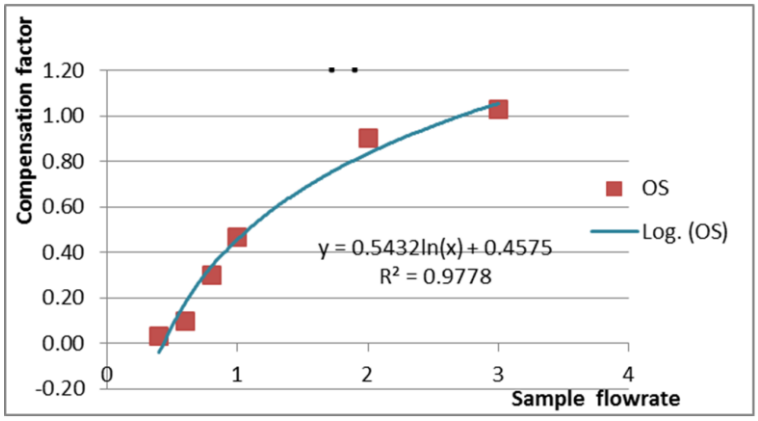

Figure 7-8: Estimating the response curve by a formula. This formula is used for calculating the compensation factor that will be used to adjust flow rate of the dilution pump

7.7 *Separating Effects from Micro Reactor Flow Rate*

Another idea is to avoid the variation of input flow rate to the MRA by using another multiport valve with a larger loop volume to transfer bulks of sample. The sample in this loop is sent to the splitter by a stable flow supplied by the flushing pump. This flushing flow can be controlled to fit with a certain split factor. The dilution pump is controlled to give a desired dilution ratio and the diluted solution is sampled by the second switching valve and sent to MS via a carrier solvent flow. The concept is presented in Figure 7-9.

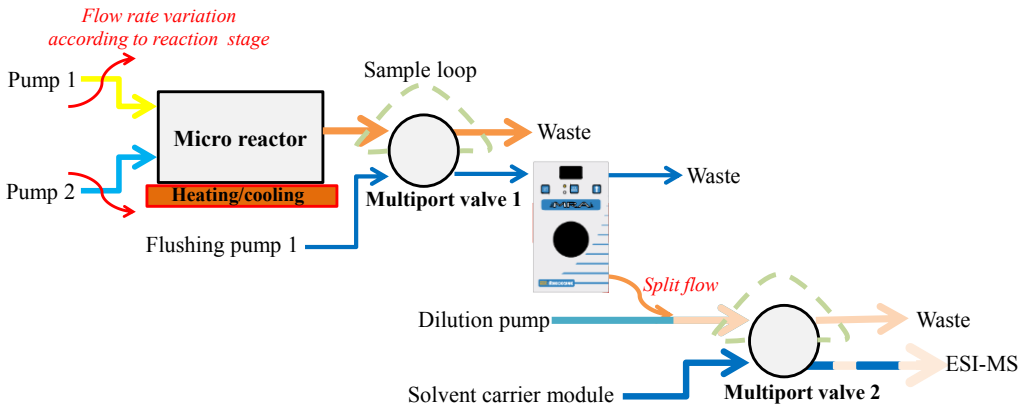

Figure 7-9: Separating effects from micro reactor flow rate

This concept has been tested which shows its diluting capability and less dependence on the fluctuation of micro reactor flow rate. A further test was performed using similar stock solution (4-MOS in MeOH) with dilution ratio 1:50, 1:25, 1:12.5. The result is plotted in Figure 7-10 that shows a logical increase of peak area as dilution ratio decreases from 1:50 to 1:12.5. However, the concept is quite complicated with more hardware requirements; System operation is delayed for filling the large sample loop; the MRA can work with only some split factors that require low input flow rate.

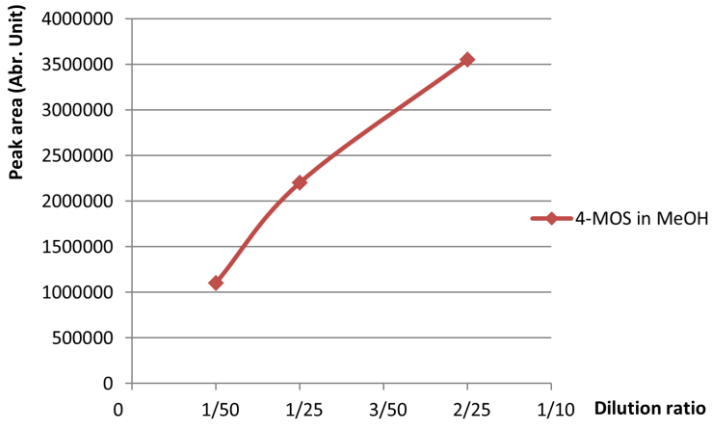

Figure 7-10: The concept of separating the effects from micro reactor flow rate variation. Dilution ratio: 1/50, 1/25, 1/12.5. Stock solution: 4-MOS in MeOH

7.8 *Flow Compensation Concept*

Another idea is to compensate for the micro reactor flow. By observing that the split flow is more stable with micro reactor flow rate greater than 3 mL/min, an isocratic pump (G1310A, Agilent Technologies, Waldbronn, Germany) for low flow compensation has been added to circumvent this problem. This compensation pump will be triggered when the main flow is lower than the threshold (3 mL/min). In turn, the flow rate of the dilution pump (Smartline 100, Knauer, Germany) will be reduced corresponding to the added portion to the main stream. This dilution process is automatic so that the *split factor*, *dilution flow rate* and *compensation flow rate* are automatically selected based on the dilution ratio and reaction stages set by users. As an example, given a dilution ratio 1:100, if micro reactor flow rate is 4 mL/min (>3 mL/min), the *split factor* will be 1 and *dilution flow rate* will be 1 mL/min (refer to Table 7-1). However, when micro reactor flow rate is 1 mL/min (<3 mL/min), the *compensation flow* will be 2 mL/min. In that case, the original solution is diluted 2/3 or 66.7%, or the required dilution ratio is now only 1:33. Therefore, the dilution flow reduces to 0.33 mL/min to achieve the desired dilution ratio (1:100). The concepts are presented in Figure 7-11.

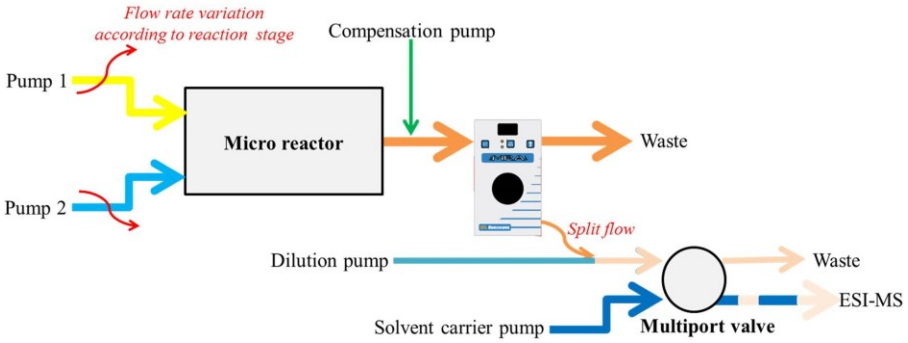

Figure 7-11: Flow compensation concept

7.8.1 *Diluting Algorithm*

The dilution module is integrated into the control software for automatic operation. GUI for this module is presented in CHAPTER 9. The diluting algorithm is shown in Figure 7-12. There are two possible routes. One has no knowledge about the micro reactor flow rate. That is when the user enters a desired diluting ratio. All data in Table 7-1 is loaded into a 59x3 matrix for convenient reference. 59 rows correspond to 59 *split factors* available in the table. Every *split factor* (1 → 59) is stored in column 1, its corresponding *split ratio* is stored in column 2 and its corresponding *micro reactor flow rate* is stored in column 3. For example, the first row has *split factor* = 1 in column 1, *split ratio* = 100 in column 2 and *micro reactor flow rate* = 1 in column 3. The algorithm then searches for a *split factor* that has its corresponding *split ratio* closest to the input dilution ratio. The dilution flow rate is calculated afterward. If this value is not smaller than 0.4 mL/min (practical experiments in the laboratory showed a signal reduction when the dilution flow rate got below 0.3 mL/min), the *split factor* and dilution flow rate are set onto the relevant devices. Else, the next *split factor* of the same *split ratio* is selected to recalculate the

dilution flow rate. In the second route with knowledge about the current micro reactor flow rate (when the automatic operation mode starts), the compensation flow rate is calculated first. Due to the possible compensation flow, the micro reactor flow rate might be partially diluted (if micro reactor flow >= 3 mL/min, no compensation flow is added). As a result, the dilution ratio is re-calculated. The new dilution ratio is then used for finding the *split ratio*, *split factor* and dilution flow rate. This process again follows some of the steps in the first route.

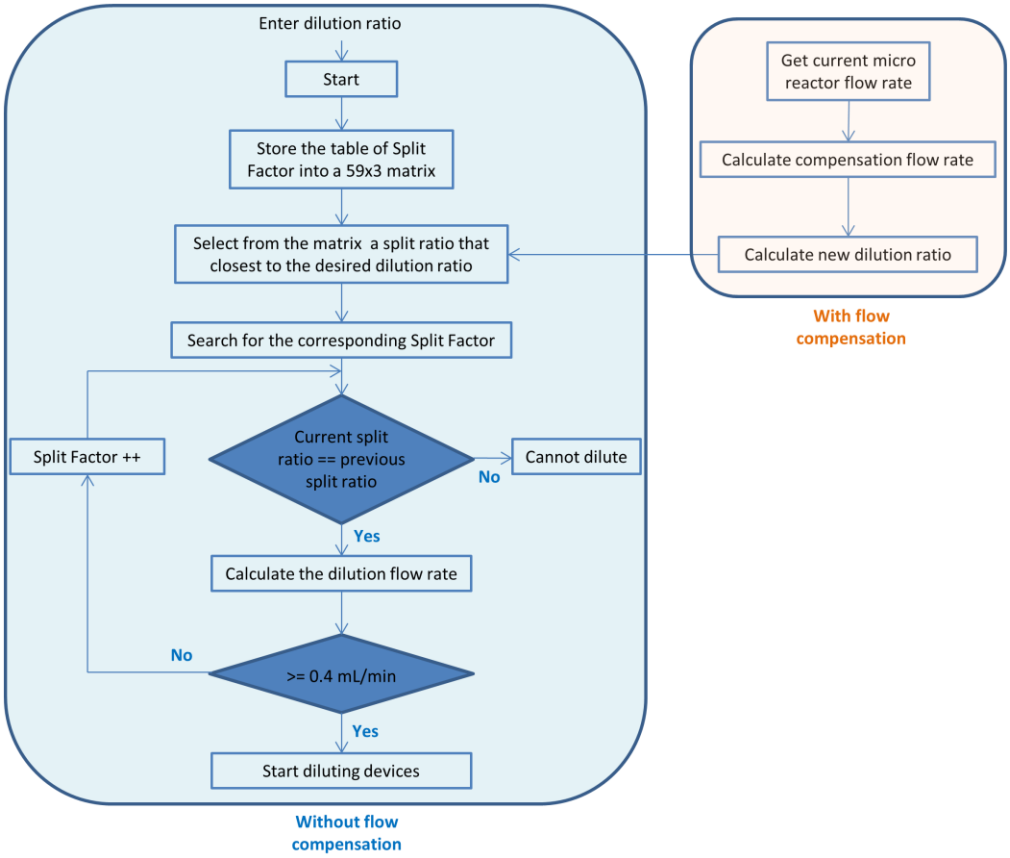

Figure 7-12: Algorithm for diluting with the flow compensation concept

7.8.2 Testing and Results

7.8.2.1 Testing for Diluting Performance Before and After Flow Compensation

OS and 4-MOS in MeOH solvent were used for comparing between dilution using MRA with and without flow compensation. The micro reactor flow rate was varied from 0.6 mL/min to 6 mL/min, meanwhile, other parameters were kept unchanged (Refer to *Experiment 5* in Section 11.2). The result is shown in Figure 7-13. The plot (a) shows a strong dependence of the diluted solution on flow rate variation of the micro reactor. Meanwhile, the diluted solution on plot (b) is more stable, especially from the flow rate larger than 1 mL/min. This result proves the stability of this concept to the instability of the input flow rate.

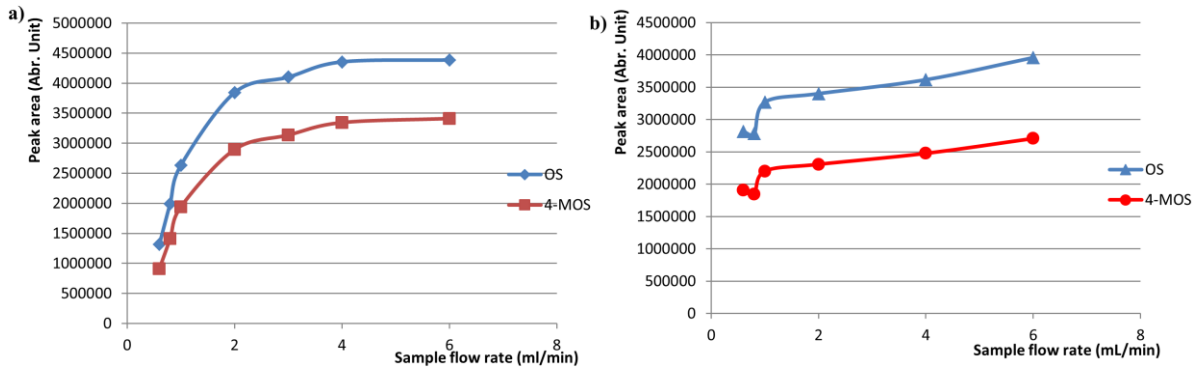

Figure 7-13: Improvement in dilution with the flow compensation concept
a) without flow compensation, b) with flow compensation

7.8.2.2 Automatic vs. Manual Dilution

A comparison between automatic and manual dilution was performed using OS and 4-MOS in MeOH with 4 dilution ratios 1/500, 1/300, 1/100, 1/50. For every dilution ratio, different micro reactor flow rates (4, 2, 1 mL/min) was attempted. Detail settings can be found in *Experiment 6* in Section 11.2. Some of the results are shown in Table 7-2 and Figure 7-14b.

In every dilution ratio, the average peak area and STD of every reaction flow rate (4, 2, 1 mL/min) for 3 runs are calculated, which gives STD in a range of 1.9% - 10.5%. The average peak area and STD of all peaks for every dilution ratio are also calculated. Those results show a logical increase of the sampling peak areas (from 428,582 to 4,322,822 for OS and from 503,726 to 5,737,318 for 4-MOS) as dilution ratio decreases (from 1:500 to 1:50). They are also approximate to the manually diluted solutions of similar ratios (from 609,015 to 5,148,866 for OS). It should be noticed that the manual dilution is not affected by the micro reactor flow rate variation in the testing range (1 – 4 mL/min) because the sampling loop is only 5µL. Due to the (possibly) different settings of the dilution module (split factor, compensation flow rate and dilution flow rate) and different micro reactor flow rate for every reaction stage, the standard deviations measured with automatic dilution (3.3% - 9.7% for OS) are normally higher and in larger range than those measured with manual dilution (3.9% - 6.4%). Further comparison the signal intensity between different dilution ratios (1:50, 1:100, 1:300) with dilution ratio 1:500, we get values in two rows “expected quotient” and “actual quotient”. It is expected that the signal intensity of dilution ratio 1:50 would be 10 times larger than that with dilution ratio 1:500. The actual quotient in this case (4,322,822/428,582) is 10.09 which is very good. Other logical quotients are also obtained for other ratios such as with dilution ratio 1:100 (expected quotient: 5 – actual quotient: 5.08 (2,178,413/428,582)) and with dilution ratio 1:300 (expected quotient: 1.67 – actual quotient: 1.61 (690,117/428,582)).

This experiment shows the approximation between automatic vs. manual dilution in one concentration of stock solution. Further questions are how the module performs in different concentrations of stock solution or in different solvents. These issues will be presented in the next two sections.

Table 7-2: Automatic dilution and manual dilution of OS in MeOH (Run 2, 91 mg/L OS + 91 mg/L 4-MOS in MeOH)

Automatic Dilution				
Dilution ratio	**1:500**	**1:300**	**1:100**	**1:50**
Average peak area (4 mL/min)	428,506	657,404	2,222,846	4,256,341
STD	21,959	32,704	50629	80,670
STD in %	5.1	5.0	2.3	1.9
Average peak area (2 mL/min)	403,190	675,048	2,127,199	4,163,563
STD	20,444	69,761	77,942	158,831
STD in %	5.1	10.3	3.7	3.8
Average peak area (1mL/min)	454,051	737,899	2,185,195	4,548,562
STD	20,374	62,335	45,233	478,179
STD in %	4.5	8.4	2.1	10.5
Average of all peaks	428,582	690,117	2,178,413	4,322,822
STD	29,488	66,839	71,478	337,210
STD in %	6.9	9.7	3.3	7.8
Expected quotient	1	1.67	5	10
Actual quotient	1	1.61	5.08	10.09
Manual Dilution				
Average of all peaks	609,015	1,013,662	2,758,547	5,148,866
STD	38,835	61,433	105,813	216,010
STD in %	6.4	6.1	3.9	4.2

7.8.2.3 Dilution in Different Concentrations of Stock Solution

The dilution using different concentrations of stock solution was performed with the same settings as in the previous experiment. Stock solution one (low concentration) contained 45.5 mg/L OS and 45.5 mg/L 4-MOS; stock solution two (high concentration) contained 136.5 mg/L OS and 136.5 mg/L 4-MOS.

Measurement results are plotted in Figure 7-14a and Figure 7-14c which present the comparison of automatic vs. manual dilution. As in the previous case with medium concentration of stock solution, both automatic and manual dilution give logical results with higher peak area obtained as dilution ratio to be lower. And the performance of automatic dilution and manual dilution are approximate to each other. Furthermore, Figure 7-14c also indicates a situation where the diluted solution does not fall in the linear dynamic range of the MS. This makes these lines curve instead of linear. Therefore, a higher dilution ratio would be recommended to this case.

Figure 7-15 summarizes the automatic dilution with same dilution ratios but different concentrations of stock solution (low concentration, medium concentration and high concentration). As it can be seen, for every concentration of the stock solution, signal intensity of the diluted solution increases as the dilution ratio decreases from 1:500 to 1:50. In addition, for every same dilution ratio, peak areas of stock solution

with higher concentration are higher. This results in a much steeper slope of the green curve (from stock solution 3) over the steeper slope of the red curve (from stock solution 2) and over the blue curve (from stock solution 1).

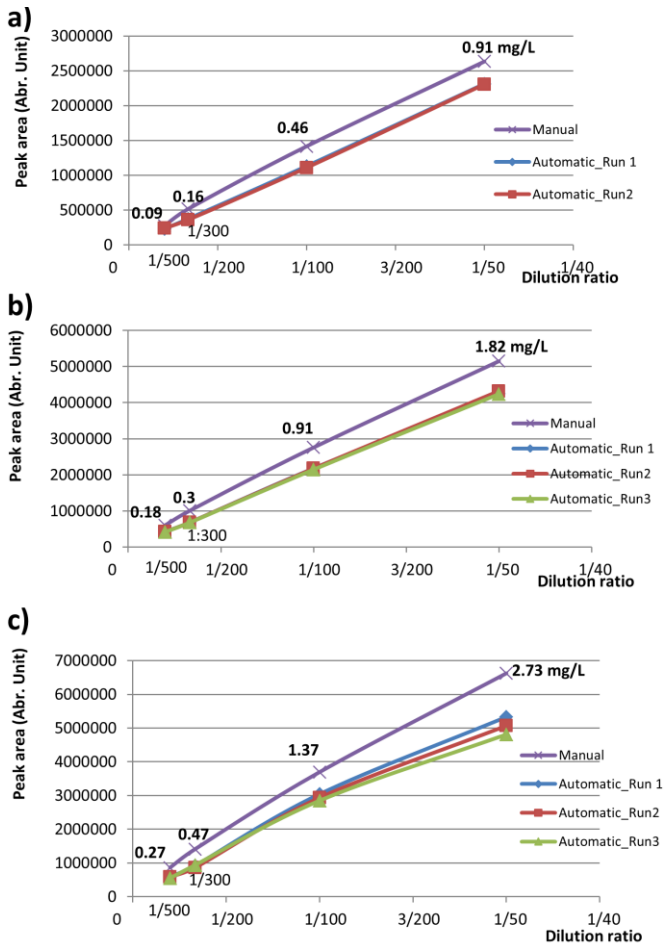

Figure 7-14: Automatic dilution and Manual dilution with dilution ratios of 1:500, 1:300, 1:100 and 1:50 of OS in MeOH a) 45.5 mg/L OS in MeOH (low concentration), b) 91 mg/L OS in MeOH (medium concentration), c) 136.5 mg/L OS in MeOH (high concentration)

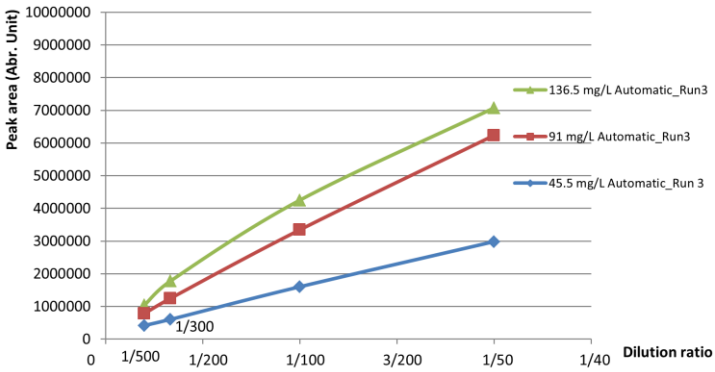

Figure 7-15: Diluted concentration vs. concentration of the stock solution

7.8.2.4 Dilution in Different Solvents

In this test, the dilution with same dilution ratios was performed using another solvent, pure ACN. Similar stock concentrations (solution 1: 45.5 mg/L OS + 45.5 mg/L 4-MOS; solution 2: 91 mg/L OS + 91 mg/L 4-MOS; solution 3: 136.5 mg/L OS + 136.5 mg/L 4-MOS) were prepared. Pure ACN was used as the diluent by both dilution pump and compensation pump. A summary of dilution in different solvents are shown in Figure 7-16.

The first column in the figure presents automatic dilution and the second column presents the corresponding manual dilution. Each row presents the dilution with same concentration of analytes in different solvents. In all plots, the dilution using ACN solvent gives larger signals than with MeOH. The effect of different solvents (with different characteristics such as specific conductance, surface tension, and viscosity) to the analytes (OS, 4-MOS) in this case is clearly seen for both automatic and manual dilution. This phenomenon was confirmed by doing another experiment in which the MRA was set to a fixed *split factor* (SF=3). The dilution was conducted with 2 stock solutions sequentially (91 mg/L OS and 91 mg/L 4-MOS in MeOH; 91 mg/L OS and 91 mg/L 4 MOS in ACN). In order to further confirm the impact of abrasion to the *rotor seal* and *stator face assembly* for their continuous contacting, the test was repeated after replacing a new pair of those components. As can be seen in Figure 7-17, ACN gives the higher signal intensity of analyte (OS) than MeOH does both with the old pair (2,034,084 vs. 1,590,062) and the new pair (2,819,071 vs. 2,013,855). The results also confirm the abrasion of the rotor seal and stator face assembly with time by lessening the aliquot volume and so the split amount of sample. Further literature review solidifies the influence of the make-up flow/dilution flow solvent on the mass spectrometry data [160]. Bristow et al. monitored the starting material amide (*m/z 325*) (in the reaction to form isocyanate intermediate) and plotted its absolute abundances as a function of reaction temperature for different sampling make-up flow compositions (50:50 acetonitrile:water + 0.1% formic acid; 20:80 acetonitrile:water + 0.1% formic acid; and 50:50 acetonitrile:water + 0.05% TFA). He reported that the absolute abundances varied depending on the composition of the make-up flow used in which acetonitrile:water (50:50) + 0.1% formic acid produced the highest ion abundance for the amide (from 20^{o}C – 80^{o}C) compared with the other two make-up flows.

7.9 *Summary*

A dilution module, which is based mainly on the MRA, has been presented for solving the problem of high concentration solution to the mass spectrometer. The approach of low flow compensation is applied to circumvent the strong dependence of diluted solutions on the low flow rate of the micro reactor. Different tests were performed that show the module's ability in diluting different solutions at their different initial concentrations. In addition to decreasing human labor, automatic dilution can help reduce potential errors made by operators via manual dilution. Although there are high standard deviations due to effects from different flow rates and device performance, the process is automated and able to perform various dilution ratios starting from 10. Finally, due to the contact and abrasion of the *rotor seal* and *stator face assembly* pair, a regular replacement to these essential components is recommended.

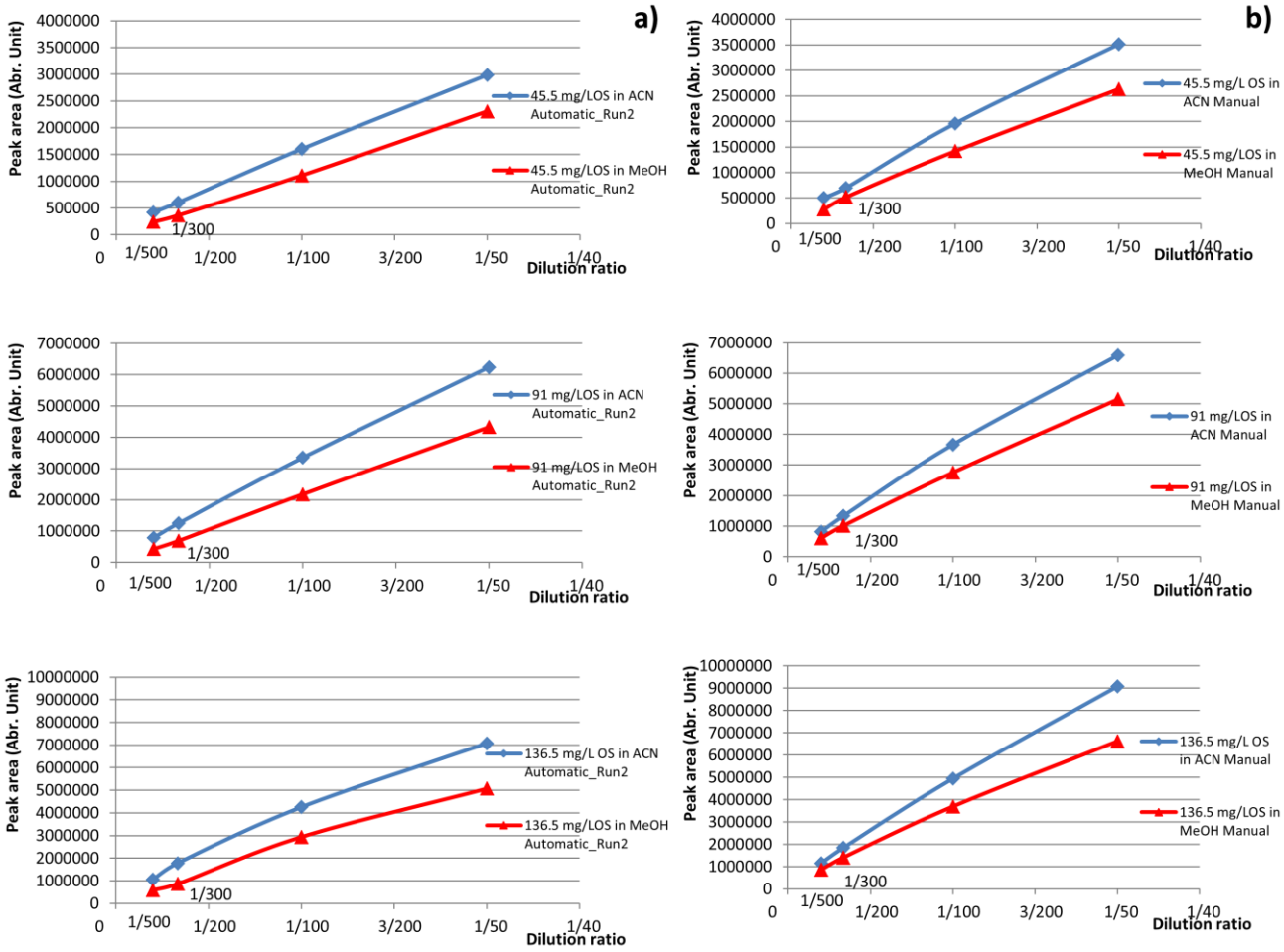

Figure 7-16: Diluted concentration vs. different solvents
a) automatic dilution, b) manual dilution

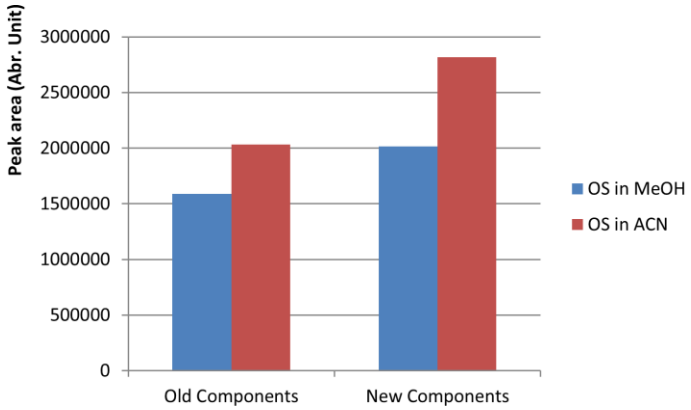

Figure 7-17: Influence of different solvents and component's age on the dilution

CHAPTER 8 INTEGRATION THE MICRO REACTOR SYSTEM TO THE ICP/MS

8.1 *Overview*

Atomic spectroscopy with different optical and mass spectrometric methods such as atomic absorption spectroscopy (AAS), atomic emission spectroscopy (AES or optical emission spectroscopy - OES), atomic fluorescent spectroscopy (AFS) and mass spectrometry, are the most powerful methods for elemental analysis for a variety of sample types and concentrations [162]. Inductively coupled plasma (ICP)-MS offers a wide elemental coverage, high sensitivity (ng/L range) and low background, fast analysis times, wide linear dynamic range of operation (up to nine orders of magnitude), and isotopic information. These advantages compensate the limitations of graphite furnace AAS (GFAAS) for single element measurement or of ICP-OES for complex interferences, quite complex emission spectrum and accuracy at ultra-trace levels [163] [164]. As a consequence, ICP-MS has become a growing technique in analytical laboratories at the expense of other atomic spectroscopic techniques [110]. However, the instrument is very costly to afford, non-availability of certified reference standards for most of the pharmaceutical products, or the problem of polyatomic ions due to the combination with argon from the plasma or components from solvent or from the sample matrix [165][164].

ICP-MS can be used for metal speciation, quantification of proteins and biomolecules (metal-coded affinity tags – MeCAT) and elemental analysis. It finds its application in medical and forensic field, specifically, toxicology such as metal assay from blood, urine, plasma, serum. In environmental field such as metal analysis for drinking water, sea water, or water and other material analysis in industrial process. In industrial and biological monitoring such as analysis of blood or urine for metal toxicity of individuals working in battery factory or in environment exposed to metals. In geochemistry for radiometric dating. In pharmaceutical industry, for detection of inorganic impurities in pharmaceuticals and their ingredients [166][167].

8.2 *Integration Schemes and Applications*

As a standalone device, an ICP-MS does not provide information about the structural form of analytes. Therefore, a combination of ICP-MS with separation techniques (or in short “hyphenated techniques”) such as gas chromatography (GC), liquid chromatography (LC), ion chromatography (IC), or capillary electrophoresis (CE) are popular in research and application areas [110]. Micro reactors which are widely integrated to molecular mass spectrometric techniques find little application in the field of atomic spectrometry in general or with ICP-MS in specific. In the found literature, when being coupled to ICP-MS, the micro reactor was only functioned as a separation element (as a column to separate analytes) but not as its main purpose of a compartment in which chemical reaction can take place.

HSU ET AL. coupled an ICP-MS with a polyoxometalate cluster (POM)/microfluidic (MF) separation system for determination of trivalent [Cr(III)] and hexavalent [Cr(VI)] chromium species in aqueous samples (water) [114] (Figure 8-1). $Cs_{2.5}H_{0.5}PW_{12}O_{40}$ (CsPOM) as an immobilized reagent was coated in the micro reactor chamber. The Cr(III) was absorbed by CsPOM, meanwhile, the Cr(VI) was sent to the

ICP-MS by the carrier solvent. After that, HNO_3 as eluent solvent eluted Cr(III) directly to the ICP-MS. The system was tested for its optimal operating conditions such as the effects of pH, diluent flow rate, adsorption flow rate, reactor chamber, etc. Another technique named capillary micro extraction (CME) in which the inner surface of an open tubular capillary column is coated with extraction medium. HU ET AL. coated the capillary with Al_2O_3 and coupled it to ICP-MS for trace analysis of inorganic As(III)/As(V) and Cr(III)/Cr(VI) in natural waters [168]. A similar application of CME-ICP-MS for determination of trace Co, Ni and Cd in water, rice and urine samples can be found in [169]. WANG ET AL. fabricated a chip-based liquid phase micro extraction (LPME) device for metal extraction [170]. The aqueous flow and organic flow from the inlets formed a lamina stream in the micro channel. Their interfacial contact was where the target reagent dispersed to the organic phase. The organic phase was then collected and analyzed via the electro thermal vaporization (ETV) – ICP-MS. The method was applied for metal ion determination (Cu, Zn, Cd, Hg, Pb, Bi) in $HepG_2$ cell, Jurkat T cells and human serum sample. In another example of detecting rare earth elements in sea water, a commercial SEAFAST (Elemental Scientific, NE, USA) column was used to preconcentrate the target analyte and eliminate sample matrices. All the carrier streams were operated by peristaltic pumps for their low cost and non-contact with chemicals [171]. Another configuration which used Integrated sample Introduction system (ISIS, Agilent Technologies, Waldbronn, Germany) was employed for loading sample to the sample loop [172]. A second pump continuously transferred carrier and internal standard solution (mixed at the mixing T) to the ICP-MS's nebulizer. Samples were injected discretely to the carrier flow by switching the valve to the injection mode. The system was used to detect 13 trace elements in tea infusion.

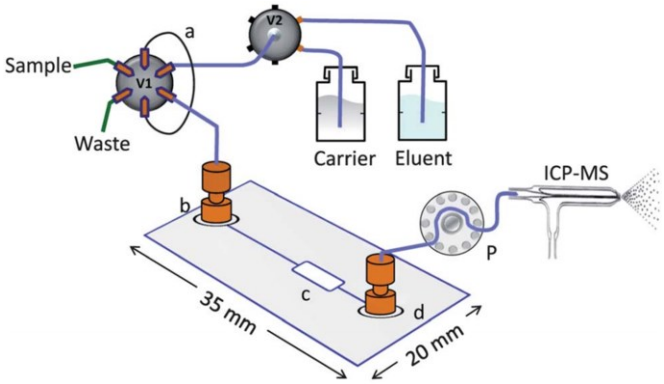

Figure 8-1: Schematic representation of the online CsPOM-MF/ICP-MS system [114]

8.3 *Integration Concepts*

A stable and "in the working range" input flow rate to an analyzer is required in order to insure measurement stability. However, the flow rate in micro reactor depends on the reaction stage accordingly and is normally larger than the accepted threshold (< 1 mL/min) of an MS. Therefore, using the complete outflow from the micro reactor is not usually suitable.

Two integration schemes between the micro reactor system and the analyzer are proposed: The first scheme is the same as that used in connection to the ESI-MS with the FIA approach. The carrier solvent through the multiport valve is directly connected to the nebulizer inlet of the ICP-MS via a 0.25 mm ID capillary (as in Figure 8-2). The micro reactor stream, which is supplied by two HPLC pumps, fills in the sample loop (5µL) and goes to waste. At injection position of the valve, the carrier stream flushes the sample loop content and send it to the ICP-MS. One channel of the peristaltic pump/nebulizer pump is used to drain waste from the nebulizer.

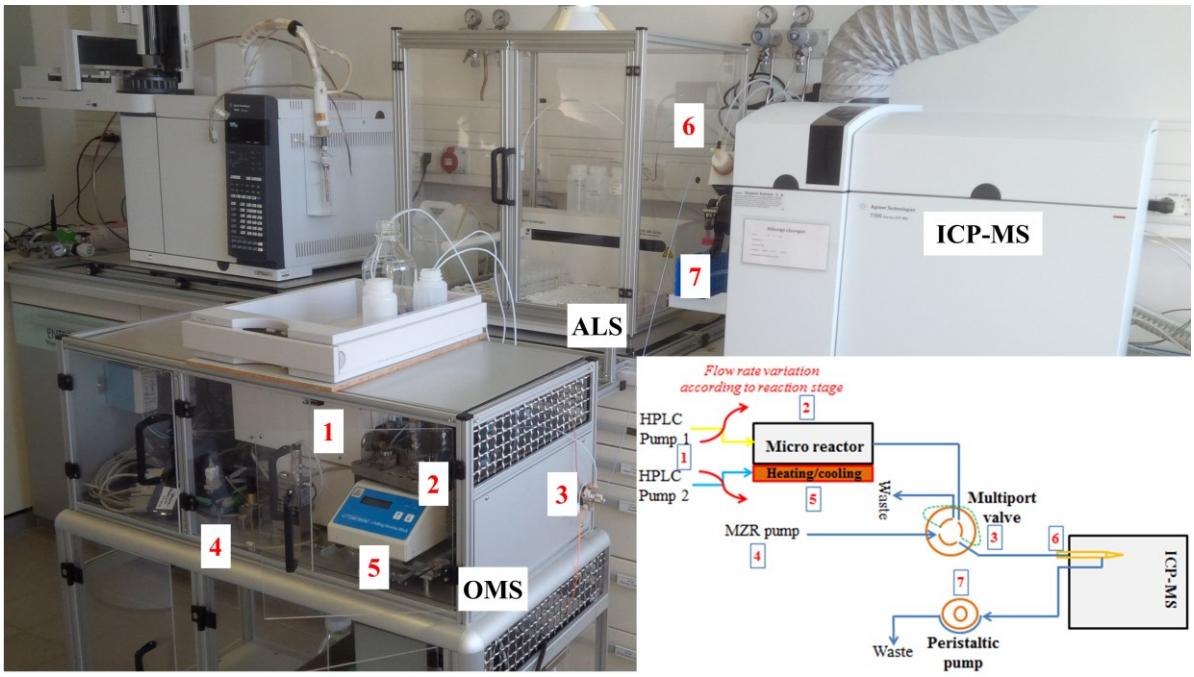

Figure 8-2: First configuration: Direct integration of the micro reactor system to ICP-MS. 1) HPLC pump, 2) micro reactor, 3) multiport valve, 4) micro annular gear pump, 5) heating/cooling module, 6) nebulizer, 7) peristaltic pump

This scheme offers a simple connection. Multiple samplings per reaction stage are possible as in the integration to the ESI-MS. However, tuning and optimization of the Agilent 7700x ICP-MS are missing in this scheme due to the exclusion of the auto sampler (ALS). These procedures are required so that the plasma gives efficient ion production; the ion optics give the best sensitivity; the Quadrupole gives optimal mass resolution and mass calibration; and the detector gives optimal sensitivity and linear dynamic range [110]. Thus, the second scheme which cooperates ALS, ORMS, and ICP-MS is implemented as in Figure 8-3.

Both the ALS and micro reactor are connected to the multiport valve in which one of them can be selected at a time. In position 1 of the multiport valve, the ALS flow is connected to one of the channels of the peristaltic pump (using a Peri-pump tubing, internal diameter (ID) = 1.02 mm), which supplies solution (via a capillary, ID=0.5 mm) for the nebulizer. In position 2, the solution from micro reactor flow is connected to the peristaltic pump. The peristaltic pump plays the main role in regulating sample flow rate to the nebulizer. Whenever flow rate from the micro reactor is higher than flow requirement of the

peristaltic pump, the excessive flow will be discharged via the drainage line (number 8 in the figure). The drainage line (ID = 0.5 mm) with an adjustable back pressure regulator is used not only for releasing excessive flow from the micro reactor but also to prevent ambient air from sucking into the main stream.

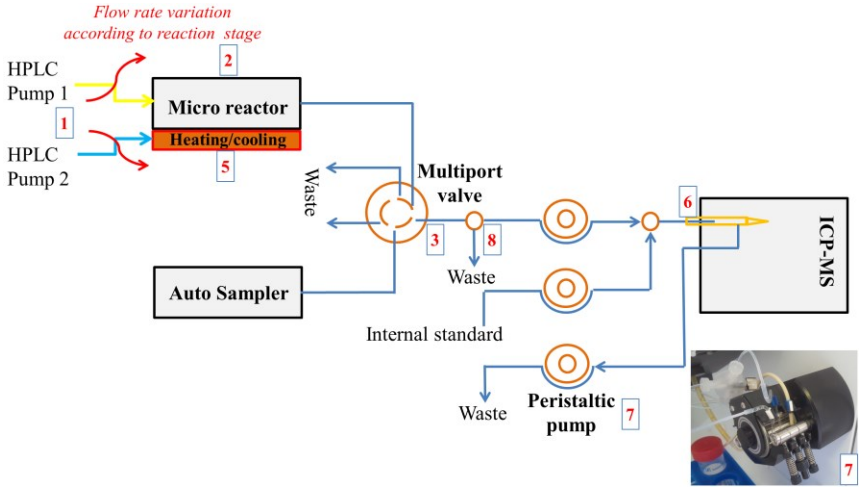

Figure 8-3: Second configuration of integration the micro reactor system to ICP-MS. 1) HPLC pump, 2) micro reactor, 3) multiport valve, 4) micro annular gear pump, 5) heating/cooling module, 6) nebulizer, 7) peristaltic pump, 8) Tee joint

In this concept, the micro reactor system is added to the standard configuration of the ICP-MS system. In more details, the system starts up with warming, calibration, and tuning. After that, the valve is switched so that analytes from the micro reactor can be supplied and mixed with the internal standard line before entering the nebulizer. In addition, the carrier solvent pump of the micro reactor system is not required, instead, the peristaltic pump is used, which is standard for introducing sample to ICP-MS.

8.4 *Testing and Results*

The purpose of integration to ICP-MS is to enable the capability of the system to detect metals. However, the system itself contains different parts made of metals which directly contact to solutions such as micro reactor, pumps, multiport valve. Therefore, apart from testing the feasibility of the two integration concepts, testing for contamination caused by the micro reactor system is also important.

CertiPUR® ICP multi-element standard solution IV and CertiPUR® Lutetium ICP standard were used for the testing purpose. Sample solution was prepared with 100 µg/L ICP multi-element standard solution IV in HNO_3 (1%, v/v). Internal standard solution contained 500 µg/L lutetium in HNO_3 (5%, v/v). Two separate solutions as carrier solvent were prepared: ultrapure water and HNO_3 (1%, v/v). Detailed settings for all measurements are summarized in *Experiment 7* section 11.2.

8.4.1 Variation of Carrier Solvent Flow Rate (Configuration 1)

In this test, different flow rates of carrier solvent (from 0.2 mL/min to 0.6 mL/min) were attempted in order to determine their influence on the measured signal.

As flow rate of the carrier solvent is varied from 0.2 mL/min to 0.6 mL/min, the response time reduces from 13s to 7s and the peak width is reduced from 21s to 11s. This enables the peak to peak sampling time to be lower than 30s. However, starting from 0.6 mL/min, the drain tube from the nebulizer is filling since more large droplets are formed and the peristaltic pump drains the waste at 0.1 rps (≈ 0.4 mL/min).

As more carrier solvent enters the plasma, the baseline is higher. Meanwhile, the amount of sample is unchanged (5µL). As a consequence, the measured signal for each element is reduced as the carrier solvent flow rate increases (see Figure 8-4). In addition, as flow rate increases, the residence time of analytes in the plasma is shorter that reduces their ion quantity passing through the skimmer to the MS.

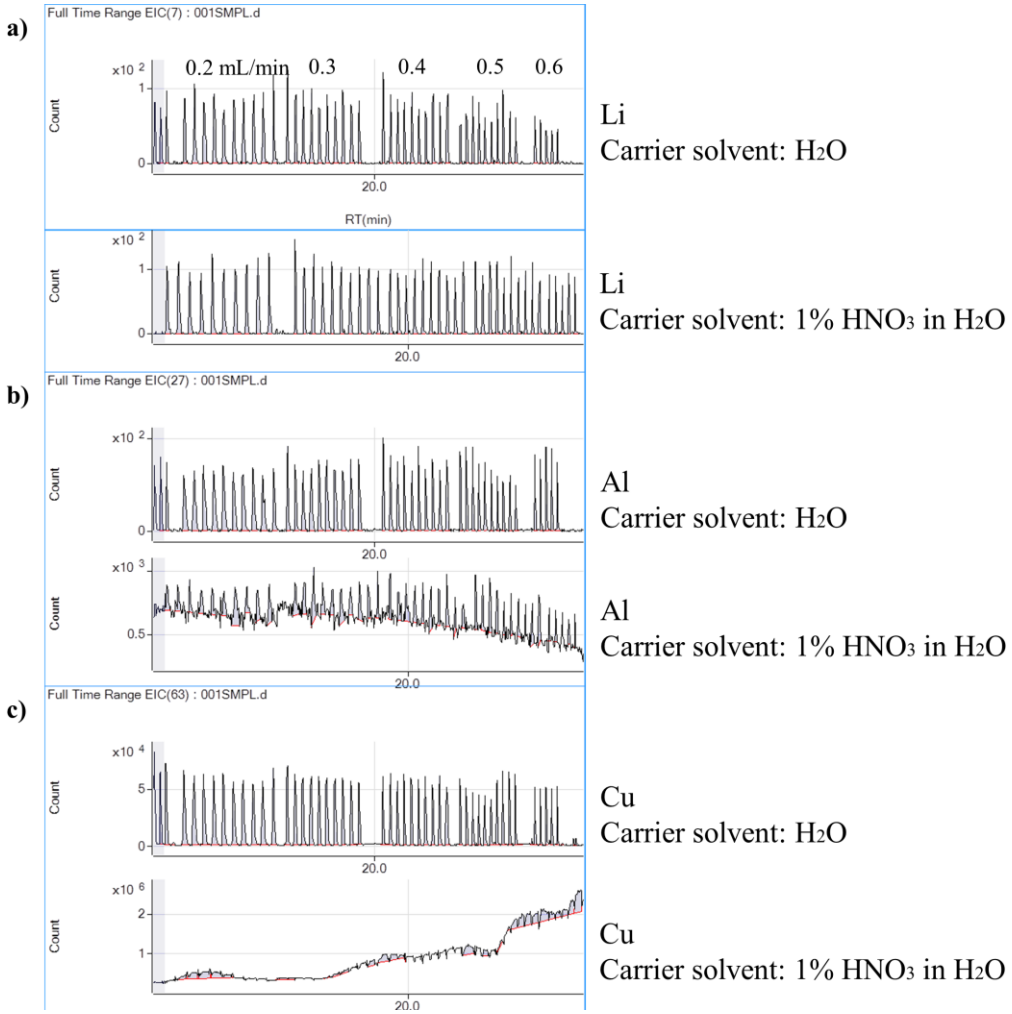

Figure 8-4: Li (a), Al (b) and Cu (c) elements measured with H_2O as carrier solvent and with 1%HNO_3 as carrier solvent. The carrier solvent was from 0.2 mL/min to 0.6 mL/min

8.4.2 Changing of Carrier Solvent Type (Configuration 1)

The solvent carrier pump is manufactured from metallic materials which might affect the analytical results. In order to see how different solvents may influence on the carrier pump's metal dissolution, two different

carrier solvents (H_2O and 1% HNO_3) were used to transfer samples and results are shown in Table 8-1 for selected elements. The average peak areas of 10 samplings for each flow rate are calculated as well as their relative percentage (RP). The result is, some elements are not influenced by different carrier solvents since they are not present in the pump materials or not influenced by the solvents. They have similar peak profiles and peak areas in H_2O and in 1% HNO_3 at different flow rates (Figure 8-4a), such as Li, Co, and Pb. Their relative percentage is in the range 74.3% – 110.4%. Some elements including Mg, Al, and Zn are slightly impacted. This results in different peak profiles and peak areas in H_2O and in 1% HNO_3 (Figure 8-4b). The RP values in this case are normally higher and in a larger range (69.7% – 144.7%) than in the previous case. This indicates their existence in the pump material. Finally, elements such as Cu and Fe are heavily influenced by 1% HNO_3 solvent (Figure 8-4c). No peaks are observed because the baseline is too high. This indicates the high concentration of Cu and Fe in the pump and the pump is the main source of metal contamination to the solution.

Table 8-1: Measured peak area (signals) of selected elements in two carrier solvents at various flow rates. Relative percentage (RP): variation of the signal in the carrier solvent HNO_3 related to the signal in the carrier solvent H_2O

Elements	**Flow rate (mL/min)**	**0.20**	**0.30**	**0.40**	**0.50**	**0.60**
	Carrier solvent	**Average peak area (arbitrary unit)**				
Not influenced						
Li (7)	**H_2O**	931	723	552	344	324
	1% HNO_3	1,006	764	622	463	313
	RP (%)	*92.5*	*94.6*	*88.7*	*74.3*	*103.5*
Co (59)	**H_2O**	874,211	700,319	491,116	341,324	281,131
	1% HNO_3	815,822	667,652	544,645	415,372	339,279
	RP (%)	*107.2*	*104.9*	*90.1*	*82.2*	*82.9*
Pb (208)	**H_2O**	332,471	248,627	183,496	137,731	86,382
	1% HNO_3	301,252	253,760	199,020	159,221	98,477
	RP (%)	*110.4*	*98.0*	*92.2*	*86.5*	*87.7*
Slightly influenced						
Mg (24)	**H_2O**	12,077	10,133	6,858	4,992	4,092
	1% HNO_3	9,473	8,073	6,416	4,760	3,548
	RP (%)	*127.5*	*125.5*	*106.9*	*104.9*	*115.3*
Al (27)	**H_2O**	4,136	3,352	2,701	1,629	1,906
	1% HNO_3	2,859	2,862	1,891	1,665	1,427
	RP (%)	*144.7*	*117.1*	*142.8*	*97.8*	*133.6*
Zn (66)	**H_2O**	106,559	82,996	58,430	44,234	26,179
	1% HNO_3	83,230	75,982	55,886	45,070	37,582
	RP (%)	*128.0*	*109.2*	*104.6*	*98.1*	*69.7*
Strongly influenced						
Fe (56)	**H_2O**	1,195,177	930,988	649,684	478,419	380,292
	1% HNO_3	no signal, baseline too high				
Cu (63)	**H_2O**	740,151	568,158	422,849	303,414	211,554
	1% HNO_3	no signal, baseline too high				

Additionally, the corresponding standard deviations (STD) in % of the measurements are calculated and presented in a separate table (Table 8-2) for easier interpretation of the results. The STD in this configuration is mainly determined by the stability and the dynamics of the carrier solvent (that depends on the flow rate and flow interruption as the multiport valve switches), the abrasion and dissolution of pump materials to the carrier solvent. These parameters contribute to the rather high STD in the range of 0.9% - 26.1% for the first group of elements and 2.7% - 43.7% for the second group of elements. This is logical because the second group is more sensitive to different carrier solvents.

Table 8-2: Standard deviation of elements in different carrier solvents at different flow rate

Elements	**Flow rate (mL/min)**	**0.20**	**0.30**	**0.40**	**0.50**	**0.60**
	Carrier solvent	**STD in %**				
Not influenced						
Li (7)	**H_2O**	11.0	7.2	26.0	22.0	21.6
	1% HNO_3	7.2	12.5	7.8	24.2	24.7
Co (59)	**H_2O**	3.0	8.4	13.4	21.8	17.8
	1% HNO_3	0.9	3.8	13.3	14.7	1.8
Pb (208)	**H_2O**	6.0	4.5	12.7	23.8	9.1
	1% HNO_3	1.8	4.1	13.5	16.7	26.1
Slightly influenced						
Mg (24)	**H_2O**	7.3	6.1	19.5	19.2	4.7
	1% HNO_3	11.8	6.7	18.6	29.7	23.6
Al (27)	**H_2O**	11.6	11.0	17.3	24.4	20.6
	1% HNO_3	43.7	28.6	37.5	26.9	43.7
Zn (66)	**H_2O**	2.7	8.8	15.8	19.2	23.6
	1% HNO_3	8.3	5.1	22.0	22.6	38.1
Strongly influenced						
Fe (56)	**H_2O**	4.0	3.4	12.8	11.2	14.9
	1% HNO_3	no signal, baseline too high				
Cu (63)	**H_2O**	5.0	12.0	14.2	22.4	23.6
	1% HNO_3	no signal, baseline too high				

8.4.3 Variation of Micro Reactor Flow Rate (Configuration 2)

Flow rate in the micro reactor were changed from 0.6 mL/min to 8 mL/min in order to examine the stability of the measured signal. In addition, a suitable working range of the micro reactor could be estimated.

As shown in Figure 8-5, the total ion current (*TIC*) signal as well as other component signals Fe, Cu, Al, etc. show a slight slope as the micro reactor flow rate increases. Although the drainage line functions well,

a higher pressure is created in the suction line of the peristaltic pump that causes a higher sample amount entering the analyzer. This variation of the acquired signal can be reduced by using a bigger drainage diameter or longer capillary from the tee joint to the suction point of the peristaltic pump. However, the variation of the signal intensity is not significant in this case. Therefore, this second configuration can be considered stable for large variations of the flow rate of the micro reactor.

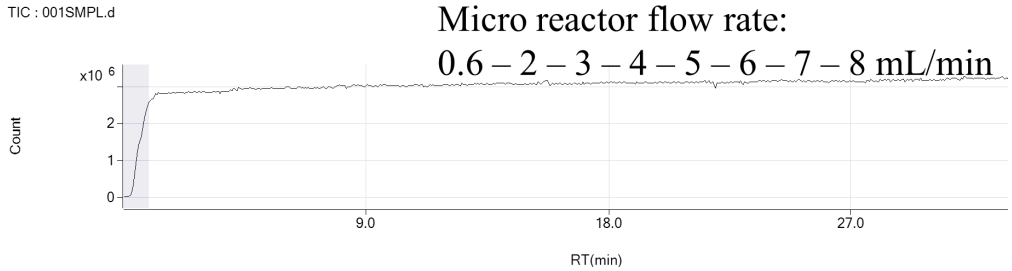

Figure 8-5: *TIC* signal according to the changing of micro reactor flow rate

Some advantages and disadvantages of the two connection concepts are listed in Table 8-3. In general, the second concept offers a stable and continuous sample flow from the micro reactor to the peristaltic pump, inclusion of the ALS and especially exclusion of the carrier solvent pump (P_3) which is the main source of metal contamination to sample. As a consequence, this concept is selected for further testing the dilution module in the connection to ICP-MS.

Table 8-3: Advantages and disadvantages of the integration concepts to ICP-MS

	Concept 1	**Concept 2**
Advantages	Simple and direct connection. Multiple peaks per reaction stage.	Continous flow from the micro reactor to the peristaltic pump. Including ALS. Not including the *mzr* pump. Large range of flow rate from ORMS to ICP-MS (>0.4 mL/min).
Disadvantages	Not including ALS: no suitable warm-up, tuning, and calibration for ICP-MS. A small range of flow rate from ORMS to ICP-MS (<0.6 mL/min). Including the *mzr* pump which is the main source of metal contamination from the ORMS system.	

8.5 *Dilution with ICP-MS in Spectrum mode*

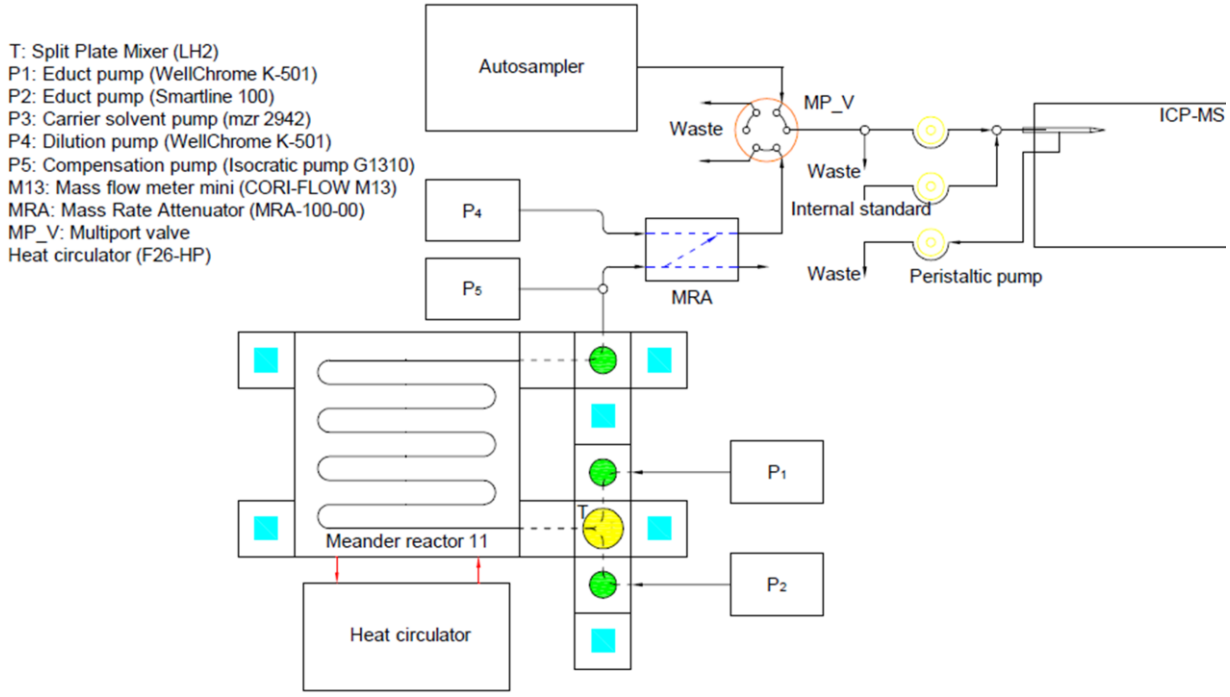

Figure 8-6: Second concept for integration to ICP-MS including the dilution module

The second integration scheme is selected for quantitative verification of the dilution module. As shown in Figure 8-6, flow from the micro reactor after diluted using the flow compensation approach is connected to the multiport valve. The valve's position decides either ALS or the diluted flow to be linked to the peristaltic input flow.

For every reaction stage, flow rate of the micro reactor system is fixed. For ICP-MS, flow rate of the peristaltic pump at its default settings is different (Sample uptake: 0.4 rps ≈ 1.6 mL/min; Probe rinse: 0.1 rps ≈ 0.4 mL/min; Probe rinse 1: 0.3 rps ≈ 1.2 mL/min). Therefore, the flow requirement from the peristaltic pump would be often greater than what ORMS can supply (sometimes only 0.4 mL/min). This would result in air bubble in the main stream that enters via the drainage line. The issue is circumvented at a cost of time increasing up to 4 minutes per sample by changing settings for the peristaltic pump (Table 8-4). In all steps of a sampling cycle, flow rate of the peristaltic pump/nebulizer pump is fixed at 0.1 rps which is equal to the smallest flow rate from the ORMS. Due to flow reduction, the uptake time is increased from 30s to 140s to guarantee the sample to arrive and to be stable at the acquisition period. This value is estimated by manually monitoring the signal changes (from low to high or high to low) in the tuning step of ICP-MS. In addition, the ALS measures calibration samples from low to high concentration and it is not used when the OMRS line is connected to MS that the rinse time can be set to 0s to save time.

Table 8-4: Change settings for the Peristaltic pump

Steps	Time (s)	Speed (rps) of Nebulizer Pump
Sample Uptake	140	0.10
Probe Rinse (Sample)	0	0.10
Probe Rinse (Std)		
Rinse 1	0	0.10
Probe Rinse 1		
Rinse 2	0	0.10
Probe Rinse 2		

8.5.1 Experimental Procedure and Setup

By enabling a stable flow to the nebulizer the ICP-MS is also enabled to work with the spectrum acquisition mode. This helps to make the calibration curve conveniently and therefore the quantitation of the dilution can be done easily. Because the procedure for performing the experiment includes ALS and ORMS with some steps, it is necessary to enumerate them. The following steps and values were used in the third experiment to measure quantitatively the dilution of 5 mg/L ICP multi-element standard in 1% HNO_3 with 1% HNO_3 as a diluent (Section 8.5.2.3).

- Prepare samples for a standard calibration (1 – 5 – 10 – 50 – 100 µg/L ICP multi-element standard in 1% HNO_3).
- Prepare stock solution for automatic dilution (5 mg/L ICP multi-element standard in 1% HNO_3).
- Manually dilute the stock solution in different dilution ratios (1:1000 – 1:500 – 1:100 – 1:50). These manually diluted samples are used to compare with automatic dilution. These samples as well as samples for calibration are sent to the analyzer via the ALS.
- Set the multiport valve in a position (position A – default) so that the ALS connects to the peristaltic pump.
- Start the ICP-MS as normal and remember to tighten up the back-pressure regulator for no suction of air bubbles.
- Create a batch and a list of samples for the ICP-MS to measure. Then, change settings as in Table 8-4 for the peristaltic pump at Batch\Acq Method\PeriPump-ISIS.
- Set one dilution ratio (from high to low, 1:1000 – 1:500 – 1:100 – 1:50), flow rates (4 – 2 – 1 mL/min), sampling interval and other parameters for the ORMS as in *Experiment 10* Table 11-12.
- Manually switch the multiport valve in order to connect the ORMS to ICP-MS after ICP-MS tuning has finished. Then, release the back-pressure regular for no pressure accumulation in the main stream and start the ORMS.
- Set a new dilution ratio after the previous measurement finishes.

These steps were applied to perform dilution with different solutions: (1) blank solvent (1% HNO_3), (2) blank solvent (ultrapure water), (3) solution with 5 mg/L ICP multi-element standard in 1% HNO_3 and (4) solution with 5 mg/L ICP multi-element standard in ultrapure water. The results are presented for every experiment separately.

8.5.2 Results

8.5.2.1 Dilution in Spectrum Mode of ICP-MS with 1% HNO_3 Blank Solvent

Detail settings for the experiment can be found in *Experiment 8* Section 11.2. In general, the experiment first runs calibration samples, then blank solvent (1% HNO_3) via ALS and finally, automatic dilution via the ORMS system. The results are plotted in Figure 8-7a for some representatives (Fe, Mn, Li). The yellow bar shows the average value from 4 vials of the blank solvent transferred via ALS. Other bar groups indicate results of automatic dilution with blank solvent at ratio 1/500, 1/100 and 1/50 with micro reactor flow rate from 4 mL/min to 1 mL/min.

As it can be seen, there is contamination from ORMS to the solution in micro reactor because contaminant's concentration before the ORMS is smaller than that after the ORMS such as Fe and Cr. More specific, Fe and Cr contaminate sample the most with their high concentration difference before and after ORMS (1.274 µg/L for Fe and 0.520 µg/L for Cr). Some elements such as Mn, Ni, Cu and Al contaminate sample with lower concentration (0.156 µg/L for Mn and 0.073 µg/L for Cu). Other elements such as Li, B, Mg, Co, Zn, Ga, Ag, Cd, Ba, and Pb have very little or no contamination to sample due to the difference in their concentration before and after the ORMS is very small.

8.5.2.2 Dilution in Spectrum Mode of ICP-MS with Milipore water

A similar experiment was performed for Milipore water. Detail settings are stored in *Experiment 9* Section 11.2. Results are plotted in Figure 8-7b for some selected elements (Fe, Mn, Li).

In this case, Fe is a higher contaminant than other elements with its concentration difference before and after the ORMS is 0.289 µg/L. Some elements such as Cr, Mn, Ni, Cu and Al contaminate sample with a lower concentration (0.189 µg/L for Cr and 0.102 µg/L for Mn). Other elements such as Li, Mg, Co, Zn, Ga, Ag, Cd, Ba, and Pb have very little or no contamination to the sample due to the difference in concentration before and after the ORMS is very small. It can also be seen that the contamination for most elements in ultrapure water is smaller than in 1% HNO_3.

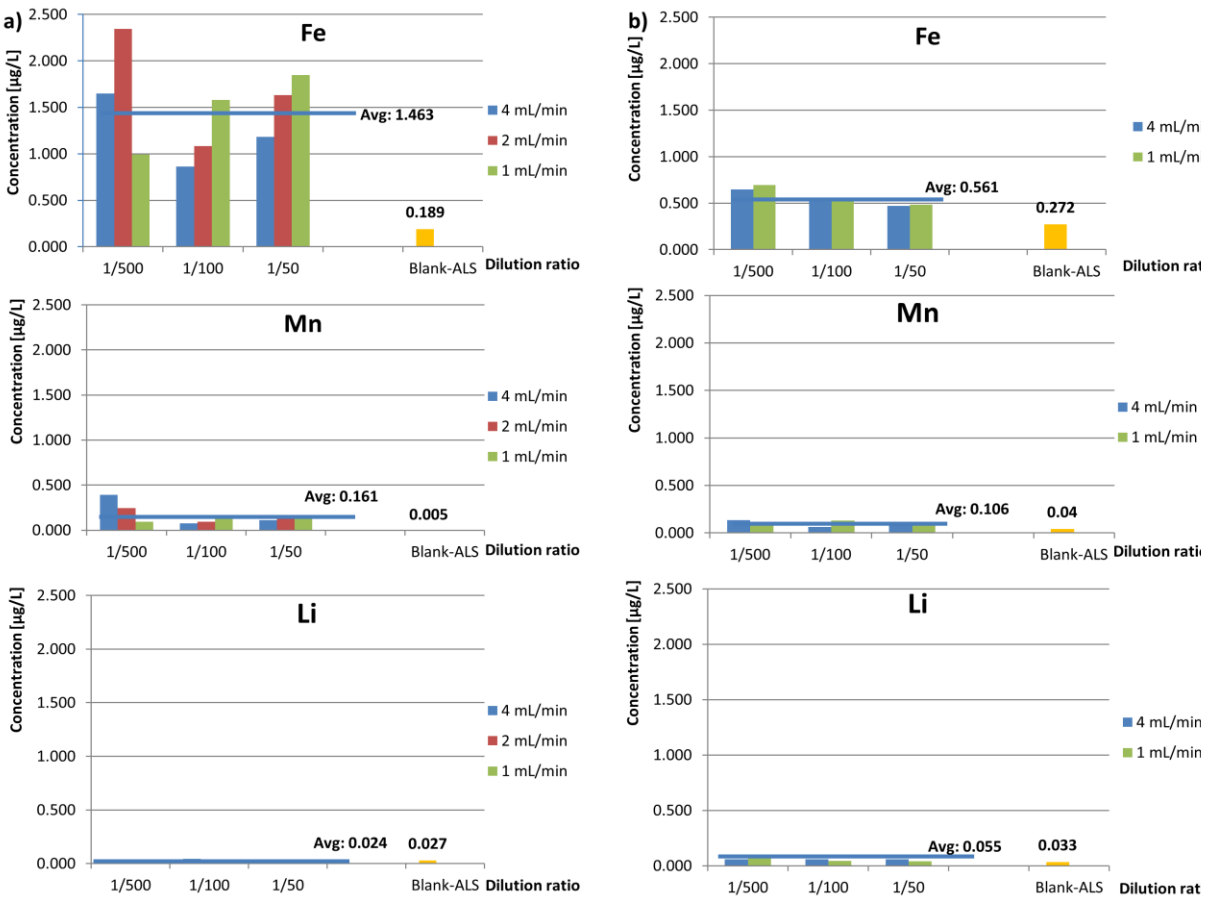

Figure 8-7: Concentration of Fe, Mn and Li in blank solution of 1% HNO_3 and ultrapure water sampled by ALS and by ORMS system at different dilution ratios and different flow rates of the micro reactor
a) in 1% HNO_3, b) in ultrapure water

8.5.2.3 Dilution of 5 mg/L ICP multi-element standard in 1% HNO_3

Details settings for the experiment has been explained in Section 8.5.1 and summarized in *Experiment 10* Section 11.2. Results for some selected elements (Li, Mn, Fe) are shown in Figure 8-8. Plots on the left compare manual vs. automatic dilution; and plots on the right show details measurements of automatic dilution. In the top left plot as for Lithium (Li), values from manual dilution plotted in blue (1:1000 – 1:500 – 1:100 – 1:50) are linear and close to the expected concentrations (5 – 10 – 50 – 100 µg/L). Automatic dilution at different micro reactor's flow rates gives equivalent results to manual dilution of the same dilution ratio as indicated by green line (4 mL/min), red line (2 mL/min) and yellow line (1 mL/min). This automatic dilution is further displayed in the plot besides that shows detail measurement for each diluting condition (each diluting condition is measured 4 – 5 times). In general, results of automatic dilution are logical (higher dilution ratio-lower concentration of the diluted solution and vice versa), stable with various flow rates of the micro reactor and in accordance with the expected concentrations as well as with results of manual dilution. Dilution 1:1000 (with expected concentration 5 µg/L, manual dilution: 4.94 µg/L) is displayed at the left most bar group. This group shows a good dilution in different flow rates of the micro reactor such as 4.90 µg/L at 4 mL/min (green bars), 4.94 µg/L

at 2 mL/min (red bars) and 4.77 µg/L at 1 mL/min (yellow bars). The dilution is stable because different sampling repetition (one bar represents one sampling's result) gives similar values. Similarly, the dilution results are good with >90% the expected concentration for other dilution ratios such as 1:500 (second bar group - expected concentration: 10 µg/L, manual dilution: 9.82 µg/L), 1:100 (third bar group - expected concentration 50 µg/L, manual dilution: 51.47 µg/L) and 1:50 (last bar group - expected concentration 100 µg/L, manual dilution: 108.34 µg/L). However, at ratio 1:50 (flow rate 1 mL/min), the dilution gives about 80% of the expected concentration. This makes the yellow bar group lower than two other bar groups. The reason might come from the change to another split factor (from SF=2 to SF=3) which does not work as well as the previous one.

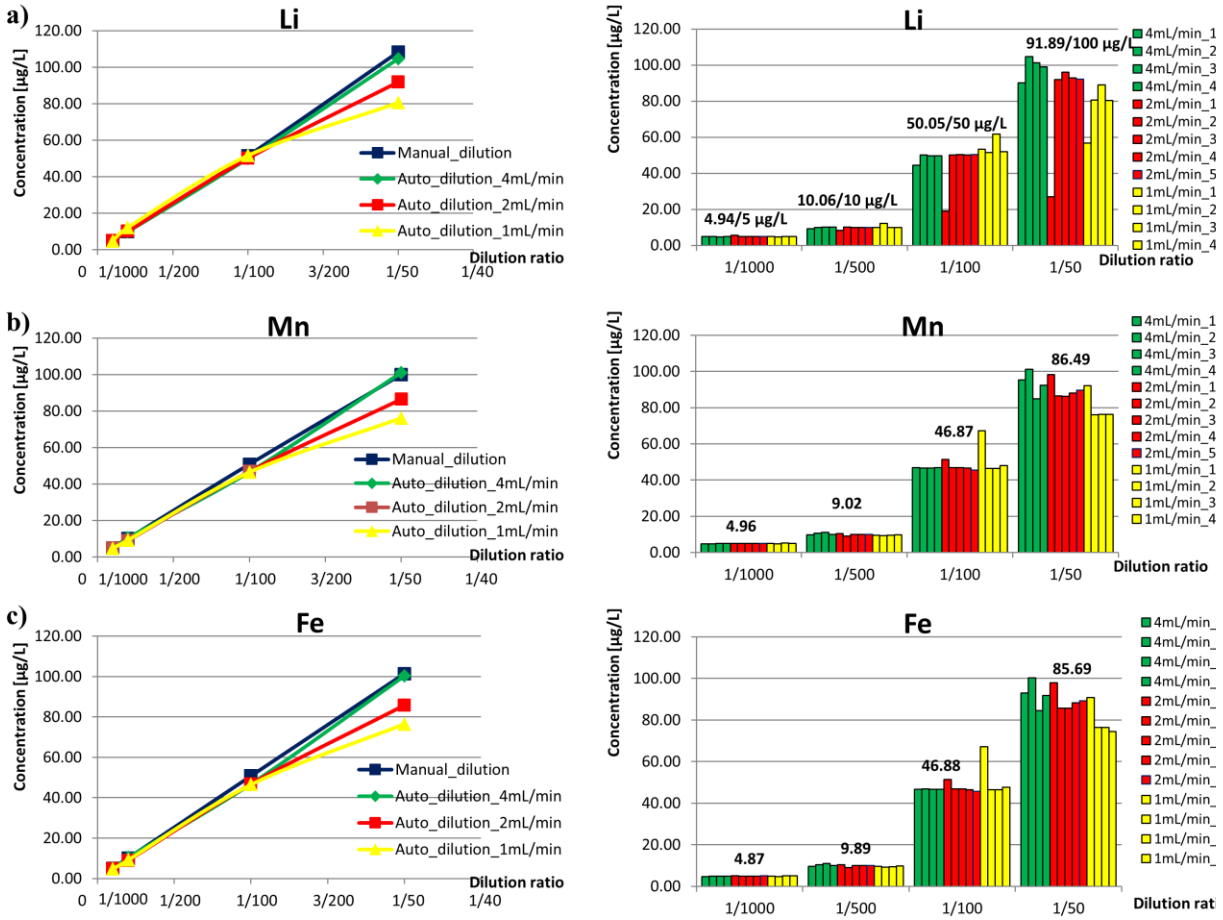

Figure 8-8: Manual vs. automatic dilution of 5 mg/L ICP multi-element standard in 1% HNO_3 at dilution ratios 1:1000, 1:500, 1:100 and 1:50 (left) and its automatic dilution in more details (right) for some representatives Li (a), Mn (b), Fe (c)

Every sampling set on ICP-MS is taken at every 4 minutes without knowing about the ORMS's operation. The ORMS changes its working conditions for every new reaction stage or dilution ratio that it requires some time to be stable. If ICP-MS's sampling period falls into that transient period, the measured signal will be not good. This normally occurs in the first sampling of every new reaction stage and every new dilution ratio as seen at ratio 1:100 – flow rate 2 mL/min or 1:50 – flow rate 2 mL/min and 1 mL/min. As a result, the first sampling in every new reaction stage or new dilution ratio should be omitted.

The calibration and dilution for other elements are not much different. Plot *b* (Mn) and *c* (Fe) that respectively belong to group "slightly influenced" and "influenced" by metal dissolution from the micro reactor (as in two previous experiments) show a good dilution. There is no or very little influence from the contaminants to the dilution because the measurements are approximate to the expected concentrations; calibration curves for Mn and Fe are linear (not shown); and the automatic dilution for Mn, Fe is as good as that of Li.

8.5.2.4 Dilution of 5 mg/L ICP multi-element standard in Ultrapure water

Dilution of 5 mg/L ICP multi-element standard in ultrapure water was carried on with ultrapure water as a diluent. Detail settings for the ORMS can be found in *Experiment 11* Section 11.2. Main settings are: dilution ratio 1:1000 – 1:500 – 1:100 – 1:50; micro reactor flow rate: 4 mL/min - 2 mL/min – 1 mL/min (reaction stage: 3 min – 6 min – 12 min).

The results for some selected elements (Li, Mn, Fe) are shown in Figure 8-9 with its arrangement in the same way as in the previous figure. Results for diluting with ultrapure water are not remarkably different from the previous case with HNO_3 (1%, v/v). In the top left plot as for Li, values from manual dilution plotted in blue (1:1000 – 1:500 – 1:100 – 1:50) are linear and close to the expected concentrations (5 – 10 – 50 – 100 µg/L). In the top left plot, automatic dilution at different micro reactor's flow rates gives stable and equivalent results to manual dilution of the same dilution ratio as indicated by green line (4 mL/min), red line (2 mL/min) and yellow line (1 mL/min). In the top right plot, dilution 1:1000 shows a good dilution at different flow rates of the micro reactor such as 5.11/5 µg/L at 4 mL/min (green bars), 4.78/5 µg/L at 2 mL/min (red bars) and 4.40/5 µg/L at 1 mL/min (yellow bars). Similarly, the dilution results are good with >90% the expected concentrations for other dilution ratios 1:500 (second bar group - expected concentration 10 µg/L, manual dilution: 10.51 µg/L), 1:100 (third bar group - expected concentration 50 µg/L, manual dilution: 53.54 µg/L) and 1:50 (last group - expected concentration 100 µg/L, manual dilution: 103.72 µg/L). At flow rate 1 mL/min of ratio 1:50, the dilution again gives smaller value (78.45/100 µg/L) than at other flow rates due to the change to another split factor which does not work very well. There are also some abnormal bars at the first sampling in every new reaction stage or new dilution ratio. This can be similarly reasoned as in the previous experiment for 1% HNO_3. Finally, dilution for other elements is also not much different to that of Li as shown in plot *b* for Mn, except for Fe in plot *c*. The calibration curve for Fe as well as its dilution are not good which may be reasoned by effects from the sample matrix.

In comparison to the previous test using 1% HNO_3, dilution using ultrapure provide similar results. The concentration of diluted solution with ultrapure water is a bit smaller than that of the previous test with 1% HNO_3 for all dilution ratios. However, the reason comes from the physical abrasion of the *rotor seal* and *stator face assembly* pair. This reduces the amount of transferred sample as the aliquot volume get smaller over operation time. The effect of different solvents is not clearly observed in this test because both concentration and Count per second (CPS) of the diluted sample in both cases are not remarkably different. It is also observed that, the CPSs for different elements with same concentration in a solution

are different. For example, 100 µg/L of Cu (in the calibration solution) gives a CPS of 997,839 but 100 µg/L of Zn (in the same calibration solution) gives a CPS of 167,990.

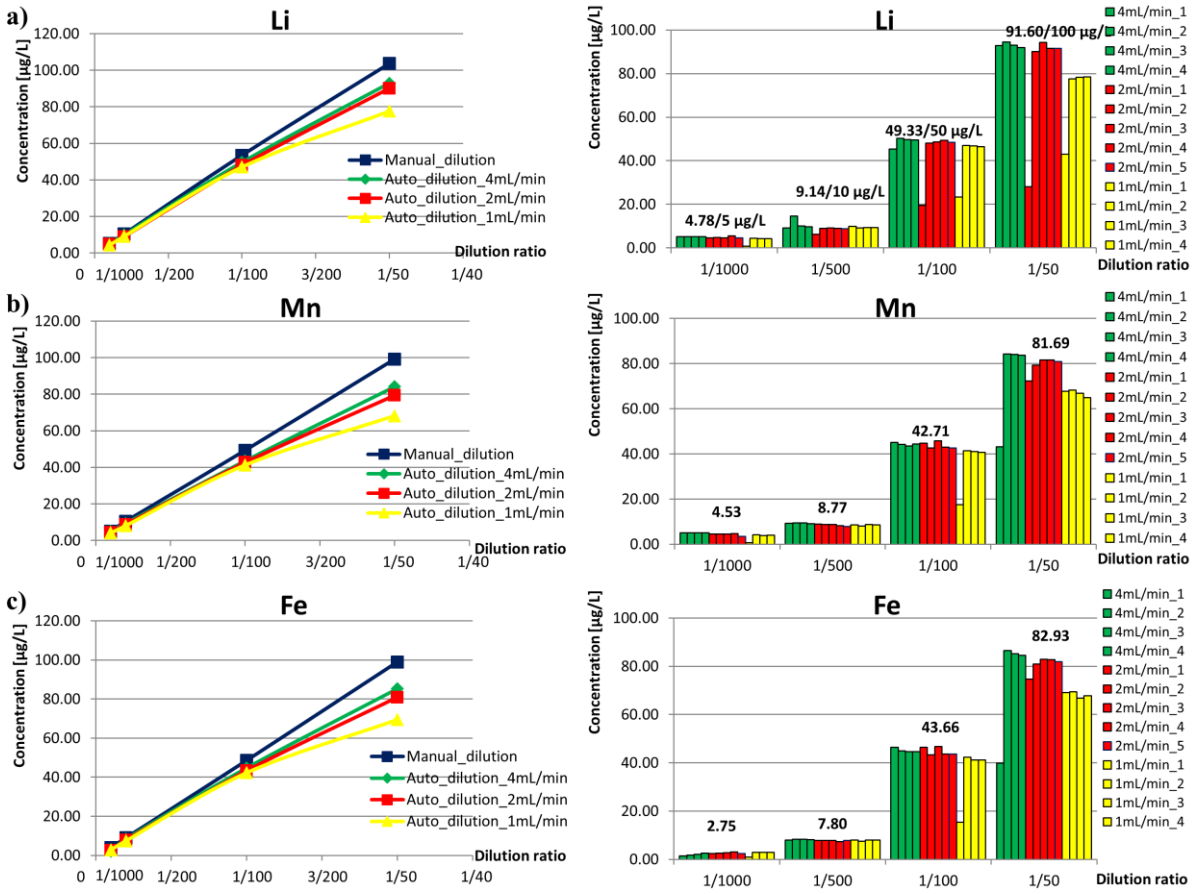

Figure 8-9: Manual vs. automatic dilution of 5 mg/L ICP multi-element standard in ultrapure water at dilution ratios 1:1000, 1:500, 1:100 and 1:50 (left) and its automatic dilution in more details (right) for some representatives Li (a), Mn (b), Fe (c)

8.6 *Dilution with ICP-MS using Time-Resolved Analysis (TRA) Mode*

One drawback of using the previous concept is its high sampling cycle time (approx. 4 minutes for each sample). Another attempt has been made in order to reduce this sampling period by modifying the integrating configuration (Figure 8-10) and using the TRA mode of ICP-MS. At normal operating condition, diluted solution runs through a sample loop (5µL) to waste and the ALS connects to the peristaltic pump via the multiport valve. When this valve switches, sample in the sample loop is withdrawn and sent to the MS. ALS plays a role supplying carrier solvent to carry sample to MS. The direct connection approach (configuration 1) as presented in Section 8.3 is not selected because it does not include the ALS; it has strong contamination of Fe and Cu from the *mzr* carrier solvent pump and this pump is not suitable for working in acidic environment.

8.6.1 Experimental settings

A familiar experiment diluting 5 mg/L multi-element standard solution in 1% HNO_3 was performed. Manual dilution was also conducted in order to compare with automatic dilution. Detail settings for the

experiment are shown in *Experiment 12* Section 11.2. Main settings are: dilution ratio 1:500 – 1:100 – 1:50; micro reactor flow rate: 4 mL/min - 2 mL/min – 1 mL/min (reaction stage: 3 min - 6 min – 12 min); and diluent is 1% HNO_3.

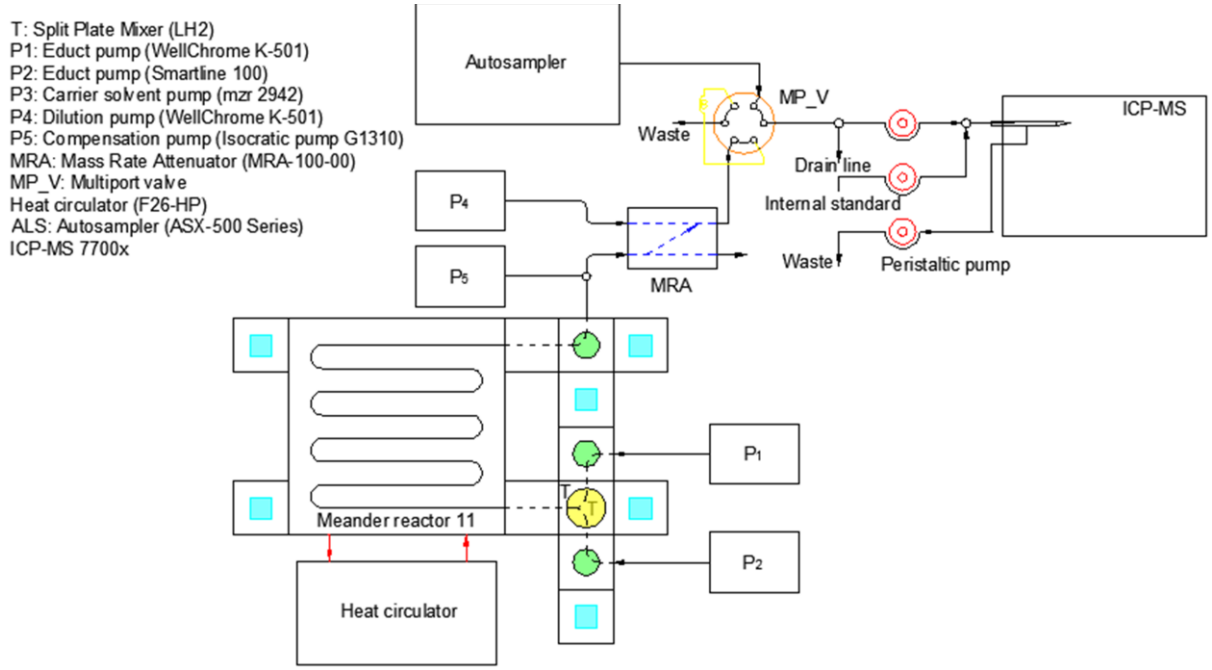

Figure 8-10: Integrating configuration used for testing the dilution module with ICP-MS in TRA mode

8.6.2 Results

The results are presented for some elements that are not or very little contaminated and contaminated by the micro reactor system. Figure 8-11 is the dilution result of Pb with the first 4 groups displaying manually diluted samples and the last 3 groups displaying automatic dilution. Each diluting condition is sampled 5 times. In general, results of automatic dilution are logical (higher dilution ratio-lower concentration of the diluted solution and vice versa), stable with various flow rates of the micro reactor system (4 – 2 – 1 mL/min). More details of the measurement are presented in Table 8-5. In every dilution ratio, the average peak area and STD of 5 peaks for every reaction flow rate (4, 2, 1 mL/min) are calculated, which give STD in the range of 1.2% - 16.7%. The average peak area of all peaks for every dilution ratio is also calculated which equals approximately 75% of manual dilution. Further comparison of the signal intensity between different dilution ratios (1:50, 1:100) with dilution ratio 1:500, we get values in two rows “expected quotient” and “actual quotient”. It is expected that the signal intensity of dilution ratio 1:50 would be 10 times larger than that with dilution ratio 1:500. The actual quotient in this case (438,216/44,556) is 9.84 which is very good. Another logical quotient is also obtained with dilution ratio 1:100 (expected quotient: 5 – actual quotient: 5.08 (226,424/44,556)). For other elements which are not or little influenced by the micro reactor such as Li, Cu, Mg, Co, Zn, Ga, Ag, Cd, Ba, … the dilution results are logical and can be interpreted the same as for Pb. These dilution results once again confirm the diluting capability of the module.

Table 8-5: Measurement results of Automatic vs. Manual dilution for Pb

Automatic dilution				
Dilution ratio	**1/1000**	**1/500**	**1/100**	**1/50**
Average peak area-4 mL/min (Abr. unit)		48,121	225,370	477,826
STD		8,042	10,549	11,765
STD in %		16.7	4.7	2.5
Average peak area-2 mL/min (Abr. unit)		38,394	220,908	459,192
STD		1,696	5,948	5,603
STD in %		4.4	2.7	1.2
Average peak area-1 mL/min (Abr. unit)		47,152	232,993	377,629
STD		1,626	2,899	9,821
STD in %		3.4	1.2	2.6
Average of all peaks (Abr. unit)		44,556	226,424	438,216
STD		6,522	8,751	44,520
STD in %		14.6	3.9	10.2
Expected quotient		1	5	10
Actual quotient		1	5.08	9.84
Manual Dilution				
Average of all peaks (Abr. unit)	30,019	57,750	288,660	597,681
STD	1,742	3,459	13,241	24,221
STD in %	5.8	6.0	4.6	4.1

However, for those elements that are influenced by the micro reactor such as Fe, Cr, Mn, the dilution is not good that signals measured from both manual and automatic dilution at different dilution ratios are not clearly different. All the peaks measured almost have similar areas as shown in Figure 8-12 for Fe. Those results are also different from those measured in Section 8.5.2.4 using the spectrum mode although they are supposed to be similar. The difference, however, has not had an explanation currently. In general, the measurement for the dilution module with TRA mode gives as logical results as with the spectrum mode except for some elements contaminated by the ORMS such as Fe, Cr, and Mn.

Using the TRA mode and the current configuration, the *mzr* pump is not included that prevents a strong contaminating source of Fe and Cu; the ALS is included that the warming up and tuning procedure are performed conveniently. In addition, using the TRA mode allows consecutive measurements without fear of significant contamination from previous measurements [173]. However, due to pressing effects from the peristaltic pump, the sample is dispersed which results in wide peak (normally >60s depending on the diluted concentration). In addition, it requires about 50s for the sample to reach the detector. These make the sampling interval be selected as long as 160s. Although this value is rather high, it is smaller than in the previous configuration (≈ 240s). In addition, the sample-dispersing effect also reduces the

measurement sensitivity of elements, for example, Li and Al, which can be quantified in spectrum mode, give weak signals in TRA mode.

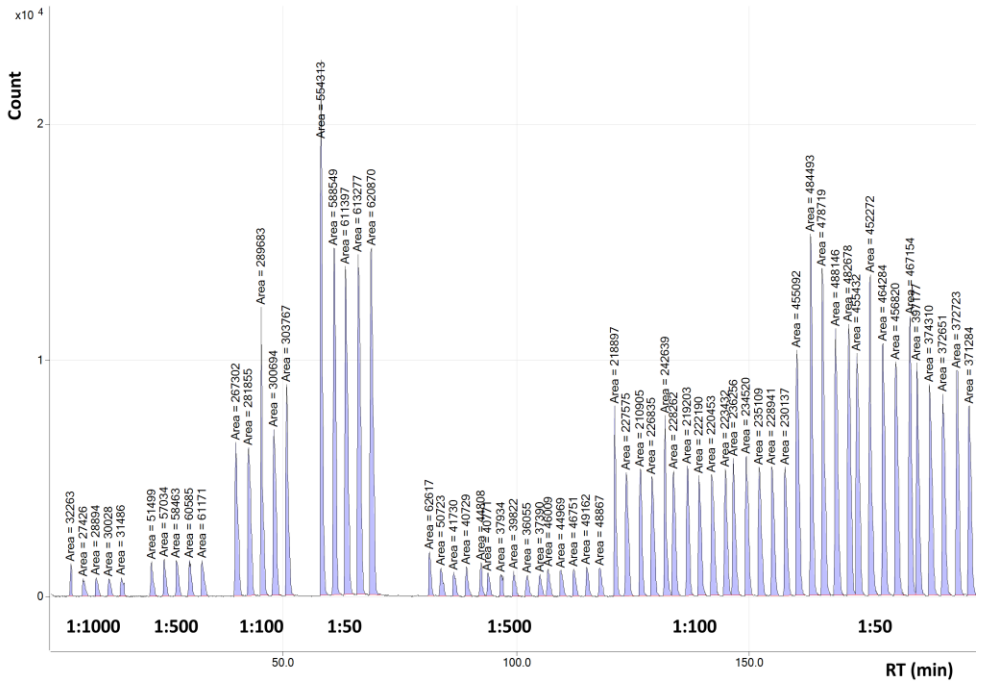

Figure 8-11: Manual and automatic dilution in TRA mode for Pb (207)

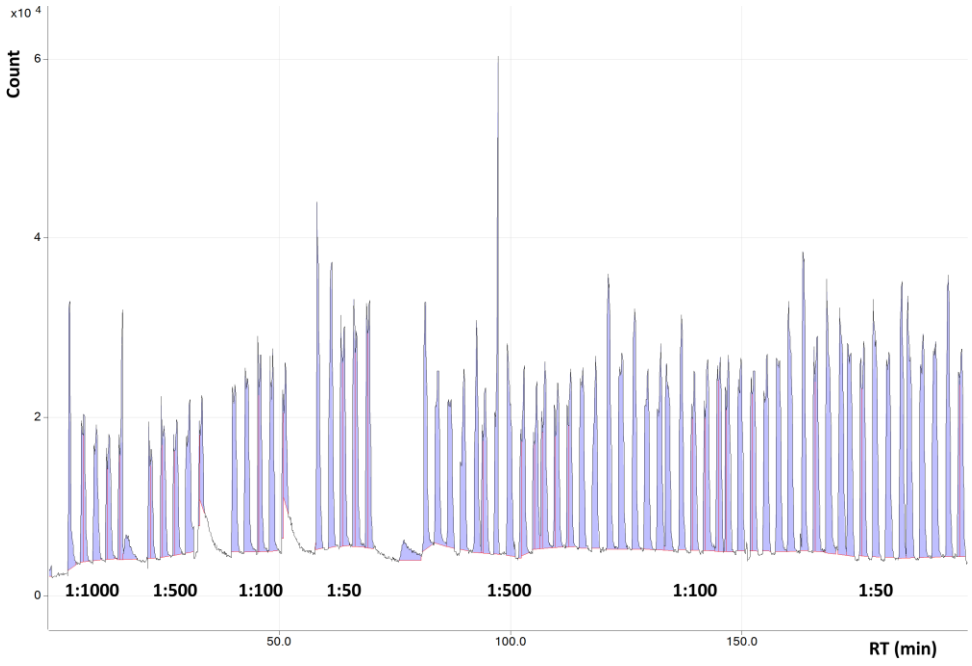

Figure 8-12: Manual and automatic dilution in TRA mode for Fe (56)

8.7 *Summary*

Two concepts for coupling the micro reactor system to an ICP-MS have been proposed. In both concepts, the micro reactor system is successfully coupled to the ICP-MS that elements in the standard solution from the micro reactor system are detected. Testing results in the first concept shows a strong contamination of Cu and Fe from the system materials to the sample due to the *mzr* carrier solvent pump. It also shows more abrasion of the carrier pump's materials with 1% HNO_3 solvent than with ultrapure water. The second concept, which includes an ALS, provides more flexibility in sample handling and is stable to flow rate variations of the micro reactor. This second concept is further applied in determining the contaminants from the ORMS (excluding the *mzr* pump) to the sample such as Fe, Mn, Cr and quantify the dilution using 1% HNO_3 and ultrapure water as diluents in which the ICP-MS operates in spectrum mode. An attempt to reduce the time gap between each sampling has also been made with the ICP-MS in TRA mode. This helps decrease the sampling interval from 240s to 160s although the dilution result in TRA mode is not as good as that in the spectrum mode. However, in both operating modes of ICP-MS, the dilution module again shows its capability to give logical results at various dilution ratios.

In order to prevent air bubble from the drainage line, an inline check valve (CV-3323, IDEX Health & Science LLC, Oak Harbor, WA, USA) was used. However, it did not help that a back-pressure regulator was finally chosen. When the ALS connects to the peristaltic pump, this regulator is manually turned to maximum pressure to prevent air from the ambient. Later, it is manually released to atmospheric pressure when the micro reactor flow is connected to the peristaltic pump so that there is no pressure built up in the main stream and the excessive flow is easily discharged.

CHAPTER 9 MODIFICATION OF THE GRAPHICAL USER INTERFACE

A software module programmed in C++ (ORMS software) controls the system operation. Initially, the control software was realized to automate some core functions of the system as described in Section 3.2. It also monitors the status of main components of the system and records actions performed by the system in a log file. In addition, the ORMS software can communicate with the Data Acquisition software of the MassHunter Workstation Software series for the ESI-TOF-MS (Agilent Technologies, Waldbronn, Germany) using the classical Windows API approach. Due to the integration of new modules and new functions, the control software has been modified in order to adapt with the system expansion. However, the overall structure of the system is unchanged as shown in Figure 9-1.

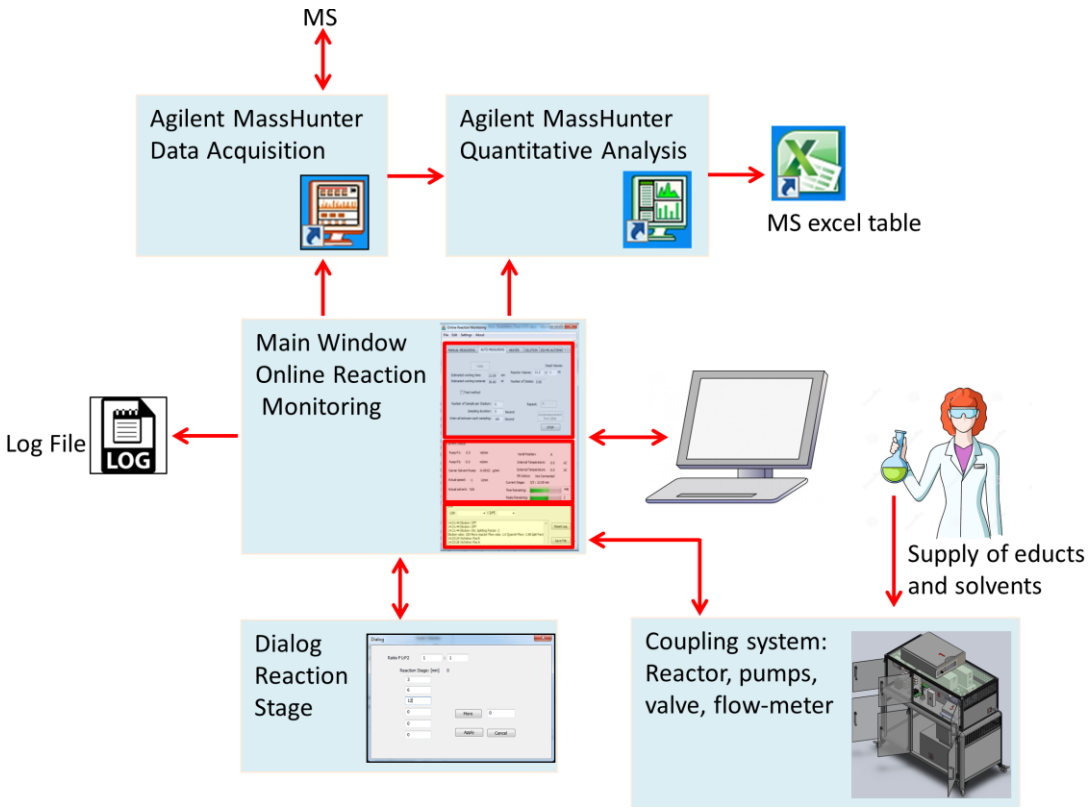

Figure 9-1: Schematic view of the workflow in the control of online reaction monitoring process [19]

9.1 *System GUI*

The modified graphical user interface (GUI) has three sections: *control section*, *status section* and *log section*. The *control section* involves different tabs in which each tab manipulates one functioning module of the system. The *status section* monitors the current status of main components. The *log section* is used for saving and archiving activities of the system. The system GUI is presented in Figure 9-2.

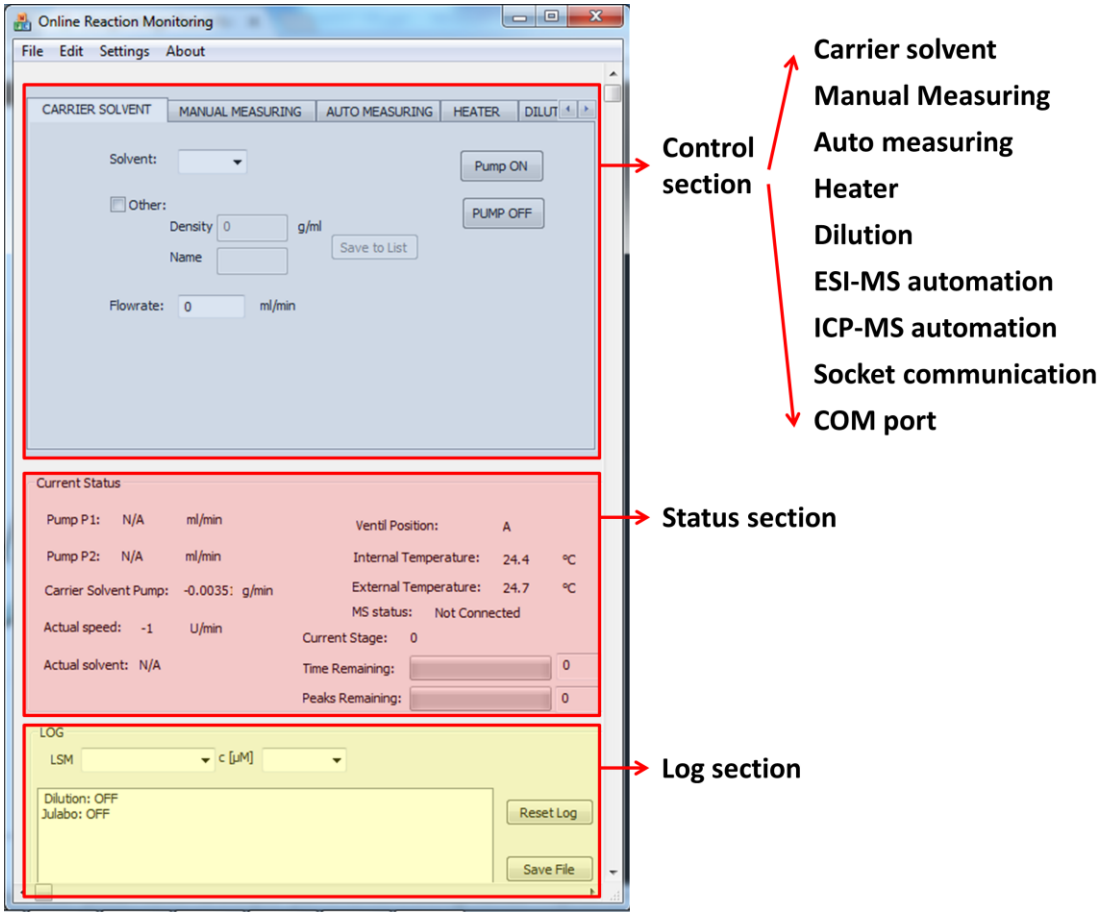

Figure 9-2: The modified GUI

9.1.1 Control Section

The *control section* is responsible for manipulating all component devices and linking them so that desired operations can be realized. In this section, there are different tabs with different control functions. Functions of each tab will be described in details.

CARRIER SOLVENT: This tab is used for selecting a carrier solvent that carries sample to the MS. In addition, users can set its flow rate so that the mass flow meter (Coriflow) can control the carrier pump's speed (Figure 9-3). The flow rate of this pump (P_3) is calculated based on the specific density (g/mL) of the solvent. The permissible flow rate is in the range of 0.1 to 1 mL/min. In addition, users are allowed to add new solvents to the list one by one by specifying their name and density.

MANUAL MEASURING: This tab is used for manually testing individual devices of the micro reactor module. Users can directly set the reactor volume and flow rate of HPLC Knauer pumps (pump P_1 and pump P_2), which transfer educts to the reactor (Figure 9-4a). Residence time can be set so that flow rates of these pumps are automatically calculated with 50-50% contribution from each stream. In addition, manual switching of the multiport valve, to position A or to position B, can be performed here. Other

sampling parameters can be edited such as sampling duration, sampling interval and number of repeated sampling so that a specified number of samplings can be executed.

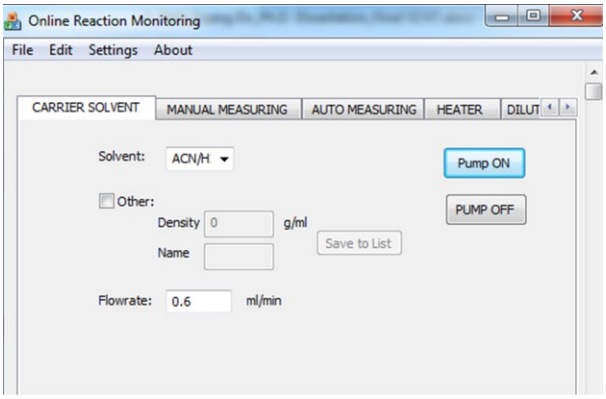

Figure 9-3: Control section: carrier solvent

AUTO MEASURING: The *automatic operation mode* of the system is set in this tab (Figure 9-4b). Users can click on "Table" button to specify a sequence of reaction stages in time ascending order as well as to set flow rate ratio for two educt pumps. The reactor volume and additional volume (for volume of mixer, capillaries, etc.) can be set. After either the *fast sampling method* or *slow sampling method* is selected, total time and volume requirement are estimated. Other sampling parameters (sampling repetition, sampling duration, sampling interval) have to be defined in this tab before automatic measurement (or *automatic operation mode*) can be started. For fully operated in automatic mode including automatic heating and automatic dilution, these modules must be set and triggered first. After settings for reaction stages completes and the "automatic measurement" button is clicked, the heating module and dilution module will be automatically activated to work in the auto mode.

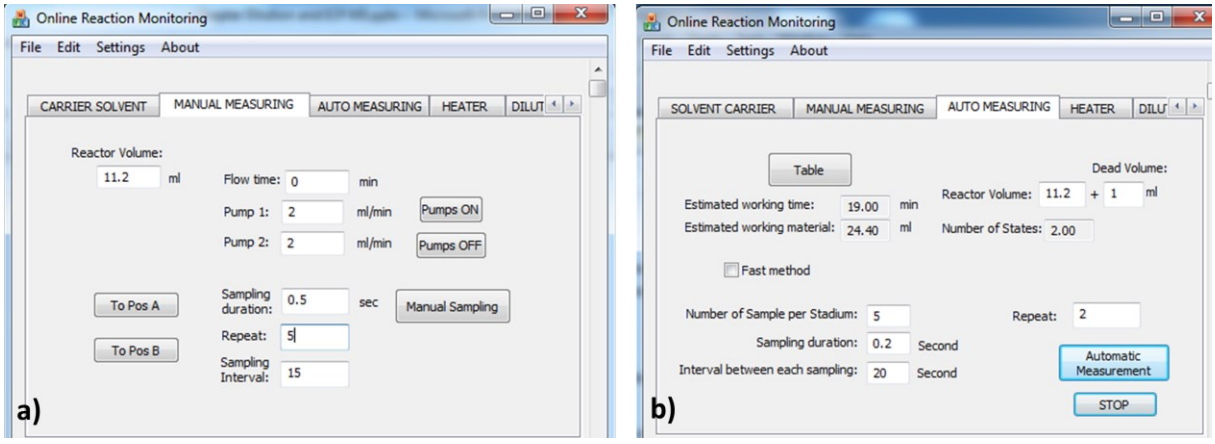

Figure 9-4: Control section: a) manual measuring, b) auto measuring

HEATER: Temperature for the circulator and heating plate can be set in this tab (Figure 9-5a). When the "Preheat" button is pressed, the circulator works in the internal heating mode. It will switch to the

external heating mode when the system starts measuring with the *automatic operation mode*. Temperature of the heating solvent and of the analytical solution as well as heater status are displayed. This module can also be referred to in CHAPTER 6.

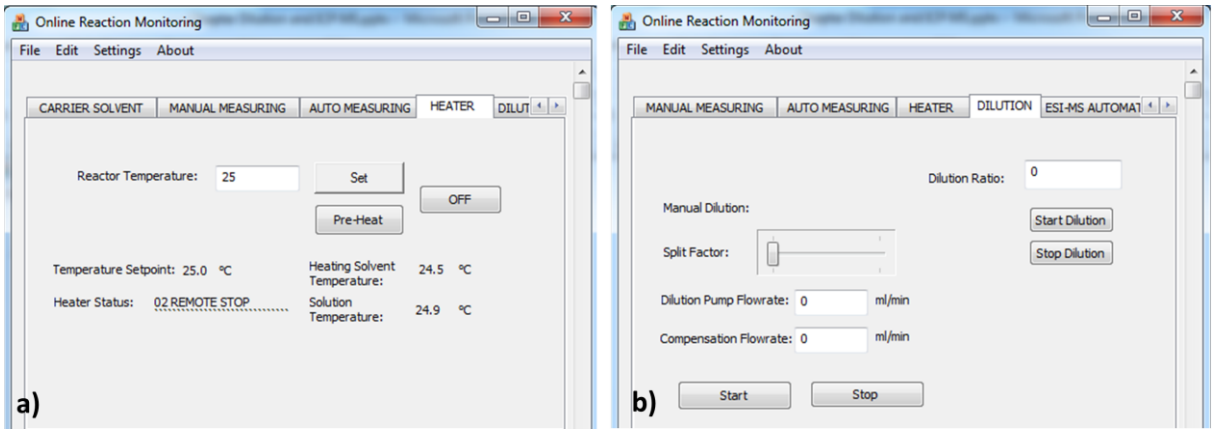

Figure 9-5: Control section: a) heater, b) dilution

DILUTION: In this tab, users can specify and start a desired dilution ratio, then splitting factor and dilution flow rate is automatically selected (Figure 9-5b). This is the initial selection without considering to the variation of the micro reactor flow rate. Similar to the heating module, when the *automatic operation mode* begins, those dilution parameters are recalculated based on the micro reactor flow rate and the module restarts. For more flexibility to the system, all diluting components such as the MRA, dilution pump and compensation pump can be manually controlled.

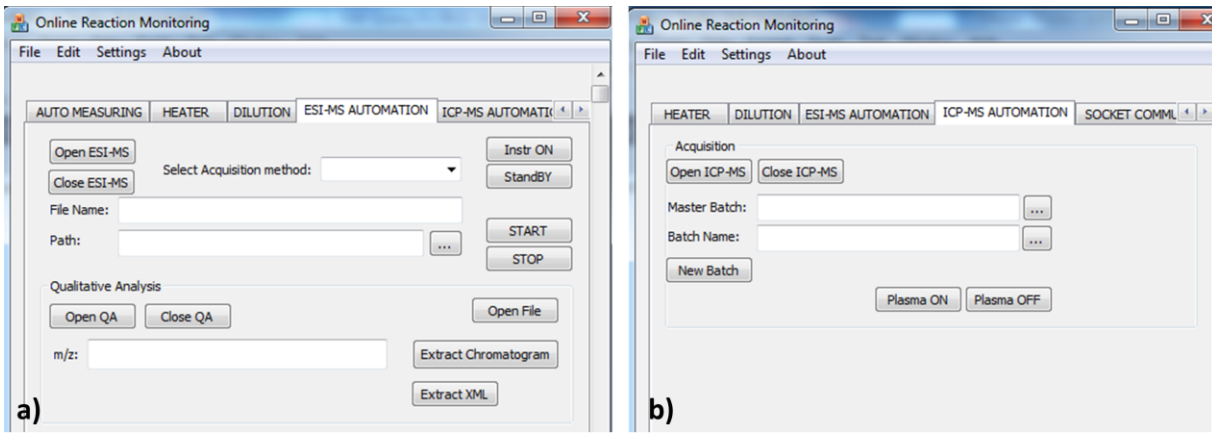

Figure 9-6: Control section: a) ESI-MS automation, b) ICP-MS automation

ESI-MS AUTOMATION: In this tab (Figure 9-6a), some basic operations of the Data Acquisition software for the ESI-TOF-MS can be performed via the ORMS software such as open/close the MassHunter, select an acquisition method. Users can update a file name and path name to store data; turn on the MS instrument/put it in standby mode; and start/stop an acquisition. In addition, the Qualitative Analysis software can be automated as well: open/close the software, and open a data file so that specific

m/z values can be sequentially extracted for its chromatogram. This tab is responsible for data acquisition. Therefore, if an ESI-MS is connected to the ORMS, it should be activated before the OMRS starts to transfer sample.

ICP-MS AUTOMATION: In this tab (Figure 9-6b), some basic operations of the ICP- MS Instrument Control software can be performed via the ORMS software such as open/close the MassHunter; Create a new measurement series (also called: batch) by using an existing master batch template; ignite and shutdown the plasma. This tab is responsible for data acquisition. Therefore, if an ICP-MS is connected to the ORMS, it should be activated before the OMRS starts to transfer sample.

SOCKET COMMUNICATION: The ORMS software can communicate with a server via Internet by specifying the IP address and Port of the target sever (Figure 9-7a). A file in **.xml* format can also be received or transferred. The CSocket class and a library called TinyXML2 were implemented to fulfill this task. This tab is built for future usage when the ORMS might communicate to a server program in the laboratory (i.e. SAMI®).

COM PORT: There are different devices such as pumps, heater, multiport valve and MRA under control by the software via RS232 and then USB hubs (Figure 9-7b). Since COM Port assignment for a device is different from computer to computer and from USB port to USB port of a computer, a manual assignment of each device for initial connection is necessary. After an initial selection, the choice is stored and retrieved every time the software to be launched. Connection status of every device to the software is indicated in a list box so that users can select another COM port if the connection status is failed. This tab should be checked first to make sure all devices be successfully communicated by the software so that further tasks from users could be executed.

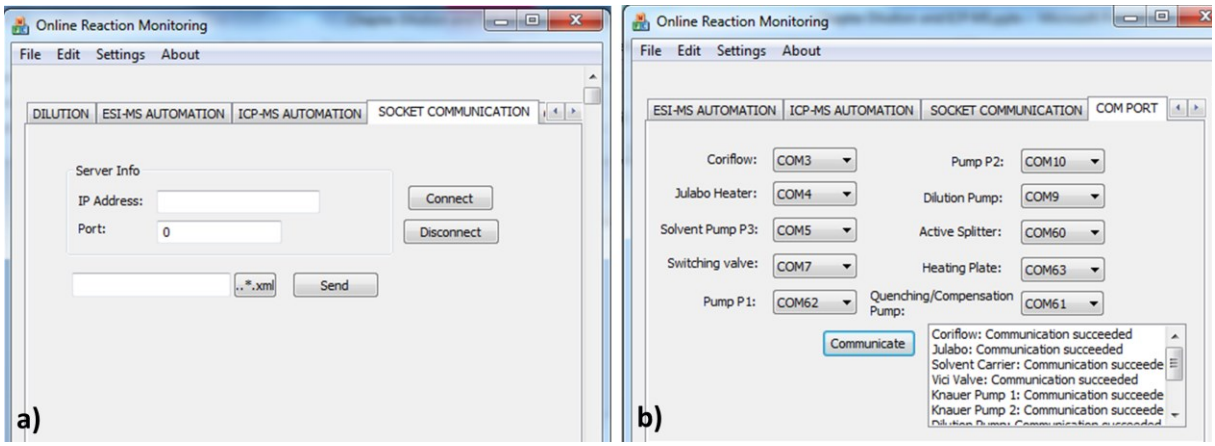

Figure 9-7: Control section: a) socket communication, b) COM port

9.1.2 Status Section

Monitoring of the current status of the system is necessary so that suitable actions could be taken in time. The monitored states are displayed in one separate section for some devices, and some other less

important are distributed in their corresponding tabs (Figure 9-8). In the main status section, calculated flow rate of two educt pumps (P_1, P_2); flow rate and speed of carrier solvent pump (P_3); temperature of heating solvent and reagent solution, etc. are indicated. Current reaction stage, time remaining before a sampling action and number of remaining peaks for each reaction stage are also indicated by two slide bars with their relevant values. Current status of the ESI-MS such standby, wait, ready is also included when it is connected to the ORMS software. Based on the current status of devices, a user has to determine himself whether an action should be taken place or not because, currently, there is no implementation of any algorithm which helps notify abnormal situations.

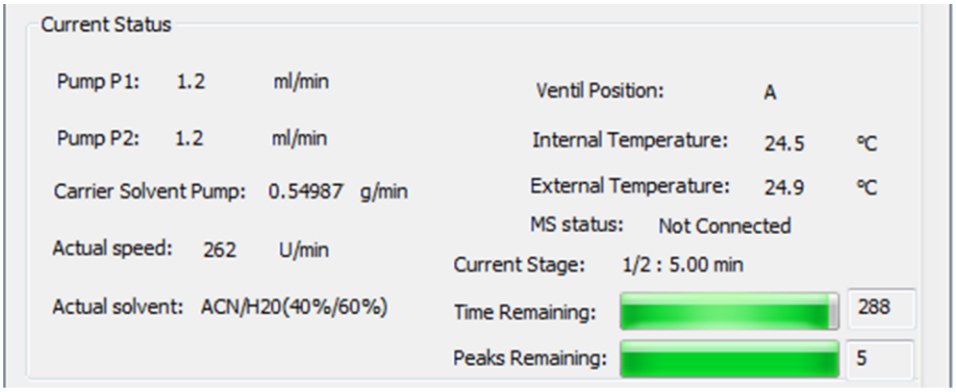

Figure 9-8: Status section of the GUI

Timers are used for updating the system status. They update the system status periodically by querying data from the system components or by taking the calculated values (flow rate of P_1, P_2, split factor, etc.). However, there exists a potential of concurrent reading and writing of commands to a device that might cause loss of commands. As a consequence, the device might not execute desired commands. This problem was experienced in the current system when there was the peak missing problem which was produced by the multiport valve for its not switching. In order to handle this problem, thread synchronization for reading and writing processes has been applied. An object of class *Cmutex,* which is a synchronization object that allows only one thread access a resource at a time, is created and commonly used for protecting the reading and writing operations onto a device. For example, the common *Cmutex* object is locked first when the reading thread is used, therefore, the writing thread will be blocked until the reading thread unlocks the *Cmutex* object. By using this technique, the reading and writing processes can be performed reliably. In addition, for write/read action, it is common to close the COM port after sending a command. However, if the system processing time is slow or the RS232 hub is slow, then, the COM port might be closed before the command actually reaches the device or data is read from the device. Therefore, it is recommended to give the system a little time after sending command for its processing (i.e. Sleep(300)).

9.1.3 Log section

The *log section* is used for showing actions performed in the system such as turn on/turn off a pump, a heater, or switch a valve as shown in Figure 9-9. Those activities can also be stored in chronological order in a text file by hitting the Save button. The file contains all settings for the system such as carrier solvent flow rate, reaction stages, sampling duration, sampling interval, time when a pump is turned on or off.

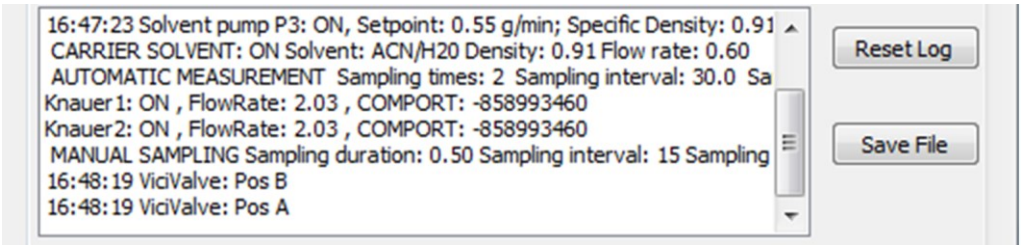

Figure 9-9: Log section of the GUI

9.2 *Graphical User Interface Automation*

9.2.1 Overview

For automation purpose, the ORMS control software not only controls the hardware devices (pumps, multiport valve etc. as described in [19]) but should also be able to control the analyzer's control software such as Data Acquisition software and Qualitative Analysis software of MassHunter Workstation Software series for the ESI-TOF-MS (Agilent Technologies, Waldbronn, Germany) and the ICP-MS Instrument Control software (or ICP-MS MassHunter, Agilent Technologies, Waldbronn, Germany) for the ICP-MS. The approach called Graphical User Inferface (GUI) automation is applied to fulfill the task. GUI automation is popularly used in testing GUI of an application (GUI testing) [174] so that repeated operations performed by humans (keystrokes, mouse movement and mouse click) can be automated via a software. This would be an equivalent ideology of implementing a robot for repeated tests of durability of a device/system before putting it on massive production.

The GUI automation process can be done through mouse clicks and through control actions. The first technique imitates the mouse movement, mouse click, and keystroke, therefore, the controlled GUI must be active and shown on the top window. This imitation is not a reliable method because "the coordinates of the controls on the screen are subjected to changes in screen resolution" [175]. The second technique obtains handles of the windows/controls (on the target GUI, the MassHunter) before sending command. The controlled GUI does not need to show on the top window. This method is considered more reliable than the first because the handle is specific to a window/control. The Application Programming Interface (API) functions from Microsoft Windows can be used directly for both methods, however, the implementation often requires more effort. Therefore, using a software or library specialized in GUI automation is more preferred. There are many relevant softwares available such as UIPath, Automa, Selenium, JUnit, AutoHotKey, AutoIt, etc [176]. Among those, UIPath is a commercial product that offers many functions such as Web automation, GUI automation, Excel automation, Screen scraping.

However, it is not straightforward to use and is not free. Automa is a high-level command tool which is very easy to use. However, the tool is not a free product and its library supports for Python only. Selenium is free tool but it is built for Web applications only. Meanwhile, AutoIt is free and it offers the scripting tasks through mouse-clicks and through control-actions. In addition, its library with lots of functions that wrap around the core API can be conveniently incorporated into C++ code. As a consequence, AutoIt is selected for the GUI automation purpose. Table 9-1 summarizes some mains features for these utilities.

Table 9-1: Some main features of GUI automation utilities

	UIPath	**Automa**	**Selenium**	**AutoIt**
Features	Web automation. GUI automation. Excel automation. Screen scraping. Good record/playback support.	GUI automation. Good record/playback support.	Web automation. Good record/playback support.	GUI automation. Good record/playback support. A simple scripting language.
Advantages	Various functions and capabilities. UiPath API can be used from a wide variety of languages: C++, VB6, C#, VB.NET, and Delphi.	Simple to use.	Free. Selenium can convert its scripts to several different formats such as Java (JUnit), Python, Ruby, C#, Perl, and PHP.	Free. Written in C++ so that the library is conveniently used in a C++ program. Library includes functions for accessing and controlling SQLite databases, Excel spreadsheets, and the Internet Explorer browser. An active user community.
Disadvantages	Commercial product. Not easy to use.	Commercial product. Automa is a Python library which is not easily integrated into a C++ program.	Not suitable for use in GUI automation.	

9.2.2 Introduction to AutoIt

"AutoIt v3 is a freeware BASIC-like scripting language designed for automating the Windows GUI and general scripting" [177]. AutoIt is a powerful scripting language[2] that can be used for automating administrative tasks and anything in a Windows environment [178]. AutoIt source is coded completely in C++ however, AutoIt itself is procedural but not object-oriented [176]. AutoIt offers the Dynamic Link Library/Component Object Model (DLL/COM) and GUI so that it can be used conveniently not only by external projects but also to create applications from its Integrated Development Environment (IDE).

[2] A scripting or script language is a programming language that supports scripts, programs written for a special run-time environment that automates the execution of tasks that could alternatively be executed one-by-one by a human operator. Scripting languages are often interpreted (rather than compiled). (Wikipedia)

With AutoIt, the GUI automation can be completed conveniently using the Record/Playback technique (using AU3Recorder utility). The keystroke and mouse activities from operators are recorded. After that, code of these activities is automatically generated so that these activities can be played back effortlessly. In addition, an application can be written in script so that a system testing/automation framework with different test cases is possible. AutoIt can be found in some publications as the case studies such as: to automate the connection of a phone support service to a Macintosh or Windows 2000 computer; to automate a virus updating and burning into CD on demand; or to automate the closing of Ariel software and opening of Acrobat software and vice versa [175][176][179] or laboratory applications such as automation of three dimensions - energy dispersive X-ray spectroscopy (3D-EDXS) reconstruction process of the Genesis software [180] or automated scanning electron microscope data [181].

The applications of AutoIt found in literature were directly created on the GUI of AutoIt. There have not been any publications applying the open library of AutoIt as well as the automation of the MassHunter software.

9.2.3 Automation of the MassHunter GUI using AutoIt library

In our software, the library of AutoIt was used by incorporating the AutoItX3_DLL.dll, AutoItX3_DLL.lib file, and AutoItX3_DLL.h to the project. In general, the inclusion of other libraries into our project is done by copying the LIB file (*.lib) and header file (*.h) to the folder where the main file of the project (*.sln) locates. And, the DLL file (*.dll) is copied into the same folder (Debug or Release) of the execution file (*.exe) that is generated when the project has compiled. Then, the Linker/Input/Additional Dependencies (in Property page) has to include the file name of the LIB file.

The windows/controls (of the target GUI) can be treated depending on (1) their handles[3] being available (using AU3_WindowGetHandle, AU3_ControlGetHanlde to obtain) and (2) their handles not being available. In the first case, handles of controls can be manipulated by sending them relevant commands, for examples AU3_ControlSend/AU3_ControlSetText to send text to an Edit box control; AU3_ControlSend/AU3_ControlCommand to manipulate ComboBox or Tab controls; or AU3_ControlClick to simulate click action on a button. The automation is also possible by using the menu bar (using functions: AU3_WinMenuSelectItem or sending keystroke i.e. AU3_Send("!f{n}"))). As an personal experience with the ICP-MS MassHunter, the control ID obtained from the AutoIt Window Info tool (similar to Spy++ utility in Visual Studio) such as: "INSTANCE", "CLASSNAMENN", "ID", "CLASS" and handle, is highly possibly changed in every new software launching. Therefore, it is recommended to use "NAME" and "TEXT" to obtain the current Window/Control handles.

In the second case when control handles are neither available nor possibly performed by keyboard control such as "Auto Sampler", "Nebulizer Pump Speed", mouse-click simulation is the only choice. This can be done simply by moving the mouse cursor to a predefined position on the screen and click (function:

[3] A handle is an abstract reference to a resource. It is often an integer number or it can be a pointer that allows access to further information. (Wikipedia)

AU3_MouseClick). This method is not reliable as explained above. Therefore, another way by matching image of a control on its containing GUI is implemented. This can be done by using MatchTemplate function in OpenCV library or ImageSearch function in external library of AutoIt. With ImageSearch, an image of a control (or template image) is required so that it could be compared with the current top most window for the matched area. The return location is then supplied to the AU3_MouseClick function. The function is fast. However, it only works well if the template is taken from the current GUI. In other words, it does not work when being used in another PC with different screen size. Therefore, a new template has to be taken every time using on a new PC. With MatchTemplate, the template image of the control is compared to the GUI image (instead of a top most window), which is obtained by screenshot function. The minMaxLoc will include the position which is best fit the template on the GUI image. The function gives more reliable result even with different PCs. Its drawback is required more processing time. Therefore, it should be used only when the handle of a control is not available.

With these techniques at hand, some basic functions of the softwares for ESI-MS and ICP-MS have been automated as presented in tabs “ESI-MS automation” and “ICP-MS automation” in Section 9.1.1.

CHAPTER 10 SUMMARY AND FUTURE WORKS

In this work, an online reaction monitoring system combining the advantages of micro reactor systems and analytical devices has been improved in performance and scope of functions. The system is computer-controlled with all actions are automated via the GUI. From the initial setup as described in Section 3.2, the system has improved through different works.

1) The addition of the dilution module enables the system to work with high concentrated solution without sample overloading problems for the MS. An active flow splitter (or mass rate attenuator) in combination with a compensation pump is applied that permits a dilution ratio from 10 to 100,000. The dilution is possible with different solvents and stable in different flow rates of the micro reactor.

2) The online reaction monitoring system (ORMS) including the dilution module can be integrated with an ESI-MS operating in time-resolved analysis (TRA) mode to measure the diluted solution online. Different concentrations of stock solution and different types of solvent (MeOH, ACN) for stock solution are used. The dilution gives logical results (higher dilution ratio gives lower concentration and vice versa) for all tested stock solutions. The effects of different solvents onto the obtained peak areas are also observed.

3) The micro reactor system was integrated with an ICP-MS for metal detection. Two integration schemes are proposed and tested. The results show a strong contamination of Fe and Cu from the carrier pump to the sample. There is also a strong influence of solvents to metal dissolution of the carrier pump to the sample.

4) The dilution was quantified using the ICP-MS in spectrum mode. The dilution is able to give >90% accuracy under various micro reactor's flow rates. It is also observed that, CPSs (count per second) for different elements with a similar concentration in a solution are different.

5) The dilution system was evaluated using ICP-MS in TRA mode. The dilution gives logical results (higher dilution ratio gives lower concentration and vice versa) and is stable in different flow rates of the micro reactor. In general, measuring in TRA mode gives as logical results as with the spectrum mode.

6) The sampling method was modified for saving time and materials. Two algorithms are further developed and both of them fulfill this purpose.

7) The second algorithm in which the total time and material consumption for a series of reaction stages equals the sum of the first and the last reaction stages is selected for implementation in the control software. The test with 6 reaction stages showed a reduction larger than 55% in time and material consumption. Moreover, the more reaction stages in a series are, the higher reduction percentage the system gets.

8) The heating module was modified to allow a faster heating rate (about 5^{o}C/min). The temperature of the reagent solution can be conditioned from -20^{o}C up to 180^{o}C. The internal and external working modes of the circulator are also used to heat the micro reactor block safely.

9) A chemical reaction was performed successfully at 25°C and 55°C to demonstrate the working possibility of the heating module and the influence of temperature on reaction kinetics.

10) The errors of simultaneous reading from and writing to devices which caused peak missing and double sized-peak in sampling of the existing system were corrected. This reduced the standard deviation in sampling replication down to less than 10%.

11) The existing control software was modified for accommodation of new functions and modules. The modified GUI has tab structure and each tab manipulates a functioning module.

12) A communication was established with the analyzer's control software for a convenience in operation and data processing. The AutoIt library is implemented for this GUI automation purpose. Basic functions in the MassHunter Workstation software for ESI-MS and ICP-MS are automated.

However, some drawbacks in the system and possible solutions are worth mentioning:

1) The problem of first smaller sampling peak when using acetic acid solvent as presented in section 5.4.2 has not yet been solved.

2) The slow heating/cooling rate of the system due to heat requirement by 4.5L of heating solvent, 2,200g of the metallic micro reactor block and smaller inlet/outlet of the heat exchanger. For further testing, the heating/cooling module could be connected to other types of micro reactor to check for the heating/cooling rate.

3) High STD of measurement with the dilution module due to different settings in the MRA for different flow rates of micro reactor.

4) The small housing does not conveniently include all system components. A bigger design for the system compartment is preferred.

For future work,

1) Different types and sizes of micro reactor could be connected for various possible measuring time and heating rate.

2) For different layers of automation, a microcontroller could be used to replace the USB relay board, which uses the QLIB library. This device is very expensive and its driver must be installed in the PC but it is only used to switch ON/OFF the relay for the valve of the carrier solvent flow only.

3) SAMI® AUTOMATED METHOD DEVELOPMENT INTERFACE, which is a graphical method development tool for use with automatic system to develop, schedule, monitor, and run assays, has been using in the laboratory. The OMRS is an automatic analytical system so that it is worth attempting the communication between OMRS and SAMI®. SAMI® could send commands in *.xml form to control different work stations. The ORMS control software will receive commands aimed for it from SAMI and interpret those commands in order to control its peripheral devices. In this case, different automation layers can be realized (physical layer – control layer – management layer).

4) By online reading signals of a reaction's products, reaction conditions can be influenced automatically based on these feedback data. As a result, reaction rate, product quality or product quantity can be optimized. The revolutionary algorithm or self-optimization (i.e. the Nelder-Mead simplex algorithm NMSIM or the stable noisy optimization by branch and fit SNOBFIT algorithm), design of experiments (DoE) and kinetic parameters can be used for this purpose.

CHAPTER 11 EXPERIMENTAL SECTION

11.1 *Devices and Materials*

Details of devices and chemicals used in this work are listed in Table 11-1 and Table 11-2 respectively.

Table 11-1: Main devices used in the system

Device	Name	Manufacturer	Quantity	Module
HPLC pump	Wellchrome K-501	Knauer, Berlin, Germany	2	Reactor
Micro reactor	Meander 11	Ehrfeld, Wendelsheim, Germany	1	Reactor
Micro annualar gear pump	MZR 2942	HNP Mikrosysteme Schwerin, Germany	1	Reactor
Flow meter	Mini Cori-flow, M13	Bronkhorst Mättig, Kamen, Germany	1	Reactor
Switching multiport valve	C10UW	Vici, Schenkon, Switzerland	1	Reactor
	C6UW	Vici, Schenkon, Switzerland	1	Reactor
Refrigerated/heating circulator	F26 HP	Julabo, Seelbach, Germany	1	Heating/Cooling
Chilling/heating block		Cole-Parmer, Kehl/Rhein, Germany	1	Heating/Cooling
Mass selective analysis system	ESI-TOF-MS G1969A	Agilent Technologies, Waldbronn, Germany	1	Analyzer
Mass selective analysis system	ICP-MS 7700x	Agilent Technologies, Waldbronn, Germany	1	Analyzer
HPLC pump	Smartline 100	Knauer, Berlin, Germany	1	Dilution
Isocratic pump	G1310A	Agilent Technologies, Waldbronn, Germany	1	Dilution
Active flow splitter	MRA-100-00-AG	Rheodyne, L.P., Rohnert Park, CA, USA	1	Dilution

Table 11-2: List of materials used for experiments

Name	Concentration	Manufacturer
Acetonitrile ROTISOLV® (ACN)	HPLC gradient grade	Roth, Karlsruhe, Germany
Methanol ROTISOLV® (MeOH)	HPLC gradient grade	Roth, Karlsruhe, Germany
Acetic acid ROTIPURAN®	100%	Roth, Karlsruhe, Germany
Acetic acid anhydride ROTIPURAN® (AAA)	≥ 99%	Roth, Karlsruhe, Germany
L-Tryptophan CELLPURE® (NDL)	≥ 99%	Roth, Karlsruhe, Germany
N-Formyl-DL-tryptophan (NFT)	90-100%	MP Biomedicals, Illkirch, France
Octanoic acid (OS)	> 99%	Merck-Schuchardt (Hohenbrunn, Germany)
4-Methyloctanoic acid (4-MOS)	> 98%	Sigma Aldrich (Steinheim, Germany)
CertiPUR® ICP multi-element standard solution IV	1000 mg/L	Merck (Darmstadt, Germany)
CertiPUR® Lutetium ICP standard	1000 mg/L	Merck (Darmstadt, Germany)
Nitric acid supra-quality ROTIPURAN® Supra (HNO_3)	69%	Carl Roth (Karlsruhe, Germany)

11.2 *Experimental Settings*

11.2.1 Experiment 1

Table 11-3 shows the experimental settings for estimating the time resolution of the system. A solution of 80 µL/L Octanoic acid (OS) and 40 µL/L 4-Methyl Octanoic acid in Methanol ran through the micro reactor at flow rate 2 mL/min. Acetonitrile/water (40%:60%) used as a carrier solvent ran at flow rate 0.4 mL/min and 0.6 mL/min respectively to see its influence on the signal intensity. Different sampling intervals (7, 10, 15, 20, 30, 40s) were attempted in order to observe when peak overlapping occurs. The experiment was repeated 3 times with 5 peaks for each sampling series.

Table 11-3: Settings for experiment 1 (time resolution)

Experiment 1	**Section 4.5**
Solution	80 µl/l Octanoic acid (OS) and 40 µl/l 4-Methyl Octanoic acid in MeOH
Micro reactor flow rate (mL/min)	2
Educt pump ratio (P_1:P_2)	1:1
Solvent carrier	ACN/H_2O (40%:60%)
Carrier solvent flow rate (P_3) (mL/min)	0.4, 0.6
Sampling duration (s)	0.2
Sampling interval (s)	7, 10, 15, 20, 30, 40
Peak replication	5
Number of runs	3

11.2.2 Experiment 2

Table 11-4 contains settings for testing the FSM-approach 1. The acetylation reaction with solution 1: 20 mg/L N-DL-Tryptophan and 2.5 mg/L NFT in acetic acid and solution 2: a mixture of 20 ml/L acetic anhydride acid (AAA) in acetic acid was measured at reaction stage 1.5 – 3 – 4.5 min using the FSM (*M=2, 4, 6*) and SSM. Acetonitrile/water (40%:60%) used as a carrier solvent ran at flow rate 0.4 mL/min to transfer samples to the analyzer. The experiment ran 3 times for FSM and 3 times for SSM with 5 peak replications for each reaction stage. Sampling duration was 0.2s and sampling interval was 20s for the SSM.

Table 11-4: Settings for Experiment 2 (Fast Sampling Method - Approach 1)

Experiment 2	**Section 5.4.2**	
Reaction stage (min)	1.5 – 3 – 4.5	
Temperature (^{o}C)	Ambient	
Carrier Solvent	ACN/H_2O (40%:60%)	
Carrier solvent flow rate (mL/min)	0.4	
Educt pump ratio (P_1:P_2)	1:1	
Solution 1	20 mg/L N-DL-Tryptophan + 2.5 mg/L NFT in acetic acid	
Solution 2	20mL/L Acetic anhydride acid in acetic acid	
Sampling method	**FSM (M=2, 4, 6)**	**SSM**
Peak repetition	1	5
Runs	3	3
Sampling duration (s)	0.2	0.2
Sampling interval (s)	-	20

11.2.3 Experiment 3

Table 11-5 is settings for testing the FSM approach 2 and of the SSM. The acetylation reaction with solution 1: 20 mg/L N-DL-Tryptophan and 5 mg/L NFT in acetic acid and solution 2: a mixture of 20 ml/L AAA in acetic acid was measured at reaction stage from 1 to 10 min using the FSM approach 2 and SSM. Acetonitrile/water (40%:60%) used as a carrier solvent ran at flow rate 0.6 mL/min to transfer samples to the analyzer. The experiment was run 5 times for FSM and 3 times for SSM with 5 peak replications for each reaction stage. Sampling duration was 0.2s and sampling interval was 19s for the SSM.

Table 11-5: Settings for Experiment 3 (Fast Sampling Method - Approach 2)

Experiment 3	**Section 5.4.2**	
Reaction stage (min)	1, 2, 3, 4, 5, 6, 7, 8, 9, 10	
Temperature (^{o}C)	Ambient	
Carrier solvent	ACN/H_2O (40%:60%)	
Carrier solvent flow rate (mL/min)	0.6	
Educt pump ratio (P_1:P_2)	1:1	
Solution 1	20 mg/L N-DL-Tryp + 5 mg/L NFT in acetic acid	
Solution 2	100 mL/L Acetic anhydride acid in acetic acid	
Sampling method	**FSM**	**SSM**
Peak repetition	1	4
Runs	5	3
Sampling duration (s)	0.2	0.2
Sampling interval (s)	-	19

11.2.4 Experiment 4

Table 11-6 is the settings for testing the heating module using FSM approach 1 and of the SSM. The acetylation reaction with solution 1: 20 mg/L N-DL-Tryptophan and 2.5 mg/L NFT in acetic acid and solution 2: a mixture of 20 ml/L AAA in acetic acid was measured at reaction stages 1.5 – 3 – 4.5 min at 25^{o}C and at 55^{o}C. Acetonitrile/water (40%:60%) used as a carrier solvent ran at flow rate 0.4 mL/min to transfer samples to the analyzer. The experiment was run 3 times for FSM and 3 times for SSM with 5 peak replications. Sampling duration was 0.2s and sampling interval was 20s for SSM.

Table 11-6: Settings for Experiment 4 (Heating module)

Experiment 4	**Section 6.6**	
Reaction stage (min)	1.5 – 3 – 4.5	
Temperature (^{o}C)	25 - 55	
Carrier solvent	ACN/H_2O (40%:60%)	
Solvent carrier flow rate (mL/min)	0.4	
Educt pump ratio (P_1:P_2)	1:1	
Solution 1	20 mg/L N-DL-Tryptophan + 2.5 mg/L NFT in acetic acid	
Solution 2	20 mL/L Acetic anhydride acid in acetic acid	
Sampling method	**FSM (M=2, 4, 6)**	**SSM**
Peak repetition	1	5
Runs	3	3
Sampling duration (s)	0.2	0.2
Sampling interval (s)	-	20

11.2.5 Experiment 5

Table 11-7 shows settings of a test for comparing dilution using the mass rate attenuator (MRA) with and without flow compensation. OS and 4-MOS in MeOH solvent were run through the micro reactor at flow rates varied from 0.6 mL/min to 6 mL/min while other parameters were kept unchanged. Acetonitrile/water (40%:60%) used as a carrier solvent ran at flow rate 0.4 mL/min to transfer samples to the analyzer. For the first case, the flow rate of the diluent solvent, methanol, is fixed at 0.6 mL/min and split factor is 3. Meanwhile, for the second case with flow compensation, the diluent, compensation flow rate and split factor were automatically calculated based on the dilution ratio (100) and micro reactor flow rate. The experiment was run 3 times for each scheme with 5 peak replications for each flow rate (reaction stage). Sampling duration was 0.2s and sampling interval was 16s.

Table 11-7: Settings for experiment 5 (Testing for dilution Before and After using the flow compensation approach)

Experiment 5	**Section 7.8.2**	
	Without	**With flow compensation**
Solution	OS + 4-MOS in MeOH	
Solvent carrier	ACN/H_2O (40%:60%)	
Solvent carrier flow rate (mL/min)	0.4	
Micro reactor flow rate (mL/min)	0.6 – 0.8 – 1 – 2 – 4 – 6	
Educt pump ratio (P_1:P_2)	1:1	
Sampling duration (s)	0.2	
Sampling interval (s)	16	
Peak replicate (peaks/reaction state)	5	
Number of runs	3	
Diluent	MeOH	
Compensation solvent	-	MeOH
Compensation flow rate (mL/min)	-	Automatically calculated
Diluent flow rate (mL/min)	0.6	Automatically calculated
	Split Factor: 3 Split ratio: 100	Dilution ratio: 100

11.2.6 Experiment 6

Table 11-8 shows settings of a test for comparing automatic dilution and manual dilution. Four dilution ratios (1:500 – 1:300 – 1:100 – 1:50) were tested. Initially, stock solution 1 with 91 mg/L OS + 91 mg/L 4-MOS in MeOH ran through the micro reactor at flow rates 4 – 2 – 1 mL/min. Acetonitrile/water (40%:60%) used as carrier solvent ran at flow rate 0.6 mL/min to transfer samples to the analyzer. MeOH was used as the diluent and compensation solvent for automatic dilution. The experiment ran 3 times for automatic dilution with 5 peak replications and 1 time for manual dilution with 20 peak replications. Sampling duration was 0.2s and sampling interval was 16s.

Then, the experiment was repeated with the same settings using stock solution 1 (low concentration) and later stock solution 3 (high concentration). These experiments are used to test the dilution in different concentrations of stock solution.

Finally, the experiment was repeated for stock solution 4, 5, and 6 in order to compare the dilution in different solvents. The system's settings are the same except for the diluent and compensation solvent are ACN.

Table 11-8: Settings for experiment 6 (Dilution module)

Experiment 6	**Section 7.8.2**	
Dilution	Automatic	Manual
Stock solution 1 (low concentration) Stock solution 2 (medium concentration) Stock solution 3 (high concentration) Stock solution 4 (low concentration) Stock solution 5 (medium concentration) Stock solution 6 (high concentration)	45.5 mg/L OS + 45.5 mg/L 4-MOS in MeOH 91 mg/L OS + 91 mg/L 4-MOS in MeOH 136.5 mg/L OS + 136.5 mg/L 4-MOS in MeOH 45.5 mg/L OS + 45.5 mg/L 4-MOS in ACN 91 mg/L OS + 91 mg/L 4-MOS in ACN 136.5 mg/L OS + 136.5 mg/L 4-MOS in ACN	
Dilution Ratio	1:500 – 1:300 – 1:100 – 1:50	
Micro reactor flow rate (mL/min) Or reaction stage (min)	4 – 2 – 1 3 – 6 – 12	
Solvent carrier	ACN/H_2O (40%:60%)	
Solvent carrier flow rate (ml/min)	0.6	
Educt pump ratio (P_1:P_2)	1:1	
Sampling time (s)	0.2	
Sampling interval (s)	16	
Diluent 1 Diluent 2	MeOH ACN	-
Compensation solvent 1 Compensation solvent 2	MeOH ACN	-
Run	3	1
Peaks	5	20

11.2.7 Experiment 7

Table 11-9 is the settings of the experiment for testing two schemes of integration to ICP-MS. 100 µg/L ICP multi-element standard solution IV in HNO_3 (1%, v/v) and an internal standard solution contained 500 µg/L lutetium in HNO_3 (5%, v/v) were used. In the first concept, micro reactor flow rate was fixed at 2 mL/min. Carrier solvent, ultrapure water and HNO_3 (1%, v/v), ran separately from 0.2 mL/min to 0.6 mL/min. Meanwhile, in the second concept, micro reactor flow rate varied from 0.6 mL/min to 8 mL/min and no carrier solvent was used because the carrier pump was not included. In addition, the sample flow to the ICP-MS was continuous that there was no requirement for sampling in this concept.

Table 11-9: Settings for experiment 7 (Integration to ICP-MS)

Experiment 7	**Section 8.4**	
	Configuration 1	**Configuration 2**
Solution	100 µg/L ICP multi-element standard solution IV in HNO_3 (1%, v/v)	
Internal standard	-	500 µg/L lutetium in HNO_3 (5%, v/v).
Carrier solvent flow rate (mL/min)	0.2 – 0.6	-
Carrier solvent	Ultrapure water HNO_3 (1%, v/v)	-
Sampling duration (s)	3	-
Sampling interval (s)	50 - 30	-
Peak replicate	10	-
Sample loop (µL)	5	5
Micro reactor flow rate (mL/min)	2	0.6 - 8
Speed of peristaltic pump (rps)	-	0.1

11.2.8 Experiment 8

Table 11-10 shows settings for a testing with blank 1% HNO_3 solvent in order to determine contaminants from the ORMS to sample. Five vials of calibration solution and four vials of blank solution HNO_3 (1%, v/v) were prepared and taken by the ALS. After that, four dilution ratios (1:1000 – 1:500 – 1:100 – 1:50) were tested using the ORMS with the automatic diluting mode. HNO_3 (1%, v/v) ran through the micro reactor at flow rates 4 – 2 – 1 mL/min sequentially. HNO_3 (1%, v/v) was used as a diluent and compensation solvent. The experiment was 2 times. Sampling duration was 0.2s; sampling interval was 790s so that the ICP-MS could repeat measuring 4 to 5 samples.

Table 11-10: Settings for experiment 8 (Integration to ICP-MS – Dilution with blank 1% HNO_3)

Experiment 8	**Section 8.5.2.1**	
	Automatic dilution (ORMS)	**ALS**
Calibration solution		1 – 5 – 10 – 50 – 100 µg/L ICP multi-element standard solution IV in HNO_3 (1%, v/v)
Sample for ALS		4 vials of blank HNO_3 (1%, v/v)
Solution	Blank HNO_3 (1%, v/v)	
Dilution Ratio	1:1000 – 1:500 – 1:100 – 1:50	
Micro reactor flow rate (mL/min)	4 – 2 – 1	-
Dilution solvent/Diluent	HNO_3 (1%, v/v)	-
Compensation solvent	HNO_3 (1%, v/v)	-
Educt pump ratio (P_1:P_2)	1:1	-
Sampling time (s)	0.2	-
Sampling interval (s)	790	-
Sampling repetition	2	-
Run	2 times	2 times
Speed of peristaltic pump (rps)	-	0.1

11.2.9 Experiment 9

Table 11-11 shows settings for a testing with ultrapure water solvent in order to determine contaminants from the ORMS to sample. Five vials of calibration solution and four vials of blank solution were prepared and taken by the ALS. After that, four dilution ratios (1:1000 – 1:500 – 1:100 – 1:50) were tested sequentially using the ORMS with the automatic diluting mode. Ultrapure water ran through the micro reactor at flow rates 4 – 2 – 1 mL/min sequentially. Ultrapure water was used as a diluent and compensation solvent. The experiment was run 2 times. Sampling duration was 0.2s; sampling interval was 790s so that the ICP-MS could repeat measuring 4 to 5 samples.

Table 11-11: Settings for experiment 9 (Integration to ICP-MS – Dilution with blank ultrapure water)

Experiment 9	**Section 8.5.2.2**	
	Automatic dilution (ORMS)	**ALS**
Calibration solution		1 – 5 – 10 – 50 – 100 µg/L ICP multi-element standard solution IV in ultrapure water
Sample for ALS		4 vials of ultrapure water
Solution	ultrapure water	
Dilution Ratio	1:1000 – 1:500 – 1:100 – 1:50	
Micro reactor flow rate (mL/min)	4 – 2 – 1	-
Dilution solvent/Diluent	ultrapure water	-
Compensation solvent	ultrapure water	-
Educt pump ratio (P_1:P_2)	1:1	-
Sampling time (s)	0.2	-
Sampling interval (s)	790	-
Sampling repetition	2	-
Run	2 times	2 times
Speed of peristaltic pump (rps)	-	0.1

11.2.10 Experiment 10

Table 11-12 shows settings of a test for comparing automatic dilution and manual dilution in integration with an ICP-MS system operating in spectrum mode. Four dilution ratios (1:1000 – 1:500 – 1:100 – 1:50) were tested. 5 mg/L ICP multi-element standard solution IV in 1% HNO_3 ran through the micro reactor at flow rates 4 – 2 – 1 mL/min. HNO_3 (1%, v/v) was used as a diluent and ultrapure water was used as a compensation solvent in automatic dilution. The experiment was run 2 times. Sampling duration was 0.2s; sampling interval was 790s so that the ICP-MS could repeat measuring 4 to 5 samples. The measurement of calibration solution and manually diluted samples were conducted when the ALS was connected to the ICP-MS.

Table 11-12: Settings for experiment 10 (ICP-MS in spectrum mode – Dilution of 5 mg/L ICP multi-element standard solution IV in HNO_3 (1%, v/v) with HNO_3 (1%, v/v) as a diluent)

Experiment 10	**Section 8.5.2.3**	
	Automatic dilution (ORMS)	**Manual dilution (ALS)**
Calibration solution		1 – 5 – 10 – 50 – 100 µg/L ICP multi-element standard solution IV in HNO_3 (1%, v/v)
Sample for ALS		4 vials of manually diluted solution
Solution	5 mg/L ICP multi-element standard solution IV in HNO_3 (1%, v/v)	5 mg/L ICP multi-element standard solution IV in HNO_3 (1%, v/v)
Dilution Ratio	1:1000 – 1:500 – 1:100 – 1:50	1:1000 – 1:500 – 1:100 – 1:50
Micro reactor flow rate (mL/min)	4 – 2 – 1	-
Dilution solvent/Diluent	HNO_3 (1%, v/v)	-
Compensation solvent	ultrapure water	-
Educt pump ratio (P_1:P_2)	1:1	-
Sampling time (s)	0.2	-
Sampling interval (s)	790	-
Sampling repetition	2	-
Run	2	2
Speed of peristaltic pump (rps)	-	0.1

11.2.11 Experiment 11

Table 11-13 shows settings of a test for comparing automatic dilution and manual dilution in integration with an ICP-MS system operating in spectrum mode. Four dilution ratios (1:1000 – 1:500 – 1:100 – 1:50) were tested. 5 mg/L ICP multi-element standard solution IV in ultrapure water ran through the micro reactor at flow rates 4 – 2 – 1 mL/min. Ultrapure water was used as a diluent and compensation solvent in automatic dilution. The experiment was run 2 times. Sampling duration was 0.2s; sampling interval was 790s so that the ICP-MS could repeat measuring 4 to 5 samples. The measurement of calibration solution and manually diluted samples were conducted when the ALS was connected to the ICP-MS.

Table 11-13: Settings for experiment 11 (ICP-MS in spectrum mode – Dilution of 5 mg/L ICP multi-element standard solution IV in ultrapure water with ultrapure water as a diluent)

Experiment 11	**Section 8.5.2.4**	
	Automatic dilution (ORMS)	**Manual dilution (ALS)**
Calibration solution		1 – 5 – 10 – 50 – 100 µg/L ICP multi-element standard solution IV in ultrapure water
Sample for ALS		4 vials of manually diluted solution
Stock Solution	5 mg/L ICP multi-element standard solution IV in ultrapure water	5 mg/L ICP multi-element standard solution IV in ultrapure water
Dilution Ratio	1:1000 – 1:500 – 1:100 – 1:50	1:1000 – 1:500 – 1:100 – 1:50
Micro reactor flow rate (mL/min)	4 – 2 – 1	-
Dilution solvent/Diluent	ultrapure water	-
Compensation solvent	ultrapure water	-
Educt pump ratio (P_1:P_2)	1:1	-
Sampling time (s)	0.2	-
Sampling interval (s)	790	-
Sampling repetition	2	-
Run	2	2
Speed of peristaltic pump (rps)	-	0.1

11.2.12 Experiment 12

Table 11-14 shows settings of a test for comparing automatic dilution and manual dilution in integration with an ICP-MS system operating in TRA mode. Four manually diluted solution at ratios 1:1000, 1:500, 1:100, 1:50 were sequentially run by the ORMS. After that, four diluting ratios (1:1000 – 1:500 – 1:100 – 1:50) were automatically diluted using the ORMS. 5 mg/L ICP multi-element standard solution IV in 1% HNO_3 ran through the micro reactor at flow rates 4 – 2 – 1 mL/min. HNO_3 (1%, v/v) was used as diluent and compensation solvent in automatic dilution. The experiment was run 2 times. Sampling duration was 3s; and sampling interval was 160s.

Table 11-14: Settings for experiment 12 (ICP-MS in TRA mode – Dilution of 5 mg/L ICP multi-element standard solution IV in HNO_3 (1%, v/v) with HNO_3 (1%, v/v) as a diluent)

Experiment 12	**Section 8.6.2**	
	Automatic dilution (ORMS)	**Manual dilution (ORMS)**
Stock solution	5 mg/L ICP multi-element standard solution IV in HNO_3 (1%, v/v)	
Dilution Ratio	1:500 – 1:100 – 1:50	1:1000 – 1:500 – 1:100 – 1:50
Micro reactor flow rate (mL/min)	4 – 2 – 1	1
Dilution solvent/Diluent	HNO_3 (1%, v/v)	-
Compensation solvent	HNO_3 (1%, v/v)	-
Educt pump ratio (P_1:P_2)	1:1	1:1
Sampling time (s)	3	3
Sampling interval (s)	160	160
Sampling repetition	5	5
Run	2	2
Speed of peristaltic pump (rps)	-	-

ABBREVIATIONS

AAS: Atomic absorption spectroscopy
AES: Atomic emission spectroscopy
AFS: Atomic fluorescent spectroscopy
ALS: Auto sampler
APCI: Atmospheric pressure chemical ionization
API: Application programming interface
CPS: Count per second
DART: Direct analysis in real-time
EESI: Extracted electrospray ionization
ESI: Electrospray ionization
FIA: Flow injection analysis
FSM: Fast sampling method
GC: Gas chromatography
GUI: Graphical user interface
HPLC: High performance liquid chromatography
ICP: Inductively-coupled plasma
ID: Internal diameter
IDE: Integrated development environment
LC: Liquid chromatography
LTP: Low temperature plasma
MS: Mass spectrometry
MRA: Mass rate attenuator
mzr: Micro annular gear pump
OES: Optical emission spectroscopy
ORMS: Online reaction monitoring system
P1, P2: HPLC Knauer pump
P3: Carrier solvent pump
P4: Dilution pump
PC: Personal computer
PID: Proportional - integral - derivative
SF: Split factor
SIA: Sequential injection analysis
SSM: Slow sampling method
STD: Standard deviation
TOF: Time of flight
TIC: Total ion current
TRA: Time-Resolved Analysis

REFERENCES

[1] V. T. Fabrizio Caccavale, Mario Iamarino, Francesco Pierri, *Control and Monitoring of Chemical Batch Reactors*. Springer London, 2011.

[2] J. Yoshida, *Basics of Flow Microreactor Synthesis*, 1st ed. Springer Japan, 2015.

[3] K. F. Jensen, B. J. Reizman, and S. G. Newman, "Tools for chemical synthesis in microsystems," *Lab Chip*, vol. 14, no. 17, pp. 3206–3212, 2014.

[4] A. Šalić, A. Tušek, and B. Zelić, "Application of microreactors in medicine and biomedicine," *J. Appl. Biomed.*, vol. 10, no. 3, pp. 137–153, 2012.

[5] N.-T. Nguyen and Z. Wu, "Micromixers—a review," *J. Micromechanics Microengineering*, vol. 15, no. 2, pp. R1–R16, 2004.

[6] J. I. Yoshida, A. Nagaki, T. Iwasaki, and S. Suga, "Enhancement of chemical selectivity by microreactors," *Chem. Eng. Technol.*, vol. 28, no. 3, pp. 259–266, 2005.

[7] J. H. Chun, S. Lu, Y. S. Lee, and V. W. Pike, "Fast and high-yield microreactor syntheses of ortho-substituted [18F]Fluoroarenes from reactions of [18F]Fluoride ion with diaryliodonium salts," *J. Org. Chem.*, vol. 75, pp. 3332–3338, 2010.

[8] C. Wiles and P. Watts, "Recent advances in micro reaction technology.," *Chem. Commun. (Camb).*, vol. 47, pp. 6512–6535, 2011.

[9] S. Hardt, W. Ehrfeld, V. Hessel, and K. M. Vanden Bussche, "Strategies for size reduction of microreactors by heat transfer enhancement effects," *Chem. Eng. Commun.*, vol. 190, no. 2015, pp. 540–559, 2003.

[10] J. Yue, J. C. Schouten, and T. A. Nijhuis, "Integration of Microreactors with Spectroscopic Detection for Online Reaction Monitoring and Catalyst Characterization," *Ind. Eng. Chem. Res.*, vol. 51, no. 45, pp. 14583–14609, 2012.

[11] C. de Bellefon, N. Tanchoux, S. Caravieilhes, P. Grenouillet, and V. Hessel, "Microreactors for Dynamic, High Throughput Screening of Fluid/Liquid Molecular Catalysis," *Angew. Chemie*, vol. 112, no. 19, pp. 3584–3587, 2000.

[12] "Microfluidics for Chemistry Applications." [Online]. Available: http://invenios.com/products/microfluidics/microfluidics-chemistry/. [Accessed: 25-Apr-2016].

[13] R. Halder, A. Lawal, and R. Damavarapu, "Nitration of toluene in a microreactor," *Catal. Today*, vol. 125, no. 1–2, pp. 74–80, 2007.

[14] X. Zhang, S. Stefanick, and F. J. Villani, "Application of microreactor technology in process development," *Org. Process Res. Dev.*, vol. 8, no. 3, pp. 455–460, 2004.

[15] Christian, M. Mitchell, D. P. Kim, and P. J. A. Kenis, "Ceramic microreactors for on-site hydrogen production," *J. Catal.*, vol. 241, no. 2, pp. 235–242, 2006.

[16] T. Nisisako, T. Torii, and T. Higuchi, "Droplet formation in a microchannel network.," *Lab Chip*, vol. 2, no. 1, pp. 24–26, 2002.

[17] K.-I. Sotowa, K. Irie, T. Fukumori, K. Kusakabe, and S. Sugiyama, "Droplet Formation by the Collision of Two Aqueous Solutions in a Microchannel and Application to Particle Synthesis," *Chem. Eng. Technol.*, vol. 30, no. 3, pp. 383–388, 2007.

[18] D. R. Reyes, D. Iossifidis, P.-A. Auroux, and A. Manz, "Micro total analysis systems. 1. Introduction, theory, and technology.," *Anal. Chem.*, vol. 74, no. 12, pp. 2623–2636, 2002.

[19] H. Fleischer, D. Hoffmann, N. Almahaini, V. Q. Do, and K. Thurow, "Online Coupling System and Control Software for Reaction Monitoring using Microreactors and ESI-MS," in *International Instrumentation and Measurement Technology Conference*, 2015, pp. 1561–1566.

[20] J. P. McMullen and K. F. Jensen, "Integrated microreactors for reaction automation: new approaches to reaction development.," *Annu. Rev. Anal. Chem. (Palo Alto. Calif).*, vol. 3, pp. 19–42, 2010.

[21] N. Holmes, G. R. Akien, R. J. D. Savage, C. Stanetty, I. R. Baxendale, A. J. Blacker, B. A. Taylor, R. L. Woodward, R. E. Meadows, and R. A. Bourne, "Reaction Chemistry & Engineering Online quantitative mass spectrometry for the reactors," *React. Chem. Eng.*, vol. 1, pp. 96–100, 2016.

[22] L. S. Santos, *Reactive Intermediates: MS Investigations in Solution*. WILEY-VCH Verlag GMbH & Co. KGaA: Weinheim, 2009.

[23] D. L. Browne, S. Wright, B. J. Deadman, S. Dunnage, I. R. Baxendale, R. M. Turner, and S. V. Ley, "Continuous flow reaction monitoring using an on-line miniature mass spectrometer," *Rapid Commun. Mass Spectrom.*, vol. 26, no. 17, pp. 1999–2010, 2012.

[24] J. P. Lowe and U. Hintermair, "Practical aspects of real-time reaction monitoring using multi-nuclear high resolution FlowNMR spectroscopy," *Catal. Sci. Technol.*, vol. 6, no. 24, pp. 8406–8417, 2016.

[25] K. J. Åström and B. Wittenmark, *Computer-controlled Systems: Theory and Design (3Rd Ed.)*. Upper Saddle River, NJ, USA: Prentice-Hall, Inc., 1997.

[26] D. Barrow, S. Taylor, A. Morgan, and L. Giles, "Properties and Use of Microreactors," *Microreactors Org. Chem. Catal. Second Ed.*, pp. 1–33, 2013.

[27] P. D. I. Fletcher, S. J. Haswell, and X. Zhang, "Monitoring of chemical reactions within microreactors using an inverted Raman microscopic spectrometer.," *Electrophoresis*, vol. 24, no. 18, pp. 3239–45, 2003.

[28] M. Brivio, R. E. Oosterbroek, W. Verboom, A. van den Berg, and D. N. Reinhoudt, "Simple chip-based interfaces for on-line monitoring of supramolecular interactions by nano-ESI MS.," *Lab Chip*, vol. 5, no. 10, pp. 1111–22, 2005.

[29] "Holistic approach." [Online]. Available: http://www.ehrfeld.com/en/products.html. [Accessed: 25-Apr-2016].

[30] "Flow Chemistry." [Online]. Available: http://www.chemtrix.com/flow-chemistry. [Accessed: 25-Apr-2016].

[31] G. M. F. I. James W. Robinson, Eileen M. Skelly Frame, *Undergraduate Instrumental Analysis*, 7th ed. CRC Press Inc., 2014.

[32] J. H. and J. E. Markus Sauer, "Handbook of Fluorescence Spectroscopy and Imaging: From Single Molecules to Ensembles," in *Handbook of Fluorescence Spectroscopy and Imaging: From Single Molecules to Ensembles*, 2011, pp. 1–30.

[33] A. R. de Boer, T. Letzel, D. a van Elswijk, H. Lingeman, W. M. a Niessen, and H. Irth, "On-line coupling of high-performance liquid chromatography to a continuous-flow enzyme assay based on electrospray ionization mass spectrometry.," *Anal. Chem.*, vol. 76, no. 11, pp. 3155–61, 2004.

[34] P. J. Viskari and J. P. Landers, "Unconventional detection methods for microfluidic devices.," *Electrophoresis*, vol. 27, no. 9, pp. 1797–810, 2006.

[35] S. R. Holler, F. James; Skoog, Douglas A; Crouch, *Principles of Instrumental Analysis*. 2007.

[36] S. G. Schulman, Q. Q. Di, and J. Juchum, "Organic Chemistry Applications of Fluorescence Spectroscopy," vol. 3, pp. 2040–2046, 1999.

[37] R. Matsumoto, H. F. Zadeh, and P. Ehrhard, "Quantitative measurement of depth--averaged concentration fields in microchannels by means of a fluorescence intensity method," *Exp. Fluids*, vol. 39, no. 4, pp. 722–729, 2005.

[38] S. Bargiel, A. Górecka-Drzazga, J. a. Dziuban, P. Prokaryn, M. Chudy, A. Dybko, and Z. Brzózka, "Nanoliter detectors for flow systems," *Sensors Actuators A Phys.*, vol. 115, no. 2–3, pp. 245–251, 2004.

[39] J.-C. Roulet, R. Vo¨lkel, H. P. Herzig, E. Verpoorte, N. F. de Rooij, and R. Da¨ndliker, "Microlens systems for fluorescence detection in chemical microsystems," *Opt. Eng.*, vol. 40, no. 5, pp. 814–821, 2001.

[40] K. B. Mogensen, J. El-Ali, A. Wolff, and J. P. Kutter, "Integration of polymer waveguides for optical detection in microfabricated chemical analysis systems.," *Appl. Opt.*, vol. 42, no. 19, pp. 4072–9, 2003.

[41] M. Hoffmann, M. Schlüter, and N. Räbiger, "Experimental investigation of liquid–liquid mixing in T-shaped micro-mixers using -LIF and -PIV," *Chem. Eng. Sci.*, vol. 61, no. 9, pp. 2968–2976, 2006.

[42] R. F. Ismagilov, A. D. Stroock, P. J. a. Kenis, G. Whitesides, and H. a. Stone, "Experimental and theoretical scaling laws for transverse diffusive broadening in two-phase laminar flows in microchannels," *Appl. Phys. Lett.*, vol. 76, no. 17, p. 2376, 2000.

[43] M. B. Kerby, R. S. Legge, and A. Tripathi, "Measurements of kinetic parameters in a microfluidic reactor.," *Anal. Chem.*, vol. 78, no. 24, pp. 8273–80, 2006.

[44] Q. Lu, J. H. Callahan, and G. E. Collins, "The selective detection of uranium(vi) on a microchip using a derivatized 4-sulfonic calix[6]arene," *Chem. Commun.*, no. 19, pp. 1913–1914, 2000.

[45] A. A. Edwards, U. Kent, and G. Medway, "Organic Applications of UV-Visible Absorption Spectroscopy," pp. 2030–2039, 2010.

[46] W. Ferstl, T. Klahn, W. Schweikert, G. Billeb, M. Schwarzer, and S. Loebbecke, "Inline Analysis in Microreaction Technology: A Suitable Tool for Process Screening and Optimization," *Chem. Eng. Technol.*, vol. 30, no. 3, pp. 370–378, 2007.

[47] Q. Lu, C. L. Copper, and G. E. Collins, "Ultraviolet absorbance detection of colchicine and related alkaloids on a capillary electrophoresis microchip.," *Anal. Chim. Acta*, vol. 572, no. 2, pp. 205–11, 2006.

[48] R. Barzin, S. R. A. Shukor, and A. L. Ahmad, "New spectrophotometric measurement method for process control of miniaturized intensified systems," *Sensors Actuators B Chem.*, vol. 146, no. 1, pp. 403–409, 2010.

[49] J. Yue, F. H. Falke, J. C. Schouten, and T. A. Nijhuis, "Microreactors with integrated UV/Vis spectroscopic detection for online process analysis under segmented flow," *Lab Chip*, vol. 13, no. 24, pp. 4855–4863, 2013.

[50] J.-S. Park, K.-B. Park, K.-S. Shin, H.-D. Park, M.-C. Kim, J.-R. Kim, S.-J. Park, and Y.-H. Song, "Design, fabrication and characterization of an integrated micro ammonia analysis system (IMAAS) with microreactor and in-plane type optical detector based on the Berthelot reaction," *Sensors Actuators B Chem.*, vol. 117, no. 2, pp. 516–522, 2006.

[51] N. J. Petersen, K. B. Mogensen, and J. P. Kutter, "Performance of an in-plane detection cell with integrated waveguides for UV/Vis absorbance measurements on microfluidic separation devices.," *Electrophoresis*, vol. 23, no. 20, pp. 3528–36, 2002.

[52] A. Prabhakar and S. Mukherji, "Microfabricated polymer chip with integrated U-bend waveguides for evanescent field absorption based detection.," *Lab Chip*, vol. 10, no. 6, pp. 748–54, 2010.

[53] C. A. McFaul, M. F. Drenski, and W. F. Reed, "Online, continuous monitoring of the sensitivity of the LCST of NIPAM-Am copolymers to discrete and broad composition distributions," *Polym. (United Kingdom)*, vol. 55, no. 19, pp. 4899–4907, 2014.

[54] H. Lu, M. a Schmidt, and K. F. Jensen, "Photochemical reactions and on-line UV detection in microfabricated reactors.," *Lab Chip*, vol. 1, no. 1, pp. 22–8, 2001.

[55] J. Wagner, T. Tshikhudo, and J. Kohler, "Microfluidic generation of metal nanoparticles by borohydride reduction," *Chem. Eng. J.*, vol. 135, pp. S104–S109, 2008.

[56] J. B. Edel, R. Fortt, J. C. deMello, and A. J. deMello, "Microfluidic routes to the controlled production of nanoparticles," *Chem. Commun.*, no. 10, pp. 1136–1137, 2002.

[57] A. Barth, "Infrared spectroscopy of proteins," *Biochim. Biophys. Acta - Bioenerg.*, vol. 1767, no. 9, pp. 1073–1101, 2007.

[58] S. Seiffert and J. Sprakel, *Physical chemistry of supramolecular polymer networks*, vol. 41, no. 2. 2012.

[59] R. Schindler and B. Lendl, "FTIR spectroscopy as detection principle in aqueous flow analysis," pp. 123–126, 1999.

[60] M. G. Lima, I. M. Raimundo, and M. F. Pimentel, "Improving the detection limits of near infrared spectroscopy in the determination of aromatic hydrocarbons in water employing a silicone sensing phase," vol. 125, pp. 229–233, 2007.

[61] R. Herzig-Marx, K. T. Queeney, R. J. Jackman, M. a Schmidt, and K. F. Jensen, "Infrared spectroscopy for chemically specific sensing in silicon-based microreactors.," *Anal. Chem.*, vol. 76, no. 21, pp. 6476–83, 2004.

[62] D. Lumpi and C. Braunshier, "Effective Reaction Monitoring of Intermediates by ATR-IR Spectroscopy Utilizing Fibre Optic Probes," in *Infrared Spectroscopy - Materials Science, Engineering and Technology*, T. Theophile, Ed. InTech, 2007, pp. 493–510.

[63] B. H. Stuart, *Infrared Spectroscopy: Fundamentals and Applications*, vol. 8. 2004.

[64] T. M. Floyd, M. a. Schmidt, and K. F. Jensen, "Silicon Micromixers with Infrared Detection for Studies of Liquid-Phase Reactions," *Ind. Eng. Chem. Res.*, vol. 44, no. 8, pp. 2351–2358, 2005.

[65] R. Keoschkerjan, M. Richter, D. Boskovic, F. Schnürer, and S. Löbbecke, "Novel multifunctional microreaction unit for chemical engineering," *Chem. Eng. J.*, vol. 101, no. 1–3, pp. 469–475, 2004.

[66] D. Prim, S. Crelier, and J.-M. Segura, "Coupling of a microfluidic mixer to a Fourier-transform infrared spectrometer for protein-conformation studies.," *Chimia (Aarau).*, vol. 65, no. 10, pp. 815–6, 2011.

[67] P. Hinsmann, J. Frank, P. Svasek, M. Harasek, and B. Lendl, "Time-Resolved FT-IR Spectroscopy of Chemical Reactions in Solution by Fast Diffusion-Based Mixing in a Micromachined Flow Cell," *Appl. Spectrosc.*, vol. 55, no. 3, pp. 241–251, 2001.

[68] C. F. Carter, H. Lange, S. V Ley, I. R. Baxendale, B. Wittkamp, J. G. Goode, and N. L. Gaunt, "ReactIR Flow Cell : A New Analytical Tool for Continuous Flow Chemical Processing Abstract : A newly developed ReactIR flow cell is reported as a convenient and versatile inline analytical tool for continuous," vol. 393, no. 1, pp. 393–404, 2010.

[69] J. Greener, B. Abbasi, and E. Kumacheva, "Attenuated total reflection Fourier transform infrared spectroscopy for on-chip monitoring of solute concentrations.," *Lab Chip*, vol. 10, no. 12, pp. 1561–6, 2010.

[70] J. Keybl and K. F. Jensen, "Microreactor System for High-Pressure Continuous Flow Homogeneous Catalysis Measurements," *Ind. Eng. Chem. Res.*, vol. 50, no. 19, pp. 11013–11022, 2011.

[71] T. Brodmann, P. Koos, A. Metzger, P. Knochel, and S. V. Ley, "Continuous Preparation of Arylmagnesium Reagents in Flow with Inline IR Monitoring," *Org. Process Res. Dev.*, vol. 16, no. 5, pp. 1102–1113, 2012.

[72] M. Rueping, T. Bootwicha, and E. Sugiono, "Continuous-flow catalytic asymmetric hydrogenations: Reaction optimization using FTIR inline analysis.," *Beilstein J. Org. Chem.*, vol. 8, pp. 300–7, 2012.

[73] A. Kudelski, "Analytical applications of Raman spectroscopy," *Talanta*, vol. 76, no. 1, pp. 1–8, 2008.

[74] F. A. S. H.H. Willard, L.L. Merritt, J.A. Dean, *Instrumental Methods of Analysis*, 7th ed. New Delhi: CBS Publishers, 1986.

[75] R. S. Das and Y. K. Agrawal, "Raman spectroscopy: Recent advancements, techniques and applications," *Vib. Spectrosc.*, vol. 57, no.

2, pp. 163–176, 2011.
[76] C. D. Zangmeister and J. E. Pemberton, “Raman spectroscopy and atomic force microscopy of the reaction of sulfuric acid with sodium chloride,” *J. Am. Chem. Soc.*, vol. 122, no. 49, pp. 12289–12296, 2000.
[77] P. D. I. Fletcher, S. J. Haswell, and X. Zhang, “Monitoring of chemical reactions within microreactors using an inverted Raman microscopic spectrometer,” *Electrophoresis*, vol. 24, no. 18, pp. 3239–3245, 2003.
[78] P. C. Ashok, G. P. Singh, H. a Rendall, T. F. Krauss, and K. Dholakia, “Waveguide confined Raman spectroscopy for microfluidic interrogation.,” *Lab Chip*, vol. 11, no. 7, pp. 1262–70, 2011.
[79] S. E. Slobodan Sasic, *Pharmaceutical Applications of Raman Spectroscopy*. John Wiley & Sons, Inc, 2008.
[80] D. A. Long, “Handbook of Raman spectroscopy. From the research laboratory to the process line. Edited by Ian R. Lewis and Howell G. M. Edwards. Marcel Dekker, New York and Basel, 2001. Price 225.,” *J. Raman Spectrosc.*, vol. 35, no. 1, p. 91, 2004.
[81] A. Urakawa, F. Trachsel, P. R. von Rohr, and A. Baiker, “On-chip Raman analysis of heterogeneous catalytic reaction in supercritical CO2: phase behaviour monitoring and activity profiling.,” *Analyst*, vol. 133, no. 10, pp. 1352–4, 2008.
[82] S. Kim, S. Lee, H. Y. Chi, M. K. Kim, J. S. Kim, S. H. Lee, and H. Chung, “Feasibility Study for Detection of Turnip yellow mosaic virus (TYMV) Infection of Chinese Cabbage Plants Using Raman Spectroscopy,” *Plant Pathol J*, vol. 29, no. 1, pp. 105–109, 2013.
[83] R. Wilson, S. A. Bowden, J. Parnell, and J. M. Cooper, “Signal Enhancement of Surface Enhanced Raman Scattering and Surface Enhanced Resonance Raman Scattering Using in Situ Colloidal Synthesis in Microfluidics,” vol. 82, no. 5, pp. 2119–2123, 2010.
[84] B. M. Liszka, H. S. Rho, Y. Yang, A. T. M. Lenferink, L. W. M. M. Terstappen, and C. Otto, “A microfluidic chip for high resolution Raman imaging of biological cells,” *RSC Adv.*, vol. 5, no. 61, pp. 49350–49355, 2015.
[85] R. S. Macomber, *A Complete Introduction to Modern NMR Spectroscopy*. John Wiley & Sons, Inc, 1998.
[86] M. V. Silva Elipe, “Advantages and disadvantages of nuclear magnetic resonance spectroscopy as a hyphenated technique,” *Anal. Chim. Acta*, vol. 497, no. 1–2, pp. 1–25, 2003.
[87] M. E. Lacey, R. Subramanian, D. L. Olson, A. G. Webb, and J. V. Sweedler, “High-Resolution NMR Spectroscopy of Sample Volumes from 1 nL to 10 &mgr;L.,” *Chem. Rev.*, vol. 99, no. 10, pp. 3133–3152, 1999.
[88] J. C. Chatham and S. J. Blackband, “Nuclear magnetic resonance spectroscopy and imaging in animal research.,” *ILAR J.*, vol. 42, no. 3, pp. 189–208, 2001.
[89] C. Massin, F. Vincent, A. Homsy, K. Ehrmann, G. Boero, P.-A. Besse, A. Daridon, E. Verpoorte, N. F. de Rooij, and R. S. Popovic, “Planar microcoil-based microfluidic {NMR} probes,” *J. Magn. Reson.*, vol. 164, no. 2, pp. 242–255, 2003.
[90] Y. Takahashi, M. Nakakoshi, S. Sakurai, Y. Akiyama, H. Suematsu, H. Utsumi, and T. Kitamori, “Development of an NMR interface microchip ‘MICCS’ for direct detection of reaction products and intermediates of micro-syntheses using a ‘MICCS-NMR’.,” *Anal. Sci.*, vol. 23, no. 4, pp. 395–400, 2007.
[91] M. Nakakoshi, M. Ueda, S. Sakurai, K. Asakura, H. Utsumi, O. Miyata, T. Naito, and Y. Takahashi, “Direct observation of the unstable intermediates in radical addition reaction by using an interfacing microchip combined with an NMR,” *Magn. Reson. Chem.*, vol. 45, no. 11, pp. 989–992, 2007.
[92] V. Sans, L. Porwol, V. Dragone, and L. Cronin, “Chemical Science using real-time in-line NMR spectroscopy †,” *Chem. Sci.*, vol. 6, pp. 1258–1264, 2015.
[93] R. M. Fratila and A. H. Velders, “Small-volume nuclear magnetic resonance spectroscopy.,” *Annu. Rev. Anal. Chem. (Palo Alto. Calif).*, vol. 4, pp. 227–49, 2011.
[94] T. L. Peck, R. L. Magin, and P. C. Lauterbur, “Design and analysis of microcoils for NMR microscopy.,” *Journal of magnetic resonance. Series B*, vol. 108, no. 2. pp. 114–124, 1995.
[95] M. Kakuta, D. a Jayawickrama, A. M. Wolters, A. Manz, and J. V Sweedler, “Micromixer-based time-resolved NMR: applications to ubiquitin protein conformation.,” *Anal. Chem.*, vol. 75, no. 4, pp. 956–60, 2003.
[96] C. Hilty, E. E. McDonnell, J. Granwehr, K. L. Pierce, S.-I. Han, and A. Pines, “Microfluidic gas-flow profiling using remote-detection NMR.,” *Proc. Natl. Acad. Sci. U. S. A.*, vol. 102, no. 42, pp. 14960–14963, 2005.
[97] R. C. Meier, J. Höfflin, V. Badilita, U. Wallrabe, and J. G. Korvink, “Microfluidic integration of wirebonded microcoils for on-chip applications in nuclear magnetic resonance,” *J. Micromechanics Microengineering*, vol. 24, no. 4, p. 045021, 2014.
[98] J. Bart, A. J. Kolkman, A. J. O. Vries, K. Koch, P. J. Nieuwland, H. J. W. G. Janssen, J. P. J. M. Van Bentum, K. A. M. Ampt, F. P. J, T. Rutjes, S. S. Wijmenga, H. J. G. E. Gardeniers, A. P. M. Kentgens, and F. P. J. T. Rutjes, “Communication A Microfluidic High-Resolution NMR Flow Probe A Microfluidic High-Resolution NMR Flow Probe,” *Small*, pp. 5014–5015, 2009.
[99] H. G. Krojanski, J. Lambert, Y. Gerikalan, D. Suter, and R. Hergenröder, “Microslot NMR Probe for Metabolomics Studies,” *Anal. Chem.*, vol. 80, no. 22, pp. 8668–8672, 2008.
[100] H. Ryan, S.-H. Song, A. Zaß, J. Korvink, and M. Utz, “Contactless NMR Spectroscopy on a Chip,” *Anal. Chem.*, vol. 84, no. 8, pp. 3696–3702, 2012.
[101] L. Ciobanu, D. a Jayawickrama, X. Zhang, A. G. Webb, and J. V Sweedler, “Measuring reaction kinetics by using multiple microcoil NMR spectroscopy.,” *Angew. Chem. Int. Ed. Engl.*, vol. 42, no. 38, pp. 4669–72, 2003.
[102] H. Wensink, F. Benito-Lopez, D. C. Hermes, W. Verboom, H. J. G. E. Gardeniers, D. N. Reinhoudt, and A. van den Berg, “Measuring reaction kinetics in a lab-on-a-chip by microcoil NMR.,” *Lab Chip*, vol. 5, no. 3, pp. 280–284, 2005.
[103] M. V. Gomez, H. H. J. Verputten, A. Díaz-Ortíz, A. Moreno, A. de la Hoz, and A. H. Velders, “On-line monitoring of a microwave-assisted chemical reaction by nanolitre NMR-spectroscopy.,” *Chem. Commun. (Camb).*, vol. 46, no. 25, pp. 4514–6, 2010.
[104] D. Zagorevskii, “2.28 - Mass Spectrometry,” in *Comprehensive Coordination Chemistry {II}*, J. A. McCleverty and T. J. Meyer, Eds. Oxford: Pergamon, 2003, pp. 367–380.
[105] J. S. Barnes, F. W. Foss, and K. a Schug, “Thermally accelerated oxidative degradation of quercetin using continuous flow kinetic electrospray-ion trap-time of flight mass spectrometry.,” *J. Am. Soc. Mass Spectrom.*, vol. 24, no. 10, pp. 1513–22, 2013.
[106] E. Van Duijn, “Current Limitations in Native Mass Spectrometry Based Structural Biology,” *JAM*, vol. 21, no. 6, pp. 971–978, 2010.
[107] Z. Zhu, J. E. Bartmess, M. E. McNally, R. M. Hoffman, K. D. Cook, and L. Song, “Quantitative real-time monitoring of chemical reactions by autosampling flow injection analysis coupled with atmospheric pressure chemical ionization mass spectrometry.,” *Anal. Chem.*, vol. 84, no. 17, pp. 7547–54, 2012.
[108] A.-H. M. Emwas, “The Strengths and Weaknesses of NMR Spectroscopy and Mass Spectrometry with Particular Focus on Metabolomics Research,” in *Metabonomics: Methods and Protocols*, J. T. Bjerrum, Ed. New York, NY: Springer New York, 2015, pp. 161–193.
[109] B. V Silva, F. a Violante, A. C. Pinto, and L. S. Santos, “The mechanism of Sandmeyer’s cyclization reaction by electrospray

ionization mass spectrometry.,” *Rapid Commun. Mass Spectrom.*, vol. 25, no. 3, pp. 423–8, 2011.
[110] *Inductively Coupled Plasma Mass Spectrometry Table of Contents – ICP-MS Primer*. Agilent Technologies, Inc., 2005.
[111] R. E. Oosterbroek, M. Brivio, M. H. Goedbloed, P. Guatteri, D. N. Reinhoudt, A. Van Den Berg, and E. S. Ionization, “Simple electro spray ionization mass-spectrometry coupling for organic synthesis analysis in microreactors,” *Micro Total Anal. Syst.*, pp. 837–840, 2003.
[112] L. S. Santos and J. O. Metzger, “Study of homogeneously catalyzed Ziegler-Natta polymerization of ethene by ESI-MS.,” *Angew. Chem. Int. Ed. Engl.*, vol. 45, no. 6, pp. 977–81, 2006.
[113] C. T. Martha, N. Elders, J. G. Krabbe, J. Kool, W. M. a Niessen, R. V. a Orru, and H. Irth, “Online screening of homogeneous catalyst performance using reaction detection mass spectrometry,” *Anal. Chem.*, vol. 80, no. 18, pp. 7121–7127, 2008.
[114] K.-C. Hsu, C.-C. Sun, Y.-C. Ling, S.-J. Jiang, and Y.-L. Huang, “An on-line microfluidic device coupled with inductively coupled plasma mass spectrometry for chromium speciation,” *J. Anal. At. Spectrom.*, vol. 28, no. 8, pp. 1320–1326, 2013.
[115] M. Brivio, R. H. Fokkens, W. Verboom, D. N. Reinhoudt, N. R. Tas, M. Goedbloed, and A. van den Berg, “Integrated microfluidic system enabling (bio)chemical reactions with on-line MALDI-TOF mass spectrometry,” *Anal. Chem.*, vol. 74, no. 16, pp. 3972–6, 2002.
[116] D. J. Clarke, A. a Stokes, P. Langridge-Smith, and C. L. Mackay, “Online quench-flow electrospray ionization Fourier transform ion cyclotron resonance mass spectrometry for elucidating kinetic and chemical enzymatic reaction mechanisms.,” *Anal. Chem.*, vol. 82, no. 5, pp. 1897–904, 2010.
[117] D. E. Fitzpatrick, C. Battilocchio, and S. V. Ley, “A Novel Internet-Based Reaction Monitoring, Control and Autonomous Self-Optimization Platform for Chemical Synthesis,” *Org. Process Res. Dev.*, vol. 20, no. 2, pp. 386–394, 2016.
[118] R. Arakawa, L. Jian, A. Yoshimura, K. Nozaki, and T. Ohno, “On-Line Mass Analysis of Reaction Products by Electrospray Ionization. Photosubstitution of Ruthenium(I1) Diimine Complexes,” no. 17, pp. 3874–3878, 1995.
[119] A. R. de Boer, B. Bruyneel, J. G. Krabbe, H. Lingeman, W. M. a Niessen, and H. Irth, “A microfluidic-based enzymatic assay for bioactivity screening combined with capillary liquid chromatography and mass spectrometry.,” *Lab Chip*, vol. 5, no. 11, pp. 1286–92, 2005.
[120] H. Wang, Z. Wu, Y. Zhang, B. Chen, M. He, and B. Hu, “Chip-based liquid phase microextraction combined with electrothermal vaporization-inductively coupled plasma mass spectrometry for trace metal determination in cell samples,” *J. Anal. At. Spectrom.*, vol. 28, no. 10, pp. 1660–1665, 2013.
[121] V. Sans, L. Porwol, V. Dragone, and L. Cronin, “A self optimizing synthetic organic reactor system using real-time in-line NMR spectroscopy,” *Chem. Sci.*, vol. 6, no. 2, pp. 1258–1264, 2015.
[122] R. J. Ingham, C. Battilocchio, D. E. Fitzpatrick, E. Sliwinski, J. M. Hawkins, and S. V. Ley, “A systems approach towards an intelligent and self-controlling platform for integrated continuous reaction sequences,” *Angew. Chemie - Int. Ed.*, vol. 54, no. 1, pp. 144–148, 2015.
[123] E. Miller, M. Rotea, and J. P. Rothstein, “Microfluidic device incorporating closed loop feedback control for uniform and tunable production of micro-droplets.,” *Lab Chip*, vol. 10, no. 10, pp. 1293–1301, 2010.
[124] S. Krishnadasan, R. J. C. Brown, A. J. DeMello, and J. C. DeMello, “Miniaturisation for chemistry , biology & bioengineering Intelligent routes to the controlled synthesis of nanoparticles,” vol. 7, no. 11, 2007.
[125] C. Houben and A. A. Lapkin, “Automatic discovery and optimization of chemical processes,” *Curr. Opin. Chem. Eng.*, vol. 9, pp. 1–7, 2015.
[126] R. L. McCreery, “Lasers for Raman Spectroscopy,” in *Raman Spectroscopy for Chemical Analysis*, J. D. Winefordner, Ed. John Wiley & Sons, Inc., 2005, p. 420.
[127] “What laser wavelengths are used for Raman spectroscopy?” [Online]. Available: http://www.horiba.com/scientific/products/raman-spectroscopy/raman-academy/raman-faqs/what-laser-wavelengths-are-used-for-raman-spectroscopy/.
[128] P. Vandenabeele and L. Moens, “Some ideas on the definition of Raman spectroscopic detection limits for the analysis of art and archaeological objects,” *J. Raman Spectrosc.*, vol. 43, no. 11, pp. 1545–1550, 2012.
[129] R. F. Ismagilov, A. D. Stroock, P. J. A. Kenis, G. Whitesides, H. A. Stone, R. F. Ismagilov, A. D. Stroock, P. J. A. Kenis, and G. Whitesides, “Experimental and theoretical scaling laws for transverse diffusive broadening in two- phase laminar flows in microchannels Experimental and theoretical scaling laws for transverse diffusive broadening in two-phase laminar flows in microchannels,” vol. 2376, no. 2000, pp. 1–4, 2016.
[130] B. Kuswandi, Nuriman, J. Huskens, and W. Verboom, “Optical sensing systems for microfluidic devices: A review,” *Anal. Chim. Acta*, vol. 601, no. 2, pp. 141–155, 2007.
[131] R. S. Macomber, *A Complete Introduction to Modern NMR Spectroscopy*. John Wiley & Sons, Inc., 1998.
[132] C. Massin, F. Vincent, A. Homsy, K. Ehrmann, G. Boero, P. A. Besse, A. Daridon, E. Verpoorte, N. F. De Rooij, and R. S. Popovic, “Planar microcoil-based microfluidic NMR probes,” *J. Magn. Reson.*, vol. 164, no. 2, pp. 242–255, 2003.
[133] M. R. Siddiqui, Z. A. AlOthman, and N. Rahman, “Analytical techniques in pharmaceutical analysis: A review,” *Arab. J. Chem.*, 2013.
[134] J. Christoph and G. Mathieu, “Sampling in Reaction Progress Analysis Understand Your Chemical Reaction Better,” *G.I.T. Laboratory Journal Europe*, pp. 18–19, 2017.
[135] H. F. Kevin A. Schug, “Hyphenation of Flow-Injection Analysis with Mass Spectrometry: A Versatile and High-Throughput Technique,” *chromatographyonline*, vol. Volume 10, no. 2, pp. 26–33.
[136] A. Fröhlich, “Online Monitoring von Mikroreaktorsystemen mit ESI-Massenspektrometrie,” University of Rostock, 2010.
[137] D. Hoffmann, “Konzeption und Realisierung einer Online-MS-Analytik für die Reaktionsverfolgung,” Universität Rostock, 2013.
[138] V. Miralles, A. Huerre, F. Malloggi, and M. Jullien, *A Review of Heating and Temperature Control in Microfluidic Systems: Techniques and Applications*. 2013.
[139] P. J. Hung, P. J. Lee, P. Sabounchi, R. Lin, and L. P. Lee, “Continuous perfusion microfluidic cell culture array for high-throughput cell-based assays.,” *Biotechnol. Bioeng.*, vol. 89, no. 1, pp. 1–8, 2005.
[140] G. Maltezos, M. Johnston, K. Taganov, C. Srichantaratsamee, J. Gorman, D. Baltimore, W. Chantratita, and A. Scherer, “Exploring the limits of ultrafast polymerase chain reaction using liquid for thermal heat exchange: A proof of principle.,” *Appl. Phys. Lett.*, vol. 97, no. 26, p. 264101, 2010.
[141] M. T. Guo, A. Rotem, J. A. Heyman, and D. A. Weitz, “Droplet microfluidics for high-throughput biological assays,” *Lab Chip*, vol. 12, no. 12, pp. 2146–2155, 2012.
[142] F. P. Incropera, D. P. DeWitt, T. L. Bergman, and A. S. Lavine, *Fundamentals of Heat and Mass Transfer*, vol. 6th. John Wiley &

Sons, 2007.
[143] G. Velve-Casquillas, J. Costa, F. Carlier-Grynkorn, A. Mayeux, and P. T. Tran, “Chapter 11 – A Fast Microfluidic Temperature Control Device for Studying Microtubule Dynamics in Fission Yeast,” in *Methods in Cell Biology*, vol. 97, 2010, pp. 185–201.
[144] J. Yang, Y. Liu, C. B. Rauch, R. L. Stevens, R. H. Liu, R. Lenigk, and P. Grodzinski, “High sensitivity PCR assay in plastic micro reactors,” *Lab Chip*, vol. 2, no. 4, pp. 179–187, 2002.
[145] T.-M. Hsieh, C.-H. Luo, F.-C. Huang, J.-H. Wang, L.-J. Chien, and G.-B. Lee, “Enhancement of thermal uniformity for a microthermal cycler and its application for polymerase chain reaction,” *Sensors Actuators B Chem.*, vol. 130, no. 2, pp. 848–856, 2008.
[146] R. M. Guijt, A. Dodge, G. W. K. van Dedem, N. F. de Rooij, and E. Verpoorte, “Chemical and physical processes for integrated temperature control in microfluidic devices,” *Lab Chip*, vol. 3, no. 1, pp. 1–4, 2003.
[147] J. J. Shah, S. G. Sundaresan, J. Geist, D. R. Reyes, J. C. Booth, M. V Rao, and M. Gaitan, “Microwave dielectric heating of fluids in an integrated microfluidic device,” *J. Micromechanics Microengineering*, vol. 17, no. 11, pp. 2224–2230, 2007.
[148] M. Robert de Saint Vincent, R. Wunenburger, and J.-P. Delville, “Laser switching and sorting for high speed digital microfluidics,” *Appl. Phys. Lett.*, vol. 92, no. 15, p. 154105, 2008.
[149] F. Haugen, “Ziegler-Nichols’ Closed-Loop Method,” 2010. [Online]. Available: http://techteach.no/publications/articles/zn_closed_loop_method/zn_closed_loop_method.pdf. [Accessed: 14-Nov-2016].
[150] P. Dell‘Orco, J. Brum, R. Matsuoka, M. Badlani, and K. Muske, “Monitoring Process-Scale Reactions Using API Mass Spectrometry,” *Anal. Chem.*, vol. 71, no. 22, pp. 5165–5170, 1999.
[151] H. Cai, J. P. Kiplinger, W. K. Goetzinger, R. O. Cole, K. a. Laws, M. Foster, and A. Schrock, “A straightforward means of coupling preparative high-performance liquid chromatography and mass spectrometry,” *Rapid Commun. Mass Spectrom.*, vol. 16, no. 6, pp. 544–554, 2002.
[152] A. Ainla, I. Gözen, O. Orwar, and A. Jesorka, “A microfluidic diluter based on pulse width flow modulation,” *Anal. Chem.*, vol. 81, no. 13, pp. 5549–5556, 2009.
[153] S. K. W. Dertinger, D. T. Chiu, Noo Li Jeon, and G. M. Whitesides, “Generation of gradients having complex shapes using microfluidic networks,” *Anal. Chem.*, vol. 73, no. 6, pp. 1240–1246, 2001.
[154] X. Zhang and M. G. Roper, “Microfluidic perfusion system for automated delivery of temporal gradients to islets of Langerhans.,” *Anal. Chem.*, vol. 81, no. 3, pp. 1162–1168, 2009.
[155] B. M. Paegel, W. H. Grover, A. M. Skelley, R. a. Mathies, and G. F. Joyce, “Microfluidic serial dilution circuit,” *Anal. Chem.*, vol. 78, no. 21, pp. 7522–7527, 2006.
[156] R. Clinton, C. S. Creaser, and D. Bryant, “Real-time monitoring of a pharmaceutical process reaction using a membrane interface combined with atmospheric pressure chemical ionisation mass spectrometry,” *Anal. Chim. Acta*, vol. 539, no. 1–2, pp. 133–140, 2005.
[157] D. Hoffmann, “Online-Reaction-Monitoring system with Dilution module,” University of Rostock, 2015.
[158] A. Toribio, E. Destandau, C. Elfakir, and M. Lafosse, “Hyphenation of centrifugal partition chromatography with electrospray ionization mass spectrometry using an active flow-splitter device for characterization of flavonol glycosides,” pp. 1863–1870, 2009.
[159] W. Leister, K. Strauss, D. Wisnoski, Z. Zhao, and C. Lindsley, “Development of a Custom High-Throughput Preparative Liquid Chromatography / Mass Spectrometer Platform for the Preparative Purification and Analytical Analysis of Compound Libraries,” pp. 322–329, 2003.
[160] T. W. T. Bristow, A. D. Ray, A. O’Kearney-Mcmullan, L. Lim, B. McCullough, and A. Zammataro, “On-line monitoring of continuous flow chemical synthesis using a portable, small footprint mass spectrometer,” *J. Am. Soc. Mass Spectrom.*, vol. 25, no. 10, pp. 1794–1802, 2014.
[161] S. M. F. Jeurissen, F. W. Claassen, J. Havlik, E. E. Bouwmans, N. H. P. Cnubben, E. J. R. Sudh??lter, I. M. C. M. Rietjens, and T. A. van Beek, “Development of an on-line high performance liquid chromatography detection system for human cytochrome P450 1A2 inhibitors in extracts of natural products,” *J. Chromatogr. A*, vol. 1141, no. 1, pp. 81–89, 2007.
[162] N. H. Bings, A. Bogaerts, and A. C. Broekaert, “Atomic Spectroscopy,” pp. 3917–3946, 2006.
[163] R. N. Rao and M. V. N. K. Talluri, “An overview of recent applications of inductively coupled plasma-mass spectrometry (ICP-MS) in determination of inorganic impurities in drugs and pharmaceuticals,” *J. Pharm. Biomed. Anal.*, vol. 43, no. 1, pp. 1–13, 2007.
[164] D. Beauchemin, “Environmental analysis by inductively coupled plasma mass spectrometry,” *Mass Spectrometry Reviews*, 2010. [Online]. Available: http://dx.doi.org/10.1002/mas.20257.
[165] A.-I. Stoica, M. Peltea, G.-E. Baiulescu, and M. Ionica, “Determination of cobalt in pharmaceutical products,” *J. Pharm. Biomed. Anal.*, vol. 36, no. 3, p. 653—656, 2004.
[166] “Inductively coupled plasma mass spectrometry.” [Online]. Available: https://en.wikipedia.org/wiki/Inductively_coupled_plasma_mass_spectrometry#Applications. [Accessed: 26-Nov-2016].
[167] D. Pröfrock and A. Prange, “Inductively coupled plasma-mass spectrometry (ICP-MS) for quantitative analysis in environmental and life sciences: A review of challenges, solutions, and trends,” *Appl. Spectrosc.*, vol. 66, no. 8, pp. 843–868, 2012.
[168] W. Hu, F. Zheng, and B. Hu, “Simultaneous separation and speciation of inorganic As(III)/As(V) and Cr(III)/Cr(VI) in natural waters utilizing capillary microextraction on ordered mesoporous Al2O3 prior to their on-line determination by ICP-MS,” *J. Hazard. Mater.*, vol. 151, no. 1, pp. 58–64, 2008.
[169] W. Hu, B. Hu, and Z. Jiang, “On-line preconcentration and separation of Co, Ni and Cd via capillary microextraction on ordered mesoporous alumina coating and determination by inductively plasma mass spectrometry (ICP-MS),” *Anal. Chim. Acta*, vol. 572, no. 1, pp. 55–62, 2006.
[170] H. Wang, Z. Wu, Y. Zhang, B. Chen, M. He, and B. Hu, “Chip-based liquid phase microextraction combined with electrothermal vaporization-inductively coupled plasma mass spectrometry for trace metal determination in cell samples,” *J. Anal. At. Spectrom.*, vol. 28, no. 10, pp. 1660–1665, 2013.
[171] E. C. Hathorne, B. Haley, T. Stichel, P. Grasse, M. Zieringer, and M. Frank, “Online preconcentration ICP-MS analysis of rare earth elements in seawater,” *Geochemistry, Geophys. Geosystems*, vol. 13, no. 1, pp. 1–12, 2012.
[172] R. F. Milani, L. I. Peron, E. S. Saron, M. A. Morgano, and F. F. Silva, “A Validated Method for Direct Analysis : 13 Trace Elements Determination in Tea Infusions using the Agilent 7700x ICP-MS with Integrated Sample Introduction System in Discrete Sampling (ISIS-DS),” p. 8, 2013.
[173] A. S. G. Roombridge, S. M. Iyashita, S. F. Ujii, K. N. Agasawa, T. O. Kahashi, M. O. Hata, T. U. Memura, A. T. Akatsu, K. I. Nagaki, and K. C. Hiba, “High Sensitive Elemental Analysis of Single Yeast Cells (Saccharomyces cerevisiae) by Time-Resolved Inductively-Coupled Plasma Mass Spectrometry Using a High Efficiency Cell Introduction System,” vol. 29, pp. 597–603, 2013.

[174] I. Banerjee, B. Nguyen, V. Garousi, and A. Memon, “Graphical user interface (GUI) testing : Systematic mapping and repository,” *Inf. Softw. Technol.*, vol. 55, no. 10, pp. 1679–1694, 2013.
[175] J. Brand and J. Balvanz, “Automation is a Breeze with AutoIt,” in *Proceedings of the 33rd Annual ACM SIGUCCS Conference on User Services*, 2005, pp. 12–15.
[176] J. M. Slack, “System testing on the cheap,” in *Proceedings of ISECON*, 2010.
[177] “AutoIt.” [Online]. Available: https://www.autoitscript.com/site/autoit/. [Accessed: 19-Sep-2016].
[178] A. Flesner, *AutoIt v3 : Your Quick Guide*. 2007.
[179] B. D. Blansit, “Using AutoIt to Simplify Scripting,” *J. Electron. Resour. Med. Libr.*, vol. 5, no. 3, pp. 293–306, 2008.
[180] M. Schaffer, J. Wagner, H. Schröttner, and M. Schmied, “Automated X-Ray Elemental Analysis in Three Dimensions Using a Dual Beam-Focused Ion Beam System,” *Pract. Metallogr.*, vol. 44, no. 5, pp. 248–250, 2007.
[181] A. R. Shiveley, P. A. Shade, A. L. Pilchak, J. S. Tiley, and R. Kerns, “A novel method for acquiring large-scale automated scanning electron microscope data,” *J. Microsc.*, vol. 244, no. 2, pp. 181–186, 2011.

PUBLICATIONS

[1] V. Q. Do, H. Fleischer, D. Hoffmann, and K. Thurow, “Online Reaction Monitoring System in Microreactor Using Electrospray Ionization Mass Spectrometry: A Methodology for Saving Time and Materials,” in 3rd International Conference on Automation, Control Engineering and Computer Science ACECS 2016, 2016, pp. 528–534.

[2] V. Q. Do, H. Fleischer, D. Hoffmann, and K. Thurow, “Integration of a Dilution Module in a Mass Spectrometry based Online Reaction Monitoring System,” American Laboratory, vol. 49, no. 1, pp. 36–40, 2017.

[3] V. Q. Do, H. Fleischer, K. Ramani, and K. Thurow, “Integration of a Micro Reactor System to a ICP Mass Spectrometer,” in IEEE International Instrumentation and Measurement Technology Conference I2MTC 2017, 2017, pp. 1375–1380.

[4] V. Q. Do, H. Fleischer, and K. Thurow, “Online Dilution for Elemental Measurements Using an Online Reaction Monitoring System and Inductively-Coupled Plasma Mass Spectrometry,” in IEEE International Instrumentation and Measurement Technology Conference I2MTC 2018, 2018, *Accepted*.

[5] H. Fleischer, D. Hoffmann, N. Almahaini, V. Q. Do, and K. Thurow, “Online Coupling System and Control Software for Reaction Monitoring using Microreactors and ESI-MS,” in International Instrumentation and Measurement Technology Conference, 2015, pp. 1561–1566.

THESES

1) An online reaction monitoring system (ORMS) combining the advantages of micro reactor systems and analytical devices has been improved in performance and scope of functions.

2) The system is computer-controlled with all actions are automated via the GUI. From the initial setup, the system has improved through different works.

3) The dilution module, which combines an active flow splitter (or mass rate attenuator) with a compensation pump, enables the system to work with high concentrated solution without the sample overloading problem for the MS.

4) The dilution is able to dilute automatically various ratios with various stock solutions at different concentrations and stable for different flow rates of the micro reactor.

5) The online reaction monitoring system including the dilution module can be integrated with an ESI-MS operating in time-resolved analysis (TRA) mode to measure the diluted solution online. Results from automatic dilution are comparable to manual dilution.

6) By integrating with an ICP-MS, the ORMS is capable of metal detection. Two integration schemes were proposed and tested. The results show a strong contamination of Fe and Cu from the carrier pump to the sample. There is also a strong influence of solvents to metal dissolution of the carrier pump to the sample.

7) The dilution was quantified using the ICP-MS in spectrum mode. The dilution is able to give >90% accuracy under various micro reactor's flow rates.

8) The dilution module also gives logical results (higher dilution ratio gives lower concentration and vice versa) when the ICP-MS operates in TRA mode. In general, measuring in TRA mode of ICP-MS gives as logical results as with the spectrum mode.

9) Both algorithms for sampling, which were further developed from the existing ones, are more versatile, and save time and materials more efficiently.

10) The second algorithm in which the total time and material consumption for a series of reaction stages equal the sum of the first and the last reaction stages is selected for implementation in the control software. This algorithm is simple to understand and more efficient when there are more reaction stages in a series.

11) The heating module is speeded up with the heating rate about 5^{o}C/min after removing unnecessary curve connectors and using an additional heating plate. Temperature of reagent solution could be conditioned from -20^{o}C up to 180^{o}C.

12) The internal working mode of the heating circulator is used to heat the micro reactor block safely. And its external working mode is used to heat the micro reactor block quickly.

13) The errors of simultaneous reading from and writing to devices which caused peak missing and double sized-peak in sampling of the existing system were corrected. This reduced the standard deviation in sampling replication down to less than 10%.

14) The existing control software was modified for accommodation of new functions and modules. The modified GUI has tab structure and each tab manipulates a functioning module.

15) The ORMS control software can communicate with the analyzer's control software for a convenience in operation and data processing. The AutoIt library is implemented for this GUI automation purpose. Basic functions in the MassHunter Workstation software for ESI-MS and ICP-MS are automated.

DECLARATION

I, herewith, declare the following:

1. The opportunity for this Ph.D. project was not communicated to me commercially. In particular, I have not engaged any organization that for money seeks supervisors for the drawing up of dissertations or that performs entirely or partially on my behalf the duties incumbent upon me regarding the examinations.

2. I hereby declare under oath that I have completed the work submitted here independently and have composed it without outside assistance. Furthermore, I have not used anything other than the resources and sources stated and where I have taken sections from these works in terms of content or text, I have identified this appropriately.

August 30, 2017, Rostock

Vinh Quang Do